

Sequence stratigraphy, sedimentology and provenance of the Upper Cretaceous siliciclastic sediments of South Jordan

Von der Fakultät Geo- und Biowissenschaften
der Universität Stuttgart
zur Erlangung der Würde eines Doktors der
Naturwissenschaften (Dr. rer. nat.) genehmigte Abhandlung

Vorgelegt von
Uwe Peter Baaske
aus Kaiserslautern

Hauptberichter:
Mitberichter:

PD Dr. H. Krawinkel
Prof. Dr. H. Seyfried

Tag der mündlichen Prüfung:

04.03.2004

Institut für Geologie und Paläontologie der Universität Stuttgart

2005

Ich versichere, dass ich die vorliegende Arbeit selbstständig und nur unter Verwendung der angegebenen Hilfsmittel angefertigt habe.

Uwe P. Brande

Stuttgart, den 11. November 2003

,,...After three days in the desert fun
I was looking at a river bed
And the story it told of a river that flowed
Made me sad to think it was dead...”

From “Horse with no name”
Written by Dewey Bunnell, 1971

Zusammenfassung

Das Ziel der vorgelegten Arbeit ist es einen sequenzstratigraphischen Rahmen für die oberkretazischen (Albium bis Santonium) Sedimentgesteine Südjordaniens zu schaffen. Des Weiteren wurde die Provenienz, Diagenese und Verwitterungsgeschichte der siliziklastischen Ablagerungen mit Hilfe von Sedimentpetrographie und Geochemie am Gesamtgestein bestimmt.

Das Arbeitsgebiet liegt im Wüstengebiet im Süden Jordaniens, etwa 60 km südlich der Stadt Ma'an. Entlang einer 90 bis 100 km langen, NW-SE streichenden Steilstufe („Escarment“) ist dort eine Abfolge von paläozoischen bis kretazischen Sedimentgesteinen aufgeschlossen. Als Grundlage für die Faziesanalyse und die sequenzstratigraphische Interpretation wurden 15 detaillierte stratigraphische Profile innerhalb der Kreidegesteine aufgenommen. Für petrographische und geochemische Untersuchungen wurden Sandsteinhorizonte und vereinzelt auch feinkörnigere Gesteine beprobt.

Die kreidezeitlichen Sedimentgesteine im Arbeitsgebiet wurden in einem terrestrischen bis marinen Bereich abgelagert. Insgesamt wurden zehn Ablagerungsbereiche für die untersuchte Schichtfolge definiert, die sich in vier Hauptfaziesassoziationen zusammenfassen lassen: (i) der Schelfbereich, (ii) die Küste, (iii) der randmarine Ablagerungsraum und (iv) die Küstenebene. Das wiederholte Auftreten von lateralen Verzahnungen der terrestrischen und marinen Ablagerungsbereiche innerhalb der Abfolge weist darauf hin, dass die untersuchten Sedimentgesteine in einem flachmarinen Küstensystem zur Ablagerung kamen. Durch Fazieskorrelation lässt sich dieses siliziklastisch bis gemischt karbonatisch-siliziklastisch geprägte Küstensystem in drei zeitlich getrennte Hauptablagerungssysteme unterteilen: (i) eine siliziklastische Rampe, (ii) eine gemischt siliziklastisch-karbonatische Rampe und (iii) ein Alluvialebenen System. Vertikal sind diese Ablagerungssysteme in sich wiederholenden Zyklomen angeordnet, die im Idealfall aus einem retrogradierenden siliziklastischen Rampensystem, einem gemischt siliziklastisch-karbonatischen Rampensystem, einem progradierenden siliziklastischen Rampensystem und, am Ende, einem Alluvialebenen System zusammengesetzt sind.

Die Ausbildung des Küstensystems wurde durch einen sich verändernden Meeresspiegel gesteuert. Bei regressivem Meeresspiegel bildeten sich sanddominierte Braid-Deltas aus. Transgressive Meeresspiegelbedingungen führten zu einem Küstensystem, das von wellendominierten Ästuaren und Barriere/Lagunen Komplexen geprägt war. Auf der Küstenebene bildeten sich während Transgressionen anastomisierende bis mäandrierende, sanddominierte Flusssysteme mit weiten Überschwemmungsebenen aus. Während Regressionen wandelte sich das küstennahe Flusssystem mehr zu einem verzweigten Flusssystem hin das direkt mit den „Braid-Deltas“, die sich zu dieser Zeit bildeten, in Kontakt stand.

Die untersuchte Sedimentabfolge beinhaltet acht Sequenzen dritter Ordnung. Die basalen vier Sequenzen umfassen die Ajlun Group (Cenomanium bis Coniacium), während die oberen vier Sequenzen innerhalb der Belqa Group (Coniacium bis Santonium) zu finden sind. Die Sequenzen 1, 2 und 4 der basalen Abfolge können jeweils noch in zwei Sequenzen höherer Ordnung unterteilt werden. Praktisch alle Sequenzen enthalten Hinweise auf „Forced Regressions“, die während des relativen Meeresspiegelrückgangs gebildet wurden.

Typische Charakteristika von „Forced Regressions“, wie z.B. Küstenablagerungen mit scharfem basalem Kontakt zu liegenden ‚Tiefwasser-Sedimenten‘, sind in den Profilen häufig anzutreffen. Wegen der besonderen Bedeutung der Regressionsphasen für die untersuchte Sedimentabfolge wurde das sequenzstratigraphische Model von Plint und Nummedal (2000) für die sequenzstratigraphische Interpretation gewählt. Dieses Model fasst den gesamten Meeresspiegelrückgang in einem neuen Systemtrakt, dem so genannten „Falling Stage Systems Tract“ (FSST) zusammen und stellt diesen dem LST, TST und HST gegenüber.

Der Vergleich der Sequenzstratigraphie mit den Hauptablagerungssystemen zeigt, dass diese Ablagerungssysteme sehr gut mit den vier System Trakten aus dem angewandten sequenzstratigraphischen Model übereinstimmen. Das Alluvialebenen System entwickelte sich während des LST, das retrogradierende siliziklastische Rampensystem während des TST. Das gemischt karbonatisch-siliziklastische Rampensystem entspricht dem HST und das progradierende siliziklastische Rampensystem ist mit dem FSST assoziiert. Veränderungen im relativen Meeresspiegel und die Sedimentzufuhr waren die wichtigsten Kontrollfaktoren für die Sequenzarchitektur der untersuchten Ablagerungen, wobei der relative Meeresspiegel hauptsächlich eustatischen Schwankungen widerspiegelt. Die siliziklastische Sedimentzufuhr ist mit Änderungen des relativen Meeresspiegels verbunden und mit dem rückschreitenden Einschneiden von fluviatilen Systemen während des FSST und LST assoziiert.

Der zweite Teil der Arbeit befasst sich mit petrographischen und geochemischen Untersuchungen zur Provenienz und Diagenese der kretazischen Sande und Sandsteine im Arbeitsgebiet. Die Untersuchung der Leichtminerale zeigt, dass die kretazischen Sande und Sandsteine Südjordaniens im Allgemeinen textuell und strukturell reif sind und als Quarzarenite klassifiziert werden können. Nur die fein- bis mittelkörnigen Sande und Sandsteine des Arbeitsgebietes weisen teilweise einen leicht höheren Anteil an Feldspat auf, der sie als Subarkosen klassifiziert. Der Schwermineralgehalt aller Sande und Sandsteine weist eine Dominanz der ultrastabilen Schwerminerale Zirkon, Turmalin und Rutil auf, wobei besonders Zirkon in den untersuchten Proben vorherrscht. Mit einem mittleren ZTR-Index von 97,9 spiegelt der Schwermineralanteil die mineralogische Reife der Sedimente, die sich schon in der Leichtmineralanalyse gezeigt hat, wider.

Die untersuchten Proben erfuhren nur ein begrenztes Spektrum an diagenetischen Prozessen. Hohe Intergranularvolumen-Werte und das Fehlen von destruktiven Kornkontakten und Drucklösung zeigen dass keine tiefe Versenkung oder große Auflast erreicht wurde und die Kompaktion der Sedimentgesteine nur gering war. Die Sandsteine des Arbeitsgebiets können nach den Hauptzementphasen in drei Gruppen unterteilt werden: Sandsteine die mit Tonmineralen zementiert wurden, schwach verfestigt und mit hohen Intergranularporositäten; Sandsteine die mit Kalzit und Dolomit zementiert wurden und eisenoxidzementierte Sandsteine. Die beiden letzten Gruppen sind gut verfestigt und haben meist nur geringe intergranulare Porositäten. Die Zementation mit Karbonatmineralen ist faziesabhängig und tritt nur in marinen Sedimenten auf.

Der Verwitterungstrend aller Proben kann als ‚normal‘ bezeichnet werden. In der Regel zeigen die CIA-Werte (‚chemical index of alteration‘) der Proben eine moderate Verwitterung an. Nur die Sandsteinproben und einige Tonsteinproben weisen erhöhte, für recycelte Sedimente typische, CIA-Werte auf.

Zusammengefasst zeigen die petrographischen und geochemischen Provenienzanalysen dass die kretazischen Sandsteine Südjordaniens an einem passiven Kontinentalrand zur Ablagerung kamen. Als Ausgangsmaterial für die untersuchten Proben ist der kristalline Kernbereich eines Kratons am wahrscheinlichsten. Neben der kratonalen Komponente weisen die Proben auch einen klaren Trend zu recycelten Sedimentgesteinen als Ausgangsmaterial auf. Dies wird besonders durch resedimentierte Quarzkörner und die Anreicherung von Zirkon in den Proben deutlich. Das Liefergebiet für die kretazischen Siliziklastika Südjordaniens ist der Arabo-Nubische Schild und seine paläozoische Sedimentbedeckung.

Abstract

The aim of this study was to establish a sequence stratigraphic framework for the Upper Cretaceous (Albian to Santonian) sedimentary rocks of South Jordan. This was accomplished by detailed sedimentological studies and facies analysis. Furthermore the provenance and weathering history of the siliciclastic rocks was determined by using sedimentary petrography and bulk rock geochemistry.

The study area is situated in the southern part of Jordan, about 60 km south of the city Ma'an, between the city Ras en Naqb in the West to Naqb Ataik in the East. Here a succession of Palaeozoic to Cretaceous sedimentary rocks is exposed along a NW-SE to E trending, about 90 km long escarpment. Along this escarpment fifteen vertical sections were logged in detail and samples were taken in the Cretaceous deposits. On the basis of these logs the facies analysis and sequence stratigraphic interpretation was carried out. Selected samples were used for petrographical and geochemical studies.

Facies analysis showed that the Upper Cretaceous sediments were deposited in a terrestrial to marine setting. The examined sedimentary succession comprises ten environmental depositional facies, which can be grouped into four major facies associations. These four facies associations are (i) the shelf facies association, (ii) the shoreface facies association, (iii) the marginal marine facies association and (iv) the coastal plain facies association. The repeated interfingering of terrestrial and marine environments shows, that the examined sediments were deposited in a shallow marine siliciclastic to mixed siliciclastic-carbonate coastal system. The facies correlation of the logged sections reveals that the sedimentary succession can laterally be sub-divided into three major depositional systems: (i) a siliciclastic ramp, (ii) a mixed carbonate-siliciclastic ramp and (iii) an alluvial system. Vertically these depositional systems are arranged in repeating cyclothems. An ideal cyclothem consists of a retrograding siliciclastic ramp system, a mixed siliciclastic-carbonate ramp system, a prograding siliciclastic ramp system and is ended by an alluvial plain system.

The shelf system was generally wave/storm dominated, whilst the prograding siliciclastic ramp system was supply dominated. The retrograding siliciclastic ramp, as well as the mixed siliciclastic-carbonate ramp system was accommodation-dominated. The coastal system can be divided into a regressive and a transgressive system. Under regressive sea-level conditions sand dominated braid deltas formed. Transgressive sea-level conditions resulted in a coastal system controlled by wave dominated estuaries and barrier/lagoon complexes. On the coastal plain anastomosing to meandering sand dominated river systems with wide overbank areas developed during transgressive times. During regressive sea-level conditions the nearshore river system changed to a more braided one that was directly linked to the braid deltas forming during these intervals.

The sequence stratigraphic interpretation of the correlated sections shows that the studied sedimentary succession includes eight third-order sequences. The basal four sequences comprise the Cenomanian to Coniacian Ajlun Group, while the top four sequences are situated within the Coniacian to Santonian Belqa Group. Moreover sequences 1, 2 and 4 can each be further subdivided into two sequences of higher order. Basically all sequences include forced regressive deposits formed during the relative sea-level fall. Characteristic features of forced regressions, like for example sharp based shoreface deposits, are frequently present within the logged sections. Due to the significance of the regressive part of the relative sea-level for the studied sediment succession the sequence stratigraphic model introduced by Plint and Nummedal (2000) was used. This sequence stratigraphic model combines the complete sea-level fall in a new falling stage systems tract (FSST), which opposes LST, TST and HST.

Comparison of the sequence stratigraphic interpretation with the major depositional systems shows that the depositional systems correspond very well with the four systems tracts of the applied sequence stratigraphic model. The alluvial plain system developed during the LST, the retrograding siliciclastic ramp system during the TST. The mixed carbonate-siliciclastic ramp system corresponds to the HST and the prograding siliciclastic ramp system is associated with the FSST. Relative sea-level changes and sediment supply were the main controlling parameters for the sequence architecture of the examined deposits. Since subsidence was low and no synsedimentary tectonic influenced the examined sediments, the relative sea-level changes are basically eustacy driven. Therefore the reconstructed sea-level curve resembles strongly global curves. The siliciclastic sediment supply is related to sea-level changes and associated with back stepping fluvial incision during the FSST and LST.

Light mineral analysis shows that the Cretaceous sands and sandstones of South Jordan are basically mineralogical mature and can be classified as quartz arenites. Only the fine to medium grained sands and sandstones of the study area exhibit a slightly higher content of feldspar, classifying them as subarkoses. Heavy mineral analysis reveals a dominance of the ultrastable heavy minerals zircon, tourmaline and rutile. Especially zircon is predominant in the examined samples. With a mean ZTR-index of 97.9, the heavy mineral content reflects the mineralogical maturity of the sediments shown by the light mineral analysis.

The studied sands and sandstones experienced a rather restricted spectrum of diagenetic processes. The compaction of the sediments was low to moderate, which is for example reflected by high IGV values. This and the lack of destructive grain contacts and pressure solution indicate that the sediments did not encounter deep burial or thick overburden. Concerning the cementation of the examined sediments, the sandstones display three major cementing phases. Sandstones cemented by clay minerals are only weakly lithified and display the highest intergranular porosities of all samples. Sandstones cemented by carbonate minerals (calcite and dolomite) or iron-oxides are well lithified and usually display only low values of intergranular porosities. The cementation with carbonate minerals is facies dependant and only occurs in marine sediments.

Both, petrographic and geochemical provenance analysis point to the deposition of the Cretaceous sandstones of South Jordan within a passive continental margin setting. As source rock for the studied samples a continental block and/or a craton interior is most likely. Furthermore, a clear trend towards a recycled sedimentary source is obvious in the petrographical as well as in the geochemical studies. Especially the presence of resedimented quartz grains and the enrichment of zircon in the sediments support this. The presented study shows that the Arabo-Nubian-Shield and its Palaeozoic sedimentary cover are the source area for the Cretaceous siliciclastic sediments of South Jordan.

The examined sediments follow normal weathering trends in the weathering diagrams. The corresponding CIA values point to a moderate weathering for most samples. Only the sandstone and some claystone samples have high CIA values typical of recycled sediments.

Acknowledgments/Danksagung

Die vorliegende Dissertation entstand auf Anregung von Frau PD Dr. **H. Krawinkel** am Institut für Geologie und Paläontologie der Universität Stuttgart. Frau **Krawinkel** danke herzlich ich für das entgegengebrachte Vertrauen, die Betreuung, die stete Diskussionsbereitschaft, die Möglichkeit auch in der Lehre Erfahrung sammeln zu dürfen sowie für die generelle Unterstützung während der Arbeit. Bei Herrn Prof. Dr. **H. Seyfried** möchte ich mich besonders für die Übernahme des Korreferates und sein offene Hilfsbereitschaft während der Arbeit bedanken.

Bei meinem Kollegen **Roman Berndt** vom Paläontologischen Institut der Universität Würzburg bedanke ich mich für die gute Zusammenarbeit während des Projektes und speziell bei der Geländearbeit in Jordanien. Den Herren Prof. Dr. **F. Th. Fürsich** (Würzburg), Prof. Dr. **N. Schmidt-Kittler** (Mainz), Dr. **Z. Lewy** (Geological Survey Israel), Prof. Dr. **J. Kuss** (Bremen) und **Frauke Schulze** (Bremen) sei an dieser Stelle für die Diskussion, Zusammenarbeit und die Hilfe bei verschiedenen Aspekten des Projektes gedankt. Das Projekt und die vorliegende Arbeit wurde von der Deutschen Forschungsgemeinschaft (**DFG**) gefördert (Kr 1666/3-1 & 3-3), der ich an dieser Stelle dafür danken möchte.

At this place I would like to thank the **Natural Resources Authority (NRA)** in Amman for the perfect logistic support during field work in Jordan. Without the help of the NRA and especially of the **Mapping** and the **Subsurface divisions**, fieldwork would not have been possible. Furthermore I want to thank the NRA colleagues **K. Moumani**, **H. Abu Azzam**, **M. Al'Bashish** and **A. Gharaibeh**. Their willingness to aid the fieldwork and to discuss the results contributed to the presented study. Furthermore they sacrificed a lot of spare time to accompany us to the field in the Batn El Ghul area. Batn El Ghul, "belly of the beast", is for sure a suiting name for such a 'lovely' desert place in the middle of nowhere.

I also thank the many drivers of the NRA, who brought us safely through the desert and the highways of Jordan, as well as the cooks, who managed to keep the whole group happy with local specialties when we came back from the field.

Bei Herrn Prof. Dr. **W.D. Blümel** bedanke ich mich für die großzügige Bereitstellung des Labors im Geographischen Institut der Universität Stuttgart. Herrn **J. Stettler** gilt mein Dank insbesondere für die Hilfe bei der labortechnischen Schwermineralaufbereitung. Bei Herrn **Ch. Wimmer** und Herrn **E. Wilhelm** bedanke ich mich für die Herstellung der Dünnschliffe. Für die RFA-Messungen und die Nutzung der Probenaufbereitung am Institut für Geowissenschaften der Universität Mainz bedanke ich mich recht herzlich bei Herrn Dr. **B. Schulz-Dobrick** und Frau **N. Grosschopf**. Für die Labornutzung und die XRD- sowie RFA-Analysen am Institut für Bodenkunde der Universität Hohenheim bedanke ich mich bei Prof. Dr. **K. Stahr** und besonders bei **D. Frobel** für die Messungen und die Hilfe während der Aufbereitung. Bei Herrn Dr. **K. Wemmer** vom Geowissenschaftlichen Zentrum der Universität Göttingen bedanke ich mich für die K-Ar-Datierung der Glaukonitproben. Herrn Prof. **H.-J. Masonne** vom Institut für Mineralogie und Kristallchemie der Universität Stuttgart, danke ich für die Bereitstellung der mechanischen Aufbereitungsmöglichkeiten (Scheibenschwingmühle, Magnettrennung) sowie für die Möglichkeit Kohlenstoffgehalts-(LECO) und XRD-Analysen durchführen zu können. Herrn Dr. **T. Theye** gilt hier mein Dank für die geduldige Einführung und Hilfe an diesen Geräten. Meiner Studienkollegin **Lydia Hufmann** möchte ich für viele informative Gespräche und Diskussionen, sowie die Hilfe im Mineralogischen Institut Stuttgart danken.

Für die Betreuung und die Einführung am LA-ICP-MS am Geowissenschaftlichen Institut der Universität Jena bedanke ich mich recht herzlich bei Dr. **D. Mertens**. Bei allen

Angehörigen des Instituts für Geologie und Paläontologie der Universität Stuttgart möchte ich mich für ihre Unterstützung und Hilfsbereitschaft bedanken. Weiterhin bedanke ich mich bei den Mitarbeitern und Gästen des **German Protestant Institute of Archaeology**, Amman für die angenehme und familiäre Unterkunft vor und nach unseren Geländearbeiten.

Besonders möchte ich mich an dieser Stelle bei der gesamten Arbeitsgruppe „Krawinkel“ bedanken. In vielen lustigen sowie ernsten Arbeits-, Diskussions-, Feier- und Reisetunden kam es stets zu einem wertvollen Gedankenaustausch von dem die vorliegende Arbeit profitiert hat. Ein außerordentlicher Dank gilt meinen Kollegen und Freunden **Steffen Kutterolf** und **Rüdiger Diener**. Ohne ihre stete Hilfs- und Diskussionsbereitschaft wäre so manches nicht möglich oder zu schaffen gewesen. **Margret Mohs** danke ich für die Hilfe im Gelände. **Alexander Wöhrle** danke ich für die gute Zusammenarbeit während seiner Diplomarbeit, die eine wertvolle Hilfe für diese Dissertation war. Meinem Freund und Kollegen **Cédric John** sei an dieser Stelle für vergnügliche Mittagspausen mit anregenden Diskussionen über Geologie und die Welt gedankt.

Meiner Familie möchte ich einen außerordentlich herzlichen Dank aussprechen. Ohne das Vertrauen und die stete, vielseitige Unterstützung meiner Mutter, **Gabriele Baaske**, meiner Großeltern **Lina** und **Heinrich Heblich** sowie meiner Tante **Hiltrud Heblich** wäre mein Studium und die vorliegende Arbeit nicht möglich gewesen.

Mein größter Dank gebührt meiner Frau und Mitdotorandin **Andrea Knörich** für die Hilfe im Gelände und im Labor, für die vielen Stunden Gespräch über Geologie, das Leben und den ganzen Rest, das erste Durchsehen der Arbeit, das Durchstehen von schwarzen Momenten, das entgegengebrachte Verständnis und vieles, vieles mehr. Danke!

Contents

Zusammenfassung

Abstract

Acknowledgements/Danksagung

1. Introduction	1
1.1 Aim of the study.....	1
1.2 Geographic overview.....	1
1.3 Study area	2
1.4 Previous works.....	3
2. Geological setting.....	5
2.1 General geologic overview	5
2.2 The Pre-Cretaceous geology of Jordan	6
2.3 Cretaceous stratigraphy of Jordan.....	7
2.3.1 Kurnub Group	9
2.3.2 Ajlun Group.....	10
2.3.3 Belqa Group	13
2.3.4 Batn El Ghul Group.....	14
2.4 Post-Cretaceous geology and landscape evolution of the study area.....	15
2.5 Cretaceous palaeogeography of Jordan and global sea-level.....	16
2.6 Cretaceous palaeoclimate	17

Part 1: Facies analysis and sequence stratigraphy of the Upper Cretaceous sediments of South Jordan

3. Facies analysis.....	20
3.1 Methods	20
3.1.1 Lithofacies types	20
3.2 Description and interpretation of sedimentary environmental facies.....	22
3.2.1 Shelf facies association	23
3.2.2 Shoreface facies association.....	28
3.2.3 Marginal marine facies association	30
3.2.4 Coastal plain facies association.....	34
3.3 Lateral and vertical arrangement of depositional system	35
3.3.1 Siliciclastic ramp system.....	35
3.3.2 Mixed carbonate-siliciclastic ramp system	35
3.3.3 Alluvial system.....	36
3.4 Characteristics of the mid-Cretaceous shelf system of South Jordan	37
3.4.1 Storm dominated shelf vs. tide dominated shelf, tidal regime	37
3.4.2 Supply dominated shelf vs. accommodation dominated shelf regime and cyclothems.....	37

3.5 Fluvial styles and facies models for the mid to Late Cretaceous of South Jordan.....	38
3.5.1 Fluvial styles on the coastal plain	38
3.5.2 Fluvial architectural-element analysis within the mid Wadi As Sir Formation.	38
3.5.3 The coastal system	41
3.6 Red sediment colours, ferribands, colour mottling and pedogenic features.....	43
3.6.1 Red sediment colours	43
3.6.2 Ferribands.....	44
3.6.3 Colour mottling and pedogenic features	44
3.7 Summary of the sedimentological features	46
4. Sequence stratigraphy.....	48
4.1 Definitions and key concepts	48
4.2 Sequence stratigraphy of the study area	50
4.2.1 Stratigraphic correlation of the logged sections	50
4.2.2 Sequences	53
4.2.3 Parasequences.....	53
4.2.4 Forced regressions.....	54
4.3 Facies, depositional systems and their relationship to the sequence stratigraphy of the study area	57
4.4 Parameters controlling the sequence architecture.....	63
4.5 Sequence stratigraphic results compared to forward stratigraphic computer models	65
4.6 Summary of the sequence stratigraphy of the mid to Upper Cretaceous deposits of South Jordan.....	67

Part 2: Petrography, geochemistry and provenance of the Upper Cretaceous sediments of South Jordan

5. Sedimentary petrography.....	69
5.1 Light mineral analysis.....	69
5.1.1 Methods	69
5.1.2 Analytical precision.....	70
5.1.3 Petrographic overview of the Upper Cretaceous sands and sandstones of South Jordan	70
5.1.4 Granulometry	73
5.1.5 Sandstone diagenesis.....	76
5.1.6 Rock classification	78
5.2 Heavy mineral analysis	78
5.2.1 Methods	78
5.2.2 Analytical precision.....	79
5.2.3 Controlling factors of the heavy mineral association.....	79
5.2.4 Description of the heavy minerals.....	80
5.2.5 The ZTR-index	82
5.2.6 Hierarchical cluster analysis of the ZTR-data.....	84

5.3 Provenance of the Upper Cretaceous siliciclastic sediments of South Jordan	85
5.3.1 Light mineral analysis	85
5.3.2 Heavy mineral analysis	88
5.4 Discussion and conclusion of the sedimentary petrography	89
6. Bulk rock geochemistry	92
6.1 Introduction	92
6.1.1 Analytical methods.....	92
6.1.2 Analytical precision.....	93
6.1.3. Controlling factors of the bulk rock geochemistry.....	94
6.2 Major elements	94
6.2.1 Sediment classification.....	96
6.2.2 Chemical index of alteration and weathering trends.....	97
6.2.3 Provenance	100
6.2.4 Hierarchical cluster analysis of the major elements.....	101
6.3 Rare earth (REE) and trace elements	104
6.3.1 Rare earth element geochemistry	104
6.3.2 Provenance derived from trace elements	106
6.4 Multi element plots	108
6.5 Discussion and conclusion of the bulk rock geochemistry	110
7. Summary and conclusion	113
7.1 Part 1: Facies analysis and sequence stratigraphic results	113
7.1.1 Marine depositional environments and sequence stratigraphy	113
7.1.2 Terrestrial deposits	115
7.1.3 Controlling parameters of the stratigraphic/sequence architecture	116
7.2 Part 2: Petrographic and geochemical results	116
7.2.1 Sandstone petrography	116
7.2.2 Provenance	117
7.2.3 Diagenesis	118
7.3 Stratigraphic correlation of North/Central Jordan and South Jordan	119
7.4 Discussion of the mid to Late Cretaceous climatic conditions of the study area	120
8. References	122

Appendix I – Graphic logs and sample overview

Appendix II – Tables

Lebenslauf/Curriculum Vitae

1. Introduction

This thesis is part of a cooperation of the geological and palaeontological institutes of the German universities of Stuttgart, Würzburg and Mainz with the Natural Resources Authority (NRA) of Jordan. Aim of the cooperation was the analysis of a Cretaceous terrestrial to marine depositional setting in South Jordan with regards to sedimentological, sequence stratigraphical and palaeontological aspects. The study area in south Jordan provided good and numerous outcrops along a more than 80 km long escarpment. On the German side the cooperation was financed by the Deutsche Forschungsgemeinschaft (DFG).

The palaeontological and carbonate sedimentological aspects of the studied sediments are covered by the Ph.D. thesis of Roman Berndt (Berndt, 2002). Both, the presented work and the study of Roman Berndt are based on the same stratigraphical sections, which were logged during joined fieldwork with Jordanian colleagues from the NRA. Though separate works, both studies complement each other.

1.1 Aim of the study

Aim of the presented study was to establish a sequence stratigraphic framework for the Late Cretaceous (Cenomanian to Coniacian) deposits of south Jordan. Beyond that, it was proposed to improve the correlation of the established stratigraphy of north and central Jordan to south Jordan, where facies changes and clastic dominated lithologies hamper a well defined biostratigraphic correlation. In order to achieve these goals, several methods were applied, which will be presented in two parts:

Part 1

This part focuses on the sedimentology and sequence stratigraphy of the study area. The various facies associations, depositional environments and their sequence stratigraphic framework are investigated and the controlling factors of the sequence stratigraphy are discussed. Furthermore, in order to provide a timeframe for the predominantly siliciclastic sediments, K-Ar dating on glaucony was performed.

Part 2

Part 2 provides additional petrographical and geochemical studies of the Cretaceous clastic sediments. The gathered information was used for sediment classification, provenance analysis and for palaeo-climatological aspects. The results provide information on possible changes in the hinterland/source area, which influence the stratigraphic architecture of the deposits.

1.2 Geographic overview

The Hashemite Kingdom of Jordan, “Al Mamlakah al Urduniyah al Hashimiyah” (conventional short form: Jordan), is situated between latitudes 29°30’ and 33°30’ N and longitudes 35° and 39° E of Gr. in the northern part of the Arabian peninsula (Fig. 1.1). Amman, the “White City” situated in the north-west is the largest city and capital of the country. With its 88.946 km², Jordan is slightly larger than Austria. Major rivers are the perennial Jordan and Yarmuk rivers in north Jordan, which are very important for the water supply of the country. With -408 m below sea-level (Bender, 1974), the Dead Sea is the lowest point of Jordan, and actual of the world. The highest point is the Jabal Ram with 1754 m above sea-level (Osborn, 1985).



Figure 1.1 Position of Jordan in the region.

Jordan is located in the arid subtropical zone (Alsharhan and Nairn, 1997) and has a subdivided climatic regime. In the north-west the climate is Mediterranean influenced with precipitation of more than 300 mm per year (Bender, 1968; 1974). The southern and eastern parts of Jordan are arid desert regions, with yearly precipitation below 50 mm, and cover wide areas of the country.

The term “south Jordan” is used for the area south of the small city Ras En Naqb (cf. Bender, 1963 and Fig. 1.3). This area is part of the arid southern desert region of Jordan with scarce, partly steppe like, vegetation. The major economical centres in the south are Ma’an, with its university, government agencies and a glass factory, and the E’Shedia phosphate mine, where Upper Cretaceous to Tertiary phosphates (Abed and

Kraishan, 1991; Abed and Amireh, 1999) are exploited.

1.3 Study area

The study area (Figs. 1.2 and 1.3) is located in South Jordan about 75 km north-east of the seaport Aqaba (N 29°31’55”, E 35°00’44”) and about 60 km south of the governorate city Ma’an (N 30°11’38”, E 35°44’09”). Base during field work was the NRA (Natural Resources Authority) field station close to Batn El Ghul (BEG, N 29°45’25”, E 35°55’06”), approximately in the centre of the study area.

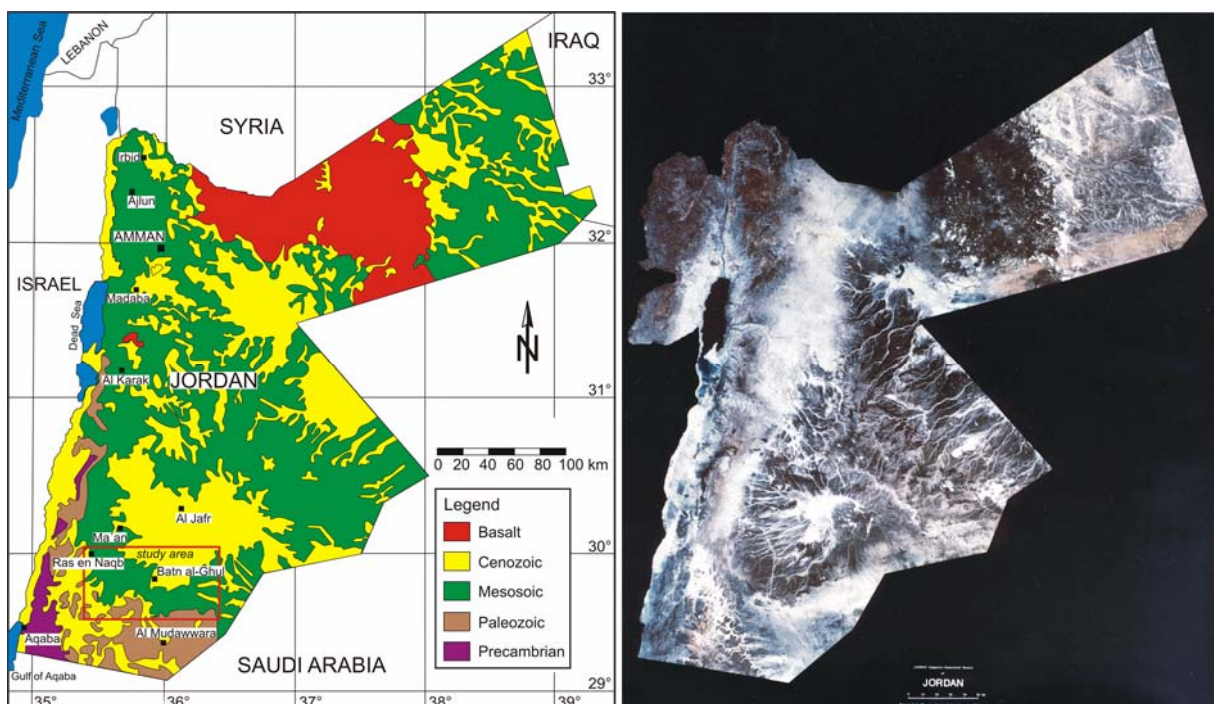


Figure 1.2 General geological overview of Jordan in comparison to a satellite image of the country. Features like the basaltic province in north Jordan and the Palaeozoic/Precambrian rocks in south Jordan are recognizable on the satellite image (Geological Map of Jordan redrawn from a map provided by the Royal Jordanian Geographic Centre www.rjgc.gov.jo/maps/geology.html; satellite image courtesy of the Natural Resources Authority, Amman, Jordan).

The presented study concentrates on outcrops along the Naqb escarpment trending NW-SE to E from Ras En Naqb (REN, N 30°00'14", E 35°29'30") in the west to Naqb Ataik (N 29°48'11", E 36°23'02") in the east. The crow-fly distance from Ras En Naqb to Naqb Ataik is 89 km. Along the up to 300-400 m high escarpment several vertical sections (sections 4 to 15) were logged in detail, further three sections (sections 1-3) were logged along the escarpment between Ras En Naqb to Petra (N 30°18'55", E 35°28'44") (Fig. 1.3). A log of a water well (courtesy of the Jordan phosphate mining company), located at the phosphate mine of E'Shedia (N 29°56'07", E 36°08'29") about 40 km south of Ma'an (Fig. 1.3), was also considered in the study. South of the Naqb escarpment an inselberg landscape, which developed in the late Cenozoic (Osborn, 1985), offers further possibilities to study Palaeozoic and Cretaceous outcrops.

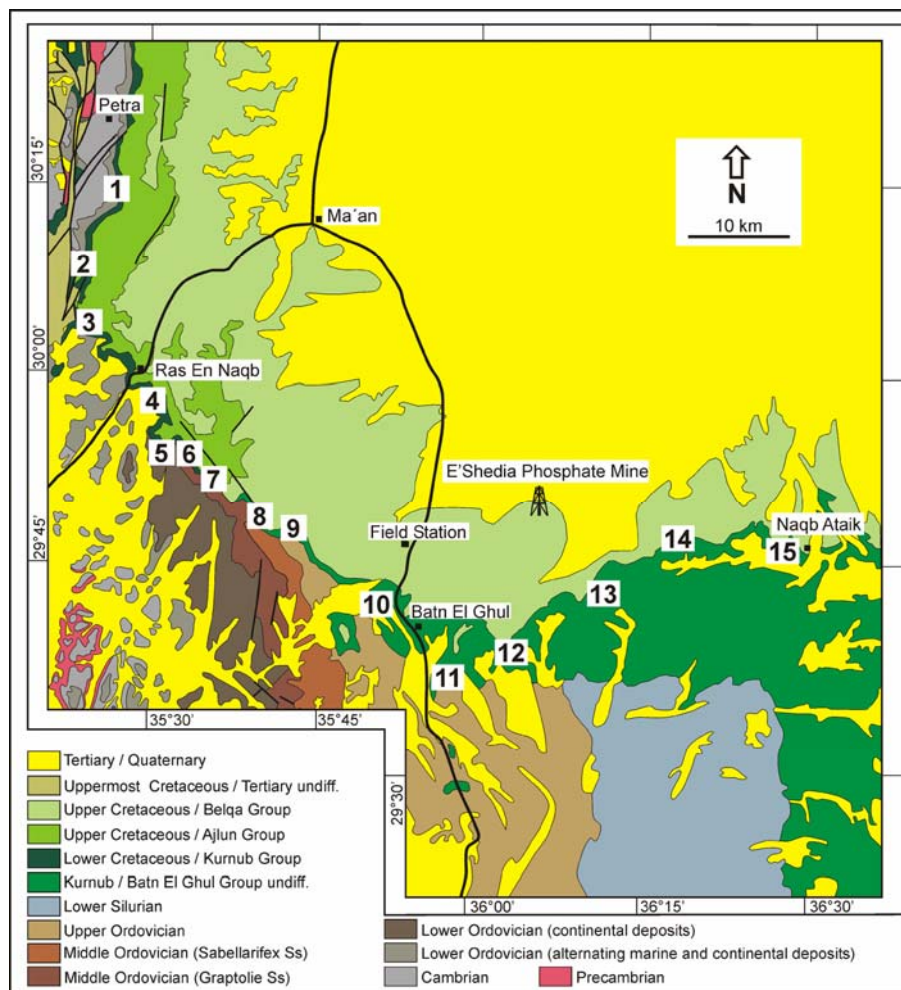


Figure 1.3 Geological overview of the study area (modified from Bender et al., 1968). The numbers represent the positions of the logged sections.

1.4 Previous works

An overview of the geology of Jordan is given in the book "Geology of Jordan" by Bender (1974), which is based on the German edition of 1968 (Bender, 1968). The evolution of the landscape of south Jordan was studied by Osborn (1985). Summaries concerning stratigraphy, sedimentology, sequence stratigraphy and hydrocarbon aspects of the Middle East region can be found in Beydoun (1988; 1995), Alsharhan and Nairn (1997) and Sharland et al. (2001). The papers of Lovelock (1984), Bowen and Jux (1987), Chaimov et al. (1992), Nasir and Safarjalani (2000) and Le Nindre et al. (2003) cover tectonic aspects of the region. The Palaeozoic sediments of Jordan are covered in Bender (1963), Bender and Mädler (1969),

Parker (1970), Amireh (1987; 1991; 1993a; 1993b), Makhlof (1998) and several Bulletins of the Natural Resources Authority in Amman (e.g. Teimeh et al., 1990 among others).

In general numerous bulletins and internal reports of the Natural Resources Authority (NRA) in Amman provide invaluable information, which is true also for the geological maps of Jordan published by the NRA. Besides the map of Bender et al. (1968) the following NRA maps were used during the fieldwork: Ibrahim (1987), Rashdan (1987), and Masri (1991; 1992; 1998).

Information on the Cretaceous stratigraphy of Jordan, including Kurnub, Ajlun and Belqa Groups, can be found in Quenell (1951), Masri (1963), Powell (1989), Andrews (1992), Makhlof et al. (1996) and Powell et al. (1996). Especially the publications of Powell are a valuable source for further references. Studies considering the petrography and K-Ar ages of glauconies from the Cretaceous strata of Jordan were presented by Abed and Mansour (1982) and Amireh et al. (1998). Cretaceous fossils of Jordan are considered in Bandel and Geys (1984) and Aqrabawi (1993). Aspects of the Kurnub Formation in Jordan are covered in publications of Bender and Mädler (1969), Abed (1978), Bandel and Vávra (1981), Abed (1982a), Houry (1986), Amireh (1987; 1991; 1992; 1993b), Nasir and Sadeddin (1989), Abu Saad and Al Bashish (1996), Amireh (1997), Amireh et al. (1998), Amireh and Abed (1999) and Amireh (2000). The nodular limestone of the Naur Formation is dealt with in Abed and Schneider (1980; 1982), while local tectonics of the Lower Cenomanian are covered in the paper of Abed (1984). Abed and El-Hiyari (1986) discuss depositional variations within the Shuayb Formation. Microfacies and depositional environment of the Wadi As Sir limestones have been studied by Abed (1982b). Studies dealing with the Amman Formation include publications of Abed and Kraishan (1991), Abed and Sadaqah (1998), Abed and Amireh (1999), Abu Saad and Al Bashish (1999). Mustafa (2000) and Moumani et al. (2001) cover palaeontological aspects of the Wadi Umm Ghudran Formation, while the thesis of Mohs (2001) deals with its sedimentological aspects. Deposits and palaeobotany of the Batn El Ghul Group are dealt with in Bender and Mädler (1969).

Works regarding the Cretaceous deposits of the surrounding areas, especially Israel and Egypt, were published by Singer (1975), Steinitz (1981), Weissbrod and Nachmias (1986), Lewy (1990), Kuss and Conrad (1991), Kuss (1992), Sandler (1996), Lüning et al. (1998a; 1998b), Abd Elwahab (1999), Buchbinder et al. (2000a; 2000b), Ibrahim (2000), Kuss et al. (2000), Lewy et al. (2000), and Salem et al. (2001) among many others.

2. Geological setting

Since the focus of the presented study is on the Late Cretaceous deposits of South Jordan, the general geologic overview will be considered only briefly. For more detailed information the reader is advised to refer to the works of Bender (1963; 1968; 1974) and the numerous publications of the Natural Resources Authority of Jordan (NRA) in Amman (e.g. Teimeh et al., 1990; Masri, 1992 among many others).

2.1 General geologic overview

Jordan is situated on the northern part of the Arabian Plate (Alsharhan and Nairn, 1997) and comprises Precambrian to Cenozoic rocks (Fig. 1.2). The Precambrian and Palaeozoic units are only exposed in South Jordan and in small parts along the Wadi Araba-Dead Sea-Rift. They are unconformably overlain by Mesozoic sediments, covering large areas. Cenozoic sedimentary deposits are exposed all over Jordan. Areas of special interest are the Jafr basin and the Azraq basin where thick clastic sediments were deposited during the Tertiary and Quaternary (Bender, 1968; 1974). A Neogene and Quaternary sheet basalt province covers large areas of the northern desert of Jordan (Bender, 1968; 1974).

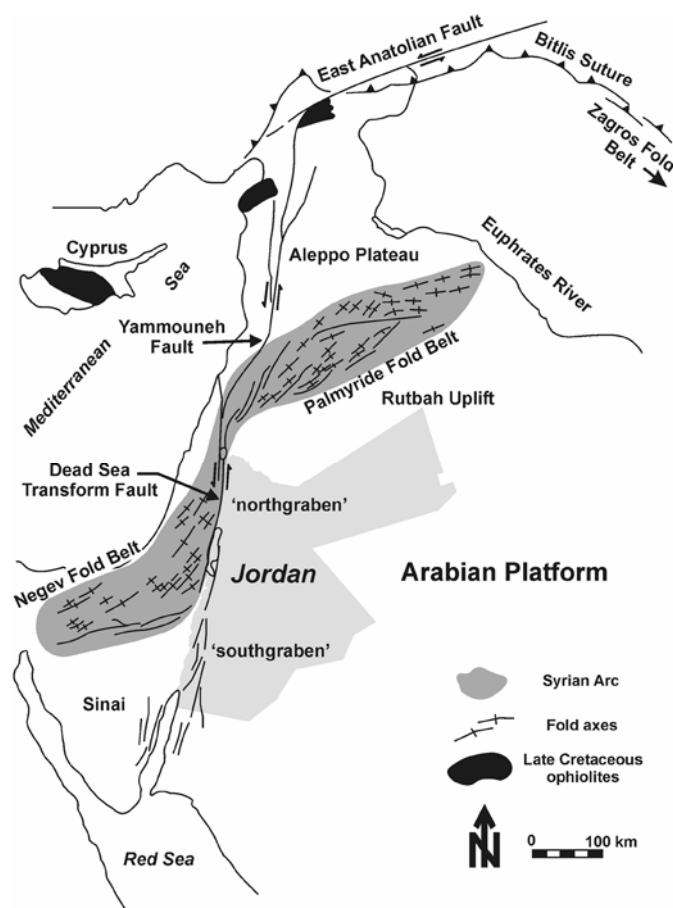


Figure 2.1 Generalized tectonic map of the north-western Arabian plate (modified from Chaimov et al., 1992).

system is still active, though the current slip-rate is less than half that of the Pliocene-Pleistocene movement (Lovelock, 1984). The rift system is filled by sediments of mid-Miocene to recent age (Andrews, 1992).

Major tectonic elements

The N-S/NNE-SSW trending Wadi Araba-Dead Sea-Rift (Bender, 1968; 1974) is the major tectonic structure in Jordan and the most important structural element in the region (Lovelock, 1984). With a length of 360 km and a varying width of 5 to 20 km, it is part of the 6000 km long East African-North Syrian fault system (Bender, 1968; 1974). It can be divided into a “southgraben”, reaching from Aqaba to the Dead Sea, and a “northgraben”, from the Dead Sea to the Lake of Tiberias (Fig. 2.1). Generally this fault system is a left-lateral (sinistral) transform fault as well as a sequence of en echelon faults whose movements have opened a number of rift troughs (Alsharhan and Nairn, 1997). The most important of these troughs are the Dead Sea and the Gulf of Aqaba. The lateral displacement, starting at the Gulf of Aqaba, amounts up to 105 km (Alsharhan and Nairn, 1997). The maximum activities of the fault system occurred during the late Miocene/Pliocene to Pleistocene, and were related to the opening phases of the Red Sea (Andrews, 1992). Today the fault

The second major tectonic element is the Syrian Arc (Fig. 2.1), an intraplate fold-thrust belt which extends from the central Sinai through Israel northward to central Syria (Chaimov et al., 1992). At least the northern part of the Syrian Arc, the Palmyride Fold Belt, started as a basin during the Jurassic, created by the opening of the Neo-Tethys (Chaimov et al., 1992). Active rifting occurred during the Early Cretaceous, leading to the formation of normal faults. The collision of the Arabian Plate with an island arc (Moore et al., 1984) or the initial closing of the Neotethys (Rigo De Righi and Cortesini, 1964) during the Late Cretaceous, conducted a compressional regime leading to the inversion of the fault system. During that time the initial folding of the Syrian Arc began and is well developed in the Negev Fold Belt on the Palestine-Sinai sub-plate (Powell et al., 1996). Basin and swell structures and compressive folds east of the Dead Sea-Rift near Amman are related to the Syrian Arc (Powell, 1989; Powell et al., 1996). The main tectonic phase of the Syrian arc occurred during the Eocene to Miocene, and continues today (Chaimov et al., 1992).

2.2 The Pre-Cretaceous geology of Jordan

The Pre-Cretaceous geology of the study area comprises the crystalline basement and its sedimentary cover. The Precambrian basement of South Jordan is part of the Arabian-Nubian shield (Petters, 1991) and includes various granites, diorites, pegmatites, aplites, rhyolites and metamorphic rocks (Bender, 1963; 1968; 1974). It is also in South Jordan where plutonic rocks are intruded by a vast number of intermediate to basic dykes, which can be observed e.g. in the Wadi Rum and along the Ras En Naqb-Aqaba highway. Above an angular unconformity, the so called 'Pre-Saq Unconformity' (Sharland et al., 2001), the Precambrian Basement is overlain by Palaeozoic clastic sediments (Bender, 1963; 1968; Bender and Mädlar, 1969; Bender, 1974). At the basement-sediment contact signs of peneplanation of the basement, e.g. levelled or filled Precambrian relief (Bender, 1963), are visible. Large outcrops, depicting the basement and the Cambrian sedimentary cover, can be found in the Wadi Rum area in South Jordan (Fig. 2.2).



Figure 2.2: Precambrian basement and parts of the Palaeozoic sedimentary cover at Wadi Rum. The Umm Ishrin and Salib formations are of Cambrian age, the Disi Formation of Late Cambrian to Early Ordovician age (Teimeh et al., 1990). The one-story houses in the foreground are outskirts of the Rum settlement. The whole outcrop is approximately 350-400 m high.

The 1600 m thick (Bender, 1974) sedimentary cover consists of Cambrian, Ordovician, Early Silurian, uppermost Permian, Triassic, Jurassic and Early Cretaceous rocks (Amireh, 1991). Dipping to the east (Bender, 1974), the Palaeozoic succession starts with Cambrian and Early Ordovician sediments in the West (e.g. Wadi Rum area). Progressively younger Palaeozoic sediments follow eastwards, ending with Silurian deposits in the Naqb Ataik area (Fig. 1.3). Deposits of Devonian, Carboniferous and Permian age are not exposed in Jordan but are present in the region, e.g. in Syria and NW-Saudi Arabia, pointing to an erosive event in Jordan. Triassic and Jurassic deposits are present in North and Central Jordan, but wedge out to the S/SE. Along the Naqb escarpment Lower Cretaceous sandstones of the Kurnub Group overlay the Palaeozoic sediments after a slight angular unconformity (Bender, 1963) created by uplift and erosion during the Jurassic (Bender, 1968; 1974; Amireh, 1997; 2000).

2.3 Cretaceous stratigraphy of Jordan

The Cretaceous deposits of Jordan are subdivided into three lithostratigraphical groups: the Kurnub Group, the Ajlun Group and the Belqa Group (Fig.2.3). The groups are separated from each other by regional unconformities (Powell, 1989; Powell et al., 1996). An overview of the stratigraphy of the single groups, including stratigraphic names and their synonyms, is given by Powell (1989) and Makhlof et al. (1996). The following paragraphs will give a short review of the Kurnub, Ajlun and Belqa groups with special regard to southern Jordan (Fig. 2.4A & B). The thickness of the single Formations/Groups in the studied sections can be found in table 2.1.

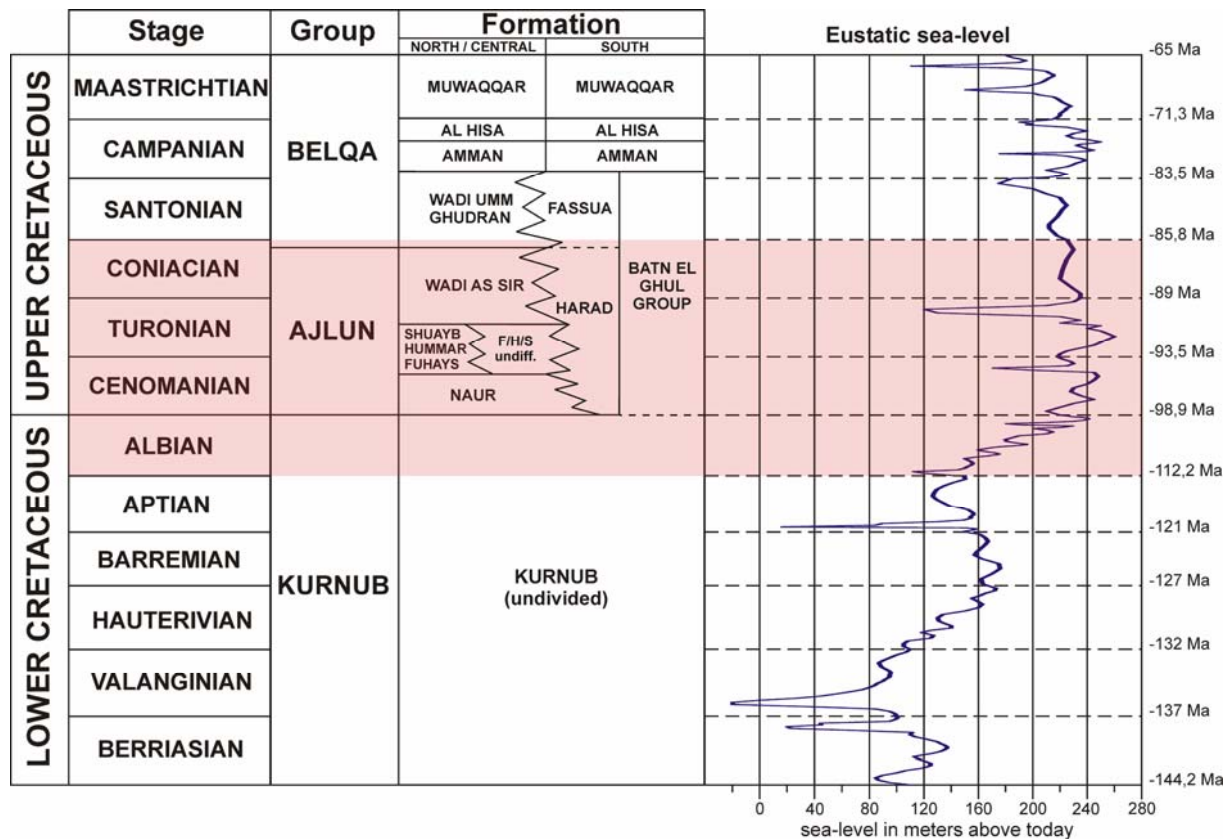


Figure 2.3: Stratigraphic table of the Cretaceous era in Jordan with regard to the different formations of North/Central and South Jordan (based on Powell, 1989). Also shown are the corresponding eustatic sea-level (Hardenbol et al., 1998) and the ages of the stage boundaries (Gradstein et al., 1995). The shaded area represents the studied time interval.

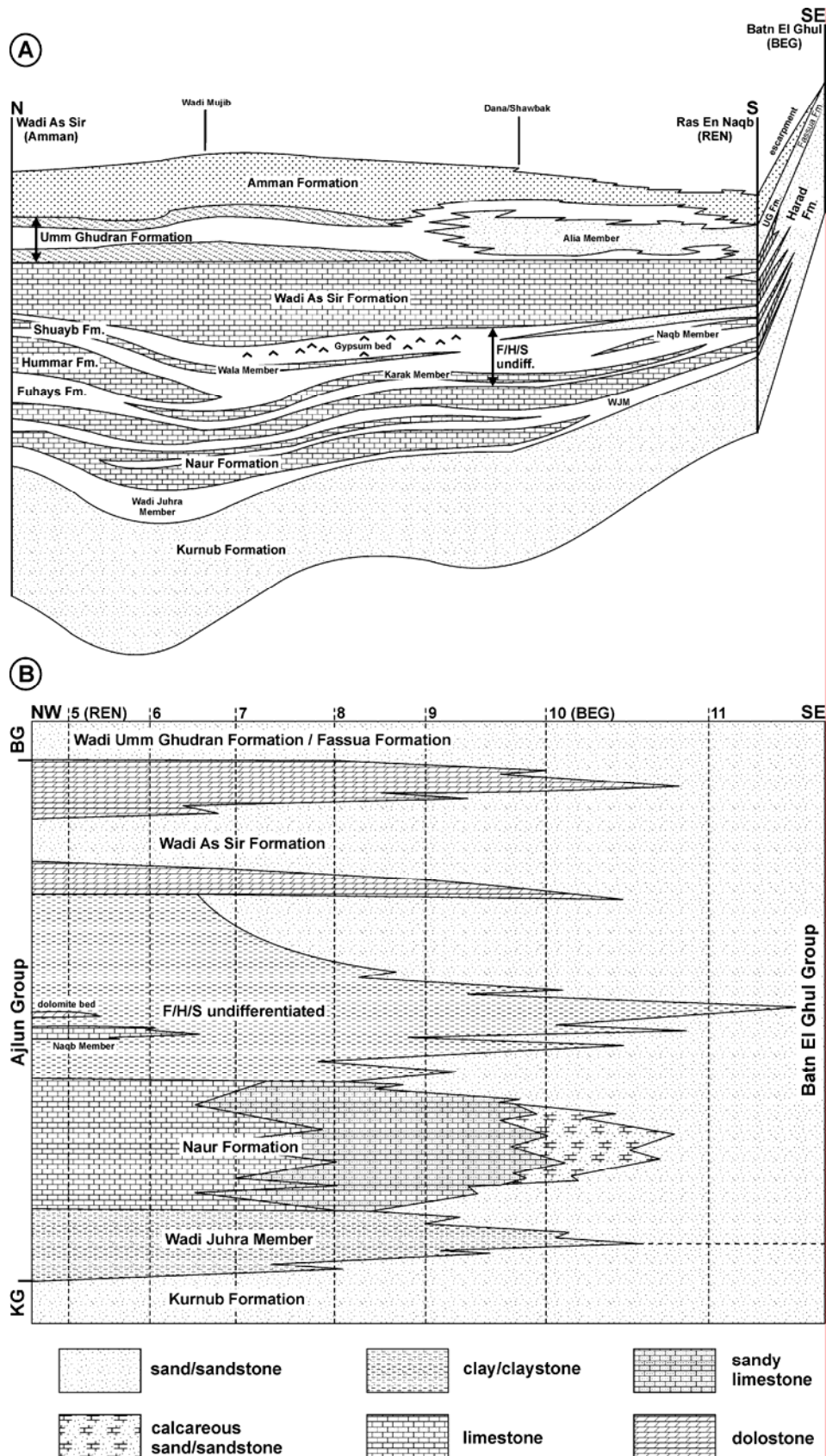


Figure 2.4 **A**) Schematic facies distribution of the Ajlun and Belqa groups along the Rift margins and the Naqb escarpment (modified after Powell, 1989). **B**) Schematic facies distribution of the Ajlun and Batn El Ghul groups along the Naqb escarpment based on the presented study (modified after Berndt, 2002). The stippled vertical lines represent the position of the logged sections (KG = Kurnub Group, BG = Belqa Group, WJM = Wadi Juhra Member).

Table 2.1 Thickness (in metres) of the Ajlun and lower Belqa Group formations in the logged sections.

Formation	Section									
	1	2	3	4	5	6	7	8	9	10
Umm Ghudran Formation							60*	80	77*	81
Wadi As Sir Formation					54.5	59.5	71	63.5	55	54.5
F/H/S undifferentiated					64	59	56	52	60.5	57
Naur Formation					20	22	16.5*	10.5	9	4.5
Naur Member B to D	14	13.5	13.5	17	14	12	10	2.5	5	?
Wadi Juhra Member					6	10	6.5	8	4	?
Kurnub Group/Formation					61.5	49		20	25	13.5

*these thicknesses represent minimum thicknesses

Though the formation names within the Cretaceous of Jordan, based on Masri (1963), are well established by the Jordan 1:50,000 Mapping Project (e.g. Powell, 1989), there are minor discrepancies in the choice of formation names. All formations bear geographical names, but most of them, such as the Naur Limestone Formation and Wadi As Sir Limestone Formation, also carry lithologic information. This might lead to misunderstandings, since the lithology of these units in South Jordan differs from the lithology in North/Central Jordan, where the formation names were usually established. The Wadi As Sir Limestone Formation in South Jordan for example, is dominated by clastic material, not by limestone which the name implies. Therefore in this study the formation names will be used **without** lithological reference as in Abed and Sadaqah (1998), following the suggestions of the International Stratigraphic Guide (Salvador, 1994) and Miall (1999; 2000) to avoid potential misinterpretations.

2.3.1 Kurnub Group (Berriasian? to Albian)

The Kurnub Group (Figs. 2.3 and 2.4) represents the complete(?) Lower Cretaceous succession in Jordan and neighbouring countries (Andrews, 1992). It comprises the “massive white sandstone unit” and the overlying “variegated sandstone unit” of Bender (1968; 1974), the later Aarda and Subeihi formations of Parker (1970). Later Amireh (1993a) proved that in some locations parts of the “massive white sandstone unit” belong to the Ordovician Disi Formation, and not to the Kurnub Group.

The white to reddish, medium to coarse grained sandstones of the Kurnub Group are approximately 200-450 m thick, thickening towards Northwest Jordan (Powell et al., 1996). In Jordan they unconformably overlie Lower Palaeozoic, Permian, Triassic and Jurassic strata (Andrews, 1992). In South Jordan, along the Naqb escarpment, the Kurnub Group unconformably overlies Palaeozoic sediments of Cambrian to Silurian age (Bender and Mädler, 1969; Powell, 1989) and youngs diachronously south-eastward (Powell et al., 1996). The reason for the unconformity is the uplift and erosion of the Palaeozoic sedimentary succession during the Late Jurassic (Bender, 1968; 1974; Amireh, 1997; 2000).

The Kurnub Group is subdivided into three regressive-transgressive depositional sequences (Amireh, 1997; Amireh and Abed, 1999), which are dominated by fluvial deposits with rare marine and paralic intercalations in Central and North Jordan (Abed, 1978; 1982a; Khoury, 1986; Powell et al., 1996; Amireh, 1997; 2000). In general the Kurnub Group shows an upward trend from a braided, low-sinuosity alluvial plain to a high-sinuosity alluvial plain, which is attributed to an overall transgressive sea-level (Powell et al., 1996). The general palaeoflow direction of the river system was north to North-West (Powell et al., 1996; Amireh, 2000) towards the Palaeo-Tethys coast (Fig. 2.8).

Based on facies interpretations Amireh (1997) presented a subdivision of the Kurnub Group for North Jordan, separating the group into the fluvial Ramel, the marine to terrestrial Jarash and the marginal marine/marine Bir Fa'as formations. Later he introduced a similar subdivision for Central and South Jordan (Amireh, 2000). Here the lower two, entirely fluvial

formations are called Karak and Hammamat, which are followed again by the marginal marine to marine Bir Fa'as Formation.

At least in South Jordan the stratigraphic position of Amireh's marine dominated Bir Fa'as Formation is an object of discussion. This is supported by Amireh and Abed (1999), who stated that the Kurnub Group of South Jordan is entirely fluvial. Amireh et al. (1998) presented K-Ar dates from glauconies taken from a dolomitic bed in the uppermost Kurnub Group, which is, according to Amireh (2000), part of the Bir Fa'as Formation. The age of 96.1 Ma for the most evolved glaucony suggests a Cenomanian age (Gradstein et al., 1995; Remane et al., 2002). Using the stratigraphic chart of Odin (1994), Amireh et al. (1998) postulated an Albian age. Besides the question which stratigraphic chart should be used, the stratigraphic position of the dolomite bed can also be discussed. Due to its direct position below the cliff of the Cenomanian Naur Formation (Amireh et al., 1998), it most probably belongs to the Wadi Juhra Member of that formation and not necessarily to the Kurnub Group.

2.3.2 Ajlun Group (Cenomanian to Upper Coniacian)

The Ajlun Group comprises Cenomanian to Upper-Coniacian sediments and is subdivided into five formations (Fig. 2.3). In central Jordan a sixth formation, the Khureij Formation, is present. The thickness of the Ajlun Group ranges from zero in the South-East to about 800 m in the North, close to the city Irbid (Powell et al., 1996). Its regional equivalents are the Judea Group in the West Bank and the Negev, and the fluvial to shallow-marine Sakaka Sandstone in Saudi Arabia (Powell et al., 1996).

In North Jordan the Ajlun Group is well exposed and the formations are well defined by bio- and lithostratigraphy. There the Ajlun Group can be divided into a lower sequence with interbedded limestones and shale, and an upper sequence of limestone all deposited on a rimmed shelf (Fig. 2.4A). Marine siliciclastics at the base of the Ajlun Group mark the major transgression of the early Cenomanian (Powell et al., 1996).

In East and South Jordan, along the Naqb escarpment (Fig. 2.4B), the shallow marine limestone lithology passes laterally into sandy limestones and calcareous sandstones to sandstones (Andrews, 1992; Powell et al., 1996). The low abundance of fossils suitable for biostratigraphy along the Naqb escarpment makes subdivision of the Ajlun Group difficult. This leads to the replacement of the term Ajlun Group by the term Batn El Ghul Group (cf. Figs. 2.3 and 2.4B). The formations of the Ajlun Group will be briefly described in the following.

Naur Formation (Upper Albian? to Lower Cenomanian)

The Naur Formation is the basal part of the Ajlun Group (Figs. 2.3 and 2.5) and represents the first transgressive phase of the Late Cretaceous Tethysian Ocean across the alluvial plain of the Kurnub Group (Powell, 1989) resulting in the drowning of the entire region (Lovelock, 1984). The exact age of this transgressive event is subject to discussion (e.g. Amireh et al., 1998), but a diachronous, approximately North-South oriented character of the Late Albian to Early Cenomanian event can be assumed. West of the Wadi Araba-Dead Sea-Rift the Naur Formation is equivalent to the lower part of the Hazera Formation (Powell, 1989).

The Naur Formation is subdivided into four members, A to D (Powell, 1989). The differentiation into Member 'B', 'C' and 'D' is only locally possible, e.g. in the western part of the escarpment near Ras En Naqb or in North/Central Jordan. Member A, also referred to as Wadi Juhra Member (Fig. 2.4), consists of a diachronously deposited, siliciclastic dominated shallow marine to marginal marine facies association (Powell, 1989). It represents the transition from the fluvial dominated clastic Kurnub Group to the marine carbonates of the Naur Formation. Powell (1989) describes paralic swamps and shallow evaporating lagoons as depositional environments for the Wadi Juhra Member. During field work the first

recognisable marine bed above the Kurnub Group was defined as the base of the Wadi Juhra Member. The bed was usually characterized by marine trace and/or body fossils or glaucony. The Wadi Juhra Member was named differently by several authors. Even its stratigraphic position is matter of discussion. Table 2.2 sums the synonyms and stratigraphic positions of the Wadi Juhra Member according to different authors.

Table 2.2 Synonyms of the Wadi Juhra Member.

Synonyms and origin	Stratigraphic position
Naur Member 'A' (e.g. Powell, 1989)	Base of Naur Formation
Wadi Juhra Member (e.g. Powell, 1989)	Base of Naur Formation
Transition zone (Makhlouf et al., 1996)	Base of Naur Formation
Bir Fa'as Formation (Amireh, 2000)	Top of Kurnub Formation/Group

The overlying cliff-forming limestones and dolomites of members B to D are traceable along the Naqb escarpment to the area West of Batn El Ghul, where they pass into marls and calcareous sandstones (Fig. 2.4B). The dolomitic, cliff-forming Member 'B' is rich in oysters, especially *Exogyra* sp. and *Ostrea* sp. and usually displays abundant *Thalassinoides* burrows (Powell, 1989) which give the rocks the distinctive nodular texture (Abed and Schneider, 1982). Chert nodules also occur within this member. Member 'C' is dominated by marly sediments and thin bedded, partially dolomitic limestones which are locally cliff forming. *Thalassinoides* and oysters dominate the fossil content (Powell, 1989). The dolomites and limestones of Member 'D' are cliff forming again and make up the well distinguishable top of the Naur Formation (Fig. 2.5). As with the former units, *Thalassinoides* dominates the trace fossil content. Shelly body fossils, including oysters and rudists, are also abundant (Powell, 1989). The three members represent an inner-shelf sequence with sediments deposited in shallow marine environments under a fluctuating, in general rising, sea-level which reaches a maximum during the deposition of the 'D' Member (Powell, 1989).

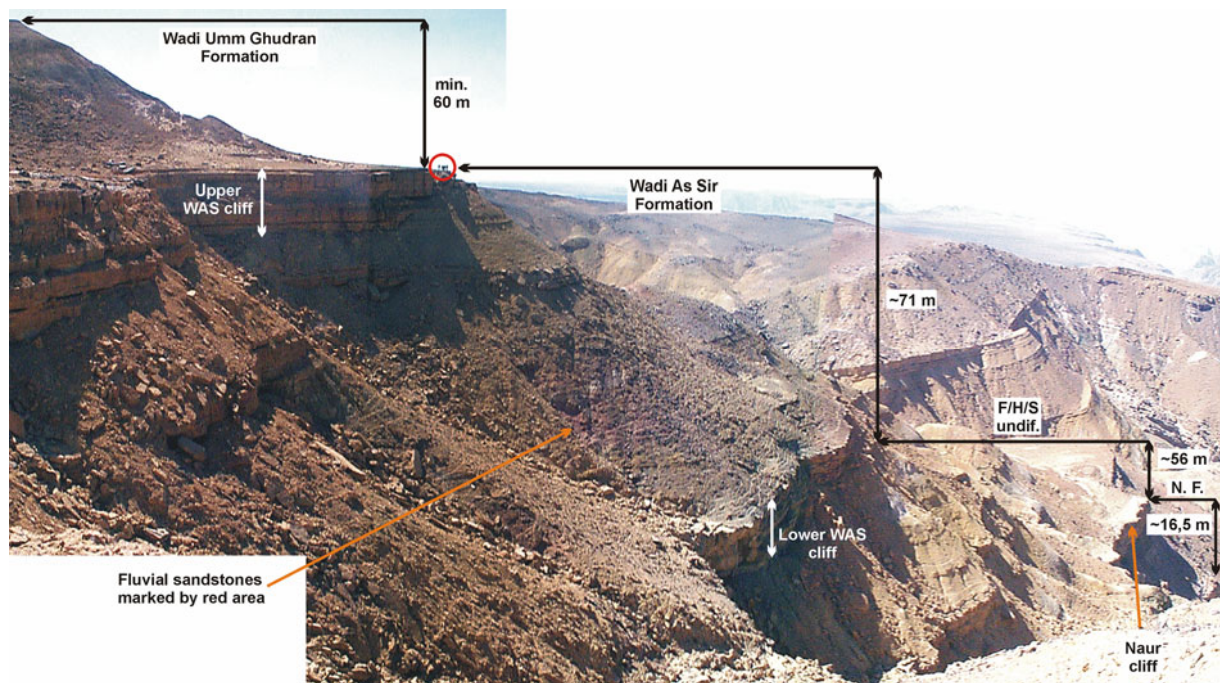


Figure 2.5 Section 7 at the Naqb escarpment, comprising the Ajlun Group. Between prominent limestone cliffs, softer sediments form steep debris covered slopes. The red circle encloses the following people as scale: H. Krawinkel, Z. Lewy, K. Moumani, and R. Berndt (N.F. = Naur Formation; F/H/S undif. = Fuhays, Hummar and Shuayb Formations, undifferentiated; WAS= Wadi As Sir Formation).

Fuhays, Hummar and Shuayb Formations (F/H/S) (Lower Cenomanian to mid Turonian)

In North Jordan it is possible to differentiate the Fuhays, Hummar and Shuayb formations in the field due to the Hummar carbonates that divide the marly deposits of the underlying Fuhays and hanging Shuayb formations. In Central and South Jordan this is not possible due to the marly expression of the Hummar Formation. Therefore the three formations are usually grouped together and called F/H/S-undifferentiated, or short F/H/S (Figs. 2.4B and 2.5). The thickness of the F/H/S differs from 50 to 150 m (Powell, 1989). A regional equivalent of the F/H/S is the Ora Formation in the southern Negev. The following brief description of the F/H/S is mainly based on Powell (1989) and Powell et al. (1996).

The lithology of the Fuhays Formation is dominated by clays, marls, calcareous siltstones and thin-bedded limestones. Prominent features are oyster packstone beds (e.g. *Exogyra* sp.) and gypsum nodules within the formation. At the top of the Fuhays Formation the Karak Limestone Member can be found (Fig. 2.4A). Though the thickness of this shelly wackestone varies locally, the *Exogyra* sp. rich limestone can be used as an indicator for the Fuhays Formation. In North/Central Jordan the Fuhays Formation usually forms a broad slope between the cliffs of the Naur and the Hummar Formations (Makhlouf et al., 1996). The beginning of the Fuhays Formation is usually defined by the first clay/marl bed above the limestones of the Naur Formation. In some locations along the Naqb escarpment, e.g. section 5, the F/H/S starts with a thin-bedded, marly limestone unit, rich in irregular echinoids (Dr. Z. Lewy, Geological Survey Israel, personal communication, 2000).

The Hummar Formation of North Jordan is mainly made up by lime- and dolostones. In several areas this formation builds a prominent cliff. In Central and South Jordan the abundance of clastic lithologies within the F/H/S increases. In South Jordan a coral bearing limestone, the Naqb Member, can be found roughly in the middle of the Hummar Formation. The following Shuayb Formation is dominated by marls, clays and thin-bedded lime- and dolostones, forming a broad slope between the cliffs of the underlying Hummar and overlying Wadi As Sir Formation. Based on ammonite biostratigraphy, the Cenomanian-Turonian boundary is located in the upper part of the Shuayb Formation, in the Wala Limestone Member (Powell et al., 1996).

The heterogeneous lithology of the F/H/S points to a deposition in marine to restricted-lagoonal environments with transgressive and regressive episodes (Powell, 1989). Though a clear identification of the three limestone members (Karak, Naqb and Wala Member) within the F/H/S is not always possible in the study area, they can locally be used for a rough division of the otherwise undifferentiated F/H/S. At least the Naqb Member can be identified in South Jordan near Ras En Naqb (Fig. 2.4B).

Wadi As Sir Formation (mid Turonian to Upper Coniacian)

The Wadi As Sir Formation is 60 to 300 m thick (Powell, 1989) and represents the topmost formation of the Ajlun Group. Only near Jabal Khureij and in the area of Mukawir it is overlain by the marls and limestones of the Khureij Formation (Powell, 1989). The Wadi As Sir Formation forms a prominent limestone/dolomite cliff in North/Central Jordan (Powell, 1989). Due to siliciclastic influence, this cliff is divided into a lower and an upper part along the Naqb escarpment. The lower cliff is close to the base of the Wadi As Sir Formation, the upper one is at the top of the formation (Fig. 2.5). The Wadi As Sir Formation is dominated by massive carbonates and dolomites (Fig. 2.4A). Marly beds occur only to a minor extent. To the East, towards the Batn El Ghul area, a transition from the marine carbonate facies to a fluvial clastic facies can be observed (Fig. 2.4B). Characteristic features of the calcareous Wadi As Sir Formation are the chert nodule layers frequently occurring in the middle and upper parts of the formation. The fossil content comprises bivalves, echinoids and gastropods. *Thalassinoides* beds also occur (Makhlouf et al., 1996).

According to Powell (1989) the Wadi As Sir Formation was deposited on a wide shallow carbonate platform. This platform extended from the present Mediterranean coastline to approximately 35 km south-east of Ras En Naqb, where shallow subtidal to intertidal conditions prevailed during the initial transgression. The depositional environments vary slightly during the sedimentation of the Wadi As Sir Formation. Occurrence of gypsum beds, rudist and bryozoan banks in Central and South Jordan within the deposits of the lower Wadi As Sir Formation, point to sedimentation under shallow subtidal to intertidal conditions. Rudist banks and the occurrence of soil calcretes in North/Central Jordan within the middle part of the Wadi As Sir Formation point to an emergence of the platform. This is supported by the presence of fluvial sediments in South Jordan along the Naqb escarpment (Fig. 2.5). The upper Wadi As Sir Formation of North Jordan was deposited under shallow-water lagoonal conditions with slightly shallower conditions towards the South. Along the Naqb escarpment the sedimentation of the formation took place under coastal margin conditions, as reflected by sandy dolomites. The deposits of the Wadi As Sir Formation represent the maximum transgression of Cenomanian to late Turonian age. Regional equivalents of the Wadi As Sir Formation are the Gerofit Formation in the Negev, the Nezer and Bina formations in the West bank as well as the Sakaka Formation in Saudi Arabia (Powell, 1989).

2.3.3 Belqa Group (Upper Coniacian to Late Eocene)

The Belqa Group unconformably overlies the Ajlun Group and comprises six formations. The Wadi Umm Ghudran, Amman and Al Hisa formations comprise Upper Coniacian to Campanian sediments. The Muwaqqar Formation spans the Cretaceous-Tertiary boundary, which is marked by a depositional hiatus (Powell et al., 1996). The lower part is of Maastrichtian, the upper part of Palaeocene to Eocene age. The Umm Rijam and Wadi Shallala formations are of Eocene age (Andrews, 1992). The thickness of the Belqa Group varies locally between 450 and 3000 m (Powell et al., 1996). Regional equivalents are the Mount Scopus, Avdat and Hashefella groups of the West Bank and the Negev. In Saudi Arabia the Belqa Group can be correlated with the Aruma Group (Powell et al., 1996).

The Belqa Group in North/Central Jordan consists mainly of chalk, chert and phosphorite sediments, deposited in a pelagic or hemi-pelagic ramp setting. The base is marked by a regional unconformity/disconformity (Powell et al., 1996). The base the Umm Ghudran Formation, defines the top of the studied stratigraphic interval west of the Batn El Ghul field station. East of the field station, the base of the Amman Formation defines the top of the studied stratigraphic interval since lateral facies changes hinder the clear recognition of the Wadi Umm Ghudran Formation. Therefore only these two formations will be described briefly in the following.

Wadi Umm Ghudran Formation (Upper Coniacian to Santonian)

The Wadi Umm Ghudran Formation represents the transition from the platform sediments of the Ajlun Group to the pelagic dominated sedimentation of the Belqa Group (Powell, 1989). In North and Central Jordan the formation consists of 50 to 75 m thick chalk dominated sediments, deposited after an erosional unconformity. Towards the South the chalk interfingers with siliciclastic sediments and dolomites, the so called Alia Member (Fig. 2.4A). Along the Naqb escarpment the siliciclastic deposits dominate and the chalky sediments disappear completely (Figs. 2.4B and 2.5). Here, the term Wadi Umm Ghudran Formation is replaced by the term Fassua Formation (Powell, 1989). The Wadi Umm Ghudran Formation was deposited in a coastal setting, influenced by rivers draining from the Arabo-Nubian shield (Powell, 1989). A regional equivalent of the Wadi Umm Ghudran Formation is the Menuha Formation west of the Wadi Araba-Dead Sea-Rift (Powell, 1989).

The base of the Wadi Umm Ghudran Formation was logged in some sections. Section 10 comprises the complete Wadi Umm Ghudran Formation. It was logged to examine possible

facies changes from the Wadi Umm Ghudran Formation to the Batn El Ghul Group. Detailed vertical sections of the Wadi Umm Ghudran Formation in sequel to sections 7, 8 and 9 are listed by Mohs (2001).

Amman Formation (Campanian)

The Amman Formation is characterized by cliff forming, massive chert beds overlaying the Wadi Umm Ghudran/Fassua Formation (Figs. 2.4A and 2.6). It comprises thin- to medium bedded heterogeneous lithologies, including chert, microcrystalline limestone, marl, chalk, grainstones and phosphate in form of granules (Powell, 1989). The Amman Formation can be traced from North to South Jordan without problem and youngs diachronously towards the Southeast of the country, overlying the Alia Member and the Fassua Formation. The Amman Formation and the overlying Al Hisa Formation are an economic significant aquifer (Abu Saad and Al Bashish, 1999) and contain most of the Jordanian phosphate reserves (Andrews, 1992). Its thickness varies from 15 to 100 m, with an average of about 50 m (Powell, 1989; Abu Saad and Al Bashish, 1999). The base of the Amman Formation is defined below the first massive thick-bedded chert and above the marly cherts or silts/sands of the Wadi Umm Ghudran/Fassua Formation (Powell, 1989). Within this study the definition was extended for the area east of Batn El Ghul (that is east of section 10). There, the base of the first unmistakable marine bed was defined as the base of the Amman Formation. The upper boundary to the overlying Al Hisa Formation is gradational. West of the Wadi Araba-Dead Sea-Rift parts of the Mishash Formation are equivalent to the Amman Formation (Powell, 1989).

The interpretation of the depositional environment of the Amman Formation is hampered by the early diagenetic silicification of the rocks (Powell, 1989). Shallow water conditions of the outer to inner shelf seem predominant in North/Central Jordan. In South and Southeast Jordan a raised content of siliciclastic deposits points to a deposition under marginal marine conditions (Powell, 1989). In general the Amman Formation represents the change from a calcareous towards a siliceous pelagic sedimentation (Powell, 1989).

Since several authors (Masri, 1963; Parker, 1970; Powell, 1989) used the term Amman Formation differently (Andrews, 1992) it should be noted that this study follows the definition of Powell (1989) as 'Amman Silicified Limestone Formation'. A compilation of the Amman Formation is given by Abu Saad and Al Bashish (1999).

2.3.4 Batn El Ghul Group (Cenomanian to Santonian)

The Batn El Ghul Group in Southeast Jordan is the counterpart of the Ajlun and lower Belqa groups of North/Central Jordan (Fig. 2.3). The reason for the introduction of the Batn el Ghul Group into the Jordanian stratigraphic nomenclature is the change from a carbonate dominated marine system in North/Central Jordan to a siliciclastic dominated, marginal marine to terrestrial system in South Jordan (Fig. 2.4A & B) and especially along the Naqb escarpment (Powell, 1989). Therefore the Batn El Ghul Group represents a facies change within the same stratigraphic framework. It comprises Cenomanian to Upper Coniacian deposits and can be subdivided into the Harad and Fassua formations. A clear geographic boundary for the use of the terms Ajlun/Belqa Group and Batn El Ghul Group can not be given. Usually the term Batn El Ghul Group is used along the Naqb escarpment, where marine deposits pass laterally into the coeval fluvial facies. This criterion is not very useful, since these facies changes take place at different localities within the different stratigraphic formations. The subdivision of the Batn El Ghul Group into Harad and Fassua Formation along the escarpment is also questionable. The use of these two formations implies that it is possible to distinguish the terrestrial equivalents of the Ajlun Group from the terrestrial deposits of the Belqa Group, which is hard to do in the field. As a result, within this study the term Batn El Ghul Group was used only for the clearly terrestrial facies east of the Batn El

Ghul field station (sections 11 to 15), where it comprises a maximum thickness of 169 metres in section 11 (Fig. 2.6) and a minimum thickness of 30.5 metres in section 12. A subdivision of the Batn El Ghul Group in its formations was not applied within this study.

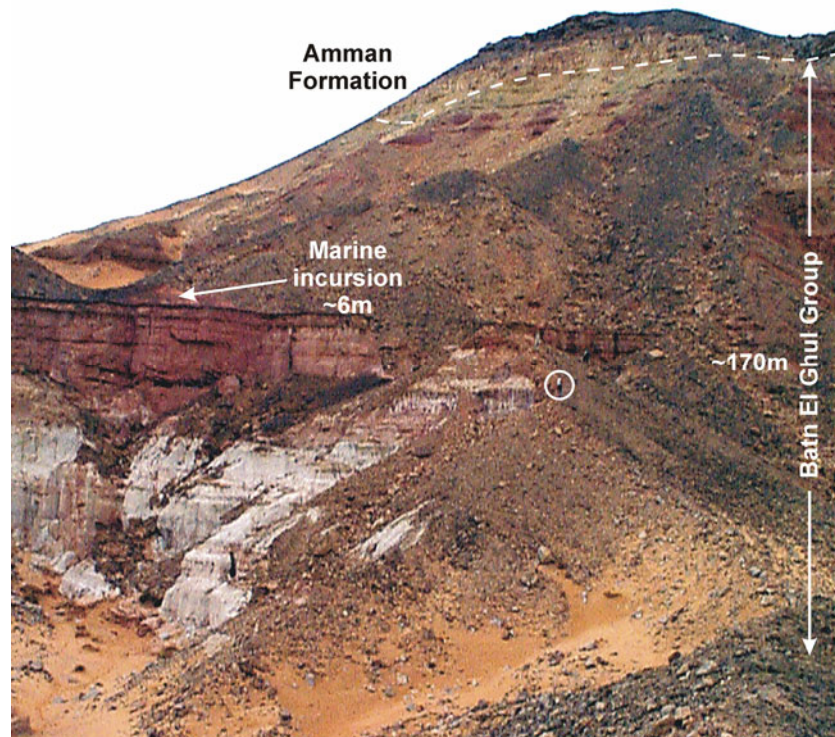


Figure 2.6 Section 11 comprising the Batn El Ghul Group east of the Batn El Ghul field station. The white deposits in the lower part of the photo are most probably part of the Kurnub Group. Since there is no significant facies difference to the hanging sediments, the white sediment colour is the only indication for the Kurnub Group. The marked marine incursion represents the maximum Cenomanian transgression. The white circle encloses H. Abu Azzam as scale.

Harad Formation

The term Harad Formation is used for the Cenomanian to mid-Coniacian stratigraphy along the Naqb escarpment. The Harad Formation replaces the Naur Formation, the F/H/S formations and Wadi As Sir Formation. Terrigenous influence to the accommodation area of South Jordan changed the lithofacies of the stratigraphic succession. Therefore a correlation with the lithofacies of northern Jordan is not always easy.

Fassua Formation

The Fassua Formation replaces the term Wadi Umm Ghudran Formation in South Jordan and can be seen as the proximal equivalent of the pelagic Umm Ghudran Formation (Powell, 1989). Along the Naqb escarpment the Fassua Formation is dominated by clay- and sandstones (Mohs, 2001). High terrigenous input changed the lithofacies in southern Jordan to in a way that a correlation with the Wadi Umm Ghudran Formation of North Jordan was not achieved yet.

2.4 Post-Cretaceous geology and landscape evolution of the study area

The deposition of marine sediments in South Jordan continued until the Eocene when regressive conditions and the uplift of the Arabian craton caused erosion and deposition of terrestrial sediments (Powell, 1989). Figure 1.2 shows that parts of the study area are covered by Cenozoic, Tertiary and predominantly Quaternary, sediments. Most of these deposits are

desert and wadi sediments of Quaternary and Holocene age. Large areas of the central desert of Jordan, north of the Naqb escarpment, are covered by chert pieces forming wide areas of Hamada (Bender, 1974). An interesting anthropologic feature is the occurrence of Palaeolithic artefacts that can be found in several places in the central desert (Bender, 1974) and sometimes along the Naqb escarpment (K. Moumani, Natural Resources Authority, personal communication, 2000).

Landscape evolution

The most striking landscape feature in the study area is the Naqb escarpment itself, which is most probably the result of erosion during the Miocene (Osborn, 1985). Subsidence of the Dead Sea rift valley and uplift of its shoulders during the Miocene lowered the local base level and led to extensive erosion (Osborn, 1985). The opening of the Red Sea during that time provided the base level for the drainage of South Jordan, while some parts also drained towards the Mediterranean. The southernmost part of the Jordan plateau was eroded by differential weathering and erosion along weak zones, e.g. faults and joints connected to the Red Sea opening and the Wadi Araba-Dead Sea-Rift. The result was the formation of the escarpment and the inselberg landscape south of it (Osborn, 1985).

The wadi erosion along the Naqb escarpment visible today, usually follows faults, while some of the wadis display signs of fluvial erosion independent of faults. The fluvial erosion was active during the last European glaciations (Osborn, 1985). Usually the wadis start as narrow canyons and tend to widen towards the South, due to slope retreat and further erosion (Osborn, 1985). The sediments filling the wadis can be considered to be of recent to sub-recent age.

2.5 Cretaceous palaeogeography of Jordan and global sea-level

During the Early Cretaceous the northern boundary of the Arabian Plate was on an equator near position (Fig. 2.7A). The area of Jordan was located at the southern shore of the Neo-Tethys Ocean (Powell, 1989; Powell et al., 1996). A low sea-level during that time (Fig. 2.3) left major parts of the continental areas exposed and allowed the deposition of the fluvial sediments of the Kurnub Group. The south-Tethyan coastline during the Lower Cretaceous trended approximately NE-SW (Powell et al., 1996) and was located in the area of northern Jordan (Fig. 2.8, "Kurnub Shoreline"). Marine incursions in the upper part of the Kurnub Group point to the rising sea levels at the end of the Early Cretaceous (Powell, 1989; Powell et al., 1996; Amireh, 1997; 2000). After a regressive phase in the Lower Aptian, the Aptian to Albian is marked as a time of strong transgression with three major flooding events in the Aptian (Gale, 2000). A steady northward movement of the Arabian Craton during the Albian to Cenomanian brought Jordan to a position approximately 7° N of the equator in late Cenomanian times (Fig. 2.7B). During this time the rising sea-level lead to a major transgression, flooding the passive continental margin of the Arabian Craton and the Lower Cretaceous terrigenous sediment cover (Lovelock, 1984; Powell, 1989). The coastline shifted further southward to South Jordan (Fig. 2.8, "Ajlun Shoreline") and the deposition of onlapping shallow marine clastic and carbonate sediments of the Ajlun Group took place. These sediments were deposited on the extensive shallow shelf sea areas typical for the mid-Cretaceous (Frakes et al., 1992). The palaeohingeline, (Fig. 2.8, "Shelf edge") separating the Tethyan basin from the shallow shelf/ramp during the sedimentation of the Kurnub and Ajlun groups, followed approximately the present Mediterranean coastline (Powell et al., 1996). During the Cenomanian the high sea-level trend continued up to the Upper Cenomanian, where a major sea-level fall occurred. The Turonian sea-levels rose even higher than the Cenomanian, producing the highest sea levels of Mesozoic time (Gale, 2000), but also displays a major regression during the Upper Turonian. The mid Turonian first-order sea-level

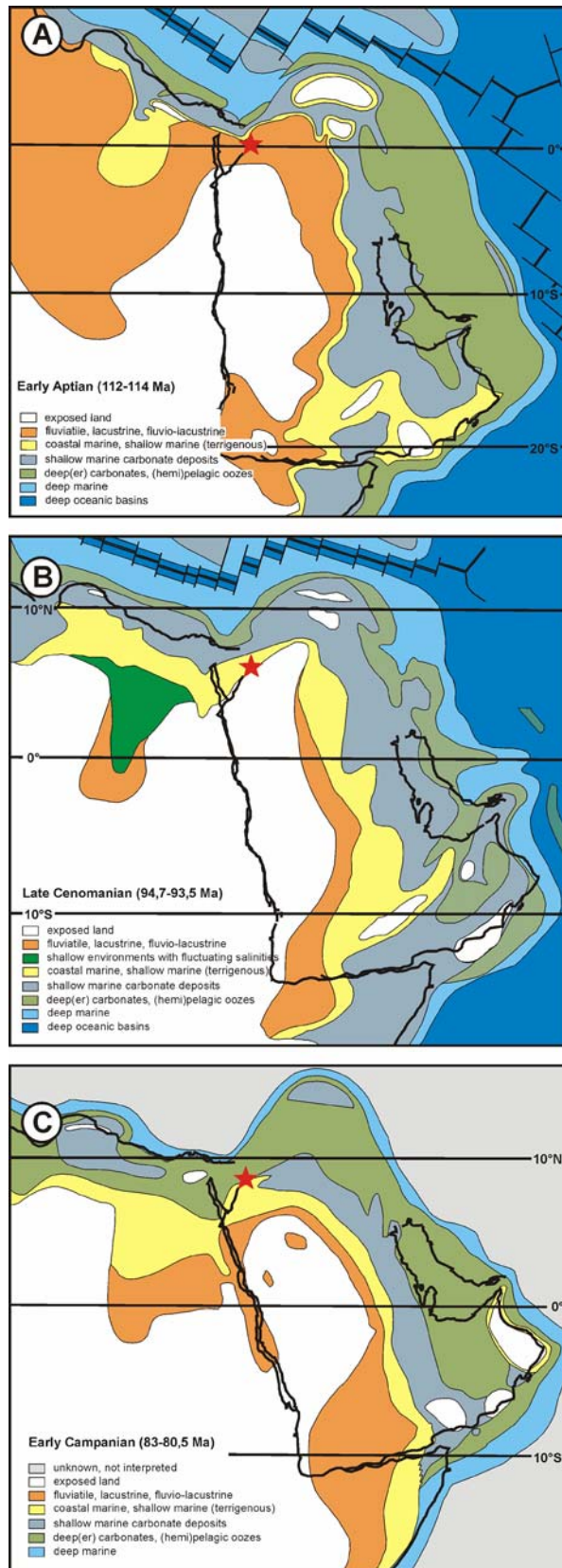


Figure 2.7 Palaeogeographic maps and depositional environments of NE-Africa and the Arabian Peninsula (modified after Dercourt et al., 2000). **A)** Early Aptian, **B)** Cenomanian and **C)** Early Campanian (red star = approximated position of Jordan).

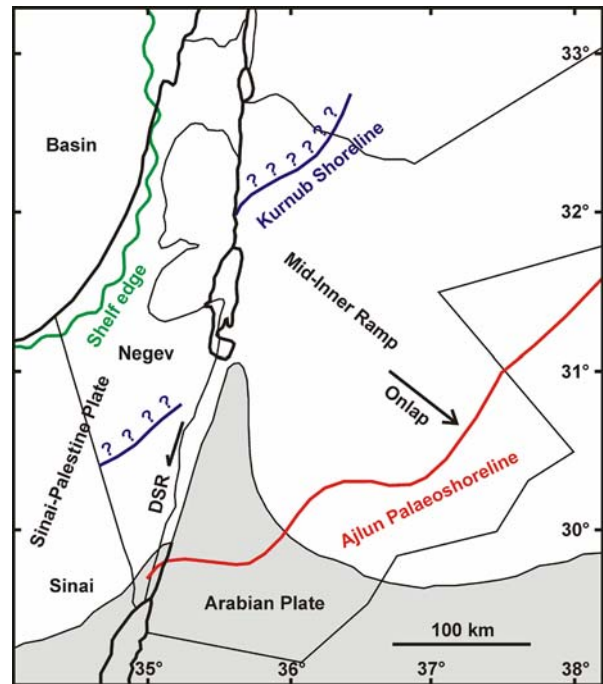


Figure 2.8 Palaeogeographic reconstruction of the Cretaceous Tethyan shoreline in Jordan and Israel (modified after Powell et al., 1996).

maximum can be related to an increased mid-ocean ridge volume and a mantle superplume (Gale, 2000). In general it can be said that during the mid-Cretaceous the sea-level was about 100-200 m higher than present and 20% of the continental area was flooded (Crowley and North, 1991).

During the Late Cretaceous the Arabian Craton drifted to 10° N (Fig. 2.7C). Fluctuating but generally high sea levels kept the major part of Jordan flooded during the Late Cretaceous, where the shallow marine sediments of the Belqa Group were deposited. The Maastrichtian sea-level shows an overall regressive trend with two major regressions during the Middle and the Upper Maastrichtian.

2.6 Cretaceous palaeoclimate

The global Cretaceous climate is seen as surpassing warm, culminating during certain intervals in “greenhouse” climatic conditions (Frakes and Francis, 1990; Powell et al., 1996; Bussert, 1998). Temperatures of Cretaceous intermediate-deep waters were about 15°C warmer than today (Crowley and North, 1991). Though temperatures were

generally high, relative warmer and cooler periods occurred, even during greenhouse conditions (Frakes and Francis, 1990). According to Frakes and Francis (1990) Berriasian, Valanginian, Albian, Coniacian and Santonian were warm periods, while Hauterivian, Barremian, Aptian, Cenomanian, Turonian, Santonian and Maastrichtian were colder. The Upper Cenomanian to Lower Turonian is interpreted as an especially 'hot' period (Frakes and Francis, 1990; MacKenzie, 1990), depicting an especially arid climatic phase.

The Early Cretaceous (Berriasian to Barremian period) represents the transition from the very humid Jurassic to the climatic zoned mid-Cretaceous. During that period the large landmasses experienced annual temperature fluctuations, especially in their inner regions which also faced low precipitation (Bussert, 1998).

A higher dispersion of the continents during the Late Cretaceous, a raised marine influence and the formation of extended epicontinental seas, lead to a more balanced climate with higher precipitation rates (Bussert, 1998). High spreading rates at the mid ocean ridges caused a high sea level and, in combination with a general high volcanic activity, high atmospheric CO₂ levels.

The high content of atmospheric CO₂ lead to raised global temperatures. The flooded continental areas added further to the CO₂ increase. Since continental areas remove atmospheric CO₂ by the weathering of silicate (Crowley and North, 1991), land areas reduced by flooding lead to decreased CO₂ removal.

The mid-Cretaceous (Aptian-Albian-Cenomanian) period was one of the warmest times of the late Phanerozoic, with average temperatures 6°C and more above today (Frakes et al., 1992). For this period and the Late Cretaceous (Cenomanian to Maastrichtian) there is no evidence for ice rafted debris in high latitudes, pointing to a time interval with ice free poles (Frakes et al., 1992; Powell et al., 1996). The late Upper Cretaceous (Campanian to Maastrichtian) is characterized by decreasing temperatures and falling sea-levels. Climate models showing high seasonal rainfalls focusing on the northern and southern borders of the Tethys are confronted with the fact that low-latitude tropical everwet vegetation is unknown (Frakes et al., 1992). This supports the point that in low latitudes evaporation, and therefore a possibly more arid climate, predominated. A strong monsoon, predicted by climate modelling, transports moisture and heat poleward (Frakes et al., 1992). According to climate models the monsoon intensities might have been driven by orbital variations (Crowley and North, 1991). Both, seasonal rainfalls and monsoonal climates point to a latitudinal climatic zonation (Fig. 2.9) and the presence of mid latitude arid belts (Frakes et al., 1992).

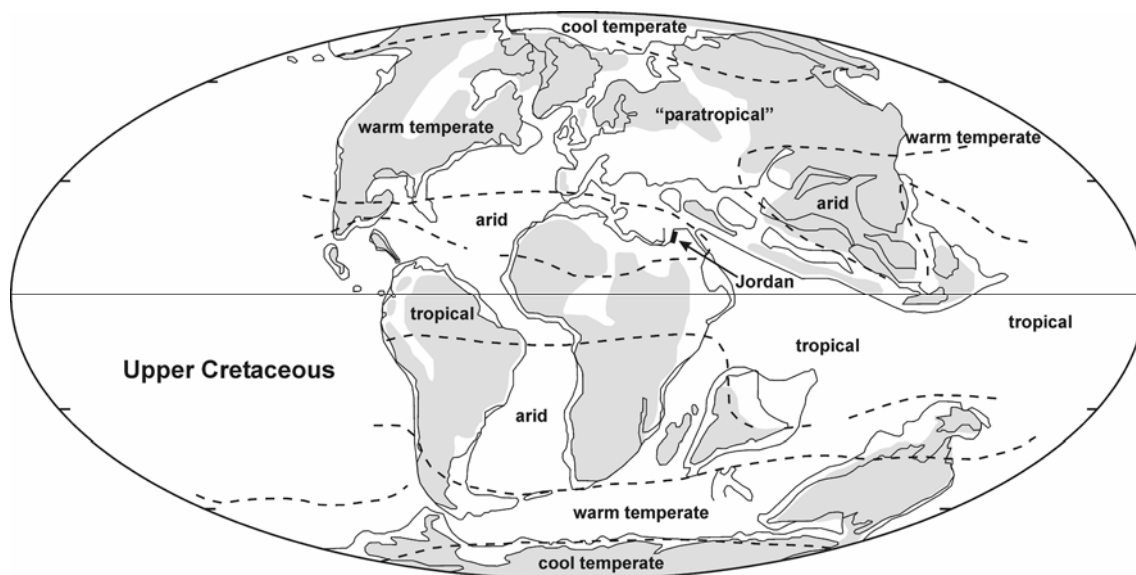


Figure 2.9 Global Late Cretaceous climate zones (modified from Scotese, 2000). The shaded areas represent terrestrial continental areas.

Though the palaeoclimate information for the Late Cretaceous is sometimes confusing (Francis and Frakes, 1993), the Aptian to mid Campanian time can in general be referred to as a greenhouse period (Frakes et al., 1992). Evidence for warmer temperatures in high latitudes are the poleward shift of coral reefs (5° - 15°) and floral provinces (15°) from present habitats. Latitudinal displacement of a larger number of invertebrates as foraminifera and rudists (Crowley and North, 1991) supports this.

Part 1:

Facies analysis and sequence stratigraphy of the Upper Cretaceous sediments of South Jordan

3. Facies analysis

3.1 Methods

Fifteen vertical sections were studied and logged in detail. Twelve (sections 4 to 15) along the escarpment between Ras En Naqb and Naqb Ataik and three (sections 1 to 3) near and west of the small town of Ras En Naqb (Fig. 1.3, Chapter 1, p. 3). Due to outcrop conditions, sections 1-4 include only the Naur and F/H/S formations of Cenomanian/Turonian age.

All sections were measured and logged on a decimetre scale. Recorded observations during field work include lithology, sedimentary structures using the cross-bedding scale after Grumbt (1969), trace and body fossil content, sediment colour using the Rock-Color Chart (Rock-Color Committee, 1963) and the mapping of discontinuity surfaces. In selected areas palaeocurrent analysis were performed.

The sedimentological information was graphically transformed into detailed textural graphic logs (e.g. Tucker, 1996). Standard lithofacies types (e.g. Miall, 1996) were defined on lithology and sedimentary structures. Graphic logs of all sections, including geographic position, lithofacies, depositional environments, sequence stratigraphic interpretation and stratigraphic position of the examined samples, are presented in Appendix I.

During field work sediment and fossil samples were collected for further analysis. A list of the studied samples and the analysis carried out is given in Appendix I. The palaeontological and carbonate sedimentological aspects are covered in detail in Berndt (2002).

3.1.1 Lithofacies types

Observation and classification of lithofacies is a standard tool of facies-analysis (Miall, 1996). The classification of sediment beds on the basis of their 'primary' depositional attributes allows a quick and effective overview of a sediment succession. Based on the classification presented by Miall (1977; 1985; 1996), a lithofacies classification for the South Jordan deposits was developed. An overview of the facies codes is presented in table 3.1.

The lithofacies scheme of Miall is focused on fluvial deposits. Therefore it had to be broadened to fit also marine deposits as well as limestones and dolomites. According to Miall (1996) lithology/grain size and the physical sedimentary structures were chosen as primary depositional attributes. Bioturbation and soil formation were added to distinguish fine-grained fluvial and marine sediments.

Applying standardized lithofacies to lithologies occurring in various depositional environments is seen critical (Miall, 1996), since not all sedimentary aspects can be recorded in the lithofacies code. In the presented classification, the carbonates are simplistic classified and do not match the classification schemes of Dunham (1962) or Folk (1959; 1962). Furthermore, some of the lithofacies classes are gradational with others, and not every single bed fits one single facies code. Therefore, a partially bioturbated massive silt with faint lamination will be classified as Fr/Fl.

Table 3.1: Litho facies classification (modified and extended from Miall, 1996)

Facies code	Facies	Sedimentary structures	Interpretation
St	Sand, fine to very coarse, may be pebbly	Solitary or grouped trough cross-beds	Sinuous-crested and linguoid (3-D) dunes
Str	Sand, fine to very coarse, may be pebbly	Solitary or grouped trough cross-beds; Bioturbation	
Sp	Sand, fine to very coarse, may be pebbly	Planar cross-beds	Transverse and linguoid bedforms (2-D dunes)
Spr	Sand, fine to very coarse, may be pebbly	Planar cross-beds with bioturbation	
Sr	Sand, very fine to coarse	Ripple cross-lamination	Ripples (lower flow regime)
Src	Sand, very fine to coarse	Ripple cross-lamination with bioturbation	
Sh	Sand, very fine to coarse, may be pebbly	Horizontal lamination parting or streaming lineation	Plane-bed flow (critical flow)
Shr	Sand, very fine to coarse, may be pebbly	Horizontal lamination parting or streaming lineation with bioturbation	
Sm	Sand, fine to coarse	Massive, or faint lamination	Sediment-gravity flow deposits
Smc	Sand, fine to coarse	Massive, or faint lamination; bioturbation, pedogenic features: colour mottling, roots	
Sl	Sand, very fine to coarse, may be pebbly	Low-angle (<15°) cross-beds	Scour fills, humpback or washed-out dunes, antidunes
Slr	Sand, very fine to coarse, may be pebbly	Low-angle (<15°) cross-beds with bioturbation	
Ss	Sand, fine to very coarse, may be pebbly	Broad, shallow scours	Scour fill
Fl	Sand, silt, mud	Fine lamination, very small ripples	Fluvial: Overbank, abandoned channel, or waning flood deposits Marine: waning storm deposits, tidal sediments, suspension fall out sediments
Fsm	Mud, silt	Massive	Fluvial: Backswamp or abandoned channel deposits Marine: suspension fall out sediments, e.g. lagoonal mud
Fr	Mud, silt	Massive, roots, bioturbation	Fluvial: Root bed, incipient soil Marine: bioturbated suspension fall out sediments, e.g. lagoonal mud
Ft	Mud, <u>silt</u>	Solitary or grouped trough cross-beds	Small sinuous-crested and linguoid (3-D) dunes in silty material
Lm	Limestone	Massive	Various limestones
Lmr	Limestone	Massive, bioturbation	
Lms	Limestone, sandy	Massive	Various limestones with obvious siliciclastic components
Lrs	Limestone, sandy	Massive, bioturbation	
Lls	Limestone, sandy	Fine lamination	Various limestones with obvious siliciclastic components and possible algal lamination
Lk	Nodular limestone	'massive'	Nodular limestone as a result of diagenesis and/or bioturbation
Lkr	Nodular limestone	clearly bioturbated	
Ll	Limestone	Fine lamination	Possible algal lamination
Dm	Dolomite	Massive	Secondary, recrystallized dolostones
Dmr	Dolomite	Massive, bioturbation	
Dms	Dolomite, sandy	Massive	Secondary, recrystallized dolostones with obvious siliciclastic components
Dls	Dolomite, sandy	Fine lamination, very small ripples	Secondary, recrystallized dolostones
DI	Dolomite	Fine lamination	Secondary, recrystallized dolostones with possible algal lamination

3.2 Description and interpretation of sedimentary environmental facies

The interpretation of the depositional environments is based on field observations and the correlation of the logs, using standard literature (e.g. Scholle and Spearing, 1982; Davis, 1985a; Walker and James, 1992; Galloway and Hobday, 1996; Reading, 1996; Einsele, 2000 among others).

Table 3.2: Summary of the ten sedimentary environmental facies types (for explanation of the lithofacies types see table 3.1).

Facies	Characteristics	Typical lithofacies types	Facies association
1 Siliciclastic shelf	Massive clays, silts and sands; interbedding of fine sand and clay layers. Plant remains; fragmented and articulated marine fossils; bioturbation.	Sm, Smc, Fsm, Fr, Fl	Shelf facies association
2 Mixed siliciclastic-carbonate shelf	Thin- to thick-bedded carbonates, dolomites, mudstones, marls, marly silts and sands; chert nodules. Fragmented and articulated marine fossils; bioturbation; plant remains.	Fsm, Fr, Lm, Lms, Lmr, Lk, Lkr, Ll, Lrs, Dm, Dms, Dl, Dls, Smc	
3 Transition zone	Thin- to thick-bedded, massive sand grading into fine-grained, bedded sand units intercalated with thick to very thick bedded silt- and claystones; thin- to medium bedded lime- and dolomites. Horizontal lamination, ripple cross-lamination, trough cross-bedding. Fragmented and articulated marine fossils; bioturbation.	Sm, Smc, Sh, St, Sp, Fsm, Fl, Fr, Dm, Dl, Dms, Lms	
4 Shoreface	Cross-stratified fine- to medium-grained, thin- to thick-bedded sandstone with few intercalations of medium- to coarse-grained units; massive lime- and dolostones. Fragmented and articulated marine fossils; bioturbation; plant remains.	Sm, Smc, Sp, Spr, St, Sh, Fsm, Dm, Dms, Lm	Shoreface facies association
5 Beach	Cross-bedded fine- and medium-grained sandstones and very thick-bedded, structureless, massive sandstones. High- and low-angle planar cross-bedding, horizontal bedding; bioturbation.	Sp, Sl, Sh, Sm, Smc, St, Fsm	
6 Estuarine facies	Interlayered massive, thin- to medium-bedded claystone and horizontal laminated fine-grained sandstone; thin- to medium-bedded sandstone. Bioturbation; abundant plant material.	Smc, Sh, St, Fsm, Fr	Marginal marine facies association
7 Lagoonal facies	Thin- to medium-bedded clay- and mudstones, intercalations of thin-bedded sand-, silt- and dolostones. Relicts of horizontal lamination. Thin- to medium-bedded lime- and dolomites; (algal-) lamination and massive. Fragmented and articulated marine fossils; bioturbation; plant material.	Sm, Sr, Fsm, Fr, Fl, Lm, Lms, Dm, Dmr, Dl	
8 Tidal flat	Thin- to medium-bedded sand- and claystones. Ripple cross-lamination, flaser bedding, horizontal lamination, trough and low-angle planar cross-bedding. Thin-bedded limestones; massive and horizontal (algal-) lamination Bioturbation; fragmented shell material; plant material.	Sm, Smc, St, Sr, Fsm, Fl, Fr, Ll, Lms	
9 Marsh	Thin- to medium-bedded sand- and claystones. Ripple cross-lamination, horizontal lamination, trough and low-angle planar cross-bedding. Colour mottling; rootlets; bioturbation.	Smc, St, Fsm, Fr, Fl	
10 Coastal Plain/ Fluvial channels and floodplain	Fine- to medium-grained, thick-bedded sandstones intercalated with clay- and siltstones; partly incised channel structures; ripple cross-lamination, horizontal bedding, cross-bedding (low-angle planar and trough). Colour mottling; rootlets; bioturbation; plant fragments.	St, Str, Sp, Sh, Ss, Sm, Smc, Fsm, Fr, Fl	

A total of ten sedimentary environmental facies were distinguished. These can be grouped into four facies associations: the shelf facies association, the shoreface facies association, the marginal marine facies association and the coastal plain facies association. Table 3.2 provides an overview of the different environmental facies, the facies associations, the corresponding sedimentary characteristics and lithofacies types.

3.2.1 Shelf facies association

The shelf facies association comprises the open siliciclastic and mixed siliciclastic-carbonate shelf and the transition zone. Both environments are part of the (siliciclastic) shoreline profile (Fig. 3.1).

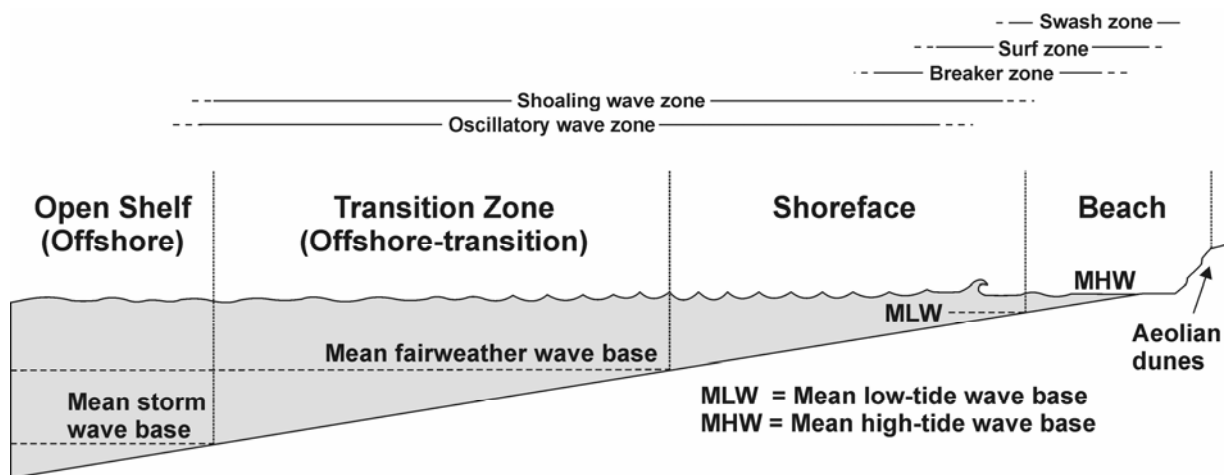


Figure 3.1: Generalized (siliciclastic) shoreline profile with depositional facies of the shelf and the shoreface facies association (modified from Reading and Collinson, 1996).

The siliciclastic and the mixed siliciclastic-carbonate shelf facies are distinguished by their content of carbonates. Within the siliciclastic shelf facies carbonates and dolomites are rare. The mixed siliciclastic-carbonate shelf facies on the other hand comprises more carbonatic, dolomitic and marly lithologies (lithofacies types: Lm, Lms, Lmr, Lk, Lkr, Ll, Lrs, Dm, Dms, Dl and Dls). Some stratigraphic intervals, as the Naur Formation, are entirely made up of carbonates. Therefore, the facies interpretation in the logged sections (Appendix I) combines the siliciclastic and the mixed siliciclastic-carbonate shelf simply as ‘Open Shelf’. ‘Open’ refers to sedimentation below the mean storm wave base (Fig. 3.1). The transition zone represents the shift from offshore to shoreface conditions (Fig. 3.1) and is characterized by regular intervals of storm influenced sedimentation.

Powell (1989; 1996) regarded the mid Cretaceous shelf system of North/Central Jordan as a carbonate ramp that was succeeded by a rimmed shelf (*sensu* Tucker and Wright, 1990b). The carbonate ramp existed during the deposition of the Naur Formation and fits well with the generalized shoreline profile. During the F/H/S and the Wadi As Sir formations a rimmed shelf with a wide shelf lagoon developed (Fig. 2A).

A shelf lagoon can be 10’s to 100’s of kilometres wide and comprise diverse sediments, ranging from low energy muddy deposits with patch reefs to high energy carbonates (Moore, 2001). The character and dimension of the shelf lagoon depends on the degree of protection provided by the barrier (Tucker and Wright, 1990b). The inner margins of the shelf lagoon may include tidal flats, sabkhas and clastic shorelines, and can be influenced by terrigenous siliciclastics.

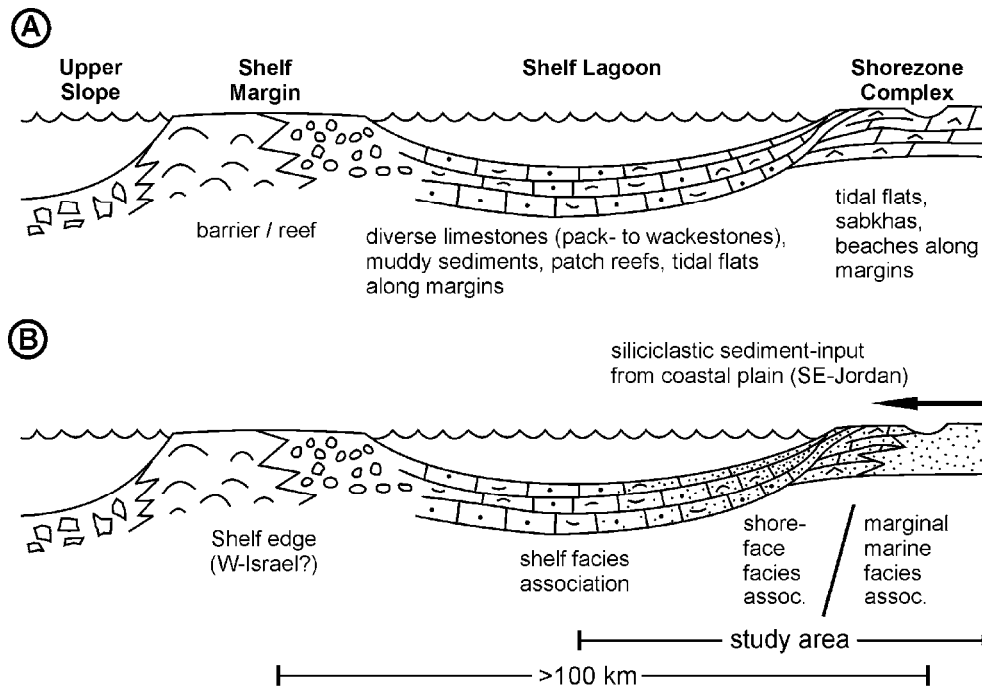


Figure 3.2 A) Facies belts of a schematic rimmed shelf (modified after Wilson, 1975). **B)** Situation in SE Jordan during the deposition of the Ajlun Group.

The mid Cretaceous shelf lagoon of South Jordan, which was more than 100 km wide, was clearly influenced by siliciclastic input from the coastal plain (Fig. 3.2B). The shelf edge was located approximately at the recent Mediterranean shoreline (Powell et al., 1996). High and low energy deposits point to moderate protection provided by the assumed shelf edge barrier, consisting most probably of patch reefs (Powell et al., 1996).

Since the shelf edge is not exposed within the study area and due to the noticeable siliciclastic input, the presented facies analysis follows the siliciclastic shoreline profile shown in figure 3.1. This approach assures a coherent analysis and description of the carbonate facies in combination with the various siliciclastic depositional facies.

Facies 1: Siliciclastic shelf

Description

The siliciclastic shelf facies mainly consists of massive silts, clays and sandstone beds (Fig. 3.3). An interbedding of thin sand and clay layers occurs and physical sediment structures are limited. Remains of lamination are sometimes present in the clays. The clays usually display a greyish colour the silts and sandstones are yellowish-brown and sometimes reddish. Articulated and fragmented bivalves, oysters, gastropods, rudists, bryozoans, ammonites, corals, crustaceans, benthic foraminifera, shark teeth, fish scales and bone fragments occur. Ichnofossils include *Thalassinoides isp.*, *Rhizocorallium isp.* and *Chondrites isp.*. Plant and wood fragments are scarce and usually restricted to clays.

Interpretation

The massive silts and clays were sedimented from suspension fall-out below the mean storm wave base and are typical for mid-shelf deposits (Walker and Plint, 1992; Johnson and Baldwin, 1996). The interbedded thin sand and silt layers are interpreted as the result of episodic storm events (Walker and Plint, 1992; Johnson and Baldwin, 1996). The lack of any primary sedimentary structures and bedding can be explained by total homogenisation of the sediment due to intense bioturbation (Walker and Plint, 1992; Bromley, 1996). The occurring ichnofossils are part of the *Cruziana* ichnofacies (Pemberton et al., 1992), which are reported from siliciclastic dominated shallow shelf environments (Bromley, 1996).

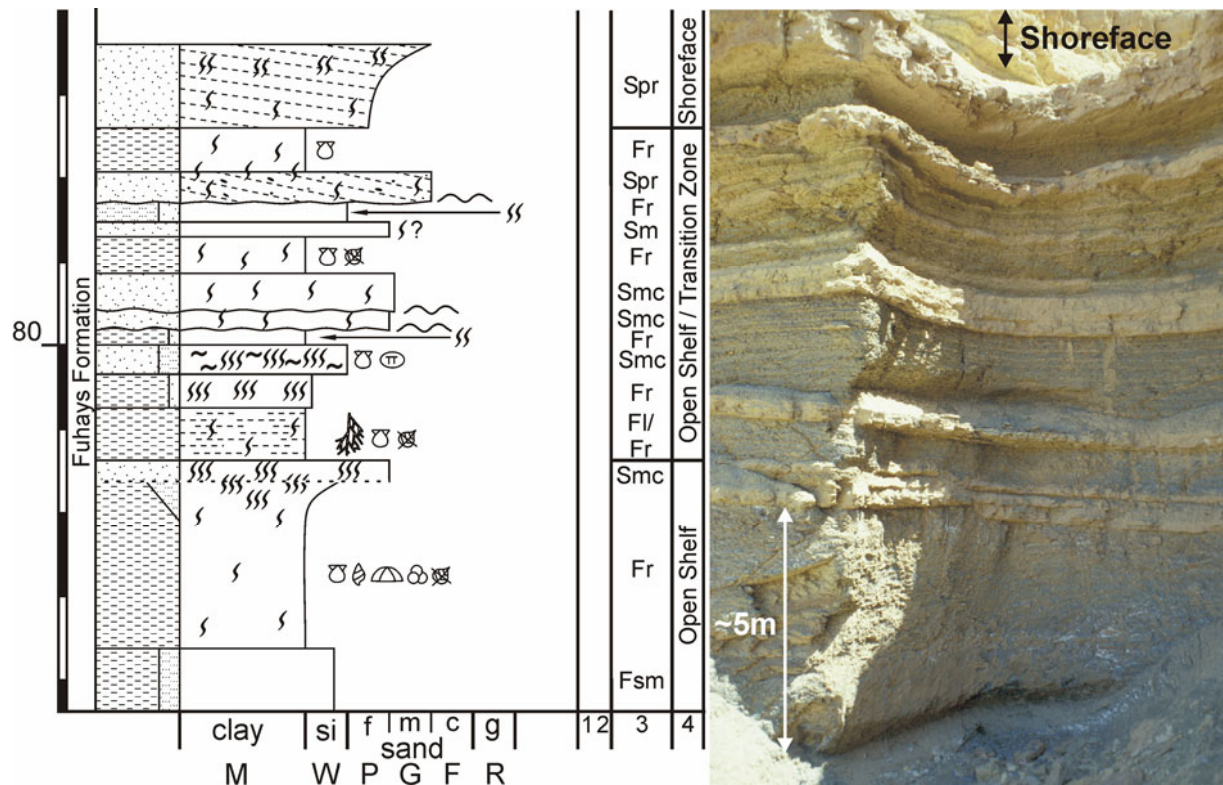


Figure 3.3 Example of siliciclastic shelf and transition zone deposits (Fuhays Formation, section 6). The interbedded sand and clay deposits are overlain by sandy shoreface sediments. The erosional features of the upper part of the outcrop point to storm events, indicating the deposition in the transition zone (legend and complete section see Appendix I).

Facies 2: Mixed siliciclastic-carbonate shelf

Description

This facies consists of thin- to thick-bedded greyish-yellow carbonates and dolomites, and greyish mudstones and marls (Fig. 3.4). Thin- to thick-bedded, yellowish-brown sand and silt beds are rarely intercalated. The limestones can be classified as wackestones, wackepackstones, grainstones and rud-floatstones (Berndt, 2002). Chert nodules (Fig. 3.5A) and matrix supported shell beds occasionally occur. Primary sedimentary structures in the limestones and dolomites include wavy bedding, horizontal bedding and lamination (Fig. 3.5B and 3.6). Mudstones, marls and sandstones are usually massive, though sandstones may also display planar cross-stratification. Bioturbation occurs in various degrees within this facies. Identifiable ichnotaxa include *Diplocraterion isp.* and *Thalassinoides isp.*. The body fossil content is very similar to facies 1. Typically are monospecific oyster associations, e.g. within the F/H/S Formation (Fig. 3.5C). These oyster beds consist of articulated individuals and internal moulds. Plant remains and glaucony grains occur scarcely.

Interpretation

According to Berndt (2002) most of the wackestones were deposited under low water energy conditions. The grainstones were sedimented in agitated water, above the mean fair-weather wave base. The rud-floatstones point to a general shallow marine environment. Wavy lamination in some limestone beds can be interpreted as algal boundstones which were deposited in an intertidal (possibly to supratidal) environment (Shinn, 1983). This means that parts of the shelf system must have been emerged, as supposed by Powell et al. (1996). Plant remains and the abundance of oysters point to a nearshore setting. All these observations fit a shelf lagoonal depositional environment. The carbonates were deposited on a shelf under low siliciclastic input conditions, as suggested by the dominantly fine grained nature of the siliciclastic sediments and the high carbonate content within this facies. An observation that

also fits a shelf lagoonal setting. To use the glauconies as an environmental indicator is critical. A 'classic' approach (e.g. Odin and Matter, 1981) favours an open marine setting and low sedimentation rates. More recent studies (Chafetz and Reid, 2000) show that a glauconite formation is also possible under shallow-water conditions (10 metres and less) and average sedimentation rates. Massive sediment beds result from intense bioturbation, homogenising the sediment (Bromley, 1996). The dolomites are most probably of secondary, diagenetic origin (Füchtbauer, 1988; Morrow, 1990). The occurrence of matrix supported shell beds (tempestites) indicates occasional major storm events (Aigner, 1985). The monospecific oyster beds with articulated individuals point to low energy environments. Such monospecific fossil assemblages may also indicate high environmental stress, e.g. hypersaline or brackish environments (Prof. Dr. F. Fürsich, personal communication, 1999). The occurring chert layers/nodules in some limestone horizons are most probably the result of bioturbation related silica diagenesis (Bromley and Ekdale, 1984; Füchtbauer and Valetton, 1988) in echinoid and *Thalassinoides*-like burrows.

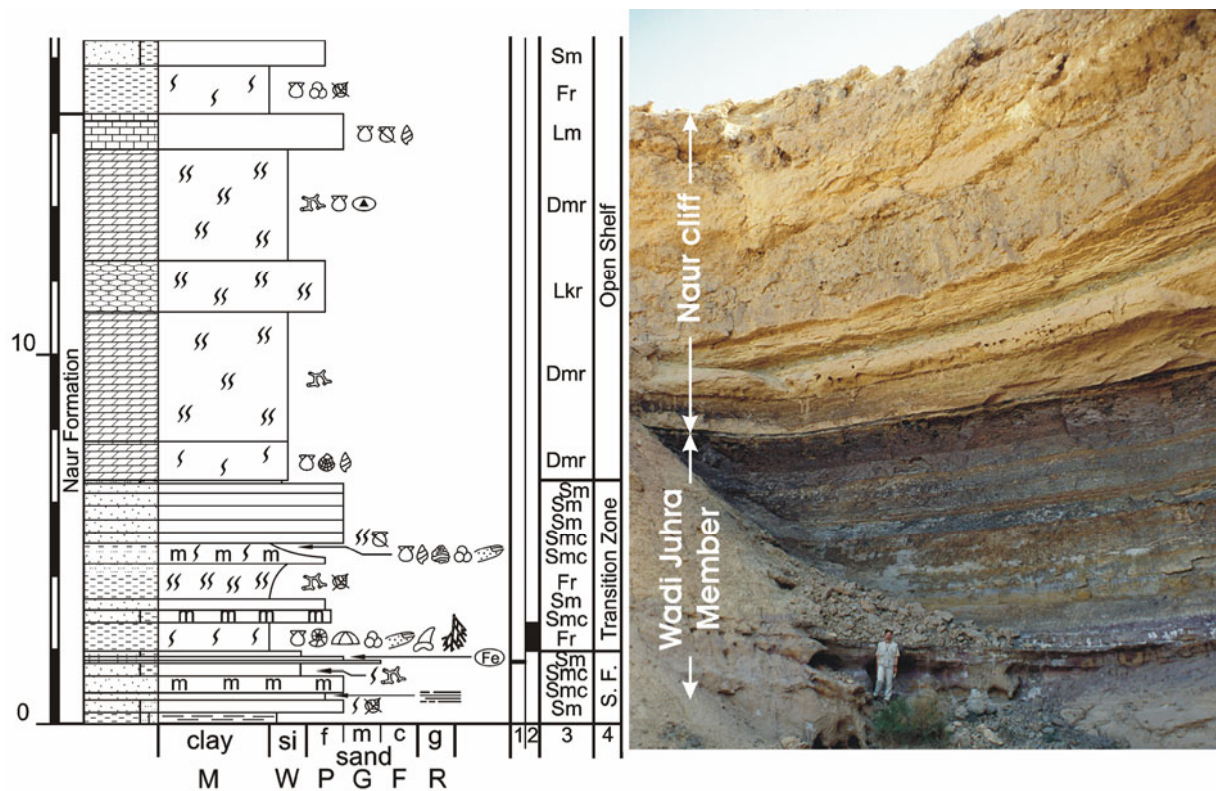


Figure 3.4 The Naur cliff as typical example for a mixed siliciclastic-carbonate shelf facies (carbonate ramp setting). The sediments of the Wadi Juhra Member represent the siliciclastic dominated transition zone. The graphic-log (part of section 7) matches the outcrop photo on the right. The yellow colours mark the beginning of the limestones and dolomites (legend and complete section see Appendix I).

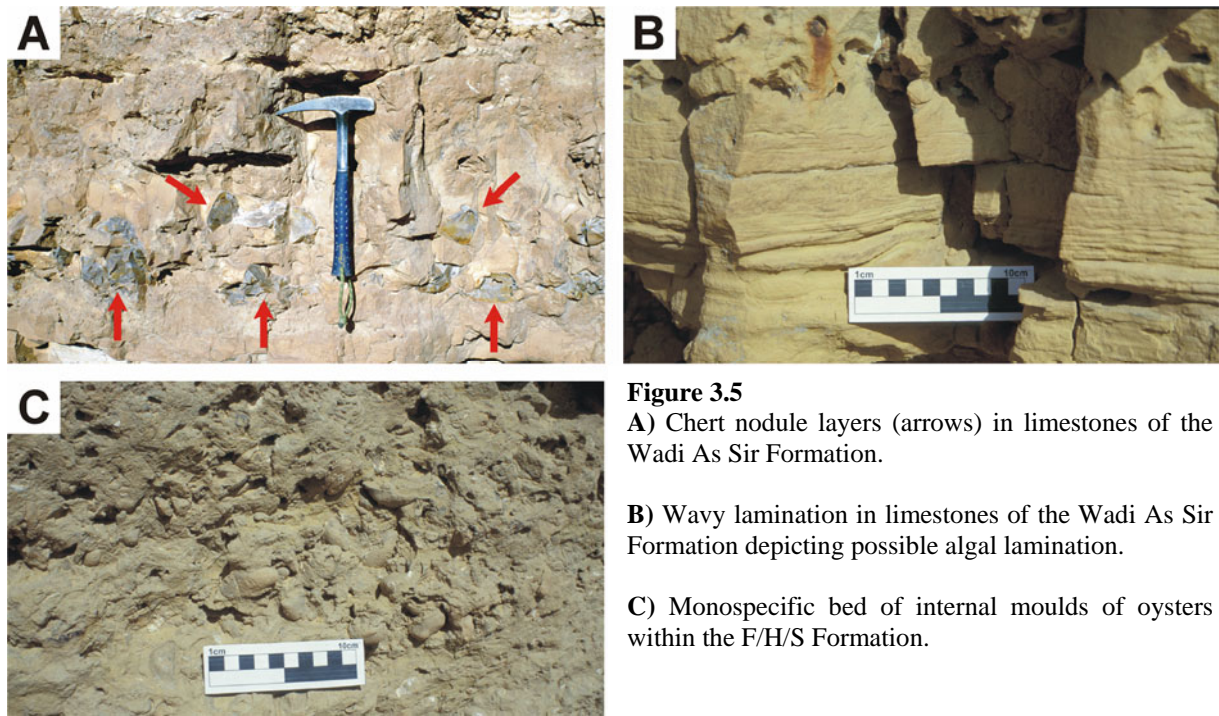
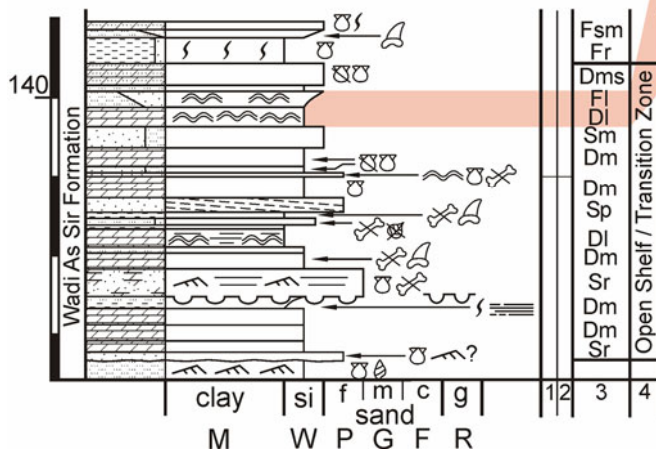


Figure 3.5
 A) Chert nodule layers (arrows) in limestones of the Wadi As Sir Formation.
 B) Wavy lamination in limestones of the Wadi As Sir Formation depicting possible algal lamination.
 C) Monospecific bed of internal moulds of oysters within the F/H/S Formation.

Figure 3.6

Parts of the Lower Wadi As Sir Formation of section 6. The dominance of dolomites and the wavy horizontal lamination, interpreted as algal lamination, point to a sedimentation within a shelf lagoon. Using the general shoreline profile, the sediments are part of the open shelf and/or the transition zone (legend and complete section see Appendix I).



Facies 3: Transition zone

Description

The transition zone is situated between the mean fair-weather wave base and the mean storm wave base (Fig. 3.1). Deposits of the transition zone comprise medium to thick bedded, calcareous and/or argillaceous sandstones as well as medium to thick bedded silt- and clay-/marlstones (Figs. 3.4 & 3.7). Intercalation of carbonates and dolomites occur and generally correspond to the carbonates of the mixed siliciclastic-carbonate shelf. Sandstones exhibit horizontal bedding, medium scale trough cross-bedding and ripple cross-lamination (Fig. 3.7

A+B). Faint lamination occurs in claystones and marls. The gross of the deposits are structureless and massive. Identified ichnofossils include *Chondrites isp.*, *Thalassinoides isp.* and *Rhizocorallium irregulare*. The fossil content of the transition zone sediments includes bivalves, brachiopods, oysters, gastropods, echinoids, rudists, benthic foraminifera, crustaceans, ammonites, fish scales, fish/shark teeth and bone fragments. Reworked material as clay clasts, shell fragments and glaucony occurs. Wood fragments and plant remains are scarce features in the transition zone. Shell beds, consisting of fragmented bivalves, occur occasionally. In general, the sediment colours of the sandstones vary from yellowish to reddish. The finer grained sediments are grey, greyish-yellowish and brown.

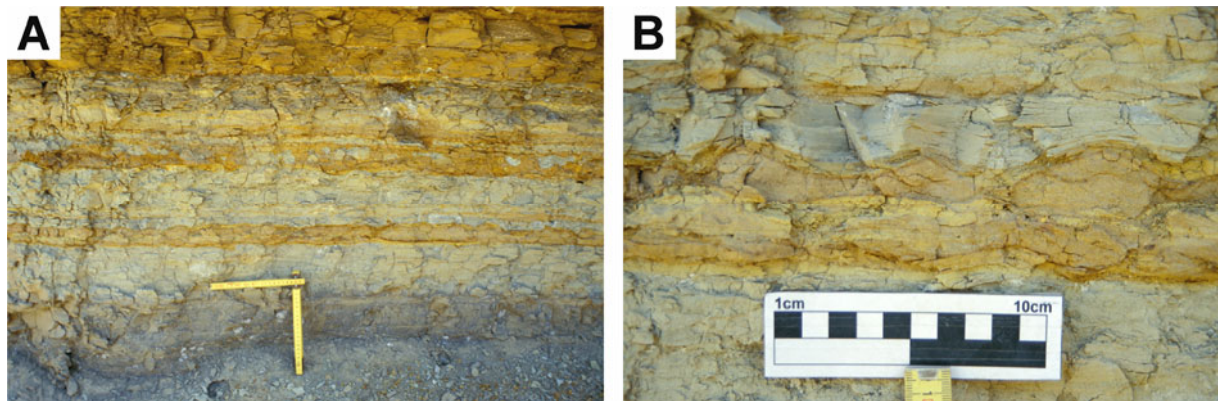


Figure 3.7 **A)** Rippled sandstone layers in mudstones (Wadi As Sir Formation of section 6, scale 20 cm). The rippled layers are interpreted to be the result of waning storm events. **B)** Close up of the lower ripple layer.

Interpretation

The gradual change in lithology to coarser grained siliciclastic sediments, the sedimentary structures and the increase in erosive contacts indicate increasing energy conditions and sedimentation between fair weather and storm wave base (Fig. 3.1). The intercalated shell beds are interpreted as tempestites/waning storm deposits (Bouma et al., 1982; Johnson and Baldwin, 1996). Ripple cross-lamination might result from currents produced by waning storm events (Johnson and Baldwin, 1996). The trough cross-bedded sand beds represent subaqueous sand dunes/waves of various sizes (Bouma et al., 1982). The finer grained, structureless sediments result from suspension fall out (Walker and Plint, 1992; Johnson and Baldwin, 1996). Limestone and dolomite beds formed under shallow water conditions, probably on morphologic highs, protected from high siliciclastic input (Wright and Burchette, 1996). Sections with thin-bedded interlayers of sand and clay might indicate a tidal influence (Terwindt, 1988). Massive sediment beds are probably the result of intense bioturbation (Walker and Plint, 1992; Bromley, 1996). The occurring ichnotaxa are part of the *Cruziana* ichnofacies and characteristic for the transition zone (Pemberton et al., 1992).

3.2.2 Shoreface facies association

This facies association includes the shoreface and the beach facies. Both depositional environments are located above the mean fair-weather wave base (Fig. 3.1) and represent dynamic high energy environments (e.g. Davis, 1985b; Reading and Collinson, 1996). Beach settings are associated with estuaries, river deltas, tidal inlets, bays and lagoons (e.g. Boggs, 1995).

Facies 4: Shoreface

Description

The shoreface sediments mainly consist of thin- to thick-bedded, yellowish-brown to red, partly calcareous, fine- to medium-grained sandstones (Fig. 3.8 and 3.9 A+B). Intercalations of medium to coarse grained sandstones and few silty and clayey beds occur. Sedimentary structures include planar cross-stratification, medium- to large-scale trough cross-bedding, ripple lamination (Fig. 3.9A), horizontal bedding and low angle planar cross-bedding. Foresets can be lined with gravel stringers (Fig. 3.9B), clay clasts, coarse sand or mud drapes and may exhibit normal grading. Massive, bioturbated sandstone units also occur. Identified bioturbation marks include the ichnofossils *Thalassinoides* *isp.* (Fig. 3.9A, arrows), *Rhizocorallium irregulare*, *Rhizocorallium jenense* and *Diplocraterion* *isp.*. Body fossils include complete or fragmented bivalves, oysters and echinoids. Wood and small plant fragments, as well as glaucony grains are common in the coarse-grained sediments.

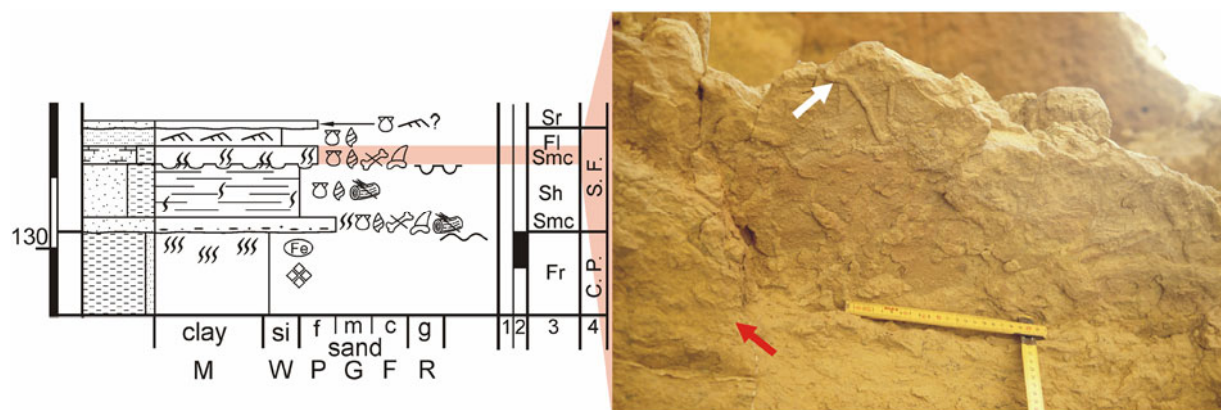


Figure 3.8 Shoreface facies in the Wadi As Sir Formation of section 6. The red shaded interval on the left hand side represents the argillaceous sandstone on the corresponding photo. The white arrow shows bioturbation, the red arrow points to a load cast (legend and complete section see Appendix I).

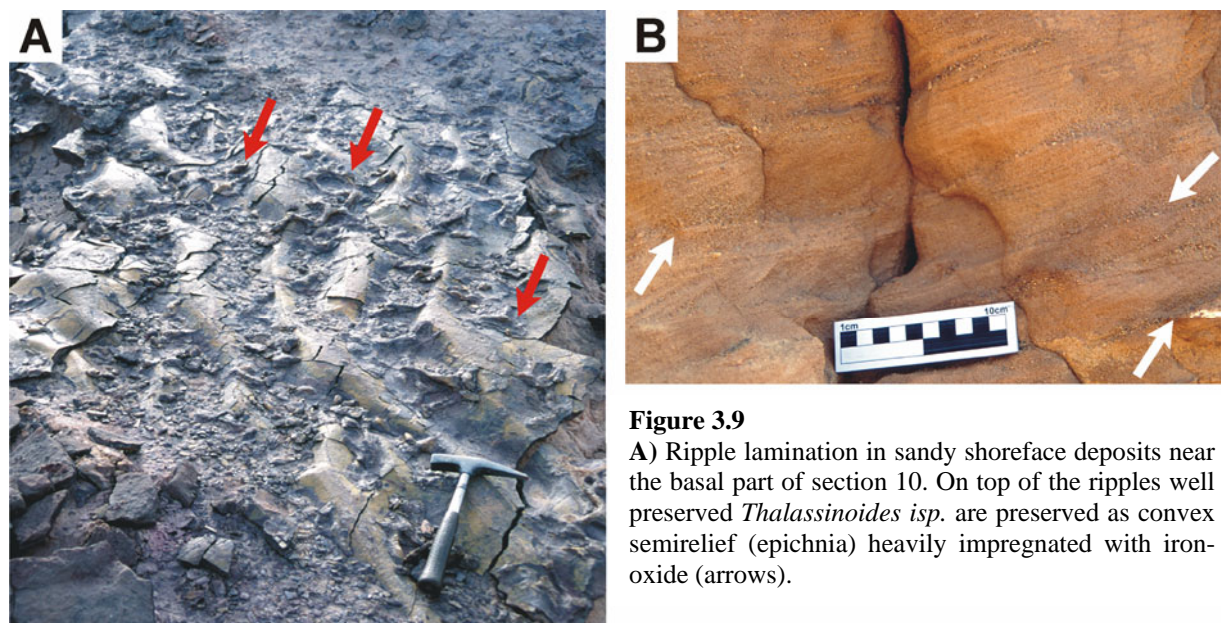


Figure 3.9

A) Ripple lamination in sandy shoreface deposits near the basal part of section 10. On top of the ripples well preserved *Thalassinoides* *isp.* are preserved as convex semirelief (epichnia) heavily impregnated with iron-oxide (arrows).

B) Gravel stringers (arrows) in a fine- to medium-grained sandstones of shoreface deposits of section 10 (basal part).

Interpretation

The predominance of physical sedimentary structures formed under high-energy conditions, supports the interpretation that sedimentation took place in a shoreface environment (Boggs, 1995). Planar and trough cross stratification, as well as ripple cross-lamination are formed under oscillatory and unidirectional flow conditions (McCubbin, 1982; Niedoroda et al., 1985; Collinson and Thompson, 1989). Planar cross-bedding for example, is formed by migrating sand waves while trough cross stratification is formed in subaqueous dunes (McCubbin, 1982). The occurrence of graded foresets and mud drapes may indicate a tidal influence, as does occasionally occurring flaser bedding (Reineck and Singh, 1973). The occurrence of shell fragments and small clay clasts points to reworking in a high-energy environment. Since in situ formation of glaucony in a sand-dominated high energy environment is most unlikely (Odin and Matter, 1981), the occurring glaucony is also interpreted as reworked material. The identified ichnotaxa belong to the Skolithos and Cruziana ichnofacies (Pemberton et al., 1992). The Skolithos ichnofacies is indicative for high energy environments with loose particulate substrates. Seaward it grades into the Cruziana ichnofacies diagnostic for medium to low energy conditions between the daily wave base and the storm wave base (Bromley, 1996).

Facies 5: Beach*Description*

The deposits of the beach facies consist of thin to thick-bedded greyish-yellow to reddish sandstones. The sediments are often structureless massive, but also display medium scale trough cross-bedding, high- and low-angle planar cross-bedding and horizontal bedding. Some foresets are lined with gravel stringers and mud drapes. Flaser bedding and bioturbation occur. The sandstones often contain small wood fragments, plant remains and shell fragments. Small to medium scale channel structures can be observed.

Interpretation

The physical sedimentary structures point to deposition under high energy, near shore conditions (Clifton, 1981; Davis, 1985b). Low-angle planar cross-bedding indicates the zone of wave swash (Davis, 1985b; Collinson and Thompson, 1989). Steep planar cross-bedded sand beds are interpreted as the result of rip currents (Gruszczynski and Rudorobek, 1993). Trough cross-bedding can form in all sub-environments of in the beach facies, e.g. in the zone of wave reformation in the surf zone (Davis, 1985b). Flaser bedding and the occurrence of mud drapes point to a potential tidal influence (Reineck and Singh, 1980). Massive sand beds are the result of sediment homogenization by intensive bioturbation (Bromley, 1996). The channel structures are interpreted as remains of small inlet (fluvial/tidal) or rip channels (McCubbin, 1982; Davis, 1985b).

3.2.3 Marginal marine facies association

The marginal marine facies association comprises estuarine, lagoonal, marsh and tidal flat facies (Fig. 3.10). For example: lagoons are areas of shallow water confined from the open sea by barrier islands (Reading and Collinson, 1996). This definition fits also to parts of the estuarine facies, e.g. the central basin (Fig. 3.10), which hinders a clear differentiation (Reinson, 1992). An overlap also exists for the marsh and tidal flat facies. Both environments are tidal influenced and can be distinguished only by an often subtle, pedogenic overprint that characterizes the marsh facies. Therefore the position of the deposits within the sedimentary succession was taken into account in addition to facies interpretation based on the lithofacies.

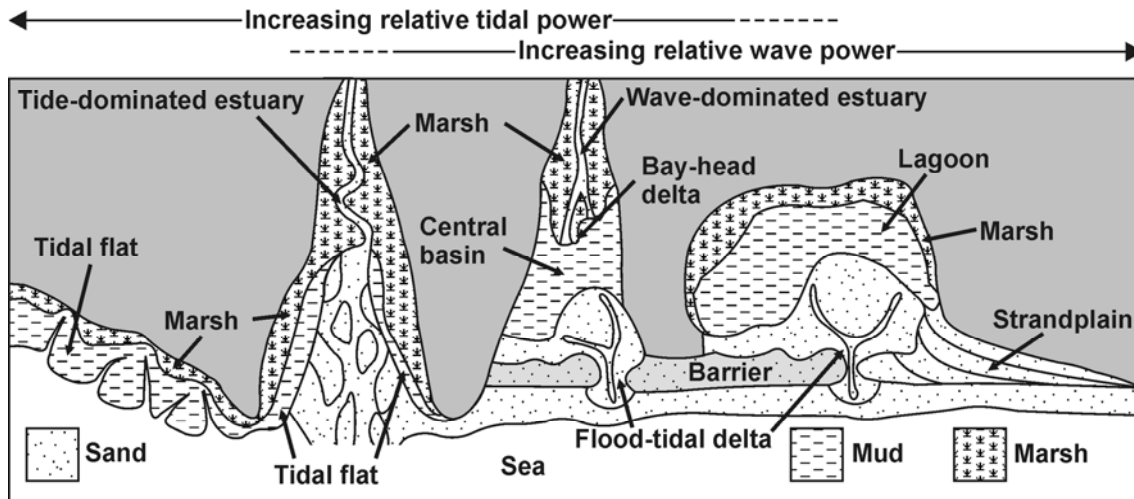


Figure 3.10 Plan view model of transgressive coasts, showing the relationship and similarities of the marginal marine environments (modified after Dalrymple et al., 1992; and Reading and Collinson, 1996).

Facies 6: Estuarine facies

Description

The estuarine facies is characterized by interlayered thin- to medium-bedded, greyish to yellow-brown clay- and yellowish-brown to reddish-brown sandstones. The sandstones often show horizontal lamination. The claystones are usually massive with rare faint lamination. Occasionally medium-bedded sandstone beds display trough cross-bedding. Bioturbation occurs throughout the facies. Identified ichnotaxa include *Thalassinoides isp.* and *Rhizocorallium irregulare*. Oysters, bivalves, echinoids, wood and plant fragments as well as few glaucony occur.

Interpretation

The occurrence of both, clay- and sandstones, suggests deposition in a tidal-influenced, estuarine environment (Reinson, 1992). Horizontal lamination in the coarse-grained sediments might be the result of plane-bed flow conditions under changing tidal currents (e.g. Reineck and Singh, 1980). The lamination in the claystones points to suspension fall out (Reinson, 1992). The trough cross-bedded sandstones can be interpreted as tidal bar, part of an inlet channel (Dalrymple et al., 1992; Reinson, 1992), pointing to a wave dominated character of the estuarine complexes. Massive sediment beds are attributed to extensive bioturbation that homogenizes the sediment (Bromley, 1996). The type of bioturbation and the scarce glaucony content point to a marine influence.

Facies 7: Lagoonal facies

Description

The sediments of the lagoonal facies are dominated by various bedded greyish clay- and mudstones. Thin- to medium-bedded, yellowish-brown sand- and siltstones are intercalated. Thin- to medium-bedded, yellowish-brown lime- and dolomites also occur. In some stratigraphic intervals, e.g. within parts of the Upper Wadi As Sir Formation (Fig. 3.6), limestones and dolomites (wackestones, wacke-packstones, grainstones and rud-floatstones) with chert nodules and shell beds are dominating. Sedimentary structures in the clay- and siltstones are limited to scarce relicts of lamination. The sandstones can exhibit planar and trough cross-bedding. The lime- and dolomites may display wavy horizontal lamination. Fragmented and articulated bivalves, oysters, brachiopods, gastropods, crustaceans, benthic foraminifera, echinoids, fish/shark teeth, fish scales, bone fragments, wood and plant remains are most abundant in mudstones. Identified ichnotaxa include *Thalassinoides isp.*, *Rhizocorallium irregulare* and *Chondrites isp.*. Glaucony (Fig. 3.11A) and occasionally small

crystals of pyrite, gypsum, baryte, calcite or dolomite are found in the claystones (Fig. 3.11B). The size of these crystals ranges from a few millimetres (dolomite) to up to 1-2 centimetres (gypsum and calcite).

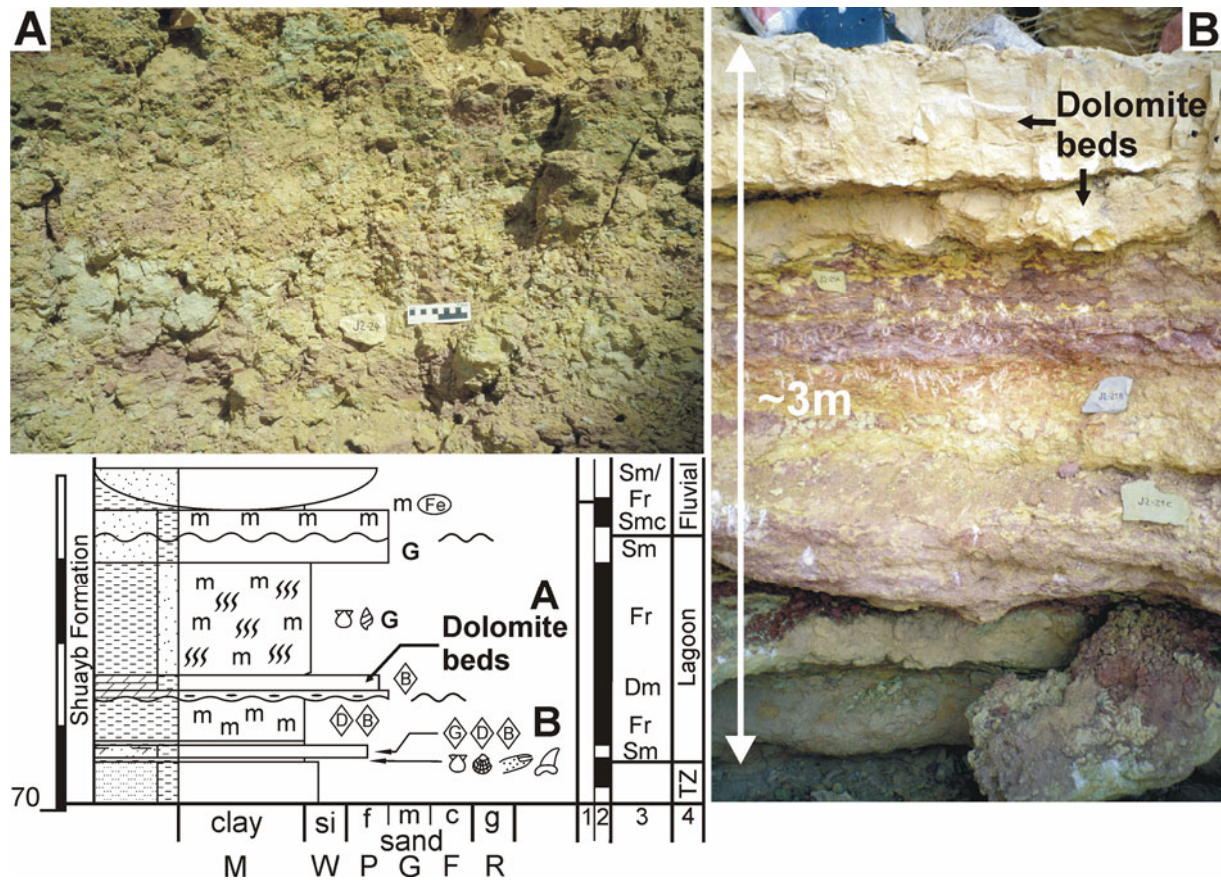


Figure 3.11 Part of the Shuayb Formation of section 8 depicting lagoonal to estuarine sediments (legend and complete section see Appendix I). **A**) Glaucony bearing, colour mottled, intensely bioturbated mudstone. **B**) Dolomitic lagoonal mudstones.

Interpretation

The dominance of fine-grained sediments and the lack of high-energy sedimentary structures indicate a protected depositional environment (Reading and Collinson, 1996). Claystone beds result from suspension fall out (McCubbin, 1982; Reinson, 1992; Reading and Collinson, 1996) and are typical of inner lagoon areas. Intense bioturbation leads to a homogenisation of the sediment, destroying most of the primary sedimentary structures (Bromley, 1996). The silt- and sandstone beds may represent deposits of small flood tidal deltas or wash-over fans (Reinson, 1992 and Fig. 3.10). The carbonate dominated successions, e.g. the upper parts of the Wadi As Sir Formation, correspond to shallow, low energy parts of a shelf lagoon. Dolomite beds are most probably of secondary, diagenetic origin (Tucker and Wright, 1990a). Wavy horizontal lamination within some limestones points to a deposition of these sediments as intertidal to supratidal algal boundstones (Shinn, 1983). The body fossil assemblage points to a restricted, hypersaline environment (Berndt, 2002), which fits the lagoonal facies. The occurrence of evaporate mineral crystals, e.g. dolomite and gypsum, within the sediments supports the interpretation of a hypersaline environment (Kendall, 1992; Kendall and Harwood, 1996). Glaucony can form especially in the inner, low energy parts of a lagoon (Galloway and Hobday, 1996).

Facies 8 and 9: Tidal flat and marsh

Description

The tidal flat and marsh facies comprise thin- to medium-bedded sand- and claystones, clayey sandstones and sandy claystones. Sediment structures include horizontal lamination, flaser bedding, ripple cross-lamination, trough cross-bedding, low-angle planar cross-bedding and mud drapes. Channel structures (Fig. 3.12) with trough cross-bedding and rip-up clasts occur in some sections. Bioturbation and plant and wood fragments are common. Roots, rootlets and small slickensides in clayey deposits are restricted to sediments of the marsh facies. Claystone beds often exhibit a characteristic colour mottling with colours ranging from pale yellowish-grey to dark red. In general, sediment colours range from white and yellowish-grey for the sandstones to yellowish-brown (Fig. 3.12) to reddish and grey for the claystones. Red colours are more often found in the marsh facies. Small shell fragments occur in more marine dominated parts of the tidal flat facies.

Interpretation

Mud drapes on the foresets of cross-bedded sandstones are clearly indicating a tidal influenced environment (Boggs, 1995). The small-scale changes in grain-size within these facies can also be explained by tidal processes (Dalrymple, 1992). Flaser bedding and ripple cross-lamination point to tidal currents (Reineck and Singh, 1980). Massive sand- and claystone beds are most probably the result of extended bioturbation of the sediment, removing any trace of primary sedimentary structures (Bromley, 1996). Bioturbation in general is a common feature in both, marsh (Frey and Basan, 1985) and tidal flat (e.g. Reineck and Singh, 1980) deposits.

Colour mottling and the formation of small dimensional slickensides within clayey deposits point to incipient soil-forming processes, indicating a prolonged period of sub-aerial exposure (Buurman, 1980; Bown and Kraus, 1981). These sediment features are common in the marsh facies. Colour mottling, however, might also occur in the tidal flat facies as a result of bioturbation (Bromley, 1996). Sandy channel structures occurring in both facies can be interpreted as fluvial channels in the marsh facies or as tidal drainage systems crossing the marsh land and/or the tidal flat (Reineck and Singh, 1980; Frey and Basan, 1985). Compared to the tidal flat facies, the marsh facies displays a noticeable pedogenic and fluvial influence (Frey and Basan, 1985). The wood fragments indicate proximity of a vegetated main land.

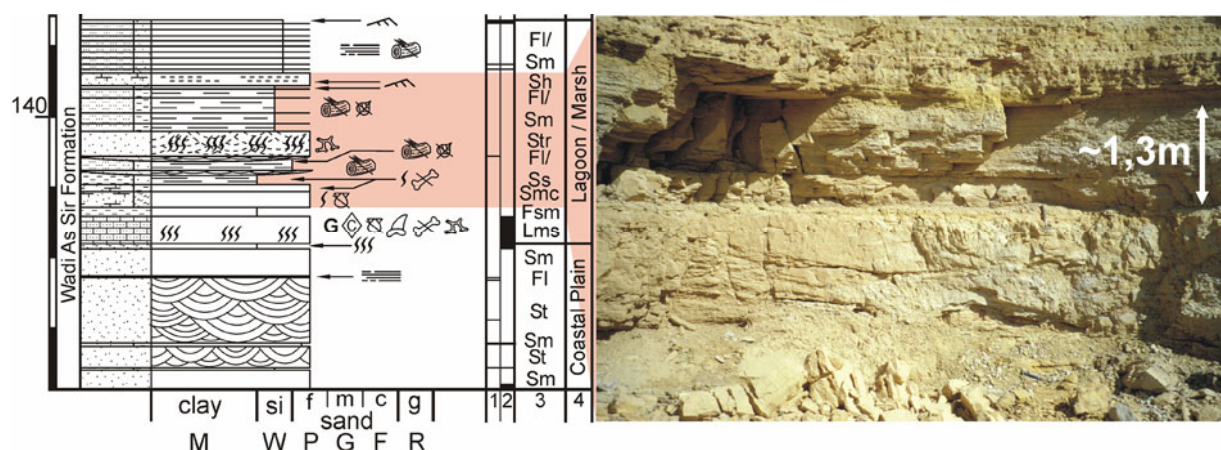


Figure 3.12 The lagoon/marsh facies in the Wadi As Sir Formation of section 8. The red shaded interval corresponds to the photo (legend and complete section see Appendix I). The lower half of the photo shows a channel-like structure that may be interpreted as small fluvial or tidal channel.

3.2.4 Coastal plain facies association

The coastal plain facies association includes coastal plain, fluvial channel and floodplain facies depositional environments. The term coastal plain was applied when sedimentary successions included marsh like deposits. The fluvial channels and floodplain facies forms the main part of this facies association. Especially the sections east of the Batn El Ghul field station, e.g. sections 11 to 15, are dominated by the fluvial channel and floodplain facies.

Facies 10: Coastal plain/fluvial channels and floodplain

Description

The sediments of this facies are dominated by fine- to medium-grained, thick-bedded sandstones (Fig. 3.13A). Argillaceous sandstones, sandy claystones, siltstone beds and sandy gravel beds occur in a minor degree. In some parts of the sections, especially within the Batn El Ghul Group east of section 10, thin- to thick-bedded claystone beds are intercalated. The sand bodies often form large channel structures, which are incised in the clay. Sedimentary structures in the sand beds include medium- to large-scale trough cross-bedding, planar cross-bedding, horizontal bedding, low angle planar cross-bedding and, to a minor extend, ripple cross-lamination. Gravel stringers may occur at the base of troughs, graded foresets, silt lenses and clayey rip-up clasts can also be found. The claystones exhibit colour mottling and small slickensides. Intercalated very thin, fine-grained sand-/siltstone layers occur in claystones. These beds sometimes display horizontal lamination or ripple cross-lamination. Bioturbation and root traces occur infrequently (Fig. 3.13B). Marine fossils are completely missing, wood and plant fragments (Fig. 3.13C) can be found occasionally. The colour of the sediments varies widely. The sandstones are greyish-white to yellow and reddish. The claystones are very often red or purple, greyish to yellow-brown colours also occur.

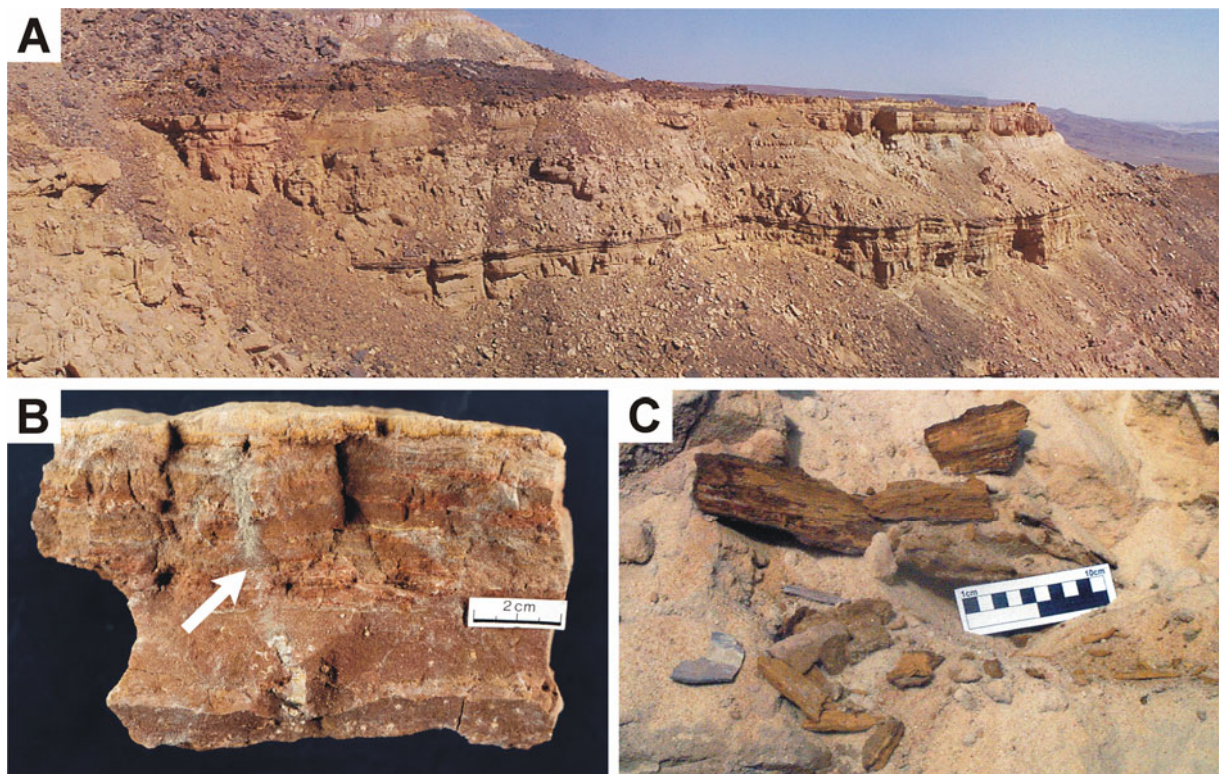


Figure 3.13 **A)** Sand dominated succession of fluvial sediments, Wadi As Sir Formation of section 9 (approximately metres 110 to 145). **B)** Specimen of a palaeosol developed on a fluvial floodplain to marsh (section 9, sample J9-36). The arrow marks a calcareous rootlet. **C)** Wood fragments in fluvial sands of section 9 (metres 106 to 110).

Interpretation

The sedimentary structures of the sandstones point to bed-load transport (Miall, 1996). The trough-cross bedded sandstones are interpreted as channel fill deposits, created by migrating subaqueous dunes. Planar cross bedding was formed by transverse and linguoid bedforms (Miall, 1996). Low-angle planar cross-stratification may be produced by downstream accretion along longitudinal bars or in scour fills and washed out dunes (Miall, 1996). Ripple cross-lamination, both in the sand- and silt-sized deposits, is the result of a low to medium flow regime. Horizontal lamination was caused by plane-bed/critical flow conditions (Collinson and Thompson, 1989). Silt- and claystones were sedimented mainly as overbank/floodplain deposit or in areas subject to low river flow velocities (Collinson, 1996). The high sand/clay ratio within the fluvial parts of the sections west of Batn El Ghul (sections 5-10) points to a low sinuosity/braided, bedload dominated fluvial system (Collinson, 1996; Miall, 1996). This is supported by the frequent occurrence of sand bars and channel fill deposits within the fluvial succession. East of Batn El Ghul (sections 11-15) the thickness and frequency of claystone beds increases, pointing to a low sinuosity/anastomosing river system with more mixed sediment load (Collinson, 1996; Miall, 1996). For further discussion of the river system see Chapter 3.5.

Colour mottling and slickensides were formed in the sediment by soil forming processes (Kraus, 1999; Tibert and Gibling, 1999). The root-horizons, usually occurring on top of overbank/floodplain deposits, are clear palaeosoils. The existence of small iron and baryte concretions/nodules and tiny caliche within the sediments also points to soil forming processes (Bown and Kraus, 1981; Kraus and Gwinn, 1997).

Parts of the coastal plain facies association might also be interpreted as a coastal sabkha depositional environment. Especially fine-grained, muddy sediments with reddish colours, e.g. around a height of 160 m in section 10, might fit into a sabkha environment. Occurring features like bioturbation, gypsum crystals and wood fragments have been reported from sabkha sediments (West et al., 1979), but are not exclusively indicative. Clear indicative characteristics of a sabkha environment, like evaporite casts/crystals or frequent occurrence of interbedded gypsum/anhydrite nodules (Kendall, 1992; Kendall and Harwood, 1996), are missing.

3.3 Lateral and vertical arrangement of depositional systems

Regarding the lateral and vertical stratigraphic relationship, genetically related facies were grouped into three major depositional systems (Baaske et al., 2001): (i) siliciclastic ramp system, (ii) mixed carbonate-siliciclastic ramp system and (iii) alluvial system.

3.3.1 Siliciclastic ramp system

The siliciclastic ramp system includes the marine and marginal marine facies associations. It comprises deposits of the siliciclastic shelf, transition zone, shoreface, beach, lagoonal/estuarine, tidal flat and marsh facies. The siliciclastic ramp system forms units between 3 m and 26 m thickness.

3.3.2 Mixed carbonate-siliciclastic ramp system

The mixed carbonate-siliciclastic ramp system comprises marine and marginal marine facies associations. It is similar to the siliciclastic ramp and comprises mixed carbonate-siliciclastic shelf, transition zone, shoreface, beach, lagoonal/estuarine, tidal flat and marsh facies. The major difference is a higher content of carbonates within the sedimentary succession. The mixed carbonate-siliciclastic ramp system forms units between 4 m and 20 m thickness.

3.3.3 Alluvial system

The alluvial system is equivalent to the coastal plain facies association, consisting of the coastal plain and fluvial channels/floodplain facies. The siliciclastic and mixed carbonate-siliciclastic ramp systems interfinger laterally with deposits of the alluvial system, representing the change from marine to terrestrial sedimentation. The alluvial system forms units between 6 m and 42 m thickness.

The lateral facies succession within the three depositional systems indicates that the predominantly marine part of the basin was located in the western/north-western part of the study area (west of section 11). The shoreline and the terrestrial part of the basin were situated in the south-eastern part (east of section 10).

The vertical facies succession shows that the position of the shoreline changed with time, and only once, during Cenomanian to Coniacian times, reached a position east of Batn El Ghul. Furthermore the vertical facies arrangement has a cyclothemic nature, indicated by a repeated arrangement of marine and terrestrial/alluvial deposits (Fig. 3.14).

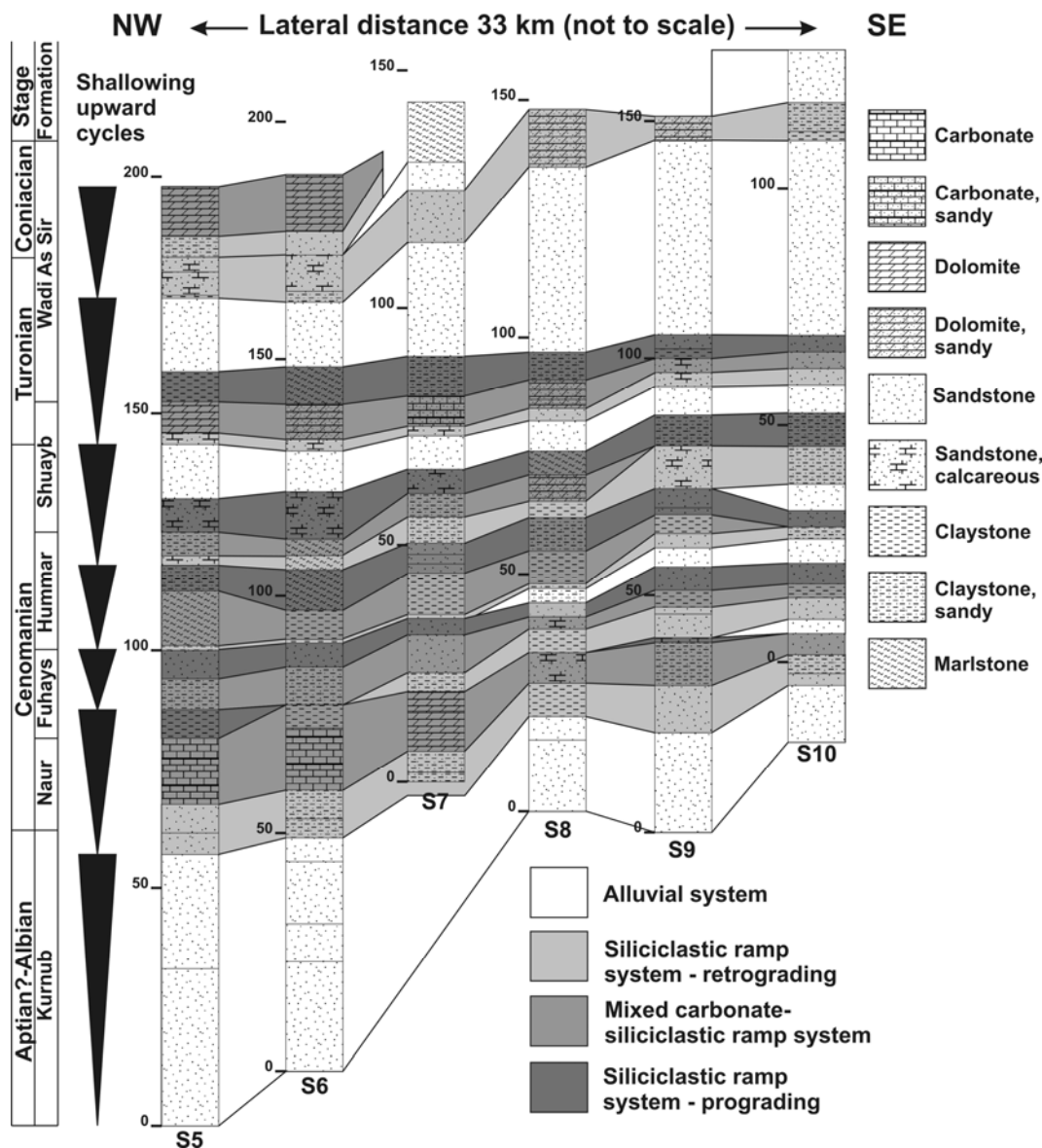


Figure 3.14 Shallowing upward cycles and cyclothem along the Naqb escarpment from Ras En Naqb (S5) to Batn El Ghul (S10).

Such a shallowing upward cyclothem starts with a first siliciclastic ramp system, which is followed by a mixed carbonate-siliciclastic ramp system, overlain by a second siliciclastic ramp system. An ideal, complete cyclothem also includes an alluvial depositional system.

Depending on the geographic position along the escarpment, a cyclothem is not necessarily completely developed. In the eastern part of the study area (east of section 10) the alluvial system makes up the bulk of the sedimentary succession, while in the western part (west of section 7) the marine depositional systems dominate (Fig. 3.14). The cyclothem is laterally remarkably continuous and display only minor changes in thickness. The cyclothem nature of the deposits is attributed to recurring sea-level fluctuations resulting in marine incursions, which reached as far as section 11, south-east of Batn El Ghul.

3.4 Characteristics of the mid-Cretaceous shelf system of South Jordan

In general, the correlation of the logged sections and the depositional environmental facies analysis show, that the proximal shelf system was mainly siliciclastic dominated (muddy to sandy), while the distal shelf was mixed siliciclastic-carbonatic to carbonatic. Even carbonate dominated stratigraphic intervals as the Naur Formation (carbonate ramp) follow that pattern.

3.4.1 Storm dominated shelf vs. tide dominated shelf, tidal regime

Facies analysis shows that both open shelf facies types contain deposits that point to episodic major storm events. Tidal signatures are limited and mainly connected to shallow water areas of the shelf. Within the transition zone the abundance of erosive sand and shell beds increases, pointing to a storm dominated shelf. Tide influenced sediments, e.g. thin interlayered sand and clays, are also present within the transition zone.

The coastal system, especially the tidal flat deposits of the marginal marine facies association, is tide influenced. Storm deposits are not present due to strong sediment reworking along the coast. Classifying the coast by its tidal range (e.g. Boggs, 1995), that is micro- (0-2 m), meso- (2-4 m) or macrotidal (>4 m), a microtidal system suits the mid-Cretaceous marine system of South Jordan best.

The fact that the storm deposits were not totally reworked by tidal influences supports the interpretation of a storm dominated shelf. The tidal influence was not strong enough to dominate the shelf system.

3.4.2 Supply dominated shelf vs. accommodation dominated shelf regime and cyclothem

According to Johnson and Baldwin (1996) variables like rate of relative sea-level rise and rate of sediment input control the sedimentation patterns of a clastic shelf. These variables result in two shelf regimes: the supply-dominated shelf regime and the accommodation-dominated shelf regime. Galloway and Hobday (1996) also conclude that the stratigraphic architecture of a clastic shelf depends on the balance of sediment supply and the creation of accommodation space. They classify the shelf systems as progradational, aggradational and transgressive. During progradation the sediment supply dominates the accommodation space (supply dominated), during aggradation both factors are balanced, while during transgression creation of accommodation space outpaces the sediment supply (accommodation dominated).

Applying the classification schemes to the mid to Late Cretaceous cyclothem of South Jordan shows that there are two types of siliciclastic ramp systems present within the cyclothem. The first is a progradational, supply dominated clastic ramp, the second a transgressive clastic ramp, where creation of accommodation space exceeds the sediment supply. The carbonate-siliciclastic ramp system is clearly accommodation-dominated. During these intervals the creation of accommodation space outpaces the siliciclastic sediment supply. The generated space on the shelf is 'filled' by carbonates, creating the mixed carbonate-siliciclastic system. Using the shelf regime classification, a complete cyclothem

starts with the alluvial system, and is followed by a transgressive siliciclastic ramp system, a mixed carbonate-siliciclastic ramp system and, finally, a progradational siliciclastic ramp system.

3.5 Fluvial styles and facies models for the mid to Late Cretaceous of South Jordan

3.5.1 Fluvial styles on the coastal plain

Looking at the fluvial intervals in the textural graphic logs reveals differences in fluvial style between the eastern sections (sections 11 to 15, east of Batn El Ghul) and the fluvial parts in the western part of the study area (sections 5 to 10, between Ras En Naqb and Batn El Ghul).

Field observations along the eastern part of the escarpment show that large sand bodies in form of channel fills are frequent, which seem to be embedded in muddy sediments. Contacts between single sand bodies seldom occur, pointing to an anastomosed to sandy meandering river system (cf. Miall, 1996, Fig. 8.8 A-P, pp. 203-205). Such a river style is sand dominated and includes fine grained sediments in form of overbank fines and floodplain deposits. Towards the West, near sections 10 and 11, the amount of sand beds increases, indicating a gradational change towards a more braided system.

The fluvial style in the western part of the study area is dominated by sand with no, or only minor, intervals of finer grained material (e.g. section 8, metres 98 to 132; section 9 metres 102 to 136). Compared to the sixteen different fluvial styles presented by Miall (1996, Fig. 8.8 A-P, pp. 203-205), the fluvial architecture points to a “deep perennial braided” or “sheetflood distal braided” fluvial system. The change from the anastomosed to the braided fluvial regime takes place between sections 10 and 11, for all stratigraphic intervals. These two sections are about 19 km apart.

3.5.2 Fluvial architectural-element analysis within the mid Wadi As Sir Formation

Fluvial architectural-element analysis is a purely descriptive method. It helps to improve fluvial facies models, since vertical profiles alone are not diagnostic for a fluvial facies. The architectural-element analysis uses eight basic elements that are proposed as constants in the fluvial environment (Miall, 1985). These elements are based on fluvial macroforms, bounded by fourth- to fifth-order surfaces (Miall, 1996), and defined by grain size, bedform composition, internal sequence and external geometry. The basic elements are: channel (CH), lateral accretion (LA), sediment gravity flow (SG), gravel bar and bed form (GB), downstream accretion (DA), sand bed form (SB), laminated sand (LS) and overbank fines (FF) (Miall, 1985; 1996). To apply this method lateral cross-sections of outcrops with at least several tens of metres width are necessary. Such a cross-section can be achieved by constructing outcrop profiles by photo mosaic. This photo mosaic is then covered by an overlay on which the architectural elements are traced (detailed method refer to Miall, 1996).

For the presented study outcrops in the fluvial part of the Wadi As Sir Formation were most suitable for an architectural-element analysis. Figures 3.14A and 3.14B display two examples from the alluvial middle part of this formation, with roughly the same stratigraphic interval in two different sections (sections 8 and 9).

Both figures show that channels (CH) of various dimensions, sand bed forms (SB) and downstream accretion elements (DA) are the dominating elements. The channel elements can include other architectural-elements of higher order. Within the studied outcrops larger channels comprise smaller channel elements, sand bed forms and downstream accretion bodies. According to Miall (1996) the dominance of DA and SB elements in sand dominated fluvial systems points to a low-sinuosity, braided river. This result supports the interpretation of the stratigraphic logs, which also point to a braided fluvial system in the western part of the study area (Chapter 3.5.1).

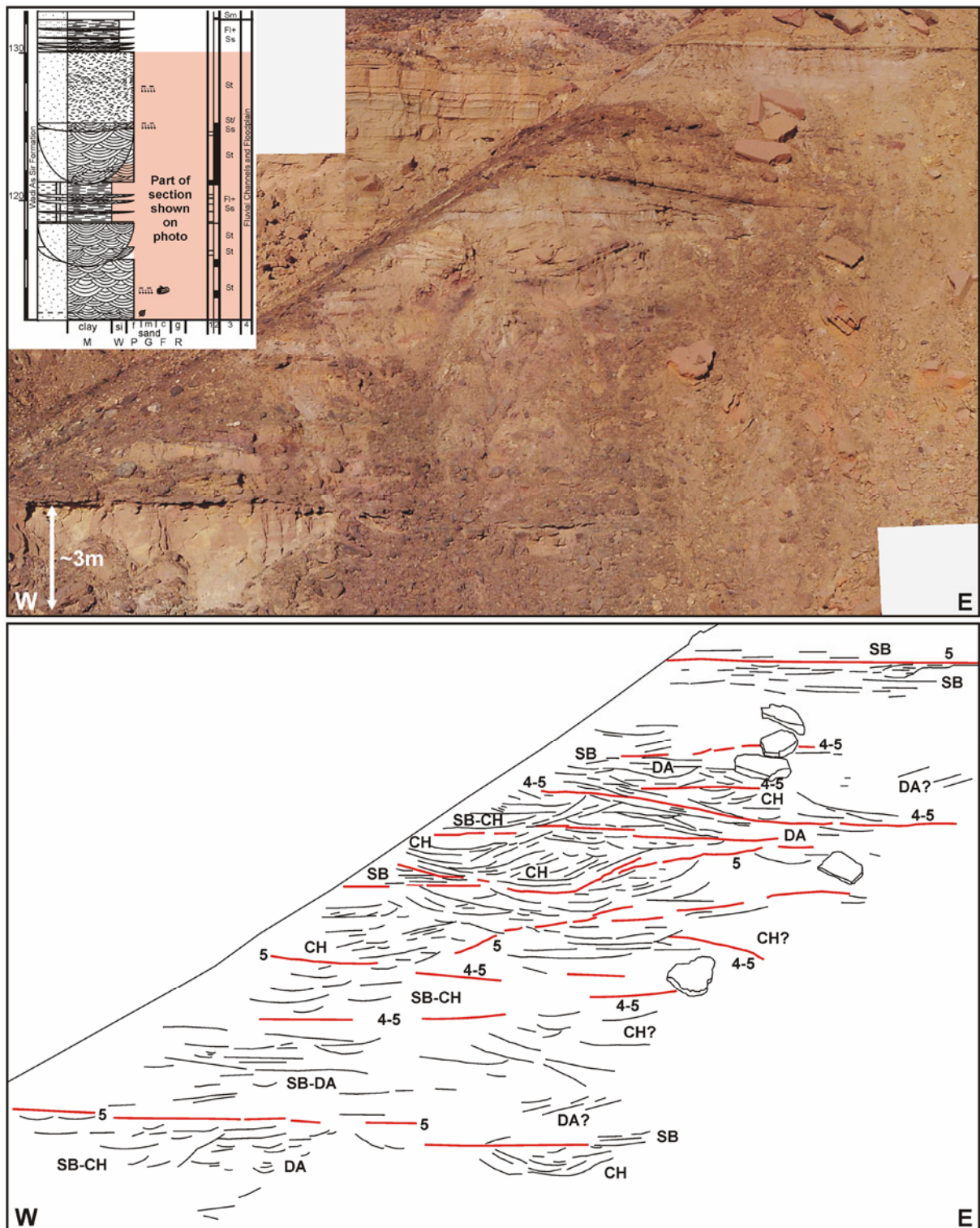


Figure 3.15A Fluvial part of the Wadi As Sir Formation of section 8. Though partly covered by scree, large channel macroforms (CH), bounded by 4 to 5-th order boundaries (red lines and numbers) can be seen. The large channels are made up by smaller architectural elements (black lines, 2nd to 3rd order boundaries), including channels (CH), sand bed forms (SB) and downstream accretion elements (DA).

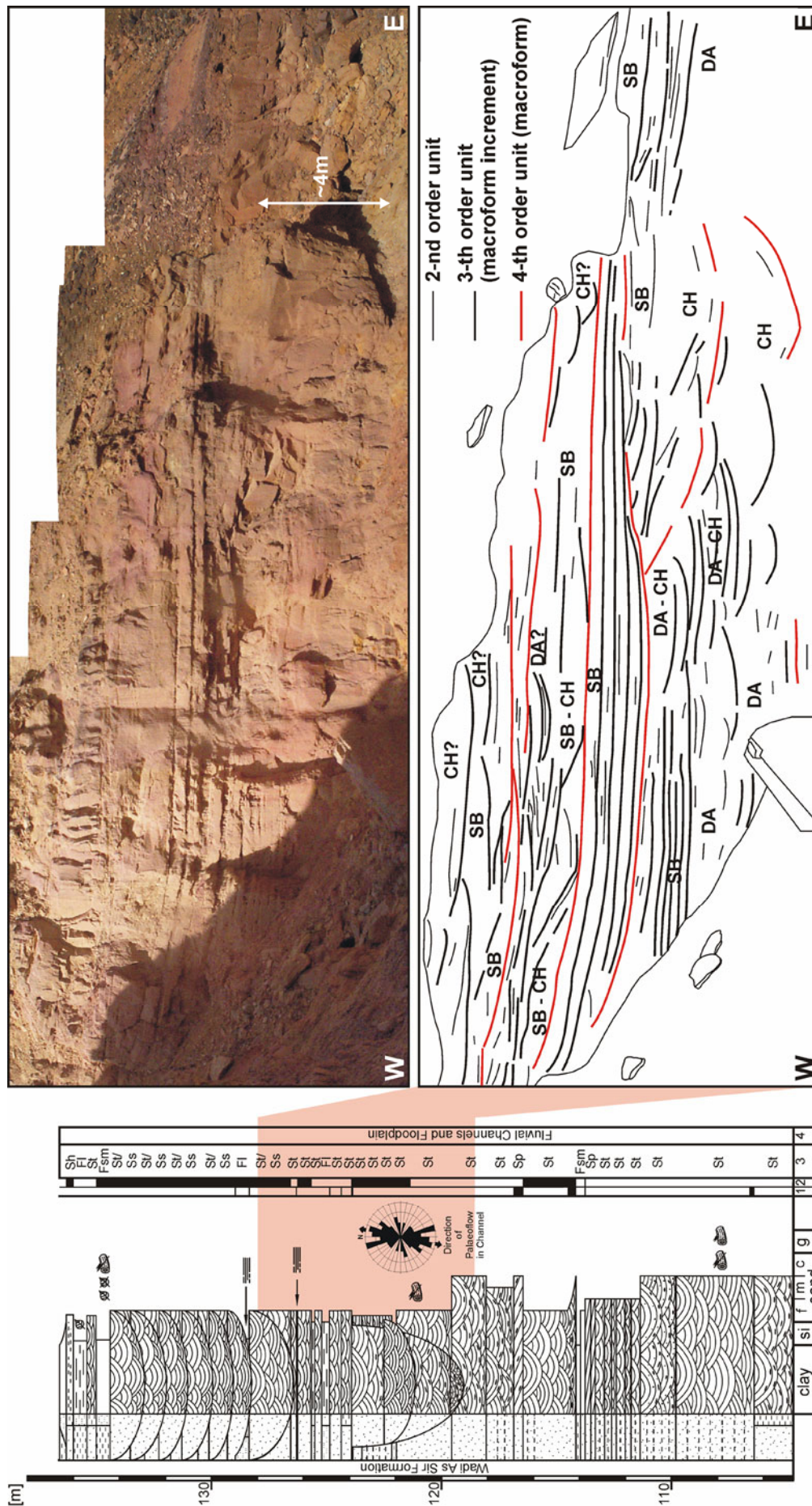


Figure 3.15B Fluvial interval from the Mid-Wadi As Sir Formation of section 9. The 33m thick fluvial succession is dominated by various bedded sandstone bodies with trough cross bedding, typical for a braided river system. The fluvial architectural element analysis (Miall, 1985; 1996) supports this interpretation. The architectural elements SB (sand bedform) and DA (downstream accretion) are typical for braided systems. CH (channel) elements of various sizes appear in all fluvial systems. The outcrop represents a large, 5-th order channel structure composed of variously sized architectural elements.

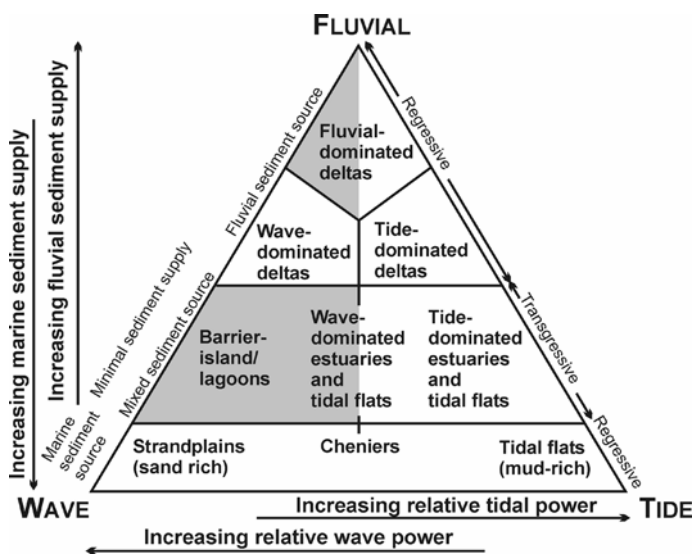
3.5.3 The coastal system

The look of a coastal system depends on several conditions like wave power, tidal power, marine sediment supply, fluvial sediment supply and fluvial gradient. Based on the interaction of these factors and the transgressive/regressive sea-level change, deltas, estuaries, braid plains, strand plains etc. may form (e.g. Walker and James, 1992; Galloway and Hobday, 1996; Reading and Collinson, 1996; Einsele, 2000 among others).

Due to facies interpretations, the depositional conditions of the mid to Late Cretaceous coastal system of South Jordan can be defined as follows:

- (i) the wave power was moderate to high (= storm dominated shelf)
- (ii) the tidal power was low (= microtidal system)
- (iii) the sediment supply was fluvial dominated, with a sand dominated load
- (iv) the fluvial gradient was low (= coastal plain system and shallow shelf)

Furthermore it can be assumed that during the studied time interval the SW-NE trending palaeoshoreline was located west of Batn El Ghul (Fig. 2.8, "Ajlun Palaeoshoreline").



Applying these depositional conditions to the coastal system classification diagram (Fig. 3.16) it follows, that during transgressive times a barrier-island/lagoon coast would have formed, while under regressive conditions a fluvial dominated delta would have characterized the coast.

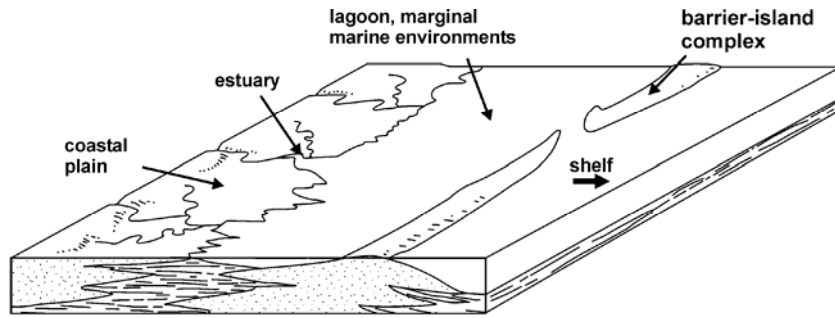
Figure 3.16 Ternary, process-based classification for all coastal system (modified from Reading and Collinson, 1996). The shaded fields indicate the mid to Late Cretaceous coastal systems of South Jordan.

Transgressive relative sea-level conditions

Figure 3.16 shows that the barrier-island/lagoonal and wave dominated estuarine environments (Fig 3.17) of the study area developed under transgressive sea-level conditions (transgressive to early highstand systems tracts in a sequence stratigraphic sense). The dominance of a fluvial sediment source decreases and a mixed fluvial-marine sediment source dominates.

Estuarine deposits, typical for transgressive sea-level conditions (e.g. Reinson, 1992; Reading and Collinson, 1996), are rare (e.g. section 7 metres 51 to 56 and lower levels of section 10). In all cases they are part of a sedimentary succession deposited under transgressive sea-level conditions. To decide which types of estuary, that is wave- or tide-dominated (Fig. 3.10), formed in the study area, a denser net of outcrop information would be necessary. Though, considering that on the shelf wave power dominated over tidal power, the formation of wave-dominated estuaries can be assumed.

The facies interpretation (Chapter 3.2.3) shows that siliciclastic dominated lagoons existed within the studied sedimentary succession predominantly during transgressive relative sea-levels (e.g. section 8, metres 33 to 38 and section 10, metres 110 to 112). Occasionally these lagoons might be part of an estuarine complex (Fig. 3.10). The lagoons might also be part of a transgressive barrier-island complex (Fig. 3.17) (Baaske et al., 2000). However, an unmistakable indication for transgressive barrier-island/lagoon complex, e.g. a clearly defined barrier, is missing within the limits of the study area.

**Figure 3.17**

Block diagram of a schematic siliciclastic barrier-island/lagoon complex. This coastal configuration is typical for transgressive sea-levels with high wave power.

It can be concluded that under transgressive sea-level conditions the mid Cretaceous coastal system of South Jordan was characterized by estuaries and lagoons.

Regressive relative sea-level conditions

It is generally assumed, that a coastal system with a fluvial dominated sediment source will form a fluvial dominated delta under regressive relative sea-level conditions (e.g. Galloway and Hobday, 1996; Reading and Collinson, 1996; Einsele, 2000 among others) (Fig. 3.16). Only the sections logged in the West (sections 5 to 10), close to the palaeoshoreline, display such a sand dominated fluvial deltaic system. The sections in the East (sections 11 to 15) are too far away from the palaeoshoreline and show the anastomosing fluvial system of the coastal plain. Therefore it can be concluded that the sand dominated fluvial deltas formed during regressive sea-level phases. Such deltaic systems can be found in the Lower Hummar, the Upper Shuayb and the mid Wadi As Sir formations of sections 5 to 10.

As described in chapter 3.5.1, the fluvial style of the western sections is that of a braided river. Therefore the examined delta systems are interpreted as braid deltas (Fig. 3.18), a subdivision of fan deltas (McPherson et al., 1988).

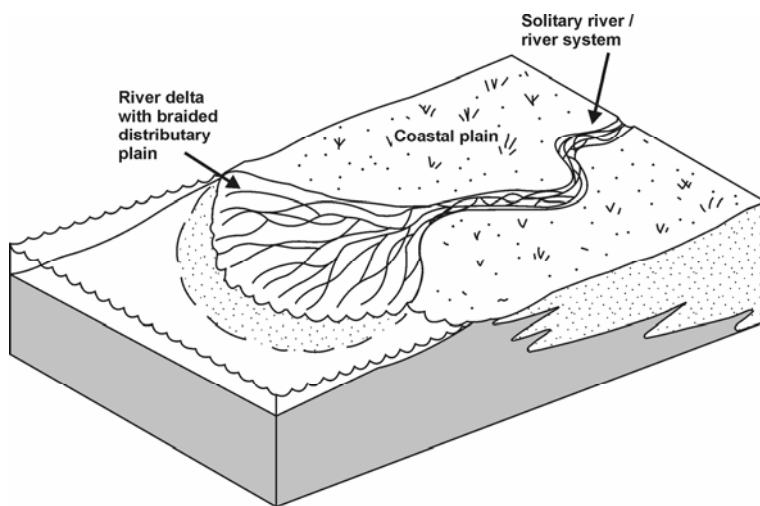


Figure 3.18 Simplified model of a braid delta, a river delta with a braided distributary plain (modified from Nemec and Steel, 1988; and Nemec, 1990).

Classically a fan delta is defined as “an alluvial fan that has prograded from an adjacent highland into a standing body of water, either a lake or the sea” (Holmes, 1965 cited in; Nemec and Steel, 1988; Orton, 1988). Nemec and Steel (1988) presented modifications to the standard definition of fan deltas, as well as a classification of twelve different fan delta types. One of their fan delta types is the braid delta (Fig. 3.18), “whose braided distributary plain has been formed by the progradation of a solitary bedload river into a standing body of water” (Nemec

and Steel, 1988). Of importance with this definition is that a fan delta is **not** necessarily directly connected to a proximal alluvial-fan system. This point is also mentioned by other authors like McPherson et al. (1988) and Orton (1988).

Using the classification schemes for coarse grained deltas after Orton (1988) and Postma (1990) leads to similar results. According to Orton’s process oriented scheme, the mid Cretaceous delta systems of South Jordan are characterized as “Gwern Gof” type deltas (Orton, 1988). The “Gwern Gof” delta is a sand dominated delta system with a high rate of sediment supply, deposited under moderate to high wave energy. Applying Postma’s facies

and architectural oriented classification the deltas can be seen as mouth-bar delta systems. The delta types of both classifications would be classified as fan deltas according to the more descriptive classification of Nemec and Steel (1988).

During the Lower Hummar Formation only the marine influenced parts of the delta complex and the distal braid delta were recorded in sections 5 to 10 (Fig. 3.19). During the Late Shuayb Formation the subaerial distal to mid braid delta and during the mid Wadi As Sir Formation the distal to proximal braid delta deposits are exposed in sections 5 to 10. In the course of the three stratigraphic intervals with delta formation, the Lower Hummar, the Upper Shuayb and the mid Wadi As Sir Formation, the lateral position of the delta complex constantly moved seawards by prograding westwards (Fig. 3.19).

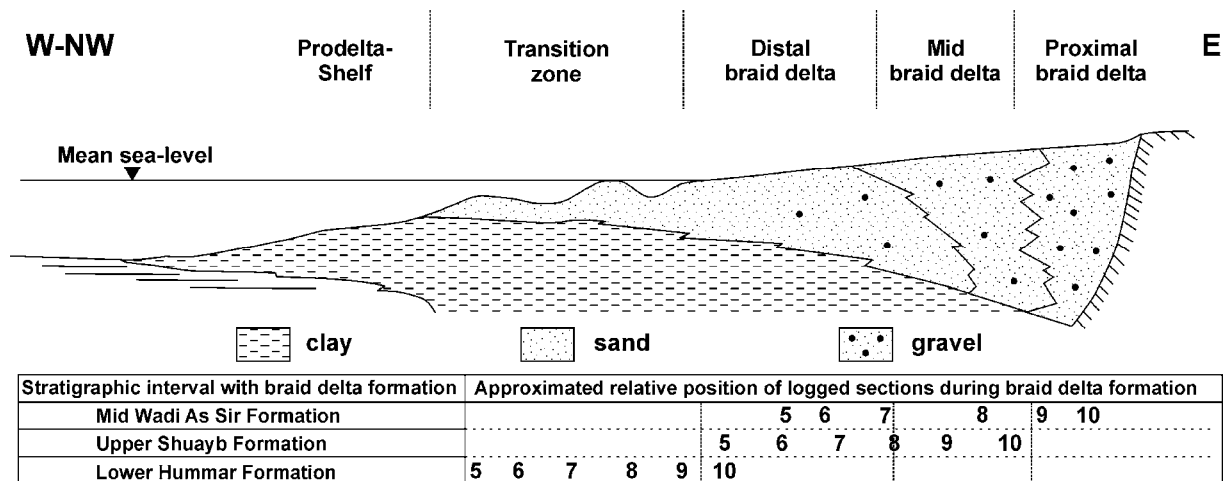


Figure 3.19 Schematic cross-section through a sand dominated braid delta (modified after Reading and Collinson, 1996). The table below the cross-section shows the approximate position of the logged sections during the stratigraphic intervals with braid delta formation.

Lagoonal systems during regressive relative sea-levels

Some of the logged sections display lagoonal depositional settings during regressive relative sea-level conditions (late highstand systems tract and falling stage systems tract in a sequence stratigraphic sense). To understand the formation of these lagoons, carbonate sedimentological aspects have to be considered. As these lagoons are parts of a wide shelf lagoon (Chapter 3.2.1 and Fig. 3.2). The falling sea-level furthers the protective role of the shelf edge barrier, successively causing a more and more protected, shallow water environment within wider areas of the shelf lagoon. Consequently the lagoonal nature of the shelf lagoon broadens. Thus, the generalized siliciclastic shoreline profile can not be applied anymore. Examples of lagoonal facies during regressive sea-level conditions occur in section 6 (metres 141 to 149), section 8 (metres 71 to 77) and section 9 (metres 69 to 73). Summing up, under regressive relative sea-level conditions the mid Cretaceous coastal system of South Jordan was characterized by sand dominated braid deltas. The delta complexes reached partially wide into the shelf during the Late Shuayb and mid Wadi As Sir formations, partly covering precursor lagoonal systems that were part of extended shelf lagoons.

3.6 Red sediment colours, ferribands, colour mottling and pedogenic features

3.6.1 Red sediment colours

Red beds are divided according to their origin into in situ/chemical red beds and detrital red beds (Pye, 1983). In situ red beds form due to chemical precipitation or pedogenic and diagenetic processes, while detrital red beds result from re-sedimentation of older red beds

after transport processes. Red sediment colour is most commonly bound to ferric forms of iron (e.g. hematite, goethite), present in the sediment in a finely divided form (Pye, 1983). In chemical red beds the source of ferric iron can be attributed to extensive post-depositional dissolution of detrital grains, e.g. iron bearing heavy minerals like pyroxene, micas and glauconite. The dissolution of the precursor mineral is usually followed by subsequent precipitation of hematite or other ferric oxides (Walker, 1974; 1976; Pye, 1983; Morton and Hallsworth, 1999). A further diagenetic process leading to intensive reddish sediment colours is the alteration of infiltrated clay minerals to hematite (Walker, 1976).

Modern red beds are, with only few exceptions, associated to terrestrial depositional settings (Pye, 1983). To see if there is a connection between terrestrial deposits and reddish/purple colours (Rock Color Chart hues 5R, 10R, 5P, 5RP) in the studied sediment succession, these colours were indicated in the logged sections of Appendix I. On first sight, red beds are fairly common along the Naqb escarpment. A closer look and a thorough “cleaning” of outcrops reveals that these surface colours are often of secondary nature, caused for example by muddy sediment drapes from the hanging sedimentary succession, covering even bright white sediments. The logged sections show that red colours are more frequent in terrestrial deposits than in marine deposits. Reddish marine sediments occur occasionally close to glauconite bearing strata, linking the sediment colour to diagenetic dissolution/precipitation processes.

3.6.2 Ferribands

Ferribands (“ironcrusts”) predominantly occur at the contact of different lithologies, e.g. sand-/claystone contact. Depending on grain-size differences and the palaeo-hydraulic regime, the lying or hanging bed displays several centimetre to decimetre thick ferribands of intense iron-oxide impregnation of the host sediment. The colour of the ferribands varies from reddish brown, brownish yellow to black, most probably representing different iron-oxide phases like hematite (α -Fe₂O₃, reddish to black colours) and goethite (α -FeOOH; brownish-yellow colour) (Scheffer and Schachtschabel, 1992; Baaske, 1999). Prominent ferribands along the Naqb escarpment are often laterally extensive and can be followed several tens of metres. The majority of the ferribands are bound to terrestrial depositional settings (“ferricretes”, Valeton, 1988). Marginal marine settings and, on few occasions, open marine settings might also display ferribands within the sediment succession.

Ferribands in terrestrial depositional environments are considered to form due to subsurface enrichment of iron oxides resulting from soil forming processes (Pye, 1983; Germann et al., 1990), but also due to iron precipitation linked to lateral influx of groundwater (Pye, 1983; Valeton, 1988). The formation of pedogenic ferricretes points to warm and humid climatic conditions (Valeton, 1988).

The occurrence of ferribands in marginal marine to marine deposits points either to a late diagenetic formation under groundwater influx in marginal marine settings or an early diagenetic formation under marine conditions. Since marine waters usually carry only minor concentrations of iron, the later would take place under climatic conditions which favour lateritic weathering and a high continental runoff (Föllmi, 1996; Mücke, 2000). The combination of these effects would provide high amounts of ferric iron in marginal marine settings to produce ferribands. Furthermore the late diagenetic/pedogenic transformation of glauconite to iron-oxides/hydroxides might also cause the formation of ferricretes (Nahon et al., 1980).

3.6.3 Colour mottling and pedogenic features

Colour mottled sediments occur in many parts of the logged sections and are usually related to the coastal plain facies association. The mottling is characteristic of sediments which have undergone modification related to soil-forming processes (Buurman, 1980; Bown and Kraus, 1981). In modern soils colour mottling is attributed to alternating wet and dry conditions

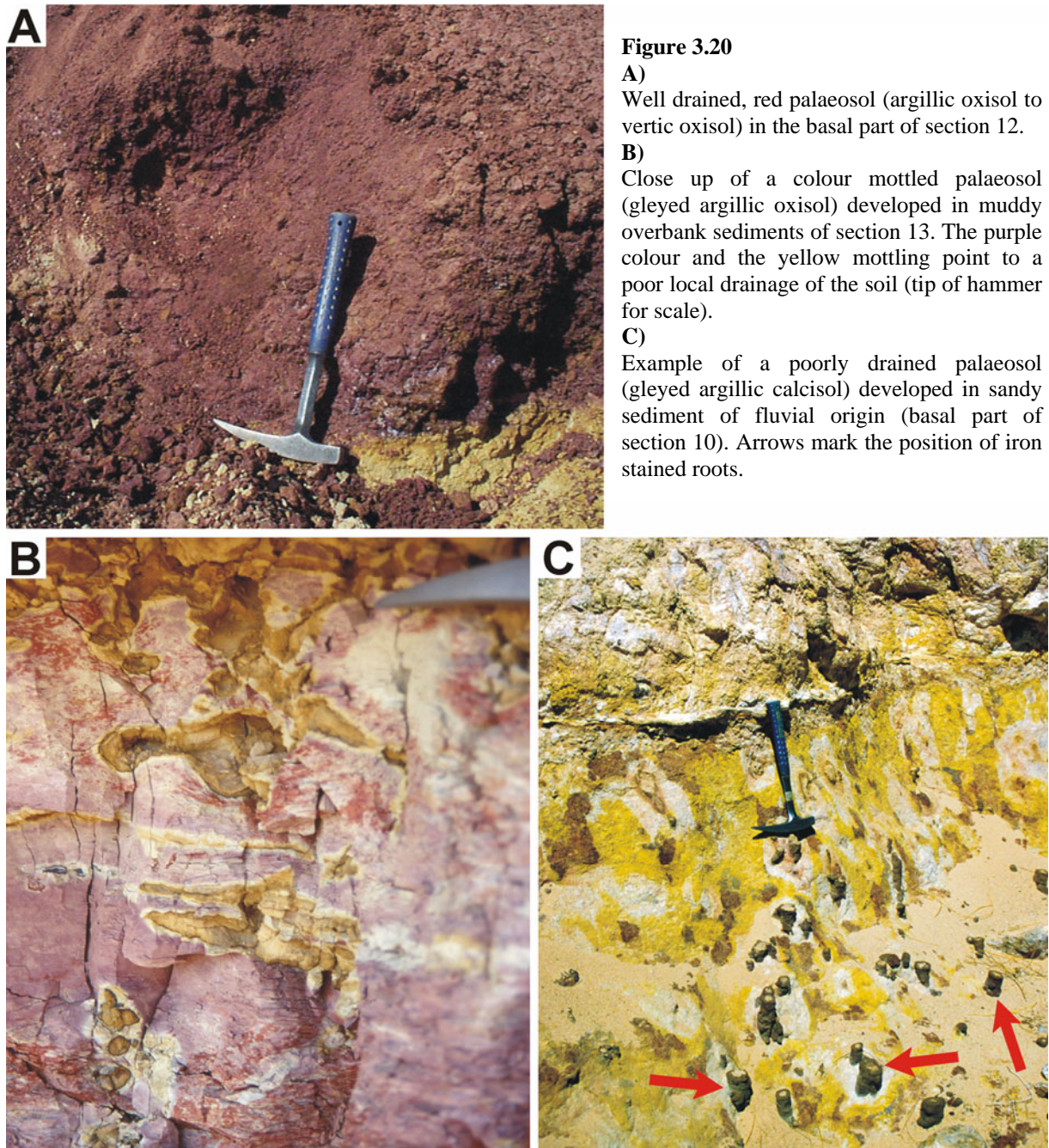
and/or fluctuating water tables, and impeded drainage which would be characteristic of modern gleys and pseudogleys (e.g. Scheffer and Schachtschabel, 1992). The wetting causes the redistribution of organic matter within the solum, leading to local reducing environments, causing iron and manganese compounds to go into solution. Under drying conditions these compounds are locally precipitated as oxides and oxyhydrates (Buurman, 1980; Bown and Kraus, 1981).

Along the Naqb escarpment colour mottling occurs in terrestrial sediments but also in marine and marginal marine deposits. Marine sediments may show colour mottling due to chemical effects of bioturbation (Bromley, 1996). So the changing oxidizing and reducing effects, connected to organic material in and around burrows, can cause mottling in marine sediments. Generally pedogenesis might also affect marine strata if sea-level fall leads to a long term exposure of the sediment (Kraus, 1999). In marginal marine settings, e.g. in the marsh facies, colour mottling might result from pedogenic processes and/or bioturbation effects.

The colour variation of the mottling and its frequency together with other pedogenic features, allows statements on the drainage condition of the palaeosol. Kraus and Gwinn (1997) showed that red palaeosols with few mottles were better drained than purple ones with yellowish-brown mottles or yellowish palaeosols with iron-oxide nodules. Examples of these different palaeosol types can be found in the study area (Fig 3.20), especially in the overbank/floodplain deposits east of section 10. The dominance of red colours (Fig. 3.20A) with few mottles points to a generally well drained coastal plain. Purple and yellow beds (Fig. 3.20 B+C) with mottles and iron-oxide nodules indicate poor local drainage conditions.

Other observed pedogenic features include the formation of small iron-oxide concretions/nodules, slickensides in muddy palaeosols, iron-oxide covered roots and rootlets (Fig. 3.20C, arrows) and small-sized calcretes within the sediment. Similar to colour mottling, iron-oxide concretions/nodules record alternating oxidizing and reducing conditions caused, for example, by variable soil drainage (Bown and Kraus, 1981; Kraus and Gwinn, 1997). Intersecting slickensides in clayey palaeosols are caused by fluctuations of the water table (Kraus, 1999) and also point to changing drainage conditions. The iron-oxide covered roots and rootlets are roughly cylindrical in shape, few centimetres in diameter and typically 10-20 cm tall. Usually these tube-like structures have a millimetre to centimetre thick iron-oxide skin and are filled with sediment. The iron-oxide precipitated in close proximity around the biogenic material due to changed chemical conditions caused by the decay of the roots (Valeton, 1988; Kraus and Gwinn, 1997). The small calcretes might have formed under warm and arid climatic conditions within the soil (Valeton, 1988).

It can be concluded that the coastal plain, developing during the Cenomanian to Coniacian in the eastern part of the study area, was variously drained and at least locally vegetated. The differentiated drainage might be connected to the fluvial architecture/topography (Kraus and Gwinn, 1997; Kraus, 1999) and the parent material/permeability of the palaeosol (Kraus and Gwinn, 1997). Considering the pedogenic features, including the ferribands/ferricretes described in 3.6.2, the soils that developed on the coastal plain are best classified as oxisols, vertisols, calcisols and argillisols (Mack et al., 1993). Due to poor palaeo-drainage these soils are often gleyed. This rough classification points to soil forming processes taking place under wet equatorial to dry subtropical palaeoclimatic conditions (Mack and James, 1994).



3.7 Summary of the sedimentological features

The sedimentological features of the mid Cretaceous depositional system of South Jordan can be summed up as follows:

- The sedimentary succession can be grouped into four facies associations which comprise ten environmental depositional facies. Ranging from open shelf to terrestrial depositional environments, the facies associations are (i) shelf facies association, (ii) shoreface facies association, (iii) marginal marine facies association and (iv) coastal plain facies association. The lateral and vertical succession of these facies associations records the repeated interfingering of terrestrial and marine environments, and shows that the mid Cretaceous of South Jordan can best be described as a shallow marine siliciclastic to mixed siliciclastic-carbonate coastal system.
- Facies-correlation of the logged sections shows that the sedimentary succession can be laterally sub-divided into three major depositional systems: (i) a siliciclastic ramp,

(ii) a mixed carbonate-siliciclastic ramp and (iii) an alluvial system. Vertically these depositional systems are arranged in repeating cyclothems. A complete, ideal cyclothem consists of:

- 4.) siliciclastic ramp system (prograding)
- 3.) mixed carbonate-siliciclastic ramp system
- 2.) siliciclastic ramp system (retrograding)
- 1.) alluvial system

- The shelf system was generally wave/storm dominated, with subordinate tidal influence. The supply dominated shelf system was represented by the prograding siliciclastic ramp. The retrograding ramp system and the mixed carbonate-siliciclastic ramp occurred during accommodation-dominated conditions.
- The character and development of the examined coastal system can be divided into a regressive and a transgressive system. Under regressive sea-level conditions delta systems formed. The delta systems are best described as sand dominated braid deltas. Occurring lagoons within the sedimentary succession are part of extended shelf lagoons. The formation of these shelf lagoons was furthered by the falling sea-level, improving the barrier effect of the patch reefs near the shelf edge.
Transgressive sea-level conditions resulted in a coastal system controlled by estuaries and barrier/lagoon complexes. Due to micro-tidal conditions, the estuaries were most probably wave dominated.
- On the coastal plain an anastomosing to meandering, sand dominated river system developed. On vegetated overbank areas extended soil formation under various drainage conditions took place. During regressive sea-level conditions the nearshore river system changed to a more braided one. This change is linked to the formation of braid deltas during these time intervals.
- Most of the terrestrial deposits display reddish colours, though red colouration alone is no indication for a terrestrial depositional environment. The formation of ferribands (“ironcrusts”) within the sedimentary succession is either directly linked to soil forming processes or to early marine diagenesis with possible ground water influence.

4. Sequence stratigraphy

Starting with the seismic stratigraphy of the 1970s, the modern sequence stratigraphic concept today is an important tool in sedimentary geology. The concept fills gaps between sedimentology, basin analysis and stratigraphy (Catuneanu, 2002). “Sequence stratigraphy is the study of rock relationships within a chronostratigraphic framework of repetitive, genetically related strata bounded by surfaces of erosion or nondeposition, or their correlative conformities” (Van Wagoner et al., 1988, p. 39). The following chapter focuses on the sequence stratigraphic framework established for the study area, based on the detailed interpretation of the logged sections (Appendix I).

4.1 Definitions and key concepts

Though sequence stratigraphy is now well established, different sequence stratigraphic concepts and definitions exist (Catuneanu, 2002). Therefore a short outline of the concept and the used terminologies will be presented. A general review of clastic sequence stratigraphy is given in Catuneanu (2002), aspects of clastic and carbonate sequence stratigraphy are covered in numerous books and articles (e.g. Wilgus et al., 1988; Van Wagoner et al., 1990; Emery and Myers, 1996; Miall, 1997; de Graciansky et al., 1998; Posamentier and Allen, 1999; Hunt and Gawthorpe, 2000 among others).

Sequence models, systems tracts and systems tract boundaries

The “classic” Exxon sequence stratigraphic model includes four systems tracts: the lowstand, transgressive, highstand and shelf-margin systems tract (Posamentier and Vail, 1988; Van Wagoner et al., 1988). Within this model both, lowstand and shelf-margin systems tract, result from sea-level fall. The difference between the two systems tracts is the rate of sea-level fall and the relationship of the rate of eustatic fall to the subsidence rate, the later resulting in “type 1” or “type 2” sequences (Posamentier and Vail, 1988; Catuneanu, 2002). The shelf-margin systems tract did not receive much acceptance (Catuneanu, 2002), for that reason only three systems tracts, lowstand (LST), transgressive (TST) and highstand systems tract (HST), are commonly used within the Exxon model (Fig. 4.1). Subdivisions of the LST and HST into early and late systems tracts refine the sequence stratigraphic model regarding different depositional conditions.

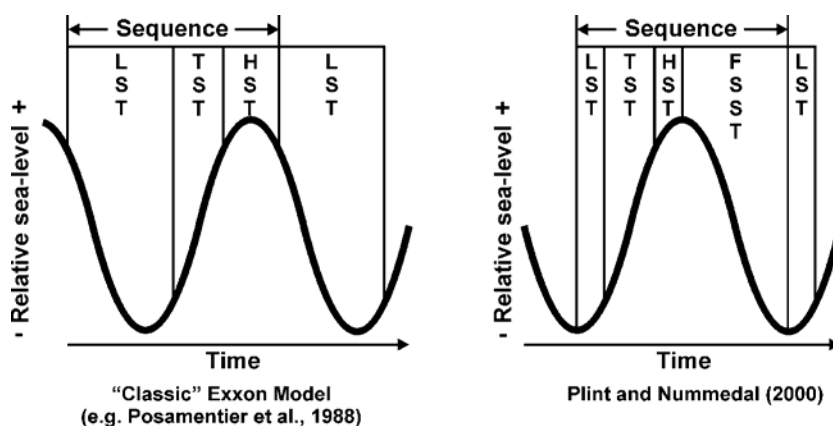


Figure 4.1

The “classic” sequence stratigraphic model introduced by Exxon researchers (e.g. Posamentier et al., 1988) and the “extended” sequence stratigraphic model by Plint and Nummedal (2000), used in this study (LST = lowstand systems tract, TST = transgressive systems tract, HST = highstand systems tract, FSST = falling stage systems tract).

Hunt and Tucker (1992) and Plint and Nummedal (2000) enlarged the original model by establishing a fourth systems tract, combining the late HST and the early LST of the Exxon model. Hunt and Tucker (1992) described this systems tract for the slope and basin floor (forced regressive systems wedge), Plint and Nummedal (2000) for the shelf setting (falling stage systems tract, FSST). The FSST comprises the complete sea-level fall and therefore

opposes the other three system tracts which jointly contain the complete sea-level rise (Fig. 4.1). In this study the concept of Plint and Nummedal will be applied, since the Late Cretaceous sediments of South Jordan were deposited in a shelf setting.

Within the concept of Plint and Nummedal (2000) the FSST is separated from the HST by the “basal surface of forced regression” (BSFR). The BSFR, introduced by Hunt and Tucker (1992), is a diachronous surface that marks the base of the marine deposits accumulated during the forced regression of the shoreline (Catuneanu, 2002). The term forced regression refers to the sediment supply independent progradation of the shoreline (Posamentier and Allen, 1999).

Table 4.1 gives an overview of a complete sequence of the “enhanced” sequence stratigraphic model, including the relative position of the systems tracts and their bounding surfaces.

Table 4.1 Position and nomenclature of the systems tracts and bounding stratigraphic surfaces in the extended sequence stratigraphic model after Plint and Nummedal (2000).

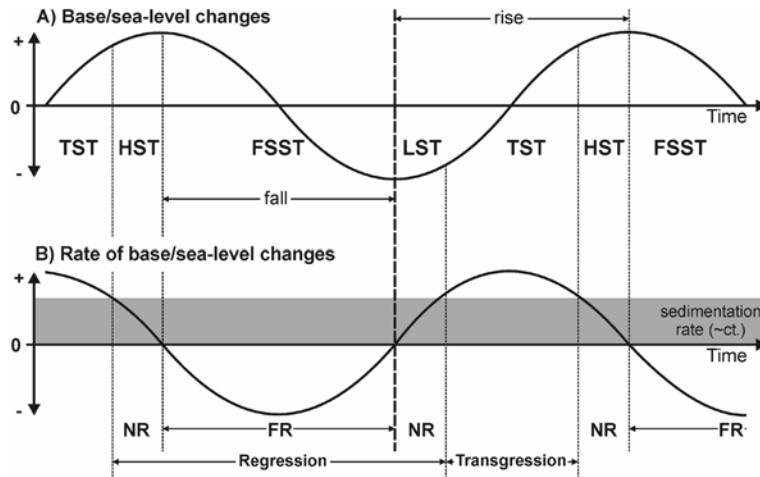
Systems tract		Bounding/stratigraphic surfaces
S E	FSST	- „Sequence boundary“ (SB)
		- basal surface of forced regression (BSFR)
Q U	HST	- maximum flooding surface (MFS)
		- maximum regressive surface (MRS)
N C	TST	- maximum regressive surface (MRS)
		- maximum regressive surface (MRS)
E	LST	- “Sequence boundary“ (SB)

To avoid misinterpretations concerning the position of the bounding surfaces in the presented study, all stratigraphic surfaces defined within the framework of this study are based on sediment stacking patterns (cf. Catuneanu, 2002). Working with outcrop based stratigraphic logs this approach ensures a consistent and practical way to trace the stratigraphic surfaces from log to log.

Forced regressions

Recent studies showed the significance of progradation of shallow marine systems during the late HST/early LST and the entire FSST respectively (Hunt and Gawthorpe, 2000). In many cases this progradation is associated exclusively with the falling relative sea-level, which is called forced regression. The term ‘forced’ expresses that the shallow marine system can only react to the relative sea-level fall by prograding seawards.

The regressive element of the relative sea-level curve can be divided into two “normal regressive” parts that enclose a larger “forced regressive part” (Fig. 4.2). During a normal regression, the sediment supply outpaces sediment dispersion and the rate of sea-level rise, filling the available accommodation space. The result is the progradation or ‘seaward movement’ of the coastline (Posamentier and Allen, 1999). During a forced regression the relative sea-level fall alone exposes sea floor, resulting consequently in the seaward migration of the shoreline. The progradation of the shoreline in this case is independent of the sediment supply (Posamentier and Allen, 1999).

**Figure 4.2**

The concept of transgression, normal regression and forced regression with regard to the systems tracts (modified after Catuneanu, 2002). Transgression occurs when the rate of sea-level rise outpaces the sedimentation rate, normal regression when the sedimentation rate is higher or equals the rate of sea-level rise or fall. Forced regressions occur only when the sea-level fall outpaces the sedimentation rate (NR = normal regression; FR = forced regression).

4.2 Sequence stratigraphy of the study area

4.2.1 Stratigraphic correlation of the logged sections

To achieve a sequence stratigraphic framework, the logged sections were first correlated using litho- and biostratigraphic characteristics. Using facies interpretation (Chapter 3) and sediment stacking patterns, the correlated logs were finally interpreted with regard to sequence stratigraphy (Fig. 4.3). Furthermore K-Ar-ages of glauconies were measured to improve and control the correlation. Due to controversial K-Ar dates, this approach had only minor success.

Litho- and biostratigraphy

For North and Central Jordan an established lithostratigraphic correlation scheme exists, which is used by the workers of the mapping division of the Natural Resources Authority (NRA) of Jordan (e.g. Powell, 1989). In the presented study this scheme was partly applied for the correlation of the logged sections. The top of the Naur Formation carbonates (HST of sequence 1.1 in Fig. 4.3) was used for correlating the western most sections (1 to 7). The base of the thick sandstone unit in the middle part of the Wadi As Sir Formation (LST of sequence 4/4.1 in Fig. 4.3), as well as the sandstone beds at the top of the Shuayb Formation (LST of sequence 3, Fig. 4.3) were used to correlate sections 5 to 10. To add the eastern most sections (11 to 15) to the correlation, the base of the Amman Formation (TST of sequence 6 in Fig. 4.3) was used.

To improve the lithostratigraphic correlation, available biostratigraphic data was incorporated. Fossil assemblages were used to control the possibility of bed to bed correlation. Index fossils like ammonites were also used for correlation and to improve the stratigraphic framework. Cenomanian to Turonian ammonites, occurring in claystones of the Hummar Formation (cf. Berndt, 2002) allowed to correlate these claystone beds in the different logs (HST of sequence 2.1 in Fig. 4.3).

K-Ar-ages of glauconite

Due to its authigenic nature glauconite, or glaucony as suggested by Odin and Matter (1981), is one of the few minerals suitable for K-Ar dating of sedimentary rocks (Télléz Duarte and López Martínez, 2002). The absolute age of glaucony is not as accurate as those of minerals of igneous origin, but gets satisfyingly close to the sedimentation age of the host sediment (Télléz Duarte and López Martínez, 2002). For this study K-Ar dating was performed on six glaucony samples from the study area in order to improve/control the stratigraphic correlation of the logged sections.

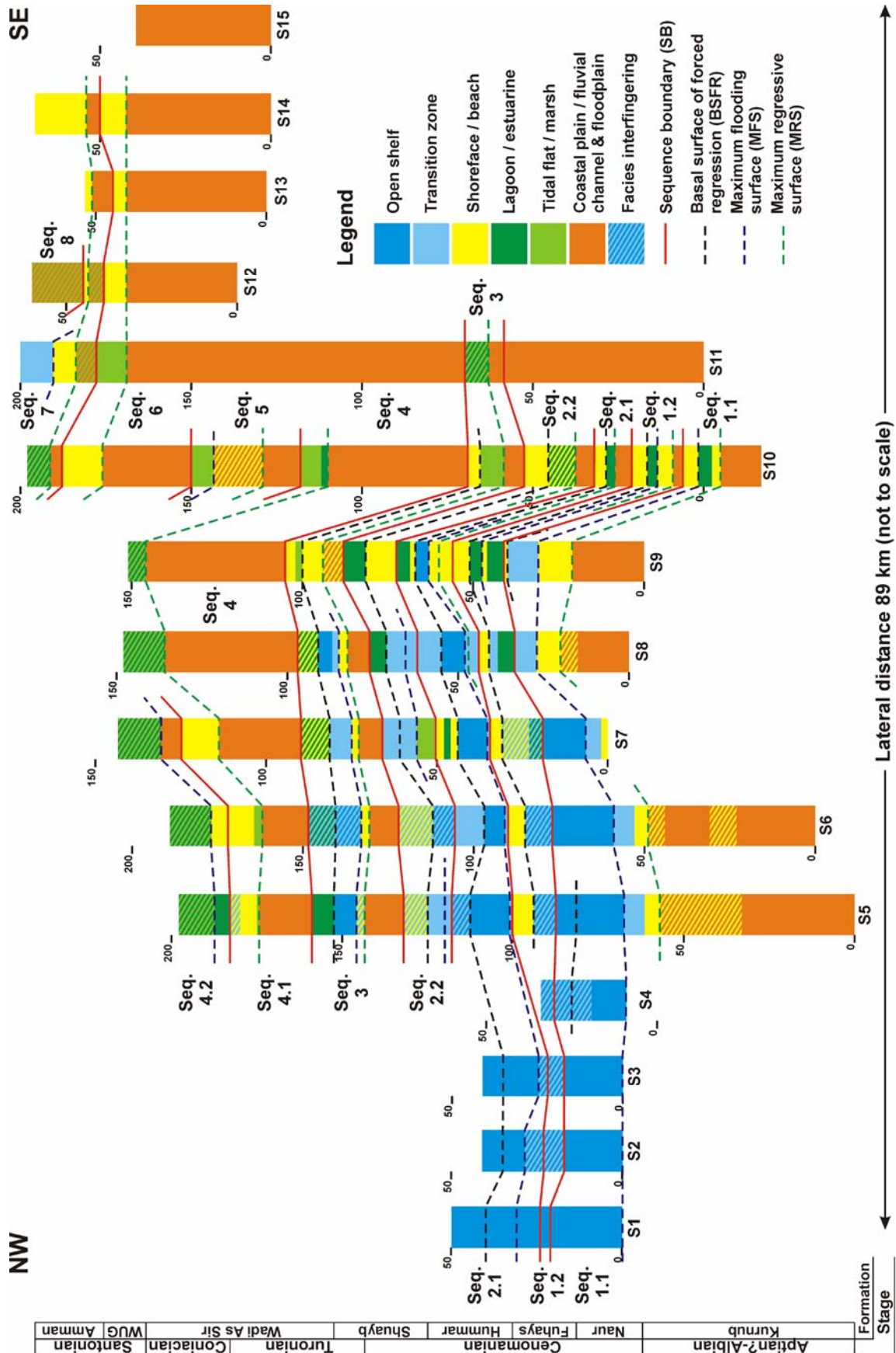


Figure 4.3 Correlation and sequence stratigraphic interpretation of the logged sections. Up to the Wadi Umm Ghudran Formation (WUG) the stratigraphy was established using section 5, the base of the Amman Formation was defined in section 10. The facies codes base on the interpreted logs in Appendix I.

Preparation

Selected glaucony bearing, unweathered mudstone samples were sieved and the sand-sized (>0,125mm) fraction was thoroughly washed with deionised water. Moderate ultrasonic treatment was used to remove possible 'neutral' non-glaucanitic and polluting fraction (Odin and Rex, 1982). Samples were dried at 30°C. For the separation of the glaucony from quartz and biogenic material, a magnetic separator was used. 100-130 mg of glaucony grains were hand picked under a binocular microscope. With regard to the glaucony evolution presented by Odin and Matter (1981), the glauconies selected for age dating were all of an evolved to highly evolved stage (Fig. 4.4). Glauconies of this stage are usually dark green and have a high potassium content (>6-7%) (Odin and Dodson, 1982). The potassium content of the examined samples from South Jordan ranges between 6.03 and 7.98 wt.% (Tab. 4.2). A concentration on the evolved glaucony fraction improves the dating, which might be unreliable with potassium contents below 6 wt.% (e.g. Kreuzer et al., 1980). The dating was performed by Dr. K. Wemmer in the K-Ar-laboratory of the IGDL of the University in Göttingen. The results are shown in table 4.2.

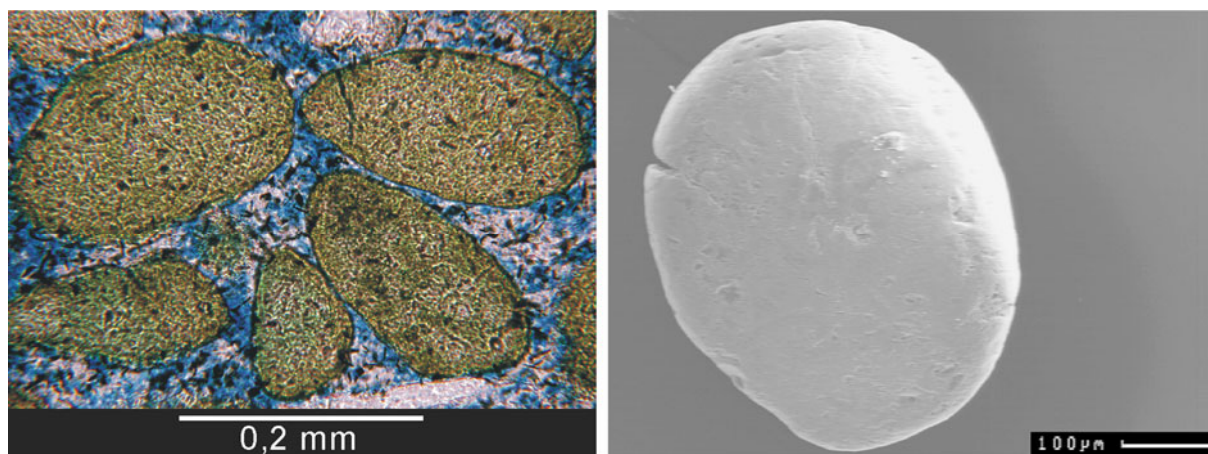


Figure 4.4 Photomicrograph (sample J7-27B) and SEM image (sample J6-68) of highly evolved glaucony grains.

Interpretation of the K-Ar-ages

Samples J5-51, J6-41, J7-27A and J7-27B were taken from the same glaucony bearing mudstone horizon just below the base of sequence 3. According to their stratigraphic position, the glaucony ages were expected to have a Lower Turonian age (about 91 to 93 Ma). The other two samples were taken for comparison. J6-68 was expected to be of Upper Turonian to Lower Coniacian age (~89 Ma), J10-X of Upper Cenomanian age (~94 Ma). As table 4.2 shows, all glaucony K-Ar-ages indicate a Santonian age, using the Gradstein stratigraphic table (Gradstein et al., 1995).

Table 4.2 K-Ar-ages of glauconite samples from the study area (K-Ar-dating by Dr. K. Wemmer, IGDL of the University Göttingen).

Sample	K ₂ O [wt.%]	40 Ar* [nl/g] STP	40 Ar* [%]	Age [Ma]	2s-Error [Ma]	2s-Error [%]
J5-51*	7.98	22.78	97.00	86.4	2.7	3.1
J6-41*	7.27	20.04	97.09	83.5	1.8	2.2
J6-68	7.17	19.88	96.20	84.0	1.7	2.0
J7-27A*	7.47	21.03	96.36	85.3	1.9	2.2
J7-27B*	7.16	20.14	97.04	85.2	1.8	2.1
J10-X	6.03	16.88	87.88	84.8	2.9	3.4

*samples from the same mudstone horizon

Lithostratigraphic correlation from North/Central Jordan with the study area and biostratigraphic data clearly indicates Cenomanian to Turonian stratigraphic ages for the examined samples. Since the isotope assemblage of the samples points to an un-weathered/un-altered state of the argon system (Dr. Wemmer, Göttingen, personal communication), the potassium system is a possible source for the age-disturbance. It is often assumed in literature that K-Ar-ages of glauconies might be too low (e.g. Kreuzer et al., 1980; Faure, 1986; Téllez Duarte and López Martínez, 2002) and that the K-Ar data therefore reflect minimum ages. According to Odin and Rex (1982) extraction of potassium from the glaucony structure by weathering might be the reason for low K-Ar-ages, even in evolved glauconies. Kohler and Köster (1982) point to the fact that diagenetic effects, like the replacement of glauconite by calcite, will also further the extraction of potassium as well as argon from the glaucony.

Weathering of the examined glauconies is most unlikely, since all glauconies display a dark green, un-weathered colour and the argon isotope system is closed. Though in the field the sampled glauconies appeared to be first cycle ones, reworking and re-sedimentation might be a point to consider. As all examined samples display a similar, apparently to young age a “diagenetic event”, resetting the K-Ar-age via the potassium system might be a more convincing explanation. This is supported by related glaucony data from the Upper Cretaceous of South Jordan presented by Amireh et al. (1998). Some of the presented ages display similar discrepancies between the stratigraphic position of the sediments and the absolute age. Some of the published glaucony ages seem also too young (samples Ka and Mr8 in Amireh et al., 1998, p. 60). This supports the speculation of a “diagenetic event” (e.g. the neo-formation of a younger potassium-bearing clay mineral phase) that resets the glaucony ages in South Jordan over a wide stratigraphic range.

4.2.2 Sequences

The studied stratigraphic interval (Albian to Santonian) displays eight third-order sequences (Fig. 4.3). Sequences 1 to 4 (Baaske and Krawinkel, 2001a; Baaske et al., 2001a; Baaske et al., 2001b), which can be found in the majority of the logged sections (sections 1 to 11), comprise the Kurnub and Ajlun groups (Albian? to Coniacian). Sequences 5 to 8 are situated in the lower part of the Belqa Group (Santonian to Lower Campanian) and are developed in sections 10 to 15. Sequences 1, 2 and 4 (Fig. 4.3), can be further divided into sequences of higher order with durations of most probably less than one million years. If these sequences are of fourth-order, it is difficult to tell with the available dataset. Third-order sequences or cycles have a duration or episodicity of a few million years (Haq et al., 1988) and reflect changes in the tectonic setting and/or the eustasy (Miall, 1997). Fourth-order sequences are often attributed to climate changes and orbital forcing (e.g. Miall, 1997; Castelltort and Van Den Driessche, 2003).

Regarding the systems tracts, most of the sequences comprise all four systems tracts of the sequence stratigraphic model of Plint and Nummedal (2000). Within the more marine parts, the bounding surfaces of the system tracts become difficult to trace. In these parts of the sections the related systems tracts are combined as LST/TST, TST/HST and HST/FSST respectively (e.g. in section 5, TST/HST in sequence 1.2 or HST/FSST in sequence 4.2, see Appendix I).

4.2.3 Parasequences

A parasequence is “...a relatively conformable succession of genetically related beds or bedsets bounded by marine-flooding surfaces and their correlative surfaces. In special positions within the sequence, parasequences may be bounded either above or below by

sequence boundaries.” (Van Wagoner et al., 1990). Parasequences in siliciclastic systems as well as in carbonate systems shoal upwards. Stacking patterns and stratal geometries define systems tracts. Within in the marine parts of the logged sections (Appendix I) shoaling upward cycles/parasequences occur (Fig. 4.5). For reasons of clarity of the figures, parasequences were not especially indicated in the logged sections of Appendix I.

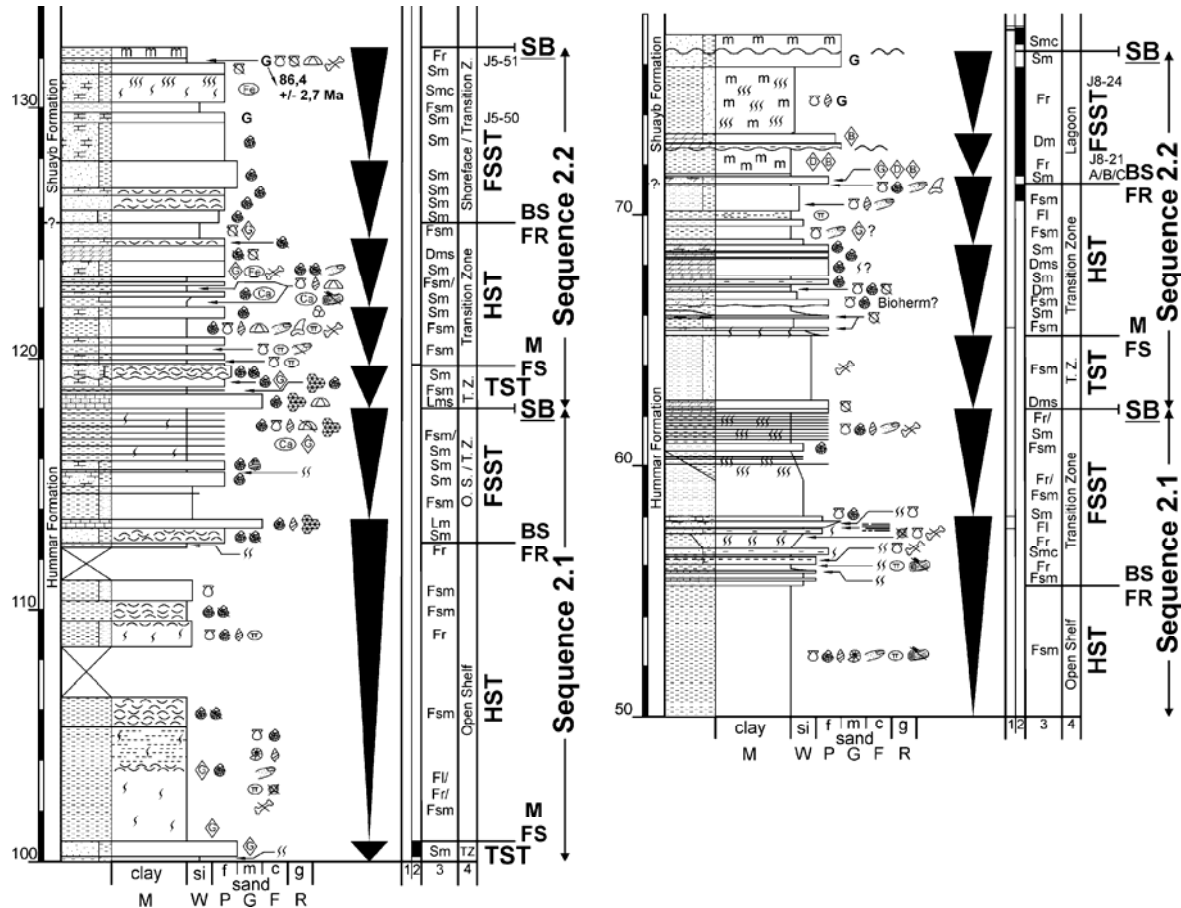


Figure 4.5 Two examples of shoaling upwards cycles/parasequences (black triangles) in the logged sections. Displayed on the left hand is section 5, on the right hand section 8. The sections, covering the same sequence stratigraphic interval, are flattened at the top of sequence 2.1 (legend and complete section see Appendix I).

4.2.4 Forced regressions

Forced regression processes are relatively common on shelf areas (Posamentier and Morris, 2000), but are often hard to find in the sedimentary record. According to Posamentier and Allen (1999) and Posamentier and Morris (2000), there are eight typical criteria to recognize forced regressive deposits. It has to be mentioned that not all criteria have to be matched to identify a forced regression and that single criteria do not necessarily proof its presence. In the following these points will be shortly illustrated. Furthermore, it will be examined if the falling stage systems tracts of the studied succession show criteria that match with the definition of forced regressions.

Seaward-dipping upper bounding surfaces

Working with outcrop and well data without seismic control or information, the seaward-dipping upper bounding surface of forced regressive deposits depends on the correlation of the logged sections. In the presented study the correlation was nearly flattened at the base of sequence 4.1. The correlation (Fig. 4.3) shows that all forced regressive deposits, i.e. all

sediments between a basal surface of forced regression and a sequence boundary, have a seaward-dipping upper bounding surface (sequence boundary).

Increased average grain size and/or diminished tendency for grain-size decrease seaward

Compared to highstand deposits forced regressive sediments of the falling stage systems tract tend to be of coarser grain size. This is due to the fact that during the FSST rivers tend to incise, cannibalizing older sediments. In addition, earlier-deposited highstand sediments of the shoreface will be reworked and dispersed during the FSST. As a result forced regressive deposits might either display an increase in grain size from proximal to distal, or show a diminished tendency for grain-size decrease seaward (Posamentier and Allen, 1999; Posamentier and Morris, 2000).

The mid Cretaceous forced regressive deposits of South Jordan do not display a grain-size increase from proximal to distal, but tend to be of the same grain size (fine- to medium grained sandstone). One reason for this might be the high content of fine- to medium-grained recycled Palaeozoic sediments (see Chapter 5).

Absence of non-marine aggradation capping proximal regressive deposits

The absence of non-marine sediment aggradation on top of the proximal part of forced regressions is linked to sediment bypass due to the seaward dipping upper surface. This feature can be noticed in sequences 1.1, 1.2 and 2.1 (Fig. 4.3).

Foreshortened stratigraphy

“Stratigraphic sections where the decompacted thickness of a shoaling upward section is significantly less than the difference in palaeo-water depth from base to top (where the top is at or near the sea level) are said to be foreshortened” (Posamentier and Allen, 1999, p. 140). The change of the relative sea-level during a forced regression can be taken into account for such foreshortened sections (Posamentier and Allen, 1999; Posamentier and Morris, 2000).

Many of the studied sequences include foreshortened stratigraphic parts. Figure 4.6 shows two examples from the logged sections. In both cases the thickness of the shoaling upward sequence, from the base of the shelf deposits to the top of the shoreface sediments, is less than the difference in palaeo-water depth from base to top. The thicknesses of the shoaling upward sequences in the examples are 12 and 11 metres respectively, while the difference in palaeo-water depth is 20 to 30 metres. As petrographic studies showed (see Chapter 5), compaction is relatively low so that all measured sediment thicknesses can be regarded as nearly decompacted.

Separation of shoreface deposits

A zone of separation between shoreface deposits located on the basin margin and shoreface deposits farther seaward indicates a zone of sediment bypass. Sediment bypass is a typical feature of forced regressions and often produces isolated sandstone deposits in shelf sediments (Posamentier and Morris, 2000). The forced regressive deposits of sequence 2.2 show a zone of separation of shoreface deposits. Within the FSST of this sequence, shoreface sediments in section 10 (basin margin) are separated from shoreface/transition zone deposits in section 5 and 6 by lagoonal and transition zone deposits in sections 7, 8 and 9.

Sharp-based shoreface deposits

Sharp-based shoreface deposits can be identified by the missing transitional facies between them and the underlying sediments (Posamentier and Morris, 2000). This effect is produced by erosion due to a lowered wave-base during the relative sea-level fall. Sharp-based shoreface deposits can be found in all studied sequences, examples are provided in figure 4.6.

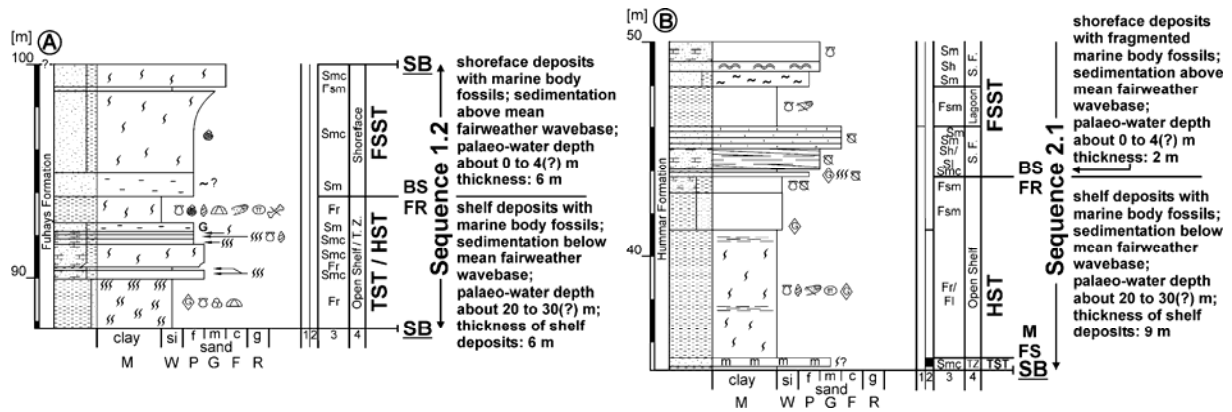


Figure 4.6 Two examples for forced regressive deposits in the falling stage systems tract (FSST), exhibiting two recognition criteria of forced regressions. The first is foreshortened stratigraphy (detailed explanation see text), the second the appearance of sharp-based shoreface deposits (directly above the basal surface of forced regression, BSFR). A) Part of section 5; B) Part of section 7; (legend and complete section see Appendix I).

Long-distance regressions

Long-distance regressions across a shelf are scarce during normal regressions because progressively more sediment is needed to fill the expanding space on the deepening shelf (Posamentier and Allen, 1999). Therefore, long-distance regressions are often associated with forced regressions, when no filling of accommodation space is needed. Long-distance regressions in the studied successions occur especially in sequences 1.2, 2.2, 3 and 4. Within these sequences regressions of more than 30 km can be traced (Fig. 4.3). The regression in sequence 4/4.1 (Turonian Wadi As Sir Formation) reaches most probably as far as Israel (Sandler, 1996; Buchbinder et al., 2000a; Buchbinder et al., 2000b) and might be also present in North and Central Jordan (personal communication F. Schulze, University of Bremen).

Progressively lower-relief clinofolds in seaward direction

Progressively lower-relief clinofolds in seaward direction are the result of progradational sedimentation in progressively shallower water, caused by forced regression. This characteristic criterion for forced regressive deposits is not present in the studied sections.

Types of forced regressions

Forced regression deposits can be differentiated into ‘attached’ and ‘detached’ deposits, due to their stratal architecture (Posamentier and Allen, 1999; Posamentier and Morris, 2000). Attached forced regression deposits are attached to the immediately preceding highstand regressive deposits. That means the regressive shoreface deposits of the two units (highstand and forced regression) are in direct contact to each other. If this is not the case and the shoreface deposits of the two regressive units are not in direct contact, the forced regression wedge is said to be detached. Which kind of forced regressive deposit occurs, is controlled by the rate of relative sea-level fall and sediment supply, the energy of the nearshore environment and the shelf gradient. The formation of attached deposits is favoured by high rates of sediment supply, low rates of relative sea-level fall, high-energy conditions and a low shelf gradient (Posamentier and Morris, 2000).

Forced regressive deposits can furthermore be classified by their upper bounding surface, which are smooth-topped or stepped-topped. Smooth-topped forced regression deposits are usually formed by a uniform rate of sea-level fall and sediment supply, while stepped-topped deposits are the result of irregular rates (Posamentier and Allen, 1999; Posamentier and Morris, 2000).

In the case of the studied forced regressive deposits, all sequences except sequence 2.1 and 2.2 contain attached forced regressive deposits (Fig. 4.3). The presence of attached forced regressive deposits points to a fairly high rate of sediment supply and a low rate of sea-level

fall during the corresponding FSSTs. The detached deposits of sequences 2.1 and 2.2, both located in the Middle to Upper Cenomanian (Fig. 4.3), are most probably the result of relatively high rates of sea-level fall during that period.

Facies analysis (Chapter 3) showed that a shelf with high-energy conditions and a low gradient is present throughout the studied time interval. Regarding the upper bounding surface of the forced regressive deposits, they seem to be smooth-topped in all sequences. This points to uniform rates of sediment supply and sea-level fall during the analogous FSSTs.

Conclusion

In each sequence of the logged sections clearly identifiable forced regressive deposits are present (Fig. 4.3), though not all eight characteristic features of forced regressions are met in each single sequence. Typical features most commonly encountered include the presence of long distance regressions, diminished tendency of grain-size decrease, sharp-based shoreface deposits and seaward dipping bounding surface. Most of studied forced regressions deposits are smooth-topped attached forced regressions. Only sequences 2.1 and 2.2 represent smooth-topped detached forced regressions.

The attached forced regressions point to a relative high sediment supply and low rates of sea-level fall in a low gradient, high energy shelf system during the corresponding FSSTs. The two detached forced regression of the Cenomanian sequence 2, formed during a phase with a high rate sea-level fall under otherwise similar conditions as during the formation of the attached ones. The fact that all the forced regression deposits are smooth-topped indicates that the rates of sea-level fall and sediment supply were rather invariable during the mid Cretaceous.

4.3 Facies, depositional systems and their relationship to the sequence stratigraphy of the study area

Facies analysis (Chapter 3) shows that the mid to Upper Cretaceous deposits of South Jordan can be grouped into four major depositional systems. The vertical stacking pattern of these depositional systems reveals shallowing upward cyclothems which ideally start with marine deposits and end with deposits of fluvial origin (Chapter 3, Fig. 3.14, p. 36). Comparison of an ideal cyclothem with the sequence stratigraphic model of Plint and Nummedal (2000) shows that each major depositional system corresponds to a systems tract of this model (Tab. 4.3, Figs. 4.7 and 4.8). The following paragraphs describe the systems tracts and the major incidents on the shelf and coastal plain that characterize them.

Figure 4.7; following page no. 58

Block diagrams of the systems tracts and corresponding major depositional systems, explanation see text. **A)** Lowstand systems tract (LST) – Alluvial plain system; **B)** Transgressive systems tract (TST) – Retrograding siliciclastic ramp system; **C)** Highstand systems tract (HST) – Mixed carbonate-siliciclastic ramp system; **D)** Falling stage systems tract (FSST) – Prograding siliciclastic ramp system.

Figure 4.8; page no. 59

Correlation of the facies (right) and the major depositional systems (left) and sequence stratigraphy. Further explanation, see text. The relative sea-level curve is based on the architecture of the major depositional systems. Due to the lack of bathymetric information, the curve does not show absolute values. The stratigraphic subdivision is based on section 5.

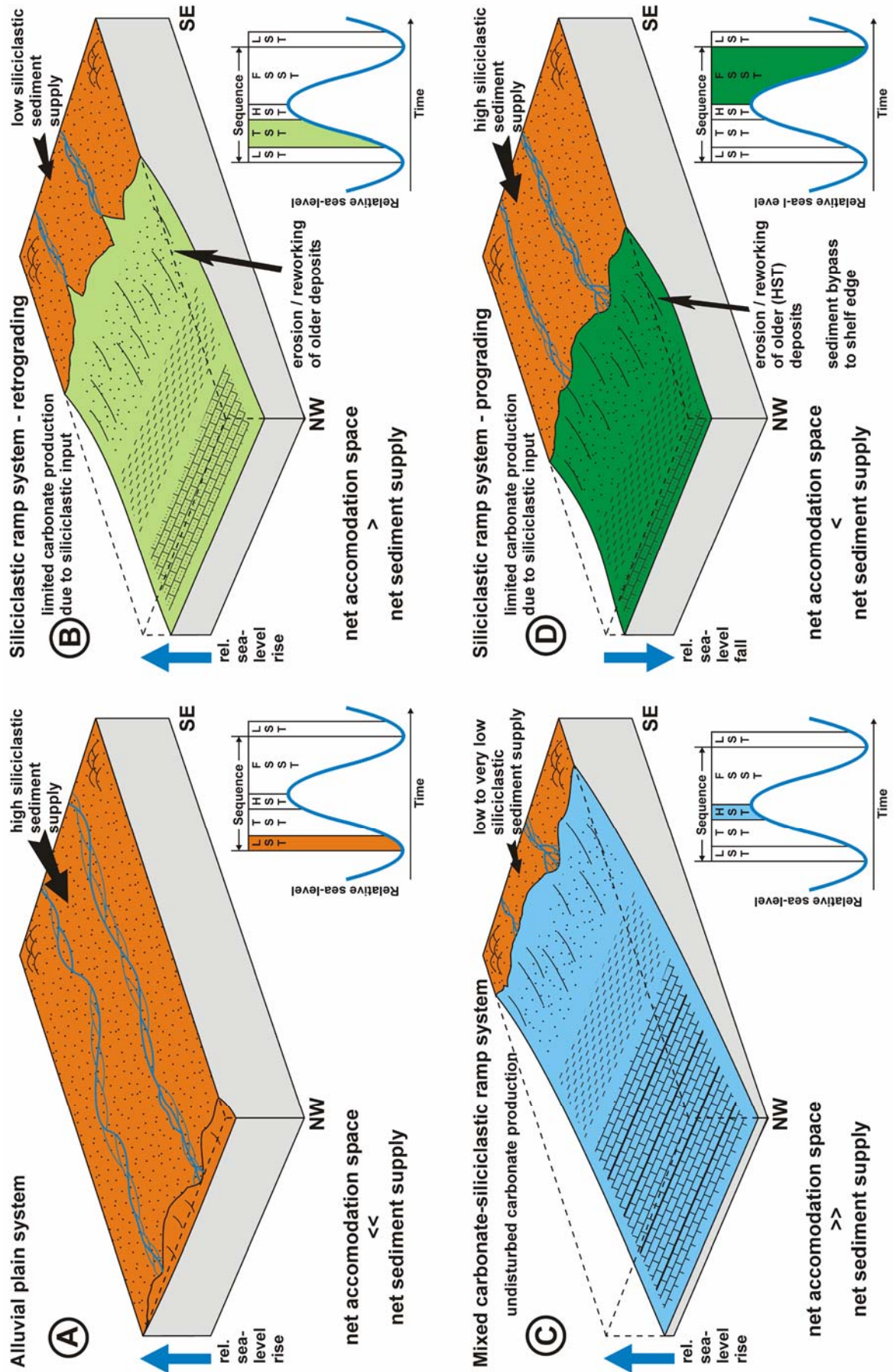


Figure 4.7 Figure captions on previous page no. 57.

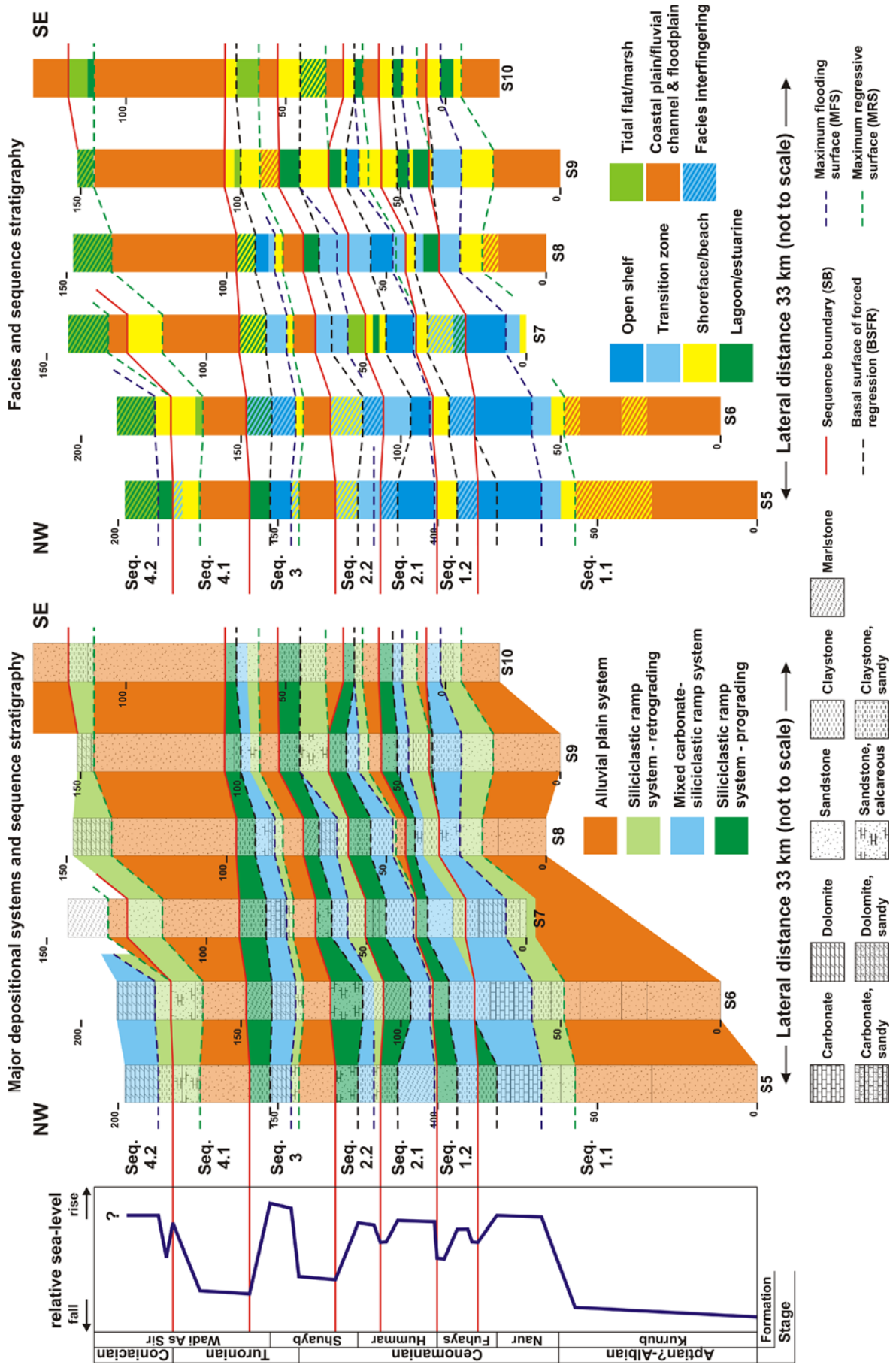


Table 4.3 Overview of the major depositional systems and their sequence stratigraphic and facies characteristics.

Major depositional system	Systems tract	Sequence stratigraphic characteristics	Facies characteristics in south Jordan
Alluvial system	LST	<ul style="list-style-type: none"> - Relative sea-level rise - Net accommodation space << net sediment supply - High siliciclastic sediment supply - Normal regression 	<ul style="list-style-type: none"> - Wide alluvial/coastal plain system - Formation of braid deltas and incised valley fills - Terrestrial depositional settings reach basinward to Central and North Jordan
Siliciclastic ramp system retrograding	TST	<ul style="list-style-type: none"> - Relative sea-level rise - Net accommodation space > net sediment supply - Low siliciclastic sediment supply - Transgression 	<ul style="list-style-type: none"> - Incipient formation of a tripartite shelf: carbonate-siliciclastic shelf, muddy clastic shelf/transition zone and sandy siliciclastic shoreface - Formation of barrier/lagoonal and estuarine coastal systems
Mixed carbonate-siliciclastic ramp system	HST	<ul style="list-style-type: none"> - Relative sea-level rise - Net accommodation space >> net sediment supply - Low to very low siliciclastic sediment supply - Normal regression 	<ul style="list-style-type: none"> - Tripartite shelf: carbonate shelf, carbonate-siliciclastic transition zone, siliciclastic shoreface - Formation of shelf lagoons (rimmed shelf)
Siliciclastic ramp system prograding	FSST	<ul style="list-style-type: none"> - Relative sea-level fall - Net accommodation space < net sediment supply - High siliciclastic sediment supply - Forced regression - Sediment bypass from coastal plain to shelf edge - Formation of broad and shallow incised valleys on the shelf edge and coastal plain 	<ul style="list-style-type: none"> - Incipient delta formation - Characteristics of forced regressions, e.g. foreshortened stratigraphy and sharp-based shoreface deposits on marine sediments occur

LST – Alluvial system (Fig. 4.7A)

Following a previous relative sea-level fall, the lowstand systems tract (LST) starts with a relative sea-level stillstand, followed by a slow rise. Due to high terrigenous sediment input, the sediment supply prevails over the newly formed accommodation space. The coastal system with large sand dominated braid delta complexes progradates seaward, resulting in a normal shoreline regression (Fig. 4.2).

The high terrigenous sediment supply is caused by recalibration of the fluvial stream equilibrium profile on the upstream alluvial plain. Though the relative sea-level stopped falling and starts to rise during the LST, the upstream parts of the river system continue to incise due to a slow upstream migration of the knickpoint. The resulting sediment is transported downstream, towards the coastal plain. On the coastal plain, now partly below the knickpoint, previously formed wide and shallow incised valleys are filled with coarse fluvial sediments (channels), representing the proximal parts of extensive braid delta systems forming at the mouth of the incised valleys (Fig. 4.9A).

Due to the shallow but wide fluvial incision during the FSST, the geometry of the valley fill are widespread sheets of amalgamated fluvial channel fill deposits, quite apart from “classical” incised valley fills. While the supply dominated coastal system progrades, the fluvial sediments on the coastal plain aggragate due to the seaward and upward migration of the fluvial equilibrium profile. The thick fluvial succession in the LST of sequence 4/4.1 is one example for aggradating fluvial deposits. Though LST-shelf deposits are rarely exposed

in the study area, it can be assumed, that the high siliciclastic input into the basin disturbed the carbonate production considerably.

TST – retrograding siliciclastic ramp system (Fig. 4.7B)

During the transgressive systems tract (TST) the relative sea-level rises constantly, causing a landward moving or retrograding coastal system. Older deposits, previously sedimented during the transgression, are constantly eroded and reworked in the shoreface area. Furthermore the rising sea-level leads to changes in the fluvial stream equilibrium profile, generating an increased sedimentary accommodation space. Fluvial sediment is stored on the fluvial and coastal plain, continuing the filling of the incised valley systems. As a result the siliciclastic sediment supply to the basin is low to very low. The lower, coastal part of the fluvial system changes due to an increased marine influence. Incised valleys become flooded and braid deltas are converted to wave dominated estuarine river mouths (e.g. Richards, 1996; Posamentier and Allen, 1999) (Fig. 4.9B).

There is still low siliciclastic sediment supply to the shelf by fluvial input and transgressive reworking and sediment dispersal. This siliciclastic input starts to disturb the carbonate production on the shelf. The formation of an incipient tripartite shelf can be noticed during the TST. On the outer shelf areas mixed carbonate-siliciclastic deposits (marls, claystones, some carbonates and sandstones) were deposited. The transition zone is often mud-dominated and usually made up by siliciclastic sediments. The shoreface is sand-dominated. The coastal system during the TST is characterized by barrier/lagoonal and estuarine systems.

HST – mixed carbonate-siliciclastic ramp system (Fig. 4.7C)

The highstand systems tract (HST) is marked by a slowly rising relative sea-level and a sea-level stillstand at its end. Compared to the TST, the rate of sea-level increase is lower during the HST. An increased sediment supply results in a stillstand and/or a slight progradation of the coastal system (Fig. 4.9C), which is part of a normal regression (Catuneanu, 2002). During the HST carbonate production on the shelf is more or less undisturbed due to a low siliciclastic input and the landward migration of the siliciclastic source. Generally the available accommodation space is superior to the siliciclastic sediment supply and gets slowly(?) filled by carbonates. The undisturbed carbonate production furthers the tripartite shelf development. The (offshore) shelf areas are dominated by carbonates and calcareous/marly sediments, while in the transition zone mixed carbonate-siliciclastic sediments are deposited. The shoreface usually consists of siliciclastic sediments. Especially during the HST the shallow, rimmed shelf becomes obvious (Chapter 3), since many of the carbonates can be characterized to be deposited within a shelf lagoon (Berndt, 2002).

FSST – prograding siliciclastic ramp system (Fig. 4.7D)

During the falling stage systems tract (FSST), the relative sea-level falls. The coastal system migrates seaward directly in response to the sea-level fall alone and not by filling of accommodation space. During the forced regression the constantly lowered wave base leads to erosion and reworking of older (HST) deposits on the constantly seaward moving shoreface. This process forms the regressive surface of marine erosion or transgressive ravinement surface (Catuneanu, 2002), and is responsible for foreshortened stratigraphy and sharp based shoreface deposits.

Since it can be assumed that the gradient of the river system on the coastal plain is less than the gradient of the shelf (Emery and Myers, 1996), a relative sea-level fall will have a stronger influence on the coastal plain, imposing a steeper gradient on the river profile than on the shelf. The increased stream power and thus raised erosion potential of the river causes fluvial incision, resulting in the formation of incised valleys during the FSST (e.g. Posamentier and Allen, 1999) (Fig. 4.9D).

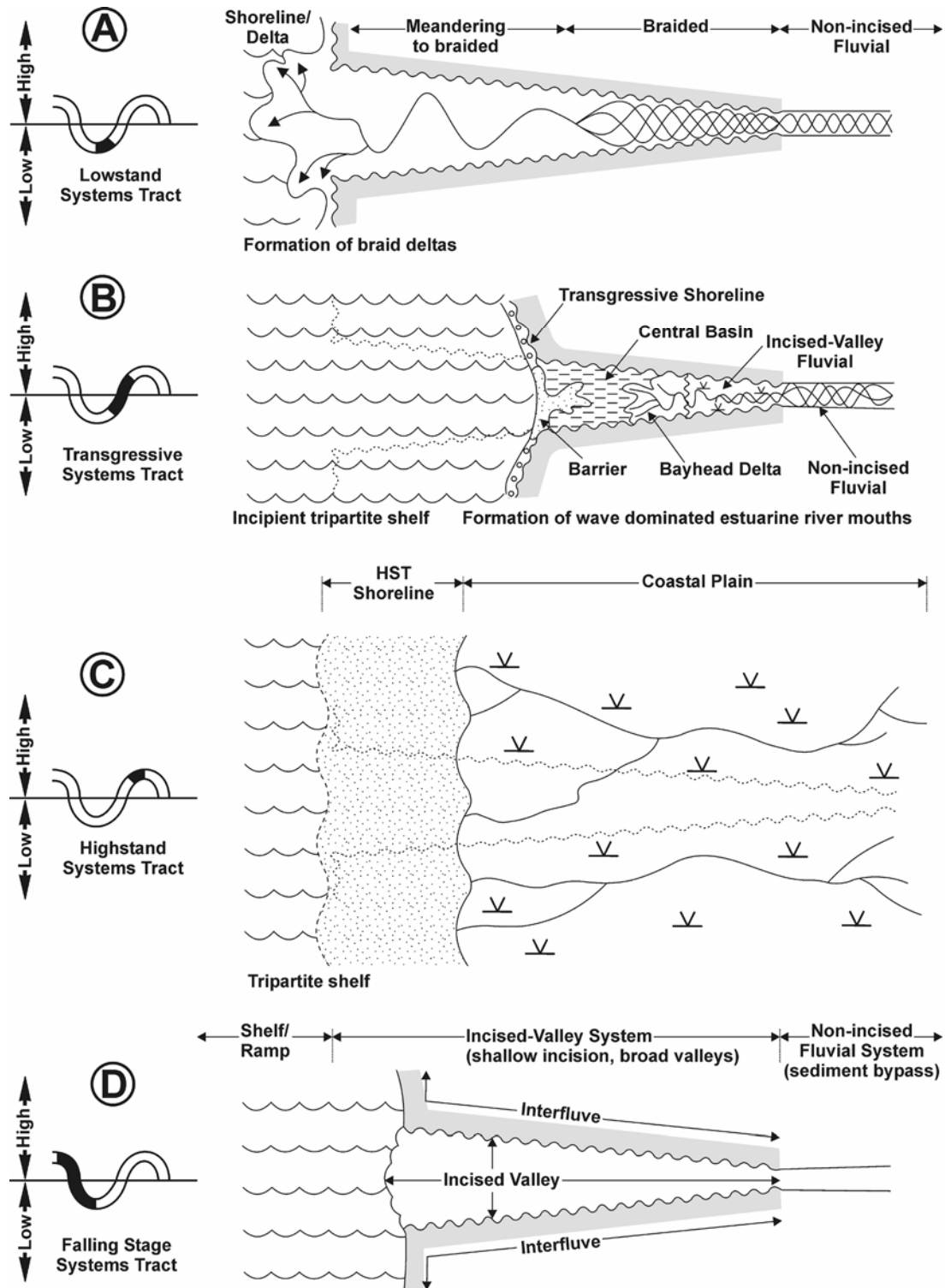


Figure 4.9 Idealized plan view of a simple incised-valley system adapted to fit the mid Cretaceous setting of South Jordan (modified after Zaitlin et al., 1994). **A)** During the FSST incised-valley systems form. **B)** During the LST braid deltas develop at the mouth of the incised valleys and fluvial aggradation “fills” the incised valley system. **C)** The TST sees the development of a wave dominated estuarine system at the mouth of the incised valley. **D)** HST with a progradational shoreface (normal regression). Further explanations see text.

Due to the constantly falling relative sea-level, the siliciclastic material is brought directly to the river-mouth, where it is target of reworking and re-deposition by shoreface powers (Posamentier and Allen, 1999). Therefore the alluvial and coastal plains become zones of sediment bypass. The formation of incised valleys (Fig. 4.9D) provides a high amount of

coarse-grained siliciclastic material and is the source of a high sediment supply to the basin. With constantly falling relative sea-level the “valley incision” moves seaward (Posamentier and Allen, 1999), often bypassing wide shelf areas where no fluvial incision might be developed. Due to the low slope angle of the shelf and the coastal plain the fluvial incision in the study area is only shallow, but relatively widespread compared to ‘steep sloped’ shelf settings.

During the FSST the shelf lagoon becomes more obvious than during the HST (see Chapter 3). The falling sea-level furthers the lagoon formation on the rimmed shelf and limits carbonate production. This is firstly caused by the falling sea level itself, constantly limiting accommodation space, and secondly by the high siliciclastic sediment input into the basin. Therefore the tripartite shelf of the HST starts to migrate seaward, restricting carbonate production to the ‘deeper’ shelf areas.

4.4 Parameters controlling the sequence architecture

The sequence or stratigraphic architecture is influenced by three major parameters: the relative sea-level, the sediment supply and the physiography (Posamentier and Allen, 1999). These major parameters are modified by subordinate second order parameters like eustacy and climate, which in turn are controlled by third order parameters (Tab. 4.4). In the following first order parameters and influencing second and third order factors will be discussed.

Table 4.4 Summary and relationship of the key parameters influencing the stratigraphic architecture (modified from Posamentier and Allen, 1999).

Key parameters influencing the stratigraphic architecture		
First order	Second order	Third order
	- Eustacy	- Climate
Relative sea-level	- Total subsidence/uplift	- Crustal cooling
		- Sediment compaction
		- Tectonics
		- Sediment loading
	- Vegetation	- Climate
Sediment supply	- Fluvial discharge	- Stream piracy
		- Palaeogeography
		- Climate
	- Provenance and Lithology	
Physiography	- Sedimentary processes	- Palaeogeography
		- Environmental energy
	- Tectonics	

Relative sea-level

The change of the relative sea-level is a major controlling parameter for the stratigraphic architecture of the mid to Upper Cretaceous (Albian to Coniacian) deposits of South Jordan. The global eustatic sea-level curve (Hardenbol et al., 1998) for the studied time period displays major changes with a total of more than 150 metres of sea-level rise and fall (Fig. 2.3, Chapter 2, p. 7).

No signs of synsedimentary tectonics were observed in the examined outcrops along the Naqb escarpment. All tectonic features are post-depositional and most probably related to the Neogene to Quaternary Wadi Araba-Dead Sea-Rift structure. Sediment compaction also was minor to normal, as proven by sediment petrography (Chapter 5). The mean sediment load from base Naur Formation to top Wadi As Sir Formation is 150 metres and can be neglected. Therefore the total subsidence and/or uplift was minimal and the relative sea-level curve resembles very much the global curve.

Using the sequence stratigraphic and depositional systems correlation, changes in relative sea-level for the mid to Upper Cretaceous of South Jordan were reconstructed (Fig. 4.8). Linked to the stratigraphy of section 5, the section which is most easily comparable to the stratigraphy of North/Central Jordan, it can be compared to regional and global sea-levels of the same period presented by other authors (Fig. 4.10). Due to the lack of bathymetric information, the presented relative sea-level reflects a pattern of changes with no absolute information on sea-level change. Comparison of the relative sea-level patterns of this study with regional and global curves shows that it resembles more the global sea-levels than the regional ones, which are influenced by regional tectonics (Lewy, 1990; Kuss, 1992) (Fig. 4.10).

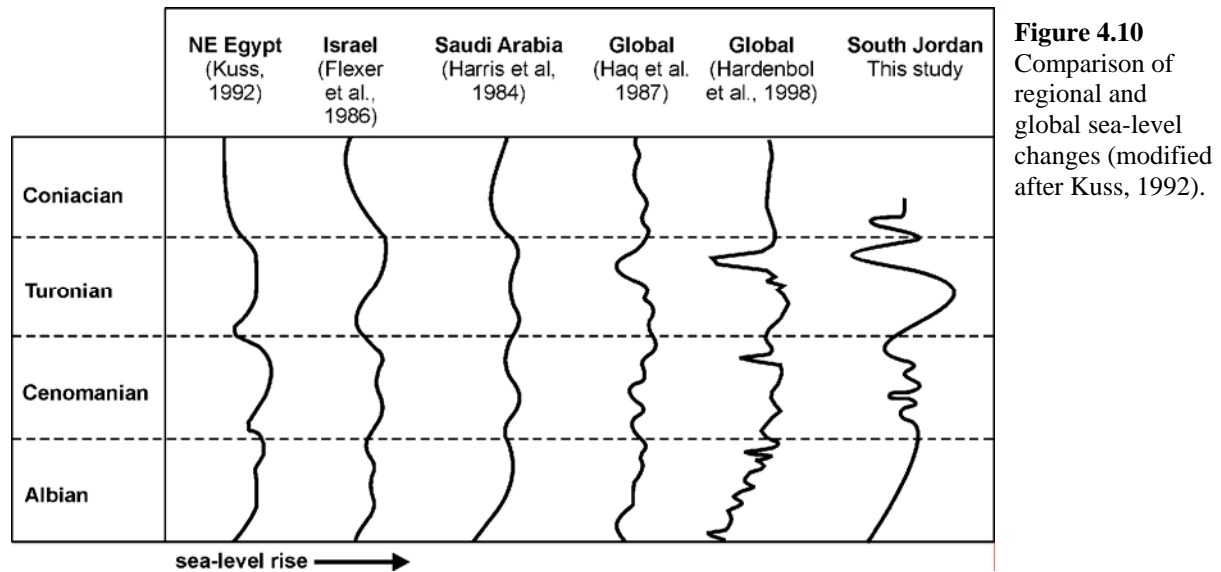


Figure 4.10
Comparison of regional and global sea-level changes (modified after Kuss, 1992).

Sediment supply

Sediment supply is also a fundamental variable in controlling the stratigraphic record (Castelltort and Van Den Driessche, 2003). As table 4.4 shows, it is influenced by several higher order parameters like vegetation, fluvial discharge and provenance. The frequent wood and plant remains and root traces within the logged sections, as well as the occurring articulated plant and tree fossils (compare Bender and Mädler, 1969; Moumani et al., 2001) point to a vegetated coastal and alluvial plain and hinterland. Vegetation might be considered a constant, since there is no real indication for a change in its density or type during the studied time interval.

The fluvial discharge is mainly controlled by the fluvial gradient. The slope of the shelf and the adjacent coastal plain was low. Stratigraphic forward computer modelling (Wöhrle, 2001) showed that a slope of about $0,035^\circ$ or lower has to be assumed. Such a low shelf gradient implies that even small changes in relative sea-level expose wide shelf areas, likewise changing the fluvial stream equilibrium profile (Miall, 1996; Posamentier and Allen, 1999). As a result of the change in fluvial equilibrium profile, the fluvial discharge and stream power increase, bearing a direct effect on the sediment load carried by the river. Since relative sea-level changed remarkably during the studied stratigraphic interval (Fig. 4.10), it can be concluded that also the fluvial discharge varied significantly.

Concerning the provenance and lithology of the source area, petrographic and geochemical provenance studies (Chapters 5 and 6) showed that these two parameters were constant during the whole studied time interval. The sediment source can be considered as a 'recycled orogen' (Arabian-Nubian shield) with a high content of recycled sedimentary material (Palaeozoic sediment cover). The Cretaceous sediments were deposited in a tectonic stable passive margin setting (Baaske and Krawinkel, 2001b), that did not change within the studied timeframe.

Physiography

Shelf width and gradient (Posamentier and Allen, 1999) are important parameters for the sequence architecture of the studied sediments. On the low gradient shelf wave energy was maximized, resulting in a wave/storm dominated shelf (Chapter 3). Depositional environments in such a shelf setting suffer high environmental energies and are susceptible to frequent reworking and erosion of sediment, disturbing the 'normal' stratigraphic succession. Furthermore the low shelf gradient enhanced the significance of the falling stage systems tract and the occurrence of forced regressions. Neither the logged sections and outcrops nor the results of the provenance analysis point to significant tectonic events which influenced the study area during sedimentation.

Conclusion

The major controlling parameters for the stratigraphic/sequence architecture of the mid to Upper Cretaceous deposits of South Jordan are the relative sea-level and, less important, the sediment supply. The total subsidence was rather low and uninfluenced by tectonics. Therefore the relative sea-level was mainly controlled by eustacy. Though a major influence of eustacy on sequence architecture is sometimes considered controversial (cf. Miall and Miall, 2001), the reconstructed relative sea-level curve of the study area is similar to the global curves (Fig. 4.10).

The siliciclastic sediment supply was important especially during the falling stage and lowstand systems tracts. The formation of incised-valleys on the alluvial plain and further upstream was the source of high sediment supply during the FSST and LST. Because of their low slope angle, shelf and adjacent coastal plain were very sensitive to sea-level falls, exposing wide areas of the shelf, leading to long-distance regressions typical of forced regressions.

4.5 Sequence stratigraphic results compared to forward stratigraphic computer models

During the course of the study a forward stratigraphic computer simulation with the Unix-based program SEDPAK was carried out by Alexander Wöhrle in order to check the significance of eustacy, sediment supply and physiography for the sequence architecture. Database for the simulation were mainly the logged and interpreted sections. Information like subsidence rates (bathymetric and sea-level corrected), sand/clay-ratios and ramp setting were taken from the logs. Carbonate production rates and eustatic sea-level curve were taken from literature (Hardenbol et al., 1998; Paola, 2000) or from the program itself. In the course of the computer modelling the sequence stratigraphic models for the mid Cretaceous of South Jordan were constantly compared to the SEDPAK result to improve both, the computer simulation and the sequence stratigraphic model. For a detailed description and work procedures refer to the Diploma thesis of A. Wöhrle (2001).

The end-model of the SEDPAK simulation (starting at the base of the Naur Formation) (Fig. 4.11) fits quite well with the sequence stratigraphic model (Fig. 4.8). The most easily recognizable matching features are the two major alluvial series (shown in each figure in orange colours) of sequences 3 and 4/4.1, which can be used as marker horizons for comparison. The SEDPAK model clearly demonstrates the significance of eustacy and sediment supply as main controlling factors of the sequence architecture (Baaske et al., 2001b). Furthermore the SEDPAK simulation verifies the point that sediment supply was especially high during FSSTs and LSTs as result of incised valley formation on the coastal/alluvial plain. The shelf gradient, as main physiographic factor, was important in the simulation for the overall distance of clastic input into the basin. The long distance/forced regressions within the simulation were mainly controlled by the low shelf gradient (about 0,035°).

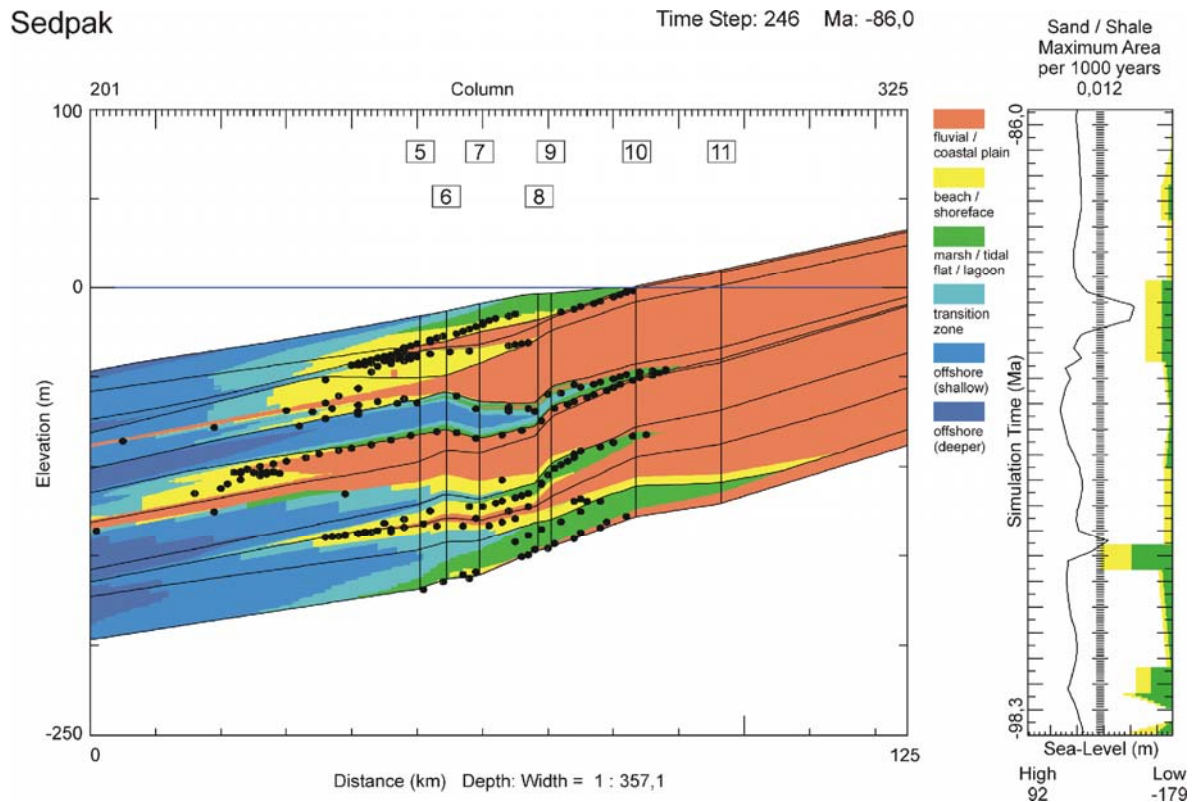


Figure 4.11 End model of the SEDPAK simulation. The column on the right represents the global sea-level curve after Hardenbol et al. (1998) and the clastic sediment supply (yellow = sand, green = clay). The colours of the depositional environments match the colours used in figure 4.2. The vertical lines in the model represent the position of the logged sections; the dots mark the coastline during the different time steps.

The computer model also produced foreshortened stratigraphy in the proximal area of the simulation (sections 8 and 9) as further hint to the presence of forced regressions (Fig. 4.12). The foreshortened stratigraphy appears in the model as low subsidence rates in sections 8 and 9, caused by ‘missing’ sediment packages.

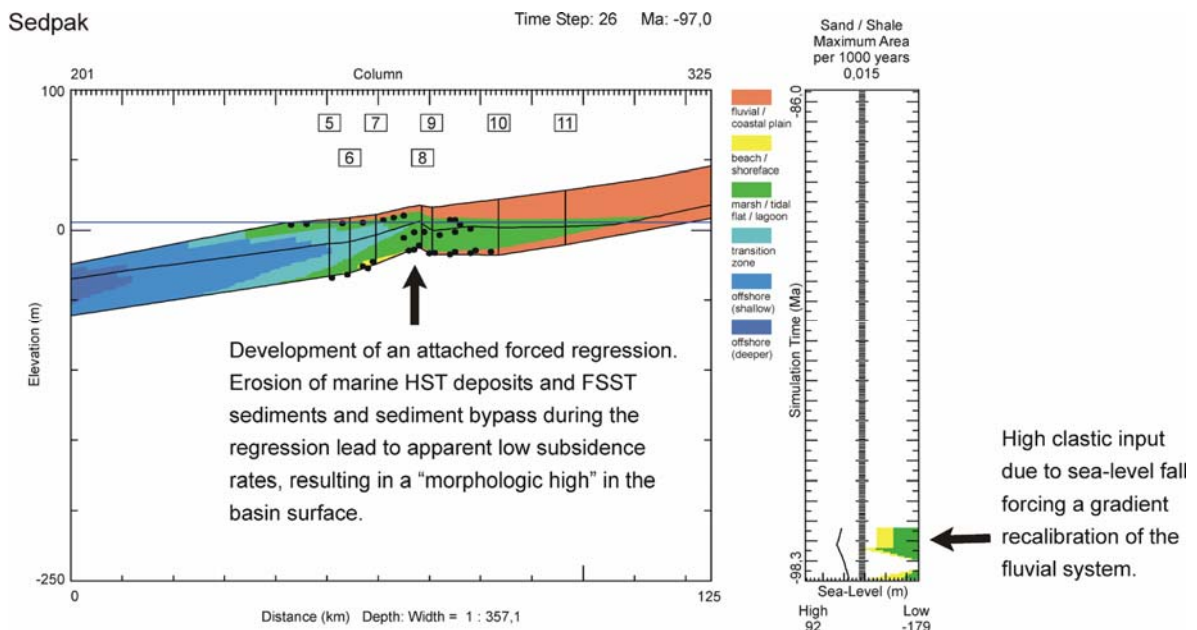


Figure 4.12 Effect of forced regressions on the SEDPAK simulation. This time step of the SEDPAK simulation shows how foreshortened stratigraphy, transferred from the logged sections into the simulation, affects the model. Due to missing sediment in sections 8 and 9 an apparent morphologic high forms due to lower subsidence rates. Further explanations see text.

In both sections the transitional facies between shelf and shoreface sediments is missing. If the transitional facies is missing due to erosion or nondeposition during the forced regressions is difficult to assess. The above mentioned low subsidence rates are clearly recognizable in the SEDPAK model as an apparent morphologic high in figure 4.12. This artificial high is the direct result of processes acting during forced regressions. It was produced by thorough transfer of field/log data into the computer model alone. The model was not initially intended to produce forced regressions, as it is often the case with other studies (e.g. Ainsworth et al., 2000).

Summing up, it can be said that the SEDPAK simulation closely resembles the sequence stratigraphic interpretation. The importance of eustacy and systems tract bound sediment supply for the sequence architecture is emphasised. Though not initially intended to include forced regressions, the computer simulation also shows evidence for their presence.

4.6 Summary of the sequence stratigraphy of the mid to Upper Cretaceous deposits of South Jordan

The different sequence stratigraphic aspects of the studied sediment succession are summed up in the following:

- Based on the correlation of the logged sections the studied sedimentary succession contains eight third-order sequences (sequences 1 to 8). Sequences 1, 2 and 4, can be subdivided into two sequences of higher order (1.1, 1.2, 2.1, 2.2, 4.1 and 4.2). The four basal sequences comprise the Cenomanian to Coniacian Ajlun Group. Sequences 5 to 8 belong to the Coniacian to Santonian Belqa Group.
- The frequent occurrence of late HST and early LST deposits in the first sequence stratigraphic interpretation using the Exxon sequence stratigraphic model showed the significance of the regressive relative sea-level in the studied succession. Such a setting is ideal to use the new, extended sequence stratigraphic model after Plint and Nummedal (2000), where late HST and early LST are combined to form a fourth systems tract, the so called falling stage systems tract (FSST). Therefore this model was applied in the presented study.
- Comparison of the major depositional systems with the sequence stratigraphic interpretation showed that the depositional systems correspond very well to the four systems tracts of the sequence stratigraphic model. The alluvial plain system developed during the LST, the retrograding siliciclastic ramp system formed during the TST, the mixed carbonate-siliciclastic ramp systems corresponds to the HST and the prograding siliciclastic ramp system is associated with the FSST.
- Basically all sequences include forced regressive deposits formed during the relative sea-level fall. Characteristic features like long distance regressions, foreshortened stratigraphy or sharp based shoreface deposits are displayed frequently within the sections. All but two of the forced regressive deposits are smooth-topped attached forced regressions. Only in sequences 2.1 and 2.2 smooth-topped detached deposits, linked to higher rates of relative sea-level fall during the mid Cenomanian, were found.
- Generally the recurring presence of smooth-topped forced regressive deposits characterizes the studied shelf system as a low gradient, high energy system.
- The reconstructed relative sea-level strongly resembles global, eustatic sea-level curves. Comparison with regional relative sea-level curves displays only marginal similarities, due to the stronger influence of tectonics in the other areas.
- The controlling parameters for the stratigraphic sequence architecture were relative sea-level changes and sediment supply. The relative sea-level changes were basically eustacy driven. Siliciclastic sediment supply was caused by sea-level changes and

associated with fluvial incision on the shelf and/or coastal plain. Consequently sediment supply was particularly high during the LSTs and FSSTs. The low gradient shelf slope was most important for the formation of the forced regressions.

- The significance of the controlling parameters was confirmed in a forward stratigraphic computer simulation carried out with the Unix-software SEDPAK. The model, based on the logged sections, showed that the stratigraphic architecture of the studied succession can be reproduced by variations of eustacy and differentiated sediment supply. The low gradient of the shelf slope was important for the formation of long distance regressions within the model. In addition to the long distance regressions, the SEDPAK simulation includes other features like foreshortened stratigraphy which directly correlates with the existence of forced regressions.

Part 2:

Petrography, geochemistry and provenance of the Upper Cretaceous sediments of South Jordan

5. Sedimentary petrography

While the Nubian Sandstones of Jordan, including the Lower Cretaceous Kurnub Group, are well examined (Bender, 1963; Abed, 1978; 1982; Khoury, 1986; Amireh, 1987; 1991; 1992; 1993; 1997; Amireh and Abed, 1999; 2000), studies of the Upper Cretaceous sandstones of South Jordan are rare. This is especially true for the petrographic aspects. Features of depositional environments were partially covered by the “Jordan Geological Mapping Project” and other publications of the Natural Resources Authority of Jordan (e.g. Powell, 1989; Andrews, 1992).

The aim of the sedimentary petrography was to determine possible vertical and horizontal variations in composition along the escarpment. Changes within the petrography of sediments can be used as possible correlation markers or even as depositional environmental indicators (Füchtbauer, 1967). Furthermore sedimentary petrography was applied to get an overview of the diagenesis of the Upper Cretaceous sandstones, e.g. to hold information on the subsidence history of the deposits. For information on the source rocks of the Cretaceous sediments the petrographic dataset was also used for provenance analysis. Tables containing the results of the petrographic analysis can be found in appendix II.

5.1 Light mineral analysis

Light mineral analysis is the basic tool in clastic sedimentary petrography. Usually following and supporting the field observations, the work on thin sections can be used in many ways. Common applications include the classification of the sediment, information on the diagenetic history and record of the source material of the sediment. The term “light mineral analysis” refers to the fact, that in a thin section of a siliciclastic sediment, the majority of the components is usually made up by minerals with a specific weight less than 2.89 g/cm^3 (Boenigk, 1983). Mineral phases with a specific weight of more than 2.89 g/cm^3 are called heavy minerals (see Chapter 5.2).

5.1.1 Methods

For the light mineral analysis 20 thin sections of sandstones and 32 thin sections of friable sand samples were point counted under the microscope, following standard point counting techniques (Tucker, 1996). The “traditional” method (Weltje, 2002) was used, distinguishing quartz, feldspar and rock/lithic fragments, where a lithic fragment is defined as a grain consisting of two or more phases. Authigenic minerals and pore space were also counted.

The point counting was carried out with a microscope (Leitz-Wild, Orthoplan) and an electronic point counter with mechanical stage (Prior, Model G). Sandstones were counted with 500 points, friable sand samples with 300. The artificial pore space in the friable sand samples was neglected during the counting. In order to compare the framework components of both datasets, the 500 point sandstone dataset had to be recalculated to a pore space free total, or to a normalized component ratio like QFL (see 5.1.4). The detrital minerals of the examined samples consist mainly of quartz (Q= 94.4%), feldspar (F= 3.9%) and rock fragments are scarce (L= 1.7%).

5.1.2 Analytical precision

The thin sections of one friable sand (J7-7) and one sandstone (J9-17 B) were selected for examination of the analytical precision. These samples were point counted three times each. The result of this analysis is summed up in table 5.1.

Composition estimates obtained by point counting are in general subject to uncertainties, resulting from various factors including the sampling scheme used in the field, the preparation technique and the counting procedure itself (Weltje, 2002). A review on this matter is given by Weltje (2002). A major factor controlling the precision is the number of points counted per thin section. Usual numbers range from 300 to 600 points per thin section (Pettijohn et al., 1987; Weltje, 2002). Higher numbers of counted points reduce the expected errors for the examined sample.

Table 5.1

Analytical precision of the light mineral analysis		friable sand (n=3; all values in vol.%)			sandstone (n=3; all values in vol.%)		
component	variety	mean	σ	range	mean	σ	range
quartz	mono	54.44	0.96	53.33-55.00	41.40	2.43	38.60-42.89
	undulose <5°	7.11	2.46	4.33-9.00	3.40	0.19	3.21-3.59
	undulose >5°	21.00	4.10	18.00-25.67	10.87	4.52	6.99-15.83
	poly. 2-3 subgrains	2.00	0.33	1.67-2.33	1.80	0.80	1.00-2.60
	poly. >3 subgrains	0.44	0.19	0.33-0.67	0.80	0.40	0.40-1.20
feldspar	plagioclase	0.11	0.19	0-0.33	0.07	0.12	0-0.20
	K-feldspar	3.89	1.68	2.33-5.67	2.13	1.40	0.80-3.59
hvy. mineral	-	-	-	-	0.13	0.23	0-0.40
lithic fragments	hematitic	0.33	0.33	0-0.67	-	-	-
	claystone	0.22	0.38	0-0.67	0.07	0.12	0-0.20
	siltstone	0.11	0.19	0-0.33	-	-	-
	carbonate	0.11	0.19	0-0.33	-	-	-
	metamorphic	0.22	0.19	0-0.33	-	-	-
authigenic minerals	quartz cement*	2.78	0.84	2.00-3.67	2.20	1.00	1.20-3.19
	feldspar cement*	0.11	0.19	0-0.33	-	-	-
	clay minerals (undif.)	3.22	1.95	1.00-4.67	3.80	0.88	2.79-4.40
	hematite	3.89	0.69	3.33-4.67	-	-	-
	Fe-oxide (undif.)	-	-	-	2.40	0.34	2.20-2.79
pore space	macro	-	-	-	30.73	3.22	27.25-33.60
	micro	-	-	-	0.20	0.20	0-0.40

*quartz and feldspar cements are inherited from recycled sediments and are no authigenic minerals sensu strictu

The analytical precision of the point counting depends also on the relative abundance of the counted components. Component abundances of up to 50% produce higher error levels, over 50% abundance lower error percentages can be observed again (Pettijohn et al., 1987). The determined errors for the examined samples (see table 5.1) are reasonable with respect to the abundances of the counted mineral phases.

5.1.3 Petrographic overview of the Upper Cretaceous sands and sandstones of South Jordan

This chapter describes the petrographic components (detrital and authigenic) of the studied samples. The following description is based on standard literature (e.g. Scholle, 1979; Adams et al., 1986 among others). Photomicrographs of the described components are shown in figure 5.1. In table 5.2 the mean values of the major petrographic components are presented.

Table 5.2

Mean values of the dominating framework components and cementing phases of the examined samples (n=53)									
	mono-quartz	undulose quartz	polyquartz	K-Fsp	plagioclase	lithoclasts	cement (total)	Fe-oxide	clay minerals
mean	62.16	20.31	2.46	3.20	0.32	1.60	9.75	5.80	2.05
σ	7.98	6.17	1.35	2.24	0.53	2.01	11.00	7.32	2.19
range	35.55-77.00	6.88-32.00	0.33-5.52	0.67-9.67	0-2.33	0-10.33	0-51.61	0-29.30	0-7.57

All values refer to 100% normalized, pore space free volume percentages

Detrital framework components

Quartz (monocrystalline quartz, polycrystalline quartz + chert)

Quartz is the dominating framework mineral in the studied thin sections (Fig. 5.1 No. 1-8, also see table 5.2). Monocrystalline quartz (monoquartz) occurs in three variants: non-undulose, slightly undulose ($<5^\circ$), and undulose monoquartz ($>5^\circ$) (cf. Scholle, 1979; Basu, 1985b and; Tortosa et al., 1991). The polycrystalline quartz (polyquartz) was distinguished into two groups: polyquartz with 2-3 subgrains and polyquartz with more than 3 subgrains. The subdivision of the polyquartz in these groups is necessary for the provenance plot after Basu (1985b). Chert, which was found only in two samples, was considered as a mono-mineral and, according to McBride (1963), added to the monoquartz fraction for classification purposes.

Re-sedimented quartz grains with thin syntaxial relictic rims of quartz cement (Fig. 5.1 No. 1-4) are often present. The frequently rounded and discontinuous cement was brought into the sediment with its host grain. During the process of re-sedimentation the cement got rounded or was partially removed from the host grain, causing the fragmented appearance of the cement rim. Though the primary origin of the quartz cement is of autochthonous nature, it is part of a sedimented grain and consequently an allochthonous element. Few quartz specimens with resorption cavities, pointing to a magmatic source for these grains, were found in some samples.

Feldspar (potassium feldspar and plagioclase)

All analysed samples contain small amounts of potassium-feldspar (K-FSP), including twinned microcline. Plagioclase occurs in some thin sections and seems to be linked to samples with smaller grain sizes (fine sand). Few K-FSP grains and even some plagioclase grains display small amounts of attached cement (Fig. 5.1 No. 9-12). The cement rims grow in optical continuity with the host mineral and display a ragged appearance. Like quartz cement this feldspar cement is inherited from the source sediment.

Potassium-feldspar might easily be mistaken for quartz under the microscope. Both minerals resemble each other in interference colour and general appearance and thus may slightly bias the point counting results. The low potassium values of the bulk rock analyses (Chapter 6) of sand sized samples back up the results of the petrography concerning the low potassium-feldspar content.

Lithic fragments (lithoclasts)

The examined samples contain only a very small amount of lithic fragments, even samples without a single rock fragment occur. Lithoclasts found in the studied samples include: claystones, siltstones, carbonate fragments, hematitic clasts, volcanic lithoclasts (including altered fragments of volcanic glass) and metamorphic lithoclasts.

Fragments of claystone (Fig. 5.1 No. 19 & 20) occur in different sizes. Often these rock fragments are bigger than the surrounding framework grains, representing reworked material brought into the sediment by erosional processes during the sediment transport. Siltstone

clasts are made up of a mixture of clay minerals and very small quartz particles and can also be considered as reworked material. Particles which might fit in both categories, i.e. claystone and siltstone, were classified as undifferentiated sediment clasts.

Carbonate fragments were found only in three samples (J7-7, J10-22A and the recent desert sand). These clasts represent material reworked from intrabasinal carbonates (e.g. from the Naur Formation). Hematitic clasts are detrital components with a lot of hematite “pseudo-matrix” in the clast. The nature of the hematite is clearly secondary and linked to diagenesis or weathering. Claystone clasts rich in Fe-oxide were also counted as hematitic clasts (Fig. 5.1 No. 17 and 18).

Small pieces of recrystallized volcanic glass or groundmass (e.g. from rhyolites, Fig. 5.1 No. 15 and 16) are scarce and might easily be mistaken for chert fragments. These volcanic lithoclasts represent primarily an acidic volcanic origin. Detrital grains with fine dark groundmass including small, lath shaped plagioclase crystals in it, were recognized as basalt grains. Generally only few samples contain such basic volcanic rock fragments.

Metamorphic lithoclasts (Fig. 5.1 No. 13 and 14) are usually made up of metamorphic polyquartz fragments of high grade metamorphic origin. The recrystallized subcrystals of a metamorphic polyquartz are lengthened and display different extinction angles under crossed polars due to variable orientation of the C-axis (Scholle, 1979). Typical source rocks for these lithoclasts would be gneisses (Scholle, 1979). Mixtures of lengthened quartz minerals with potassium-feldspar and mica flakes also occur. Lithoclasts showing an un-deformed intergrowth of quartz, feldspar and mica can belong both to the magmatic or metamorphic lithoclast group and were counted separately as “quartz-feldspar-clasts”.

Heavy minerals and opaque material

Heavy minerals and opaque materials make up less than 1% of the components. It seems that samples with smaller grain sizes contain a higher percentage of heavy and opaque minerals, which might point to hydraulic sorting during transport. Some marine sandstones (e.g. J6-43D) contain glauconite. Glauconite was counted as a heavy mineral component, since microscopic work revealed that the material was reworked and not formed in situ.

Other components

Phosphatic remains, like fish scales and fish teeth, occur in the marine sandstones along the Naqb escarpment but were not encountered during the point counting. Besides carbonate cements and glauconite the appearance of these allochthonous fragments is a good indicator for the marine nature of the host sediment. Mica minerals are present to a lower degree in some friable samples, particularly from fluvial sediments, but were lost during the preparation of the grain mounts due to buoyancy effects.

Autochthonous components

Clay minerals

Two types of clay minerals could be identified with the microscope in the studied samples: smectite and illite. Due to the small size of the minerals and the frequent covering with secondary iron-oxides a clear identification is not possible. Therefore the clays were usually point counted as “undifferentiated clay mineral”.

In all 52 examined samples the clay minerals occur as clay rims or coatings around framework grains. The appearance of clay rims mainly points to an allochthonous, “none diagenetic”, nature of the clays (Moraes and De Ros, 1992; Gaupp et al., 1993). Clay coatings may be inherited from reworked framework grains, infiltrated by sedimentary processes and meteoric water or might be the result of soil forming processes (Gaupp et al., 1993). Thus the origin of the clays might be autochthonous, at least when formed by soil forming processes.

Since the origin of the clay minerals is hard to proof under the microscope alone, the clays were considered in the calculations for cement and inter granular volume (IGV) as an autochthonous component.

Iron oxide

Iron oxide (Fe-oxide) appears in all examined samples in varying amounts. It can be encountered in the interparticle-porosity of the sandstones. Usually it fills the pore throats and even encloses several framework grains, causing the effect of floating grains. Another common occurrence of Fe-oxide in the samples is as thin, often discontinuous rims/coatings around framework grains. This appearance of Fe-oxide might be connected to the diagenetic transformation of clay mineral coatings to Fe-oxides (Walker, 1976, Prof. Dr. R. Gaupp, Institute for Geosciences, University Jena, personal communication). An exact determination of the mineral type of the Fe-oxide is not easy under the microscope. Therefore, most of it was counted as “Fe-oxide, undifferentiated”. Where hematite could be clearly identified due to its reddish-brown colour and habitus, it was counted as such.

Some samples contained larger amounts of iron oxide, forming the main cement phase of the sediment. These “Fe-sands and ferribands” (see Chapter 4: Sedimentology) usually form prominent sediment beds in the field. Samples of these sediments (e.g. J7-28 and J10-22A) show relatively few framework grains which are very often partially covered by Fe-oxide.

Carbonate cement (calcite and dolomite)

Calcite and dolomite occur in the well cemented marine sandstone samples (see Fig. 5.1). Since the thin sections were not coloured with Alizarin red it is hard to distinguish the two minerals under the microscope. A special carbonate cement feature are dedolomite rhombs, sparry calcite replacing dolomite, e.g. in sample J5-29 (Fig. 5.1 No. 23 & 24). The rhomb shapes are often outlined with iron-oxide. Replacement of quartz by calcite also occurs in the marine sandstones.

Other autochthonous minerals

Other autochthonous minerals are baryte and gypsum. Both mineral phases represent a rare feature in the samples and are interpreted as indicators for the marine origin of the sediment.

Some of the samples display a greyish-brown “groundmass” in some pore spaces, often enclosing several framework grains. Under crossed polars the colour of the material is still greyish brown, leading to the assumption that it might be a kind of phosphatic groundmass. The reddish brown colour of some parts of this material might point to the presence of iron oxide. With light microscopic analysis alone the nature of this “phosphatic groundmass” could not be determined. If this mineral phase is really phosphate, it would point to the marine origin of the sediment, or at least a marine influenced diagenesis.

5.1.4 Granulometry

Grainsize and sorting

All examined samples are fine to medium grained. Only a few samples have a coarser grain size. For preparation of the heavy mineral grain mounds (see Chapter 3.2.1) a sieving analysis of several friable sand samples was performed and interpreted with the software SediVision (Version 2.0). The results showed that the field analysis of the grain size fitted well with the grain sizes measured in the laboratory. The sediments are mainly well sorted. Very well and moderately sorted sediments also occur.

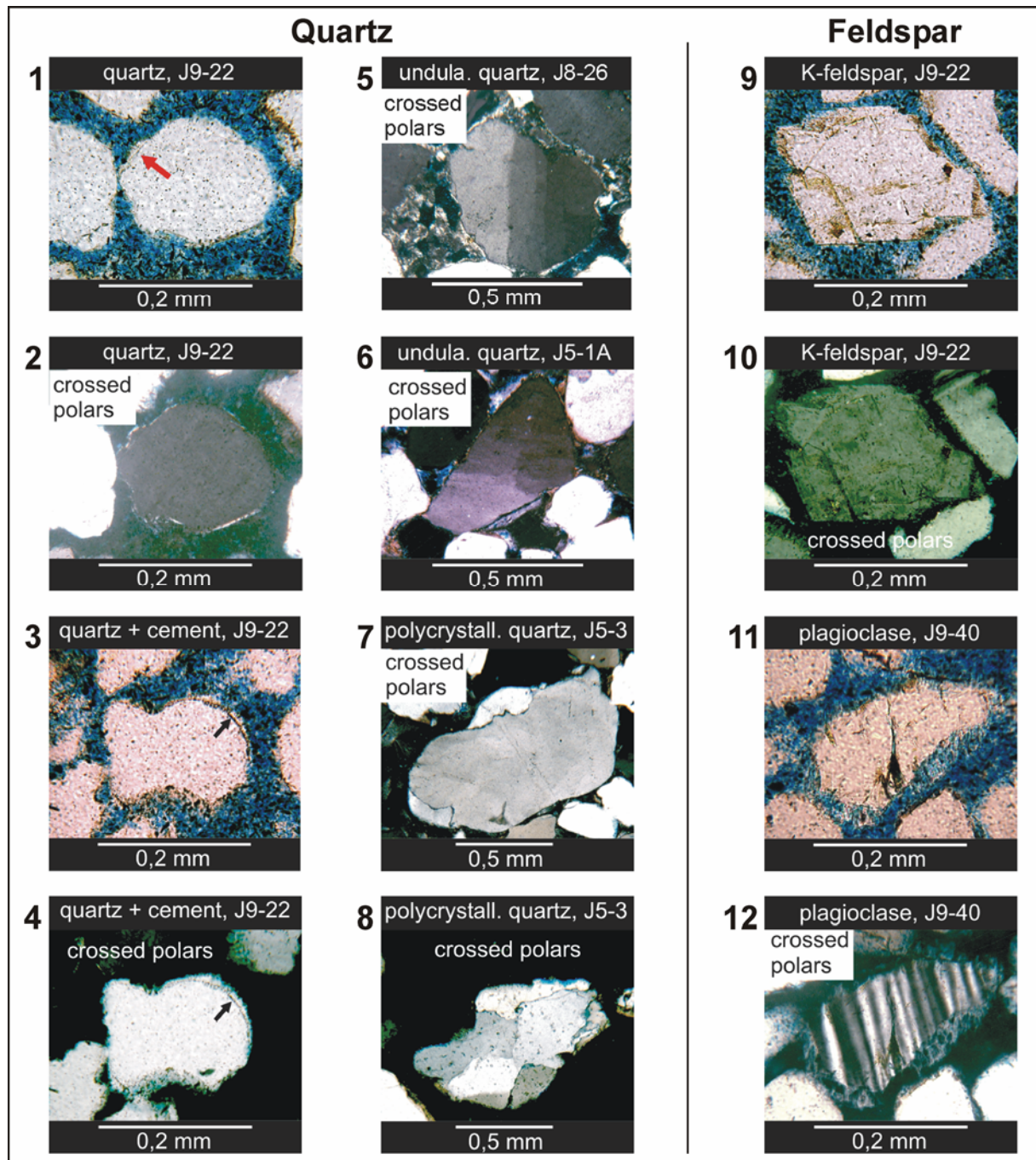


Figure 5.1 Photomicrographs of the major framework components and authigenic cementing phases.

1) rounded monocrystalline quartz with remains of syntaxial quartz cement (arrow), classifying the quartz grain as a recycled component; **2)** same quartz grain as in No. 1 photographed with crossed polars, the thin clay mineral coating around the grain becomes visible; **3)** & **4)** recycled monoquartz with thin syntaxial quartz overgrowth (arrow), a thin iron-oxide layer precedes the quartz cement; **5)** undulose quartz grain with clay mineral coating; **6)** undulose quartz grain; **7)** polycrystalline quartz with 3 sub-grains (Qp 2-3, cf. Fig. 5.10); **8)** polycrystalline quartz with more than 3 subgrains (Qp>3, cf. Fig. 5.10); **9)** & **10)** potassium feldspar with extensive syntaxial feldspar cementation, note the iron-oxide on the rims of the grain and entering joints in the cement; **11)** & **12)** plagioclase with a thin, ragged syntaxial plagioclase cement rim.

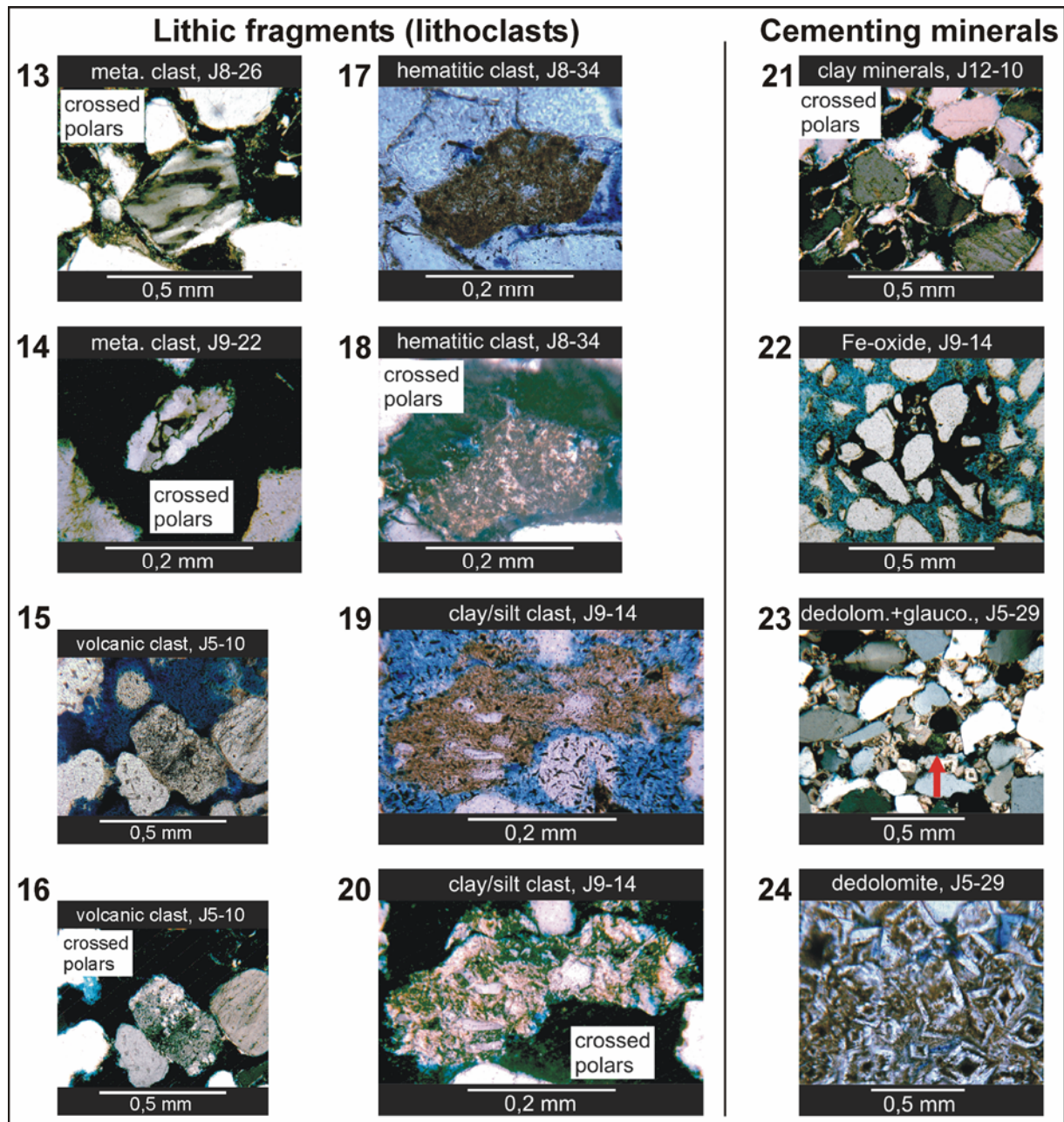


Figure 5.1 continued

13) metamorphic quartz grain; **14)** polycrystalline quartz of metamorphic origin; **15)** & **16)** rhyolitic volcanic lithoclast, the grain is a fragment of slightly altered rhyolitic groundmass; **17)** & **18)** hematitic lithic fragment; **19)** & **20)** claystone/siltstone fragment, the silt sized quartz fragments are surrounded by a clay mineral matrix (bright colours by crossed polars, photo No. 20); **21)** clay minerals visible as bright coloured clay rims/coatings around the framework grains; **22)** "floating" framework grains cemented by iron oxide; **23)** overview of a marine cemented sandstone sample, the arrow marks the position of a glaucony grain; the framework components are cemented by calcite cement and dedolomite rhombs; **24)** close up of the dedolomite rhombs, the iron oxide impregnation of the dedolomite is clearly visible.

Grain form and rounding

The grain form varies from high spherical to low spherical grains. In general the majority of the grains are rounded to sub-rounded, with angular grains occurring. The rounding of the grains depends on grain mineralogy. Well rounded grains are usually made up by quartz. The common rounding of the quartz grains ranges from rounded/sub-rounded to angular. Often the different rounding stages can be found in the same thin section. Feldspars are rarely rounded, but are frequently rimmed with feldspar cement, producing an angular appearance of the grains. Lithoclasts are usually rounded to sub-rounded. Soft, sedimentary rock fragments (e.g. claystones) are sometimes slightly deformed due to compaction.

5.1.5 Sandstone diagenesis

In general the diagenesis of the South Jordan Cretaceous sandstones is not very distinctive. Mechanical compaction is low, which points to minor burial and only little overburden. Based on field observations, sedimentology and sedimentary petrography, the sands and sandstones can be split into three diagenesis groups, which will be described in the following.

Friable and weakly cemented sandstones

The sediments of this diagenesis group are usually friable and very weakly cemented (mean cement content: 7.25%). The thin sections reveal that clay minerals (Fig. 5.1 No. 21), iron oxides (mostly hematite) (Fig. 5.1 No. 22) and sometimes some phosphate form the cement for the framework grains. Occurring quartz and feldspar cements are relictic and inherited from recycled material/sediment.

In the Houseknecht diagram (Fig. 5.2) these sandstones exhibit the highest intergranular porosities of all examined sediments. The friable character of these sandstones is a direct result of the poor “cementing” quality of the few clay minerals and iron-oxides in the sediment. Both terrigenous and marine sediments belong to this group, with only the marine samples containing the phosphatic cement phase.

Sandstones heavily cemented by carbonate minerals

Well cemented marine sandstones belong to this group. Calcite, dolomite and dedolomite are the main cementing phases forming up to 34.6 % of the sediment (see Fig. 5.1 No. 23 & 24). Open pore space, usually in form of micropores, is scarce in these sediments. Compared to the other diagenetic groups, these sandstones often display floating grains and have a high content of cementing phases. This effect might be attributed to an early cementation of the sediment and to replacement of quartz and feldspar grains by calcite cement.

The presence of dedolomite indicates the influence of meteoric fluids, leading to replacement of the dolomite by calcite (Holail et al., 1988). The precursor dolomite might be of marine origin (hypersaline) or formed in a sabkha environment. The occurrence of glaucony in some of these sediments (Fig. 5.1, No. 23) points also to the marine origin of these deposits.

Within the Houseknecht diagram (Fig. 5.2), these sediments exhibit intergranular porosities of about 10%. The sample with an intergranular volume of nearly 45% (!), points to early cementation and replacement of framework grains by calcite cement.

Fe-oxide rich sands and sandstones

Ferribands (“ironcrusts”) and Fe-sands are joined in this group and include sediments of marine and terrigenous origin. For more precise statements further studies on an enlarged dataset would be necessary.

All sediments within this group are strongly cemented with Fe-oxides. The appearance of the Fe-oxide in thin sections and its reddish-brown colour point to hematite as main mineral

phase. Often the complete intergranular pore space of the sediment is filled with Fe-oxide. The low compaction of the sediments, expressed by the dominance of point contacts within the thin sections, and the presence of floating grains give rise to the assumption that the iron-oxide is an early cement phase.

Similar to the sandstones cemented by carbonate, the Fe-sands display relatively low values of intergranular porosity in the Houseknecht diagram (red dots, Fig. 5.2).

Compaction and porosity

The examined samples show low to medium compaction. Most framework grains exhibit long contacts and fewer portions of point contacts (cf. Füchtbauer, 1988). “Floating grains” are common in the highly carbonate cemented marine sandstones and in samples intensely cemented by iron oxides.

The diagram after Houseknecht (1987) allows statements on compaction and cementation of clastic, sand grain sized sediments. To use the diagram the dataset has to include information on the intergranular pore space. Intergranular pore space and the total cement volume are combined as intergranular volume (IGV). To acquire information on the IGV of friable samples is difficult and requires extensive preparational measures. Therefore the presented data set is limited to the sandstone samples only.

Figure 5.2, the modified diagram after Houseknecht (1987), shows that about 25-40% of the primary porosity was irreplaceable destroyed by compaction. The second porosity reducing agent, cementation, splits the examined samples into two groups. Group I, marked green in figure 5.2, is only slightly cemented (up to 15%), mainly by clay minerals and some iron-oxide. Group II is cemented (20 to 40%) by carbonatic cements (marked in blue) and iron-oxides (marked in red). Group II has an intergranular porosity of at least 5-10%, while the sediments of group I display porosities of up to 35%. This clearly indicates that the cementation by different mineral phases is the main factor controlling the porosity of the South Jordan Cretaceous sandstones.

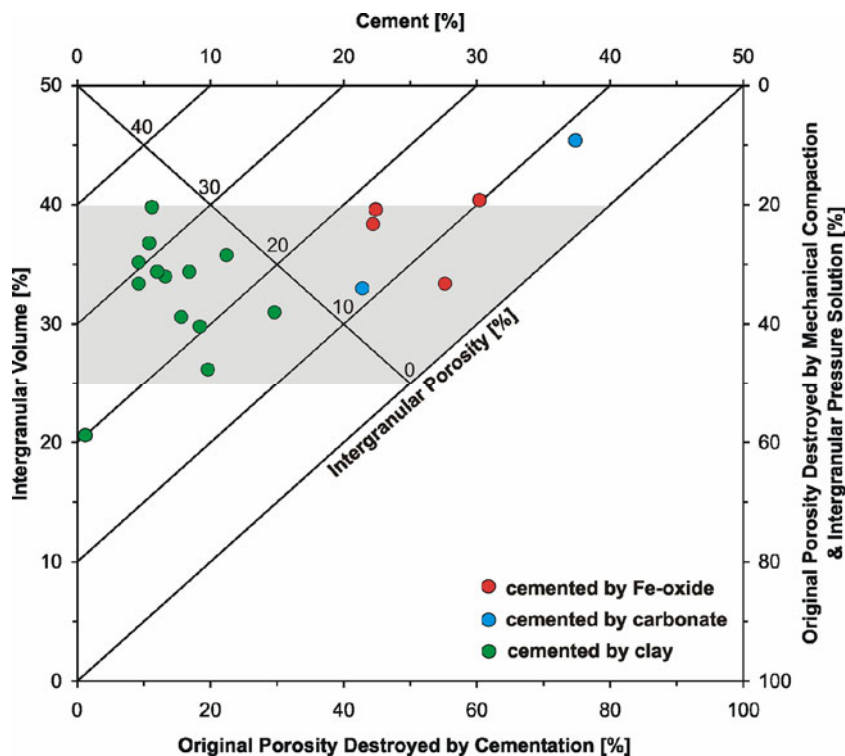


Figure 5.2

Compaction-cementation diagram after Houseknecht (1987). The majority of the samples experienced mechanical compaction (shaded area) between 20 to 45%. Two groups can be distinguished: Group I, which is slightly cemented by clay minerals, and group II, which is strongly cemented by iron-oxides or carbonates. Samples cemented by clay minerals have noticeable higher porosity values (up to 35%).

5.1.6 Rock classification

The ternary QFL-plot after McBride (1963) was used to classify the samples. For the McBride-plot all counted monoquartz, polyquartz and chert grains are combined to “quartz” (Q). K-feldspar, microcline and plagioclase are summed up in the feldspar component (F). The lithoclast (L) component includes all rock fragments. All other framework grains are neglected in this classification.

Quartz contents of 90 % and more are quite usual, classifying most sediment as quartzarenites and thus reflecting their mineralogical mature character. Depending on the content of feldspar and lithic fragments some samples plot in the subarkose and sublitharenite fields. This classification fits well with the results of the geochemical classification of the sediments (see Fig. 6.1 in Chapter 6).

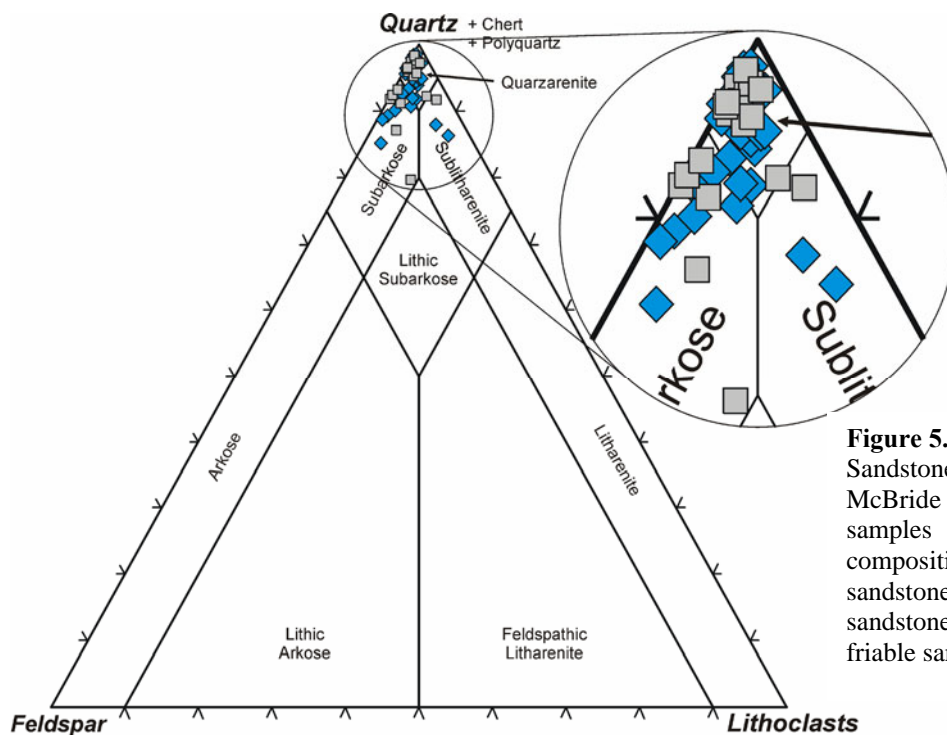


Figure 5.3
Sandstone classification after McBride (1963). Nearly all samples can be considered as compositional mature sands/sandstones (grey squares: sandstones; blue diamonds: friable samples).

5.2 Heavy mineral analysis

Heavy mineral analysis is one of the classic methods in provenance studies. The composition of the heavy mineral fraction of the sediment can provide valuable information especially on the composition of the source rock (Morton, 1985; Amireh, 1987; 1991; Kutterolf, 2001; Wozazek, 2001; Diener, 2002, among others).

5.2.1 Methods

52 friable sand samples were analysed for their heavy mineral content. To minimize influences of weathering, sorting etc. (see 5.2.3) only unweathered samples, representative for the sediment, were collected and analysed.

Separation and preparation of the heavy minerals was performed according to standard procedures as described by Boenigk (1983) and Mange and Maurer (1991). The 63-125 μm grain size fraction was obtained by sieving. The heavy mineral fraction was separated with Sodium Polytungstate (specific density 2.89 g/cm^3). Prior to the separation, the material was boiled for ten minutes in HCl (concentration: 10%) to lose iron-oxide rims and calcite, which would interfere with the Sodium Polytungstate. The drawback of the acid treatment is the loss of apatite, which dissolves during the procedure. The heavy mineral grains were mounted on standard glass slides (grain mounds) with Meltmount ($n = 1.704$).

For the analysis of the grain mounds 200 transparent grains were counted, applying the ribbon method (Mange and Maurer, 1991). To obtain more information on the heavy mineral content, zircon and tourmaline were divided into several mineral varieties (Tab. 5.3A). Until the number of 200 transparent grains was reached, all occurring opaque minerals within the 'ribbon' counting area were also counted, although not identified (see Appendix II).

5.2.2 Analytical precision

The precision of heavy mineral analysis depends, similar to the analysis of thin sections, on the number of counted minerals and factors like sample technique and preparation (Weltje, 2002). In order to get the mean heavy mineral content of a sample two methods can be applied: Some authors prefer to count less grains (e.g. 100), but more grain mounds of a single sample to get the mean composition (Boenigk, 1983). Others propose the counting of more grains (e.g. 200), to record the content of less frequently appearing heavy minerals (Mange and Maurer, 1991). This method reduces also the error of the analysis, which decreases squared to the number of the counted grains (Boenigk, 1983).

To determine the precision of the analysis, one heavy mineral grain mound (J15-4) was counted three times (Tabs. 5.3A and 5.3B). Table 5.3A clearly reveals that small relative abundances produce high errors, while combining heavy mineral varieties into major mineral groups (Tab. 5.3B) produces smaller and more reasonable error levels.

Table 5.3A Analytical precision of the heavy mineral analysis with several sub-divisions (200 grains counted; n=3; all values in %).

mineral	variety	mean	σ	range
zircon	rounded	23.67	5.75	18-29.5
	anhedral	21.50	2.50	19-24
	euhedral	7.00	1.32	5.5-8
	zoned	3.33	1.44	2.5-5
	pink	5.33	1.04	4.5-6.5
tourmaline	rounded blue	2.17	0.58	1.5-2.5
	angular blue	1.83	1.04	1-3
	rounded brown	4.67	1.04	3.5-5.5
	angular brown	3.50	2.18	1-5
	rounded green	3.50	2.29	1-5.5
	angular green	2.50	0.50	2-3
rutile	-	20.00	2.78	17-22.5
staurolite	-	0.67	0.29	0.5-1
kyanite	-	0.33	0.58	0-1

Table 5.3B Analytical precision of the heavy mineral analysis applied to the major heavy mineral components (200 grains counted; n=3; all values in %).

mineral	mean	σ	range
zircon	60.83	2.02	59-63
tourmaline	18.17	1.53	16.5-19.5
rutile	20.00	2.78	17-22.5
other heavy minerals	1.00	0.87	0.5-2

5.2.3 Controlling factors of the heavy mineral association

The heavy mineral content of a sediment is influenced by various controlling factors. These are: (1) the alteration of the source rock, (2) abrasion during the transport, (3) hydraulic processes, (4) modification during diagenesis/burial ("intrastratal solution") and (5) modification during the weathering of the host sediment (Boenigk, 1983; Morton, 1985). A detailed review of these processes is given by Wozazek (2001).

Not all of these influences had an effect on the studied material. The alteration of the source rock, for sure an important factor (Wozazek, 2001), can not be considered in this study, since the exact source rocks are not known. The alteration of heavy minerals during the transport is difficult to assess. The heavy mineral assemblage of a few samples is dominated by tourmaline (Fig. 5.5). Since all these samples are fine grained sands with higher silt and clay content, this

points to a hydraulic sorting effect. The other samples, mainly dominated by zircon or a zircon-tourmaline-rutile-mixture, do not display a hydraulic influence. The major part of the source rocks can be assumed to be multi-cycle sediments. Therefore the abrasion by transport can be inherited from an older sediment cycle and needs not be the result of the last transport. The deposits experienced only minor burial and slight diagenesis, therefore no significant intrastratal solution is to be expected (see Chapters 5.1.5 and 5.3). To minimize in situ weathering effects only fresh, unweathered samples were collected for heavy mineral analysis.

5.2.4 Description of the heavy minerals

With a mean of 97.9% of the transparent heavy mineral content, all samples display a clear dominance of the ultrastable minerals zircon, tourmaline and rutile. Other heavy minerals, like garnet, monazite and staurolite, occur only in minor percentages (mean: 2.1% of the transparent heavy mineral content). The analysed samples resemble the heavy mineral association for the Lower Cretaceous Kurnub Group as described by Amireh (1987; 1991). A summary of the heavy mineral content is shown in table 5.4.

Table 5.4 Mean values (in %) of the heavy minerals (n=52).

mineral/variety		mean [%]	σ	range [%]
zircon	rounded	26.35	11.42	1.5-49
	anhedral	12.81	4.16	5-25.5
	euhedral	7.65	3.40	2-16
	zoned	2.83	1.61	0-7
	pink	3.83	1.72	0.5-7.5
tourmaline	blue rounded	2.03	1.59	0-8
	blue angular	1.62	1.53	0-6
	brown rounded	7.80	4.30	0.5-20
	brown angular	4.23	3.94	0-21
	green rounded	6.38	3.50	0-15
	green angular	3.20	2.48	0-12.5
rutile		19.19	4.10	9-30.5
other heavy minerals		2.10	1.87	0-9

The occurring heavy minerals of the mid-Cretaceous sands of South Jordan are described in the following chapter. Photomicrographs are shown in figure 5.4. Detailed descriptions of the minerals concerning their mineralogy, optical properties and their source rocks can be found among others in Boenigk (1983), Mange and Maurer (1991) and Matthes (1990).

Zircon (ZrSiO₄)

Zircon is an ultrastable heavy mineral, frequently derived from acidic and intermediate source rocks. Rounded zircon is attributed to sedimentary source rocks (Boenigk, 1983; Mange and Maurer, 1991). Zircon is easy to recognize in grain mounds due to its extremely high relief, the usually colourless appearance and the white interference colours (see Fig. 5.4).

Based on the work of Lihou and Mange-Rajetzky (1996), 5 types of zircons were distinguished: euhedral, anhedral, rounded, zoned and pink zircons (Fig. 5.4). The pink type of zircon was established due to the possible origin from Precambrian source rocks (Zimmerle, 1972; Mange and Maurer, 1991). Within the samples rounded zircons dominate, anhedral and euhedral zircons are frequent. Pink zircons and zoned ones occur only in minor amounts but are present in all samples. Compared to tourmaline and rutile (Tab. 5.4 and Fig. 5.5), zircon forms the main heavy mineral fraction of the Cretaceous clastics of the study area.

Tourmaline ($Na(Fe, Mg, Mn, Li, Al)_3Al_6[Si_6O_{18}](BO_3)_3(OH, F)_4$)

Tourmaline is a frequent ultrastable heavy mineral within all types of clastic sediments (Mange and Maurer, 1991). The striking colours and pleochroism, the lack of any cleavage and the high interference colours are easily recognizable features under the microscope. Source rocks for tourmaline are mainly acidic magmatic rocks like granites and pegmatites (Matthes, 1990), metamorphic rocks like gneisses and contact metamorphic rocks. Due to its extreme resistance to mechanical and chemical weathering, rounded tourmaline points to a reworked/resedimented clastic source rock (Boenigk, 1983; Mange and Maurer, 1991).

A variety analysis of the tourmalines was carried out for colour and shape. Brown tourmalines (with colour variations from greyish-brown, reddish-brown to dark-brown), as well as green and blue varieties (with possible shades of greyish-blue to dark blue) were distinguished (Fig. 5.4). A further distinction for each variety in rounded and angular was made to see if an influence of reworked sediment could be found in the samples. Within the sediment rounded tourmalines dominate. Brown tourmalines are most common and are followed by the green variety (Tab. 5.4).

Rutile (TiO_2)

Like zircon and tourmaline, rutile is an ultrastable heavy mineral. In the grain mounts rutile can be identified due to its striking reddish-brown colour (often overlying the interference colour of the mineral), the high double refraction and high relief (Mange and Maurer, 1991 and Fig. 5.4). Rutile is an accessory mineral in metamorphic rocks (Boenigk, 1983; Mange and Maurer, 1991), especially in schist and gneisses and in some amphibole rich plutonic rocks (Mange and Maurer, 1991). The occurrence of well rounded rutile points to a reworked sedimentary source rock. Rutile is present in all examined samples and usually forms 16 to 20 % of the heavy mineral association. It occurs rounded as well as euhedral to anhedral.

Other heavy minerals

Other heavy minerals are staurolite, kyanite, monazite, titanite and garnet. Staurolite and kyanite occur in almost every sample, garnet is restricted to 4 samples. Monazite and titanite appear generally in most grain mounts.

Staurolite ($(Fe^{2+}, Mg)_2(Al, Fe^{3+})_9O_6[SiO_4]_4(O, OH)_2$) and kyanite ($Al_2O[SiO_4]$) indicate input from (regional-)metamorphic rocks like schist and gneisses (Matthes, 1990; Mange and Maurer, 1991). Monazite ($(Ce, La, Th)PO_4$) is an accessory mineral of granitic rocks, but also occur infrequently in metamorphic rocks (Mange and Maurer, 1991). Titanite ($CaTi[(O, OH, F)SiO_4]$) is an accessory mineral in basic and intermediate plutonic and metamorphic rocks (Mange and Maurer, 1991). It is a relatively instable heavy mineral which often forms small crystals with other Ti-minerals like rutile. Garnet ($(Fe^{2+}, Mn_3, Mg_3)Al_2[SiO_4]_3$ or $Ca_3(Al_2, Fe^{3+}, Cr_2)[SiO_4]_3$) is also an instable heavy mineral associated with a broad variety of source rocks, ranging from metamorphic rocks to volcanic rocks (Matthes, 1990; Mange and Maurer, 1991). The occurrence of garnet in some samples may point to input of primary source material and/or to the preservation of garnet by early cementation or generally impermeable sediments (Amireh, 1991).

Detailed descriptions of the microscopic features of these minerals are given in Mange and Maurer (1991) and Boenigk (1983). Besides the heavy minerals mentioned above, epidote, zoisite, brookite, anatase and mica occur. All these minerals occur seldom in the grain mounts but were not encountered during the analysis.

Opaque minerals

In addition to the counted 200 transparent heavy minerals the number of the parallel appearing opaque heavy minerals in the grain mounts was also counted (see 5.2.1: Methods). The opaque minerals were not further analysed but hematite (Fe_2O_3) and pyrite (FeS_2) occur (based on grain morphologies under the microscope and binocular). The mean ratio of transparent to opaque heavy minerals is 1.59 with a minimum of 0.25 and a maximum of 7.41. This implies that in general the transparent heavy minerals dominate the opaque heavy minerals.

5.2.5 The ZTR-index

Introduced by Hubert (1962), the ZTR-index (**Z**ircon-**T**ourmaline-**R**utile-index) can be used to express the mineralogical maturity of siliciclastic sediments. In order to get the ZTR-index the percentages of zircon, tourmaline and rutile grains among the transparent, non-micaceous, detrital heavy minerals are summed up (Hubert, 1962). The higher that number/percentage, the higher is the mineralogical maturity of the examined sediment.

The ZTR-index of the examined samples from South Jordan is extremely high. The mean ZTR-index is 97.9 with a minimum of 91 and a maximum of 100, indicating very mature sediments. Thus the ZTR-index fits quite well to the classification as quartzarenites, resulting from the QFL-classification (Fig. 5.3). Plotted into a zircon-tourmaline-rutile ternary diagram (cf. Amireh, 1991) the ZTR-results display similar ratios as the Mesozoic Nubian sandstones from South Jordan (Fig. 5.5).

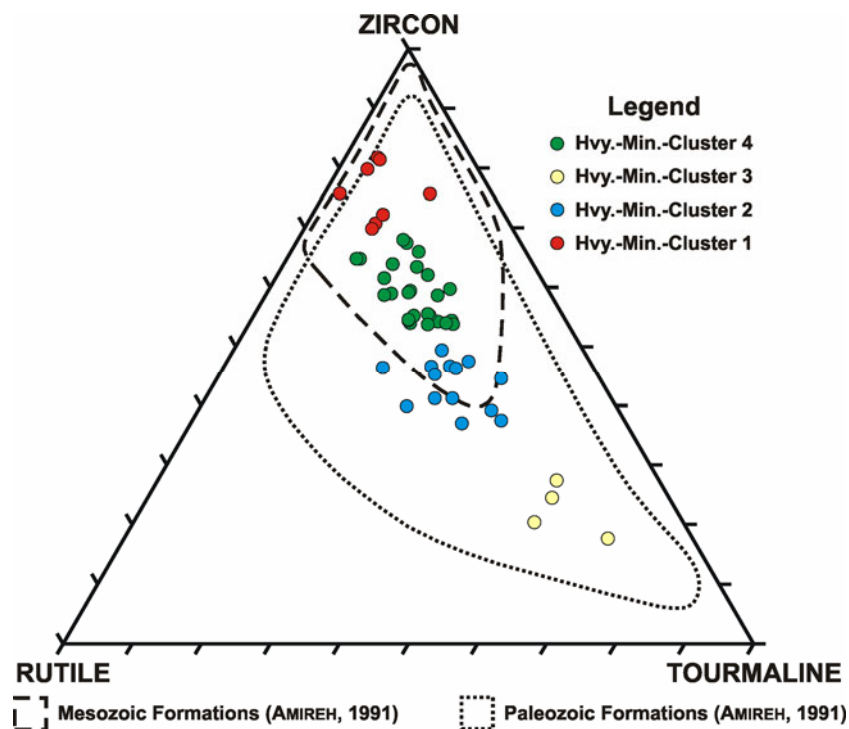


Figure 5.5 Zircon-Tourmaline-Rutile plot of the examined dataset. The colouration corresponds to the results of the cluster analysis (cf. Chapter 5.2.6). The dominance of zircon and tourmaline over rutile is clearly visible.

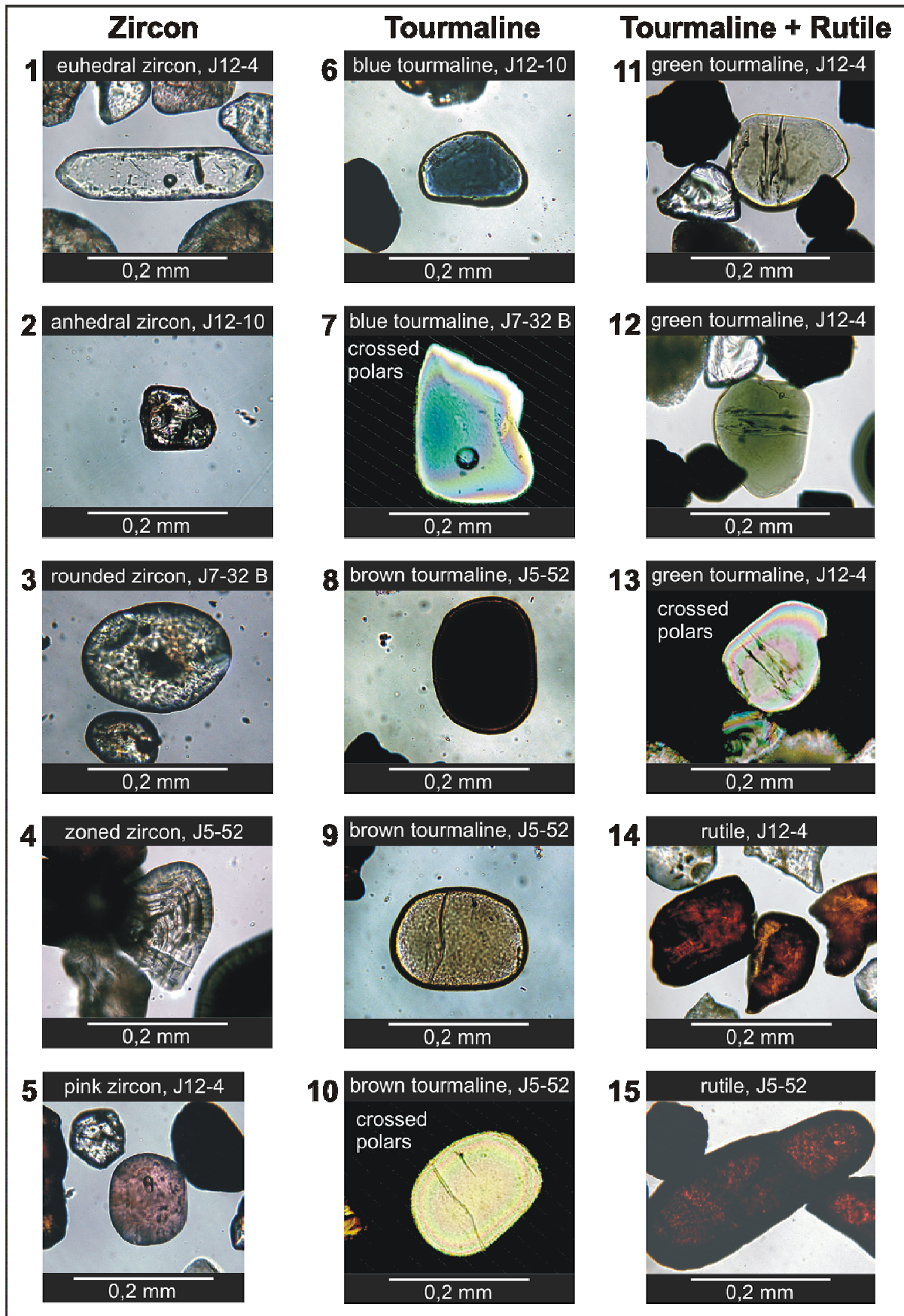


Figure 5.4 Photomicrographs of the major heavy minerals.

1)-5) typical examples of the five distinguished zircon varieties; 6) & 7) blue rounded tourmaline; 8)-10) brown rounded tourmaline with strong pleochroism; 11)-13) green rounded tourmaline; 14) & 15) typical examples of rutile.

5.2.6 Hierarchical cluster analysis of the ZTR-data

Since all studied 52 samples are clearly dominated by zircon, tourmaline and rutile (ZTR), a hierarchical cluster analysis (squared Euclidean distance, Ward method) was carried out on a data matrix determined by samples and heavy mineral content (Q-mode cluster analysis). Aim of the cluster analysis was to accomplish a subdivision of the dataset and to emphasize minor variations in the heavy mineral content.

The total zircon content, the tourmaline composition, separated in the three colour-varieties and the rutile content were normalized to 100 percent. The other heavy minerals were omitted from the dataset after a first factor analysis, as they were not significant for the dataset.

To control the significance of the 5 chosen variables, a second factor analysis was carried out before the Q-mode cluster analysis. The result (Fig. 5.6) clearly indicates that all 5 groups have to be considered within a hierarchical cluster analysis. The negative factor of 0.98 shows that zircon is the dominating heavy mineral.

A similar result is produced by the R-mode cluster analysis (“clustering the variables”). This analysis also proves the result of the factor analysis (Fischer, 1989). The dendrogram (Fig. 5.6) displays three clusters: one for the three tourmaline varieties, a rutile and a zircon cluster, fitting well with the result of the factor analysis and pointing to its reliability. Both, Q- and R-mode cluster analyses, as well as the factor analysis, were performed with the program SPSS 11.01 for Windows (SPSS Inc.).

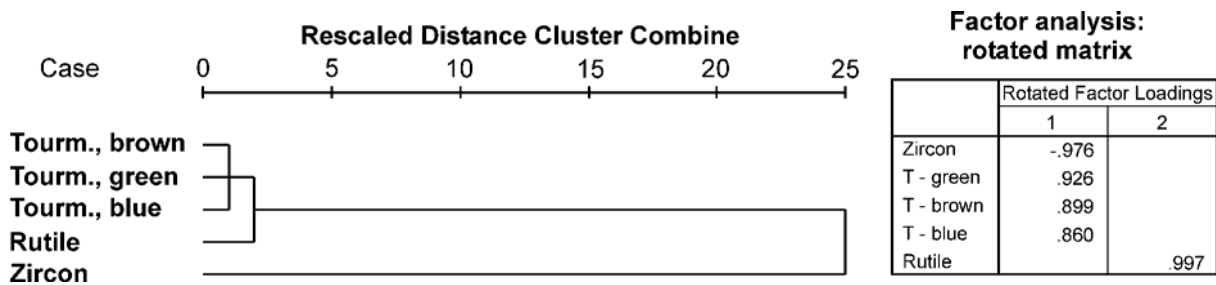


Figure 5.6 Results of the R-mode clustering (squared Euclidean distance, Ward method, total n=52) and factor analysis (right hand side) of the heavy mineral content (n=52). Further explanation, see text.

The Q-mode cluster analysis produced 4 clear clusters (Fig. 5.7) and shows that zircon is the controlling element for the production of the single clusters. In general the result can be grouped into two branches: a zircon dominated branch, including cluster 1 and 4, and a tourmaline + rutile branch, involving cluster 2 and 3. The results of the Q-mode cluster analysis are summed up in table 5.3.

Table 5.3 Results of the Q-mode hierarchical cluster analysis of the heavy mineral content (squared Euclidean distance, Ward method, total n=52; values in %).

		zircon	tourmaline			rutile
			blue	brown	green	
Cluster 1 n = 8	mean	75.96	0.95	3.74	2.85	16.51
	σ	4.76	0.96	2.05	2.29	4.31
	range	69.9-81.82	0-2.55	1.55-7.07	0.52-7.58	9.09-22.16
Cluster 2 n = 14	mean	43.29	5.58	16.11	12.88	22.15
	σ	4.06	2.73	4.19	3.34	4.68
	range	36.79-49.23	2.51-11.92	9.74-24.74	7.18-18.88	14.29-30.65
Cluster 3 n = 4	mean	22.50	8.26	31.11	21.86	16.28
	σ	4.31	1.82	6.81	2.99	3.94
	range	17.68-27.41	5.61-9.69	26.02-40.91	18.78-25.51	12.12-21.43
Cluster 4 n = 26	mean	58.92	2.91	10.01	8.42	19.74
	σ	4.74	1.29	3.38	2.84	3.18
	range	53.57-67.86	1.01-6.15	3.54-15.58	1.02-12.24	14.14-25.25

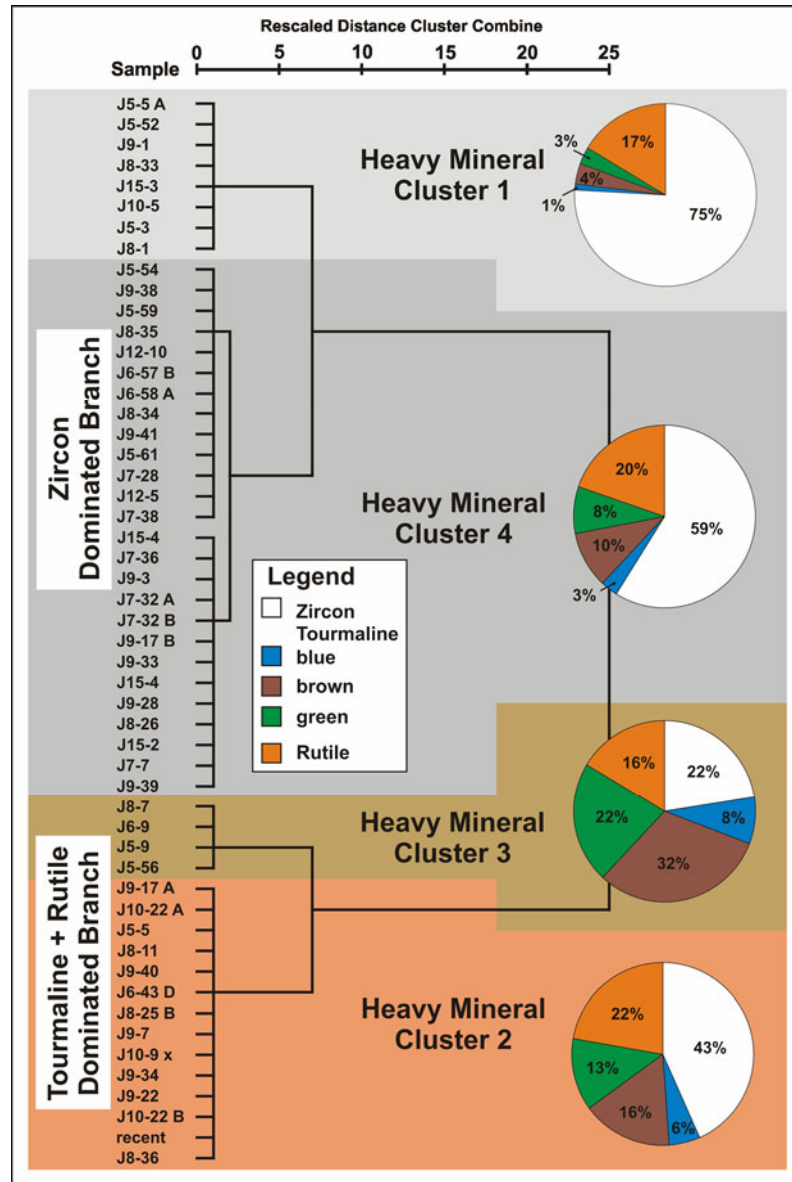


Figure 5.7 Result of the heavy mineral Q-mode hierarchical cluster analysis (squared Euclidean distance, Ward Method). The examined samples are grouped in 4 clusters, which can be combined into two branches: a zircon dominated branch and a tourmaline + rutile dominated branch.

5.3 Provenance of the Upper Cretaceous siliciclastic sediments of South Jordan

The word provenance is derived from the Latin “provenire”, meaning “origin” or “the place where produced” (Basu, 1985a). Since the tectonic history and source composition of a sediment is recorded within its modal composition (McLennan et al., 1993), sedimentary petrography can be applied to read this information. Provenance is a function of the source rock, relief, climate and sediment transport (Basu, 1985a). “Secondary” mechanisms like diagenesis and recycling add disturbance to this function (Haughton et al., 1991; Johnsson, 1993) and can seriously influence the provenance information.

5.3.1 Light mineral analysis

The quartz rich character of the clastic sediments of the study area and the poorness in various lithic fragments allow only the use of the basic quartz-feldspar-lithoclast analysis (herein referred to as QFL) to determine the provenance of the sediments.

The QFL-based ternary plots after Dickinson (Dickinson et al., 1983; Dickinson, 1985) (Fig. 5.8 A & B) display consistent results for all samples. These plots use the basic QFL information with slight differentiations: the quartz content Q is divided into Q_m , monocrystalline quartz, and Q_t , the total quartz content, including polyquartz; feldspar combines potassium feldspar and plagioclase; the lithic fragments might be separated into L_t , the total lithic fragments, including polycrystalline quartz, and L , the unstable lithic fragments (Dickinson, 1985). In both diagrams (Fig. 5.8 A & B) most of the samples plot in the “craton interior” field, representing material from a continental block, with a slight trend to the recycling fields.

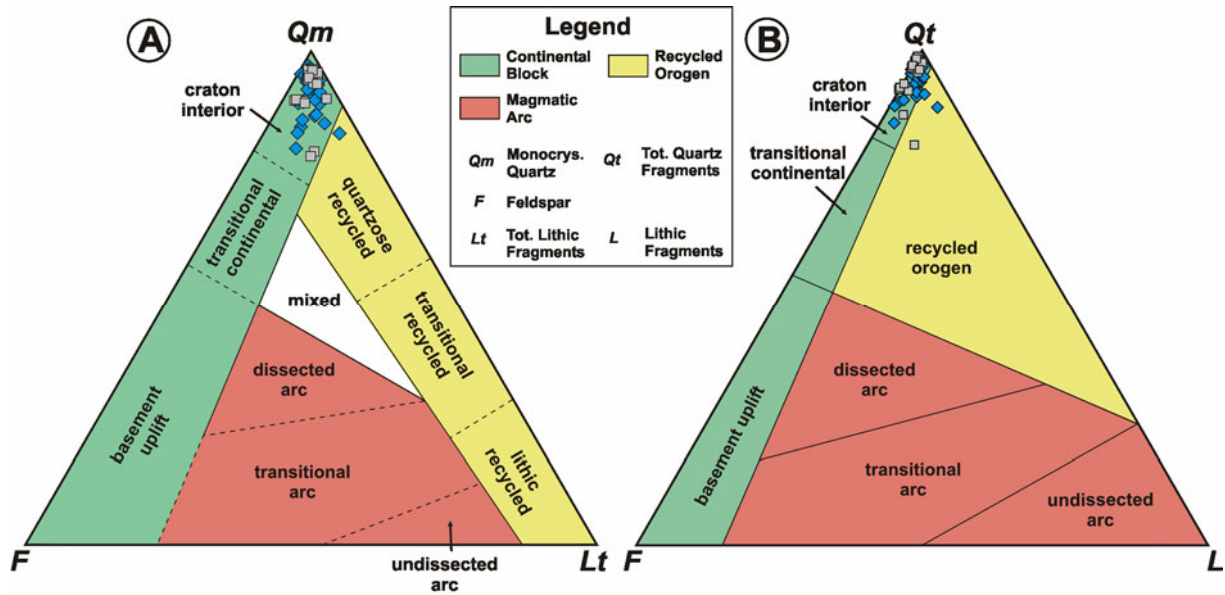


Figure 5.8 Ternary diagrams after Dickinson (Dickinson et al., 1983; Dickinson, 1985). In both ternary plots the gross of the samples plot in the continental block field (green) with tendencies to the recycled orogen field (yellow).

Based on the dataset and classification of Dickinson (Dickinson et al., 1983; Dickinson, 1985), Molinaroli, Blom & Basu (1991) developed a set discrimination functions to test this classification. The application of the functions (Fig. 5.9 A-D) to the studied data set exhibit the same clear results as with the original ternary plots of Dickinson.

Figure 5.9; following page no. 87

Scatter plots using discriminant functions from Molinaroli et al. (1991). The plots are based on the ternary diagrams of Dickinson (see Fig. 5.8) and include the same discriminant fields. Diagrams A and B are based on the QFL and diagrams C and D on QmFLt. The used discriminant functions for the scatter plots are shown in the tables below.

	A- Discrimination by QFL (3 groups)		B- Discrimination by QFL (7 groups)	
	F1	F2	F1	F2
quartz	0.05255857	0.06651623	-	-
feldspars	-	-	0.1078196	-0.08731842
lithic fragments	-0.01129834	0.1044331	0.07149468	0.07376478
constant	-3.162011	-6.221263	-3.181089	0.1149167

	C- Discrimination by QmFLt (3 groups)		D- Discrimination by QmFLt (3 groups)	
	F1	F2	F1	F2
monocrystalline quartz	0.05658474	0.2035148	0.1331829	0.1192073
feldspars	-0.001823969	0.2681704	-	-
total lithic fragments	0.004277794	0.1696830	-0.009705610	0.1734174
constant	-3.227174	-20.46354	-7.110715	-11.48198

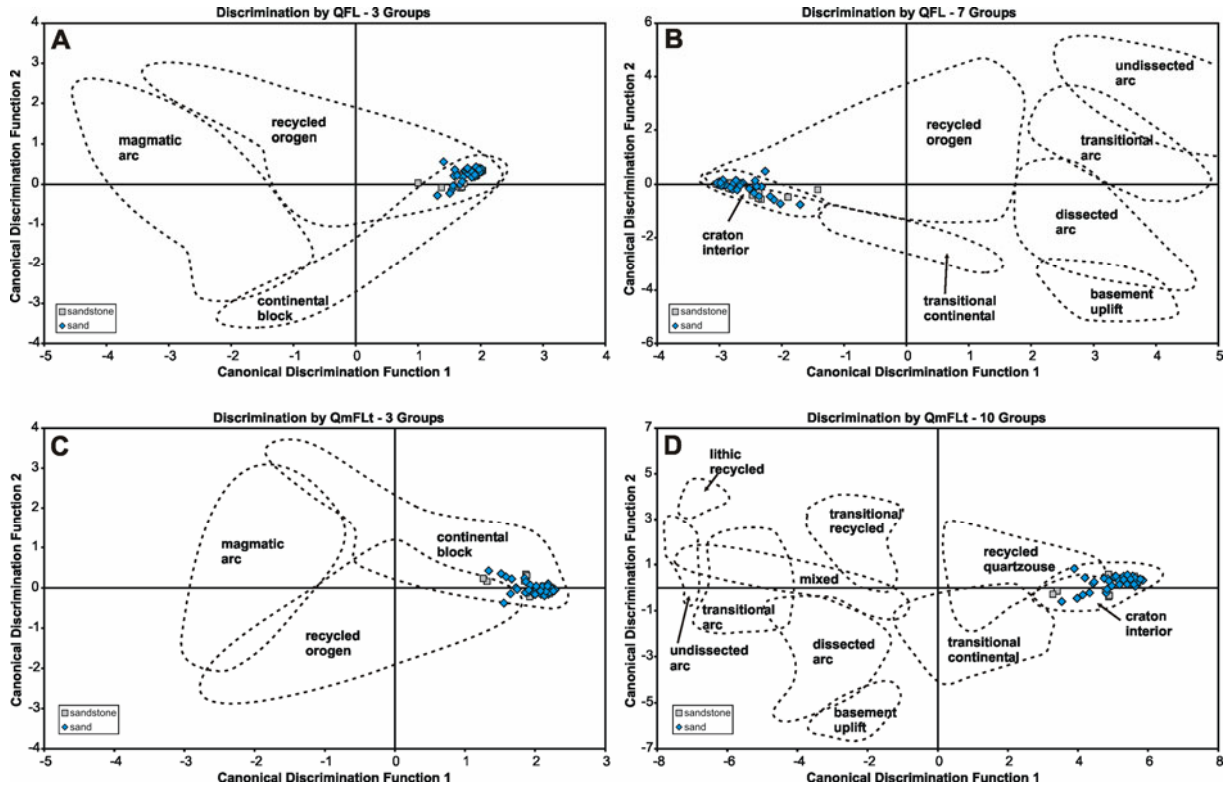


Figure 5.9 Figure captions on previous page no. 86.

Within the double ternary diagram after Basu (1985b) with modifications from Tortosa et al. (1991) (Fig. 5.10A). A plutonic to metamorphic (middle- to upper-rank) source rock, e.g. granites and gneisses is indicated for all samples. Again the ternary-plot is crosschecked by a discrimination function from Molinaroli et al. (1991) (Fig. 5.10B), showing the same result. The diagram after Basu implies that the dominance of plutonic source rocks might be possible.

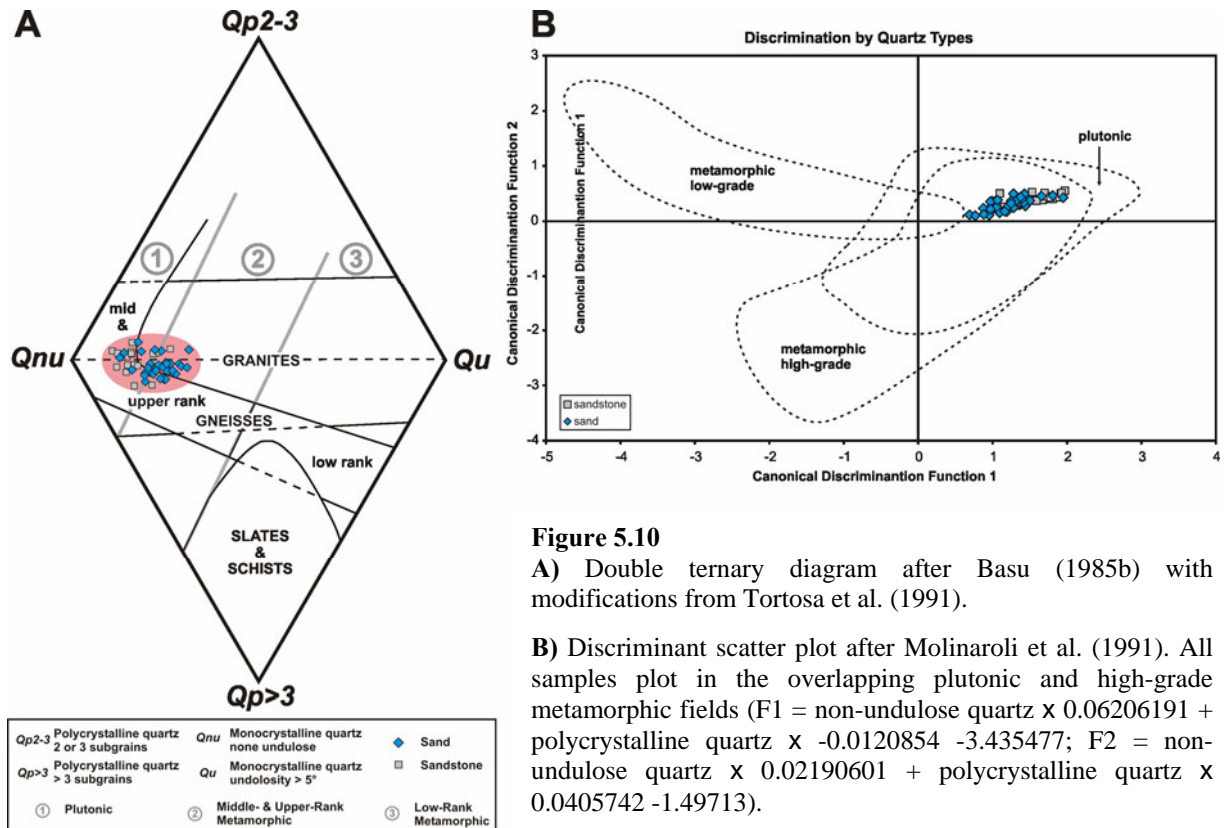


Figure 5.10

A) Double ternary diagram after Basu (1985b) with modifications from Tortosa et al. (1991).

B) Discriminant scatter plot after Molinaroli et al. (1991). All samples plot in the overlapping plutonic and high-grade metamorphic fields ($F1 = \text{non-undulose quartz} \times 0.06206191 + \text{polycrystalline quartz} \times -0.0120854 - 3.435477$; $F2 = \text{non-undulose quartz} \times 0.02190601 + \text{polycrystalline quartz} \times 0.0405742 - 1.49713$).

Figure 5.11 displays a similar result. The arrow shaped fields in the middle of the diagram represents a more or less homogenous mix of a metamorphic and plutonic source. The analysed data set plots preferably in the plutonic part of the diagram, pointing to a dominance of plutonic source material in the samples. In addition the diagram can also be used to determine the palaeo-relief of the sediments and/or the climate of the depositional environment. Most of the samples plot in the field number 4, pointing to the sedimentation in a low relief on tropical humid climatic conditions. The samples plotting in the field number 2 were either deposited on a low relief with a temperate and sub-humid climate or on tropical humid conditions within an area with a moderate relief.

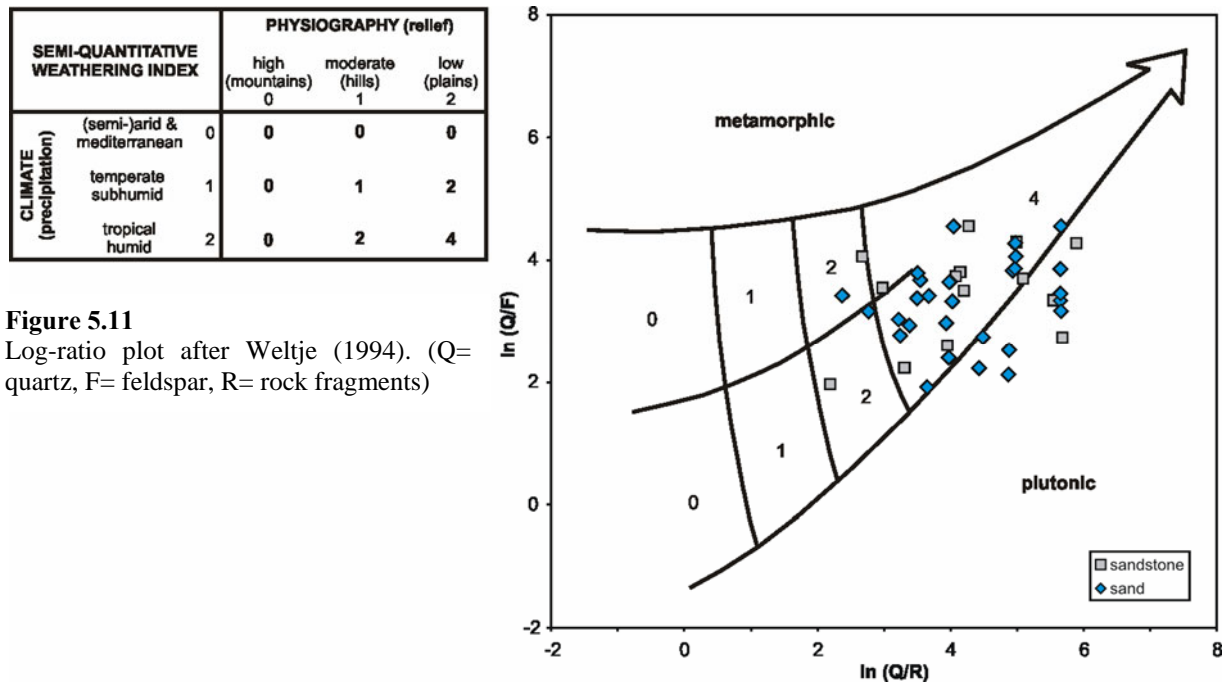


Figure 5.11
Log-ratio plot after Weltje (1994). (Q= quartz, F= feldspar, R= rock fragments)

5.3.2 Heavy mineral analysis

The heavy mineral spectrum of the studied sediments is clearly controlled by zircon, tourmaline and rutile (ZTR). Basically the occurrence of these heavy minerals is not distinctive for a source rock, since they are associated with various magmatic and metamorphic rocks. These heavy minerals are very resistant against mechanical and chemical destruction and tend to get enriched in the sediment, while other heavy minerals are removed from the sediment (Hubert, 1962). ZTR-values above 90 point to the resedimented/recycled nature of the host sediment (Hubert, 1962; Mange and Maurer, 1991), where ZTR get enriched during the re-sedimentation process.

The presence of well rounded varieties of zircon and tourmaline in the sediment, promotes the assumption that older sediments form a part of the source material of the Cretaceous sands of South Jordan. The rounded zircon and tourmaline grains, dominating their corresponding fraction (Fig. 5.12), faced a more intense or repeated transport than the angular ones. Though the appearance of angular and even euhedral variants of zircon and tourmaline further the assumption that the heavy minerals were at least partially derived from a “first cycle”, non-sedimentary source.

The occurrence of pink zircon phases indicates that parts of the sediments derived from Precambrian source rocks (Zimmerle, 1972). Some of the pink zircons are perfectly rounded (e.g. Fig. 5.4 No. 5), while others display a euhedral grain form. This points to multiple source for the pink zircon: the rounded variety was derived from an older, not necessarily

Precambrian, recycled sediment, whereas the source of the euhedral variant can be considered to be a Precambrian rock, either sediment or bedrock.

The presence of staurolite and kyanite, both accessory minerals in metamorphic rocks (Matthes, 1990; Mange and Maurer, 1991), point to a metamorphic input.

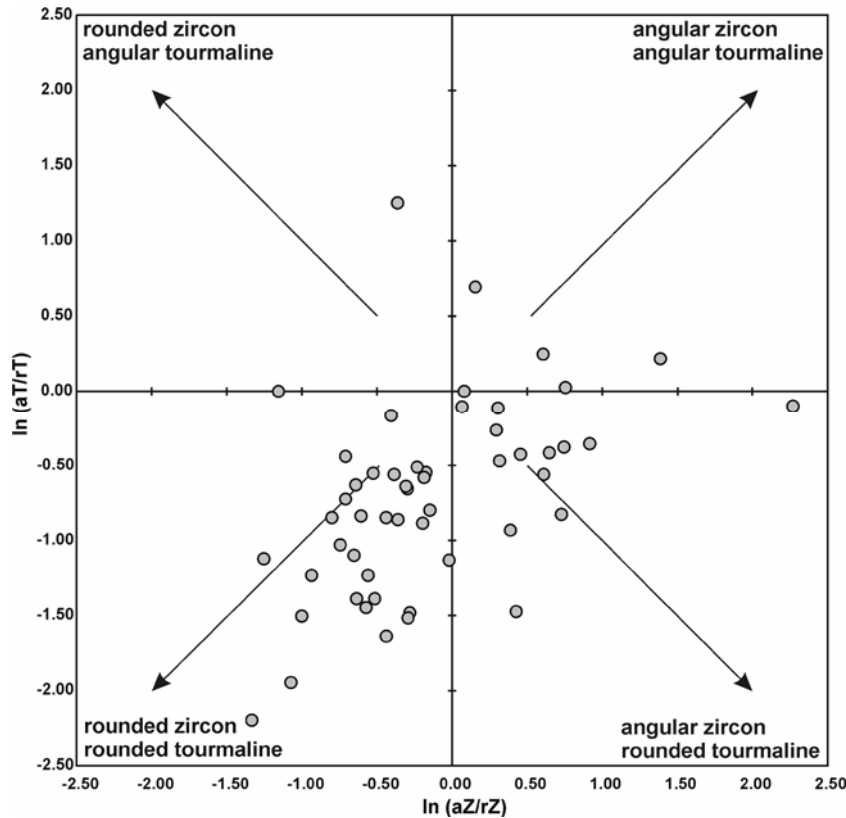


Figure 5.12

Log-ratio plot of angular and rounded zircon and tourmaline varieties.

aT = angular tourmaline
rT = rounded tourmaline
aZ = angular zircon
rZ = rounded zircon

5.4 Discussion and conclusion of the sedimentary petrography

The examined Cretaceous sands and sandstones of South Jordan are basically mineralogical mature sediments and can be classified as quartzarenites (Fig. 5.3). Their main components are dominantly quartz and less feldspar and lithic fragments. The mineralogical maturity of the sandstones is also reflected in their mean ZTR-index of 97.9 (see 5.2.3), classifying them as very mature sediments (Hubert, 1962). The fine and fine to medium grained sands/sandstones in general exhibit a slightly higher content of feldspar, classifying them as subarkoses (Fig. 5.3).

In general quartzarenites are considered to be multicycle sediments. Only in warm humid climates and slow sedimentation rates within a low relief environment first-cycle quartzarenites would form (Pettijohn et al., 1987). Such depositional conditions are indicated by the log-ratio plot (Fig. 5.11) after Weltje (1994). However, the presence of resedimented quartz grains in virtually all examined samples, points to the origin of the quartzarenites as multicycle sediment. A fact that is supported by the predominance of rounded zircon and tourmaline varieties in the heavy mineral content of the sediments (Fig. 5.12).

The studied samples of sandstones gained a rather restricted spectrum of diagenetic processes. The compaction of the sediments was low to moderate (Fig. 5.2), which is reflected by high IGV values and the lack of destructive grain contacts and signs of pressure solution. Only long and point contacts of framework grains were found. The absence of pressure solution might be the reason for the lacking of quartz cement phases, as there was not enough free SiO₂ in the fluid system to trigger a quartz precipitation (Pettijohn et al., 1987;

Füchtbauer, 1988). All of these features indicate that the studied Upper Cretaceous sediments did not encounter deep burial or thick overburden.

The Cretaceous sandstones display varying cement phases:

- clay minerals
- iron-oxides
- carbonate minerals (calcite, dolomite)

The few cement phases of the friable sandstones are clay minerals and some iron-oxides, basically hematite. The appearance of the clay minerals as rims and coatings around framework grains (Fig. 5.1 No. 21) as well as the lack of clay mineral phases in the open pore space indicate that these clays were mainly washed into the sands (Gaupp et al., 1993), or formed during soil forming processes. The friable sandstones have the highest intergranular porosities of all samples.

The cement phases of the well cemented sandstones are calcite, dedolomite, and/or dolomite (Fig. 5.1 No. 23+24) or iron oxide (Fig. 5.1 No. 22). Both sandstone groups display low values of intergranular porosity. As these sandstones have similar IGV values as the less cemented sandstones, it is assumed that they experienced the same compaction by minor burial and overburden.

The sandstones cemented by clay minerals and Fe-oxide are of both, marine and terrestrial origin. The calcareous sandstones are most probably of marine origin. Since the terrestrial sandstones of South Jordan usually do not contain carbonate cement, it can be stated, that the carbonate cement is facies dependant (Füchtbauer, 1967) and tied to the marine environment. During the early diagenesis the calcite precipitates either under influence of marine or marine derived waters (Morad, 1998) or due to the solution of biogenic material (Füchtbauer, 1988). This usually happens at the sediment-water interface or in the shallow marine burial environment (Füchtbauer, 1988; Tucker and Wright, 1990). A late precipitation of the carbonate cements can be ruled out since compaction of the sediment would have been higher during a later diagenetic state. Furthermore, such a late, burial diagenetic cementation would have affected terrestrial and marine sandstones in the same way. In some samples the calcite cement replaces quartz, a fact directly linked to the chemical properties of both mineral phases (e.g. Pettijohn et al., 1987).

Dolomite as cementing phase in sandstones is often attributed to a late diagenetic stage (Füchtbauer, 1988) or to early diagenesis associated with the sulphate reduction zone (Morrow, 1990; Morad, 1998). Special depositional environments, like sabkhas, and the possible interaction of fresh and marine waters in a mixed-water aquifer are also possible "sources" for dolomite cement (Morrow, 1990). For the studied samples the exact mechanism of dolomite production can not be stated. Since the dolomite cemented sandstones usually bear calcite cement as well as features like glaucony and phosphatic particles, a marine origin of these deposits is reasonable. Considering furthermore the minor burial depth of the sediments (cf. Chapter 5.1.5), the dolomite origin is most probably linked to a mixed-water aquifer and/or the sulphate reduction zone.

In carbonate deposits meteoric waters often cause de-dolomitization reactions (Tucker and Wright, 1990). A similar meteoric influence, consequently post dolomite formation, might have caused the occurrence of de-dolomite within the South Jordan siliciclastic sediments.

The frequent ferribands and Fe-sands along the escarpment are also a diagenetic feature. The source of the Fe-oxide might be attributed to a lateritic weathering together with continental runoff (Föllmi, 1995; Mücke, 2000). A high runoff of iron-oxide from the continent gives rise to the assumption of a warm humid (tropical) climate. This fits with palaeo-climate reconstructions for the Cretaceous (Chapter 2.6: Cretaceous palaeoclimate). Most probably the iron oxide cementation took place as an early diagenetic cementation under marine conditions, or under ground water influence and soil forming processes in terrestrial environments (Valeton, 1988; Germann et al., 1990).

The source rocks of the Upper Cretaceous sands and sandstones belong to a continental block and/or a craton interior. Evidence for sediment recycling, indicated by the trend of some samples to the “recycled quartzose” and “recycled orogen” fields (Fig. 5.8), is supported by the presence of resedimented quartz grains in the samples (Fig. 5.1 No. 1-4). The light mineral analysis points to plutonic and medium to high grade metamorphic rocks as source rock (see Fig. 5.10 A & B).

The dominance of the ultrastable heavy minerals zircon, tourmaline and rutile (ZTR) and especially the zircon predominance (Figs. 5.5 & 5.7), clearly point to a sediment recycling (McLennan et al., 1993). The less stable heavy minerals were removed from the sediment due to the repeated sedimentary recycling. The predominance of the rounded zircon and tourmaline grains is a direct hint to sediment reworking (Fig. 5.12). The occurrence of metamorphic heavy minerals like staurolite and kyanite supports the assumption that metamorphic rocks were exposed in the source area.

The Arabian-Nubian shield is build up by plutonic and metamorphic rocks and partially covered with sediment resulting from continues weathering of the basement rocks and subsequent deposition (Bender, 1963). This sedimentary cover, in South Jordan represented by the Palaeozoic “Nubian sandstones” (Bender, 1963; 1974), most probably is the source of the resedimented quartz grains in the sandstones.

All studied sand/sandstone samples are very similar in a petrographic sense. Variations, either in light or in heavy minerals, are only minor and therefore not useful for correlation attempts. In terms of facies dependency, only the calcareous sandstones are useful as indicator for marine depositional environments.

6. Bulk rock geochemistry

6.1 Introduction

Bulk rock analysis of main and trace elements is a standard tool in geochemistry and easy to perform, e.g. by XRF-spectrometry (**X-Ray Fluorescence**). Similar to sedimentary petrography, bulk rock geochemistry of sedimentary rocks can be applied to sediment classification (e.g. Pettijohn et al., 1987; Herron, 1988; McCann, 1991), information on the weathering of the sediment (e.g. Nesbitt and Young, 1982; McLennan et al., 1993) and statements on the provenance of the sediment (Bhatia, 1983; Roser and Korsch, 1986; 1988; Toulkerides et al., 1999, among others). Since the geochemistry of siliciclastic sedimentary rocks does not reflect only the detrital components but also the geochemical characteristics of authigenic material (Dinelli et al., 1999), geochemical bulk rock analysis should only be performed together with sediment petrographic analysis.

The aim of the bulk rock geochemistry was to support the petrographic examinations especially in the field of provenance analysis. With geochemical methods it is possible to use finer grained samples, like palaeosols and clays, to further the provenance statements based on sand sized samples. To exclude biasing, several methods based on major and trace elements were applied. A further aspect was the use of the chemical index of alteration (Nesbitt and Young, 1982) and weathering trends in order to get information on the weathering state of the studied samples and thus on the climatic conditions of the mid-Cretaceous of South Jordan.

6.1.1 Analytical methods

For the presented study 70 sediment samples, collected during fieldwork following standard sample collecting techniques (Tucker, 1996), were analysed for major elements (SiO_2 , Al_2O_3 , Fe_2O_3 , MnO , MgO , CaO , Na_2O , K_2O , TiO_2 , P_2O_5) and trace elements (Pb, Th, U, Sc, V, Cr, Ni, Cu, Zn, Ga, Rb, Sr, Y, Zr, Nb, Ba) by XRF-spectrometry. All samples were treated with demineralised water, dried and crushed with a W-carbide mill. Due to a Co contamination, caused by abrasion from the Co bearing W-carbide mill during crushing, Co measurements were not considered. The XRF-analysis were carried out at the Mineralogical Institute of the University Mainz (Philips: PW 104) and in the Soil Science laboratory of the University Hohenheim (Cameca). In both laboratories fusion pellets (fusion aid: lithium tetraborate; ratio fusion aid/sample 8:1) were used for major element, and pressed pellets for trace element measurements.

Selected samples were further analysed for their rare earth element (REE) and trace element content (*trace elements*: Y, Nb, Hf, Bi, Ba; *REE*: La, Ce, Pr, Nd, Sm, Eu, Gd, Tb, Dy, Ho, Er, Tm, Yb, Lu). This was done on the XRF-fusion pellets with an ICP-MS with laser ablation, at the Institute for Geosciences of the University Jena (VG Elemental: PQ3; Laser: Merchantek: Microprobe II). To achieve a higher precision, Ba was used as an internal standard for the ICP-MS analysis. For reasons of comparison and to combine the measurements from the different laboratories, all major element analysis were recalculated to a volatile free, molar base and normalized to 100 wt.% (LOI-free wt.%; cf. Roser and Korsch, 1988).

Parallel to the XRF-spectrometry the **L**oss **O**n **I**gnition (LOI) was gravimetrically determined for each sample after heating of the sample for one hour at 1005°C. The LOI represents the volatile components (H_2O , CO_2 etc.) in the sample which are lost during the preparation of the fusion pellet. In siliciclastic samples the LOI can be used to roughly estimate the amount of clay in a sample. The **T**otal **I**norganic **C**arbon (TIC) content was analysed with a carbon analyser (LECO, RC-412) at the Mineralogical Institute of the University Stuttgart.

The CO₂ value was used to evaluate the carbonate content in the examined samples. Tables containing the results of the geochemical analysis can be found in appendix III.

6.1.2 Analytical precision

Sample J9-28 was selected for repeated analysis in order to get information on the analytical precision. The sample was analysed three times on different fusion and pressed pellets with the XRF and eight times on four different fusion pellets with the ICP-MS.

Table 6.1A Precision of the XRF-spectrometry (n=3)

element	mean	σ	range
SiO ₂ [wt.%]	97.57	0.81	96.66-98.22
Al ₂ O ₃ [wt.%]	0.35	0.01	0.35-0.36
Fe ₂ O ₃ [wt.%]	0.21	0.01	0.20-0.21
MnO [wt.%]	-	-	-
MgO [wt.%]	0.03	0.01	0.02-0.04
CaO [wt.%]	0.06	0.01	0.05-0.06
Na ₂ O [wt.%]	0.01	0.01	0.01-0.02
K ₂ O [wt.%]	0.05	0	-
TiO ₂ [wt.%]	0.05	0	-
P ₂ O ₅ [wt.%]	0.01	0	-
LOI [wt.%]	0.33	0.01	0.32-0.34
Sc [ppm]	-	-	-
V [ppm]	4.33	0.58	4-5
Cr [ppm]	1	1	0-2
Co [ppm]	219.67	2.31	217-221
Ni [ppm]	3	1	2-4
Cu [ppm]	6.33	0.58	6-7
Zn [ppm]	4.67	0.58	4-5
Ga [ppm]	3	0	-
Rb [ppm]	2.33	0.58	2-2
Sr [ppm]	20.33	0.58	20-21
Y [ppm]	1.67	0.58	1-2
Zr [ppm]	72	3.61	69-76
Nb [ppm]	2	0	-
Ba [ppm]	32.67	3.51	29-36
U [ppm]	0.33	0.58	0-1
Th [ppm]	-	-	-
Pb [ppm]	9.33	0.58	9-10

Table 6.1B Precision of the ICP-MS-LA analysis (n=8, concentrations in ppm)

element	mean	σ	range
86 Sr	30.73	1.09	29.41-32.92
89 Y	2.74	0.09	2.61-2.83
90 Zr	75.98	10.64	61.45-94.88
91 Zr	76.42	10.20	63.09-94.89
93 Nb	2.26	0.09	2.15-2.40
137 Ba	internal standard		
139 La	3.79	0.16	3.57-4.01
140 Ce	14.20	0.23	13.80-14.52
141 Pr	1.39	0.03	1.33-1.41
145 Nd	4.47	0.13	4.25-4.65
146 Nd	4.41	0.13	4.21-4.60
147 Sm	0.67	0.03	0.61-0.71
149 Sm	0.67	0.03	0.63-0.71
151 Eu	0.14	0.01	0.14-0.15
153 Eu	0.15	0.01	0.14-0.16
159 Tb	0.06	0.01	0.05-0.07
160 Gd	0.38	0.02	0.36-0.41
161 Dy	0.33	0.03	0.29-0.38
165 Ho	0.07	<0.00	0.07-0.08
166 Er	0.20	0.01	0.18-0.21
167 Er	0.21	0.02	0.18-0.23
169 Tm	0.05	<0.00	0.05-0.06
171 Yb	0.24	0.02	0.21-0.28
172 Yb	0.25	0.02	0.21-0.27
175 Lu	0.05	<0.00	0.04-0.05
178 Hf	2.07	0.24	1.79-2.54
208 Pb	6.85	0.22	6.48-7.15
232 Th	0.93	0.04	0.87-0.98
238 U	1.98	0.11	1.78-2.15

XRF-analysis in general shows only minor deviations for major elements (usually 1%) and deviations of 1-5% for trace elements. The low major element concentrations of sample J9-28 produce higher errors (up to 15%). The trace elements show reasonable standard deviations.

For analysis of fusion pellets with the laser of an LA-ICP-MS (LA = laser ablation) a general error of the measurement of 10-20%, in comparison to the standard (non-laser) ICP-MS analysis, has to be assumed. The reason for that is that the element diffusion from the pellet under the laser is not linear (Dr. D. Merten, ICP-MS laboratory Jena, personal communication, 2001) and a total homogenisation of the elements in the pellet might not be obtained. The error analysis of the ICP-MS analysis showed good results. Standard deviations

(sigma) of 3-10% are reasonable for low element concentrations (Tab. 6.1 B). For higher element concentrations (e.g. Zr) sigma rises to 15%, which is still acceptable.

6.1.3 Controlling factors of the bulk rock geochemistry

The geochemical character of a sediment is directly determined by its framework components and its authigenic mineral content. Various factors control the geochemistry of siliciclastic sediments. These factors include (1) composition of the source terrain, (2) chemical weathering, (3) hydraulic sorting, (4) diagenesis, (5) metamorphism and (6) hydrothermal alteration (McLennan, 1989; Fralick and Kronberg, 1997).

All these factors change the initial geochemistry of the sediment to a certain extent. This happens either by depletion of elements, e.g. by chemical weathering, or by addition of elements, e.g. during diagenesis. A combination of several factors affecting a sediment is the usual case. Independent of these factors, chemically immobile elements, like Zr, Ti, Al, will maintain invariant ratios during rock mass change (Fralick and Kronberg, 1997). Therefore it is important to know which of these processes influenced the examined sediment.

For the studied South Jordan Cretaceous sediments the control of these factors on the bulk rock geochemistry is summed up in the following: The influence of the source terrain belongs to the field of provenance studies and will be discussed in detail in this chapter. The effect of chemical weathering will be examined in chapter 6.2.2, since mobile elements like the alkali and alkaline earths may be influenced by it. To minimize recent weathering effects special care was taken to collect only fresh, un-weathered material. To consider hydraulic sorting effects the studied samples were grouped according to their grain size. Diagenesis effects are in general negligible (compare Chapter 5.3). Only the samples which are strongly cemented by carbonates (calcareous marine sandstones) and iron oxides (Fe-sands and ferri-bands) showed raised CaO/MgO and Fe₂O₃ contents.

6.2 Major elements

The results of the major element analysis are presented in table 6.2, detailed results for each examined sample can be found in Appendix II.

In general SiO₂ is the dominating element in all samples. Especially the sand fraction (fine and medium-grained) displays high values of more than 92 wt.%. The clay rich sediments (sand/clay mixture, silt, palaeosols and clays) have lower SiO₂-values and raised Al₂O₃-values. Similar to alumina, Fe₂O₃ is also increased in these sediments, where only the Fe-sands display higher Fe₂O₃ contents. MgO and CaO are very low in the sand fraction but display high values in the fine-grained sediments. Especially the clayey palaeosols have extraordinary high contents of both elements (combined about 25 wt.%). Of the other major elements only Na₂O, K₂O and TiO₂ show a grain-size dependant variation. They are low in the sand fraction but slightly higher in the fine-grained deposits. MnO and P₂O₅ are generally low and do not show major variations within the examined sediment types.

In terms of major element composition ratios, the studied sands and sandstones are generally characterized by low Al₂O₃/SiO₂ and high K₂O/Na₂O ratios. The clayey, fine-grained sediments display higher Al₂O₃/SiO₂ and lower K₂O/Na₂O ratios. The Fe₂O₃_{total} + MgO values are basically higher in the fine-grained fraction. Only the Fe-sands have similar high Fe₂O₃_{total}+MgO values.

Additionally to table 6.2, the major element results were plotted in Harker variation diagrams (Fig. 6.1), all showing negative linear trends for the examined sediments. The clustering of the sand-size samples near the 100 wt.% SiO₂ corner of all diagrams reflects their mature, quartzarenitic character. The similar trends of the Al₂O₃ (r= -0.84) and the K₂O-plots (r= -0.77), correspond to a higher clay mineral content in the fine-grained sediments. The K₂O-plot shows that the fine-grained sands display higher K₂O-values (fsgs: r= -0.92) as the medium-grained sands (mgs: r= -0.69). These values point to a higher potassium feldspar

content in the finer grained sands, which was also observed in the thin sections (see Chapter 5).

Table 6.2 Average chemical composition (major elements, 100 wt.% LOI-free) of southern Jordan siliciclastic sediments.

		[wt.%]													[wt.%]
		SiO ₂	Al ₂ O ₃	Fe ₂ O ₃	MnO	MgO	CaO	Na ₂ O	K ₂ O	TiO ₂	P ₂ O ₅	Al ₂ O ₃ /SiO ₂	K ₂ O/Na ₂ O	Fe ₂ O ₃ +MgO	
Fine-grained sand n = 9	mean	95.47	2.20	0.71	0.01	0.09	0.10	0.09	0.94	0.35	0.04	0.02	14.27	0.80	
	ó	2.97	1.44	0.44	0.01	0.06	0.08	0.11	0.80	0.34	0.05	0.02	12.68	0.49	
Medium-grain. sand n = 23	range	89.41- 99.17	0.26- 4.95	0.21- 1.45	0-0.02	0.03- 0.23	0.01- 0.22	0-0.35	0.08- 2.33	0.13- 1.17	0.01- 0.16	0-0.06	2.50-32.71	0.24-1.68	
	mean	92.76	2.64	2.85	0.02	0.22	0.34	0.12	0.59	0.29	0.17	0.03	6.08	3.06	
Fe-sand n = 2	ó	10.14	3.94	6.33	0.04	0.40	0.62	0.15	0.94	0.33	0.34	0.05	10.37	6.50	
	range	66.77- 99.52	0.23- 17.97	0.13- 28.08	0-0.16	0-1.56	0-1.97	0-0.51	0.03- 4.01	0.04- 1.09	0-1.20	0-0.23	0.27-45	0.13-28.29	
sand/clay mix. n = 10	mean	84.52	3.26	10.70	0.11	0.17	0.19	0.30	0.32	0.39	0.08	0.04	1.06	10.87	
	ó	2.20	2.76	1.14	0.12	0.06	0.19	0.00	0.09	0.32	0.01	0.03	0.32	1.08	
silt n = 2	range	82.96- 86.07	1.30- 5.21	9.89- 11.50	0.02- 0.19	0.12- 0.21	0.05- 0.32	0.30- 0.30	0.25- 0.38	0.16- 0.61	0.07- 0.09	0.02-0.06	0.83-1.28	10.10-11.63	
	mean	86.61	4.46	6.49	0.04	0.53	0.20	0.68	0.55	0.31	0.10	0.06	0.74	7.02	
sandy palaeosol n = 5	ó	12.26	5.04	9.57	0.09	0.81	0.17	0.76	1.12	0.47	0.10	0.08	0.64	9.64	
	range	63.91- 99.02	0.42- 17.75	0.22- 32.72	0-0.29	0.06- 0.81	0.02- 0.57	0-2.11	0.03- 3.70	0.04- 1.64	0.01- 0.34	0-0.27	0.17-1.89	0.29-33.08	
clayey palaeosoil n = 11	mean	68.26	16.32	5.52	0.02	3.09	0.46	0.72	3.73	1.72	0.19	0.25	5.40	8.61	
	ó	9.79	7.79	0.76	0.01	2.21	0.02	0.44	1.88	1.00	0.14	0.15	0.66	1.45	
clay n = 8	range	61.33- 75.18	10.81- 21.83	4.98- 6.05	0.01- 0.02	1.52- 4.65	0.44- 0.47	0.41- 1.03	2.40- 5.06	1.01- 2.42	0.09- 0.29	0.14-0.36	4.93-5.86	7.58-9.63	
	mean	73.95	11.05	6.70	0.04	2.09	0.52	1.39	2.66	1.41	0.19	0.15	2.26	8.78	
clayey palaeosoil n = 11	ó	6.54	3.93	2.56	0.04	1.40	0.47	0.42	1.31	0.83	0.23	0.60	1.49	1.54	
	range	68.02- 81.96	6.30- 14.47	3.48- 10.01	0.01- 0.09	1.14- 4.46	0.09- 1.25	1.01- 1.96	1.21- 3.89	0.59- 2.52	0.02- 0.57	0.08-0.2	0.62-3.87	7.47-11.20	
clay n = 8	mean	61.58	7.13	4.27	0.07	10.96	13.46	0.51	1.44	0.54	0.05	0.15	1.70	15.23	
	ó	29.40	3.67	1.72	0.05	12.64	17.12	0.62	0.65	0.29	0.02	0.09	0.72	13.43	
clay n = 8	range	21.59- 88.59	4.33- 17.16	2.06- 7.89	0.01- 0.15	1.44- 29.53	0.38- 38.34	0-1.60	0.62- 2.93	0.23- 1.24	0.03- 0.08	0.05-0.27	0.71-2.47	3.7-34.37	
	mean	60.66	18.34	7.05	0.05	3.88	5.35	0.73	2.67	1.18	0.10	0.30	5.11	10.93	
clay n = 8	ó	17.20	7.92	5.61	0.09	6.00	13.54	0.47	1.63	0.43	0.07	0.10	3.49	10.41	
	range	20.04- 77.05	4.92- 29.53	2.21- 17.11	0-0.24	0.25- 18.57	0.02- 38.78	0.15- 1.51	0.32- 5.11	0.35- 1.66	0.03- 0.20	0.19-0.49	0.24-10.11	2.56-32.86	

The diagrams for TiO₂, Al₂O₃, Fe₂O₃ Total and MgO display general linear trends from higher values in the finer grained material to lower contents in the medium and fine-grained

sand fraction. This reflects the decreasing amount of matrix-sized detritus, e.g. clay minerals, iron-oxides and fine-grained alteration products (Roser and Korsch, 1988; Garcia et al., 1994) in the coarser material.

Values for Na_2O , P_2O_5 , MnO , and CaO correlate also negative with SiO_2 but have low correlation coefficients ($r < -0.5$ for all four elements). Again, higher element concentrations in the finer grained sediments can be observed.

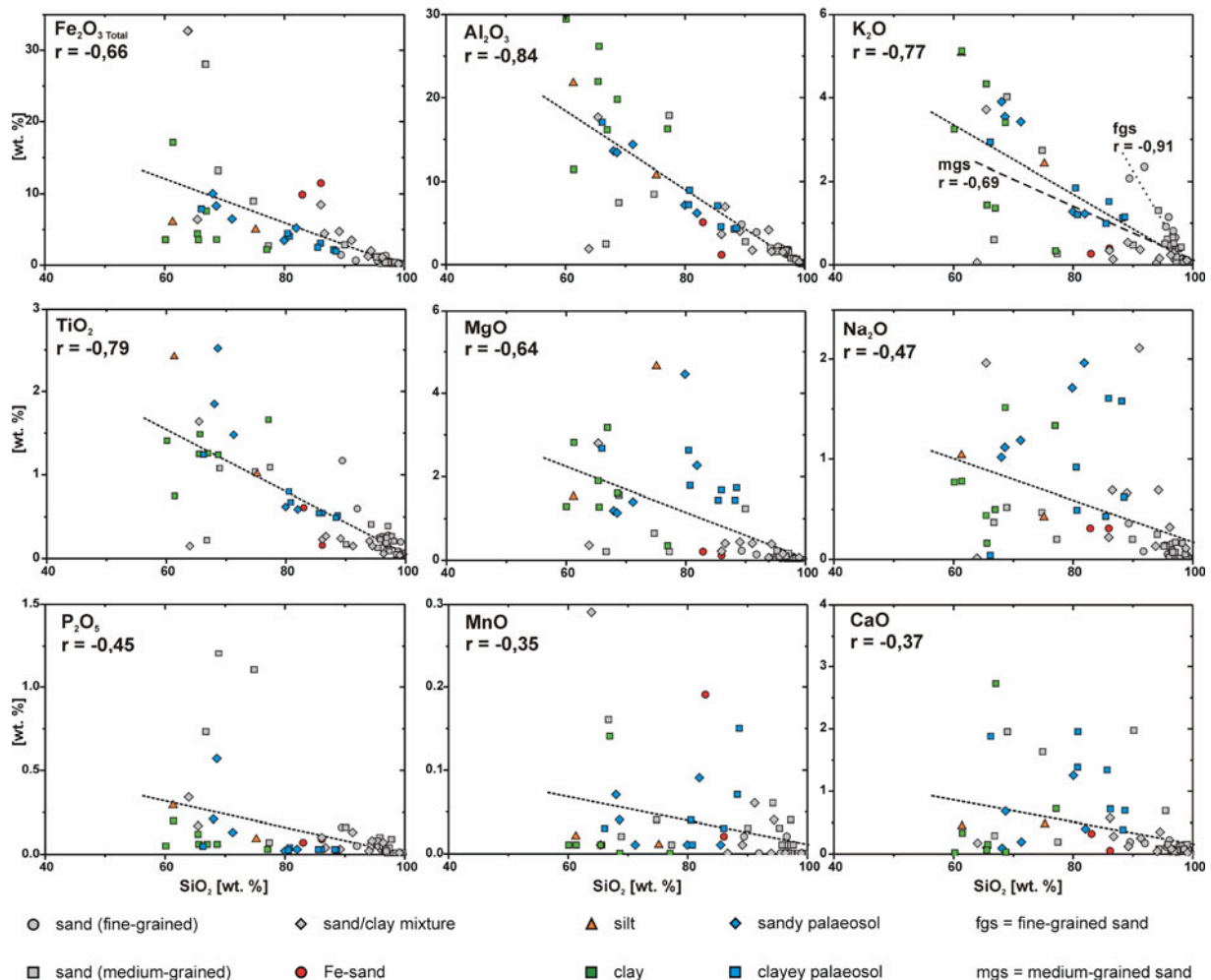


Figure 6.1 Harker variation diagrams for Cretaceous sediments of south Jordan. All data recalculated to 100 wt.% LOI-free, $n=65$.

6.2.1 Sediment classification

Similar to petrographic analysis, bulk rock geochemistry can be used to classify sedimentary deposits. The SandClass-System from Herron (1988), developed for classification of sediments in well logs, was chosen because of its classification detail and resemblance to the petrographic classification scheme of McBride (McBride, 1963, see Fig. 5.3, Chapter 5.1.4).

The representation of the field classification of the sediments fits well with the result of the SandClass-plot (Fig. 6.2). Especially sand sized samples (grey and red) and clays (green) match the corresponding classification fields. The diverse classification of the palaeosols (blue) mirrors their various sediment compositions. The predominance of quartz-rich sediments, shown in the petrographic classification, is clearly mirrored in the SandClass diagram. All plotted samples have Ca-values of less than 4% and therefore can be considered as non-calcareous sediments according to Herron (1988).

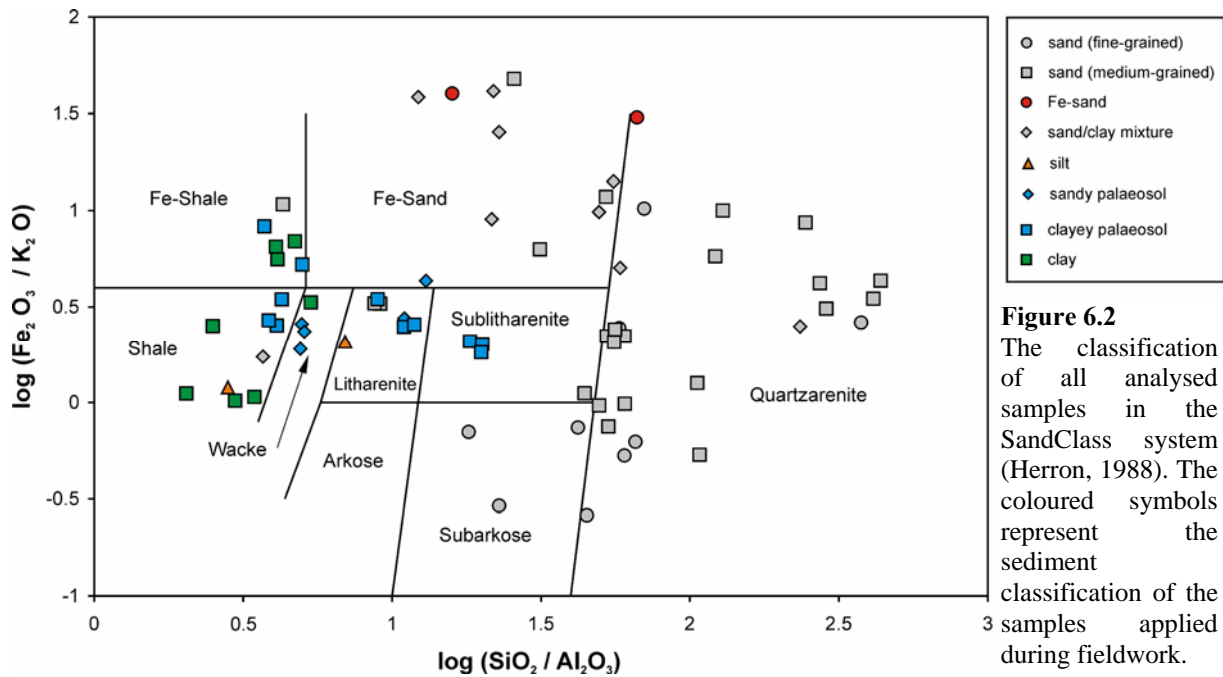


Figure 6.2
The classification of all analysed samples in the SandClass system (Herron, 1988). The coloured symbols represent the sediment classification of the samples applied during fieldwork.

6.2.2 Chemical index of alteration and weathering trends

The chemical index of alteration (CIA) was introduced by Nesbitt and Young (1982) and has been established as a general measure of the degree of weathering (McLennan et al., 1993). During the alteration of igneous rocks by weathering, alumina is enriched in sediments while alkali and alkaline earths are depleted (Nesbitt and Young, 1982; Toulkerides et al., 1999). Therefore the CIA can be calculated using the molecular proportions with:

$$\text{CIA} = \text{Al}_2\text{O}_3 / (\text{Al}_2\text{O}_3 + \text{CaO}^* + \text{Na}_2\text{O} + \text{K}_2\text{O}) \times 100,$$

where CaO* represents only that calcium that is incorporated in silicate minerals. Initially the CIA was used only on lutites to minimize the effects of size sorting and mineralogical differentiation during transportation and deposition (Nesbitt and Young, 1982).

For this study, samples with very high CaO contents, indicating the presence of calcium residing in carbonates, were not considered for the calculation of the CIA. A correction for phosphatic minerals like apatite (Toulkerides et al., 1999) could not be applied due to the loss of apatite during the heavy mineral preparation.

The average CIA of the studied samples is 67.88 (Tab. 6.3), which suggests moderate weathering degrees. The mean values for sand and silt (65 to 73) indicate similar weathering, while the value for the clayey palaeosols (53.59) is surprisingly low. The value for clays (79.47) points to a higher than average weathering, since according to Nesbitt and Young (1982) typical values for clays/shales are 70 to 75. For residual clays values approximate 100 (McLennan et al., 1993).

Table 6.3 Mean CIA-values.

sediment type	n	mean CIA	range	σ
fine-grained sand	9	64.95	55.62 - 89.54	10.11
medium-grained sand	20	69.23	43.21 - 95.16	14.71
Fe-sand	2	68.08	56.54 - 79.62	16.32
sand/clay mixture	10	66.61	29.96 - 93.29	18.38
silt	2	72.83	72.4 - 73.26	0.61
sandy palaeosol	4	65.29	54.58 - 70.81	7.38
clayey palaeosol	4	53.59	45.81 - 63.24	7.65
clay	6	79.47	60.83 - 92.73	10.77
all samples	58	67.88	29.96 - 95.16	13.88

Table 6.3 shows that the CIA-values for the different sediment types usually display wide ranges. This leads to an average CIA for all samples of around 70, suggesting a low to moderate degree of weathering for the studied samples. Still the extreme minimum and maximum values have to be explained.

For the sand sized samples the maximum values are easy to explain. Roughly all sand sized samples exhibit petrographic features of sediment recycling (see Chapter 5.4), and thus underwent repeated weathering cycles. Therefore maximum CIA-values of 90 and above are not surprising (McLennan et al., 1993). The minimum values below 50 are more difficult to justify, since unweathered igneous rocks have CIA values of 50 or below (McLennan et al., 1993). Possible explanations include the addition of alkali and alkaline earth bearing phases (e.g. clay minerals like smectite or mafic components) into the sand sized sediment during deposition (facies dependent, e.g. clay bundles), post-depositional (clay infiltration, soil forming processes) or during diagenesis (formation of a carbonate phase within the sediment).

For the fine-grained, clayey sediments the maximum values of 90 and above point to a high weathering degree. The occurring minimum values below 50 are most probably linked to the same processes that reduce the CIA of the sand sized samples. Especially the formation of microscopic calcrete and dolocrete veins in palaeosols during pedogenesis can reduce the CIA by adding non-silicate bound CaO to the sediment.

Weathering trends

Weathering trends of sediments can be shown in ternary diagrams using the molecular proportions of Al_2O_3 - $(\text{Na}_2\text{O}+\text{CaO}^*)$ - K_2O and Al_2O_3 - $(\text{Na}_2\text{O}+\text{CaO}^*+\text{K}_2\text{O})$ - $(\text{FeO}^{\text{T}}+\text{MgO})$, where CaO^* represents that of the silicate fraction only and FeO^{T} is the total Fe content recalculated to FeO. According to McLennan et al. (1993) the ternary plots will be called A-NC-K and A-NCK-FM in the following. In Figure 6.3A-C the studied samples are plotted in these diagrams. As mentioned before, Al_2O_3 is enriched in sediments during the alteration of the source rock, while alkali and alkaline earths are depleted. That means that general weathering trends will point towards the Al_2O_3 corner of the ternary diagrams, representing the conversion of unstable materials (e.g. volcanic glass) and minerals (e.g. feldspars and mica) to clay (McLennan et al., 1993).

A good example for this conversion is the transformation of potassium feldspar to kaolinite during weathering ($2 \text{KAlSi}_3\text{O}_8 + 2 \text{H}^+ + 9 \text{H}_2\text{O} \rightarrow \text{Al}_2\text{Si}_2\text{O}_5(\text{OH})_4 + 4 \text{H}_4\text{SiO}_4 + 2 \text{K}^+$; from Bjørlykke, (1989)). During this process potassium (K^+) is released and removed from the sediment. The former K^+ and Al_2O_3 bearing feldspar is transformed to a mineral predominately containing Al_2O_3 , located at the top of the ternary diagrams. The CIA changed from 50 to nearly 100 (Nesbitt and Young, 1982).

Diagenetic or metasomatic mineral transformations, like the transformation of kaolinite to chlorite, follow pathways from one mineral position in the diagrams to the other (Toulkerides et al., 1999). Therefore mineral transformations need not to follow the trend towards the Al_2O_3 corner. A mixture and interchange of several weathering trends and mineral transformations is possible.

In Fig. 6.3A the weathering trend for the fine-grained sands (grey arrows) in both ternary plots seems to be assembled. One possible trend tends to the K-feldspar point in both ternary diagrams, while the other follows a normal weathering trend towards the Al_2O_3 corner. The silt samples, displayed in orange in Fig. 6.3A, seem to follow a normal weathering trend in the A-NC-K plot, while this trend might be disturbed by $\text{FeO}^{\text{T}}+\text{MgO}$ or mica in the A-NCK-FM diagram. This is also true with the Fe-sands, shown in red. Similar to the silts, they follow normal trends in the A-NC-K plot and display a clear $\text{FeO}^{\text{T}}+\text{MgO}$ influence in the A-NCK-FM diagram. The palaeosols in Fig. 6.3A follow normal weathering trends (blue arrows) in the A-NC-K and clay mineral (smectite) influenced trends in the A-NCK-FM plot. This indicates that clay minerals dominate the palaeosols.

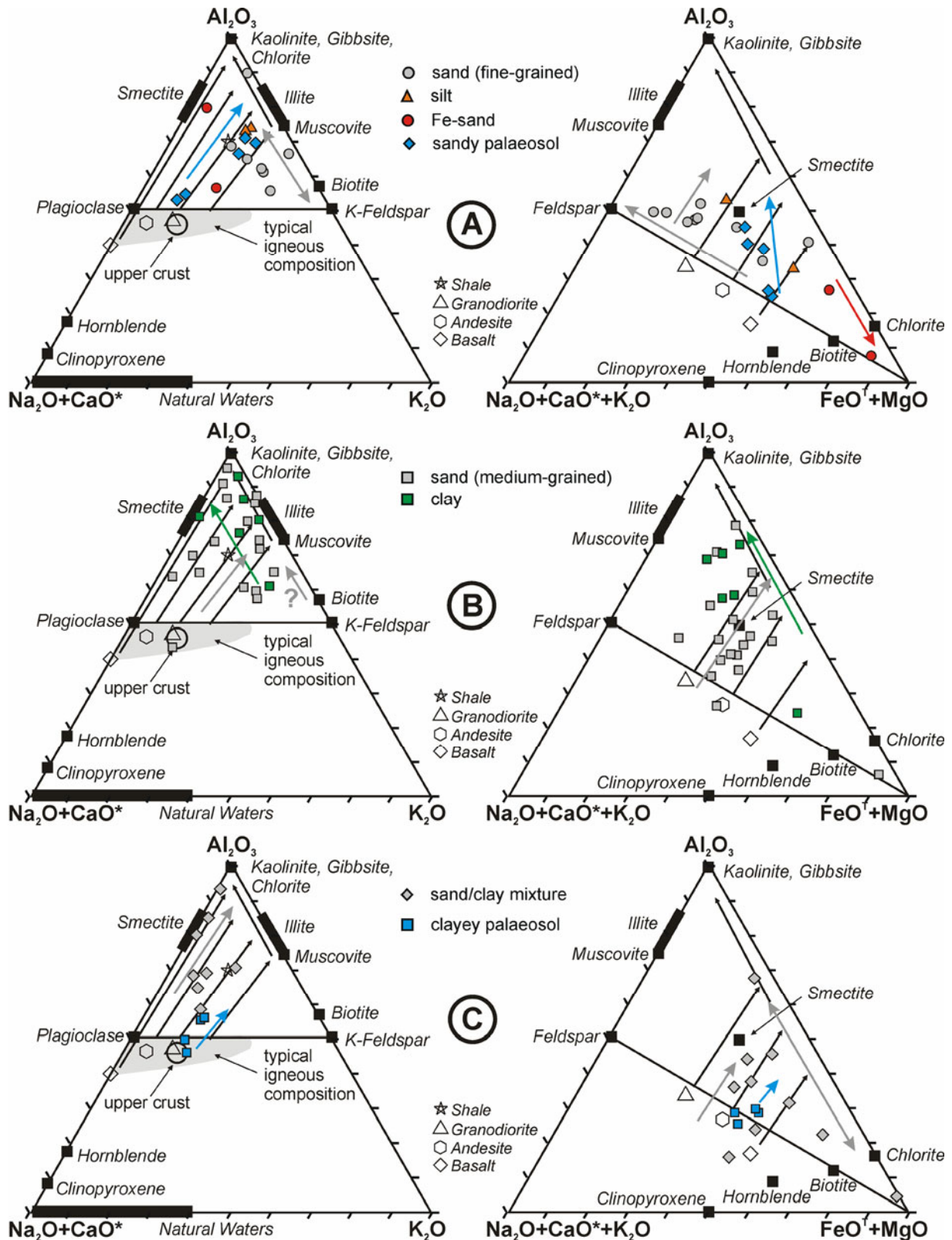


Figure 6.3 Ternary plots of molecular Al_2O_3 - $\text{Na}_2\text{O}+\text{CaO}^*-\text{K}_2\text{O}$ and Al_2O_3 - $\text{Na}_2\text{O}+\text{CaO}^*+\text{K}_2\text{O}-\text{FeO}^{\text{T}}+\text{MgO}$ after McLennan et al. (1993) and modified after Gu et al. (2002). The plots include weathering trends for some typical source rocks. A general weathering trend in all plots would tend towards the Al_2O_3 corner of the diagrams. The coloured arrows in the diagrams illustrate the assumed weathering trend of the corresponding sediments (grey = sand and sand/clay mixture; orange = silt, red = Fe-sand; blue = palaeosol and clayey palaeosol; green = clay). Explanations see text.

In Fig. 6.3B the medium-grained sands follow normal weathering trends in both diagrams (grey arrows). The clays, plotted in the same diagrams, follow the expected weathering tendency towards the Al_2O_3 corner (green arrows).

The sandy palaeosols and sand/clay mixed sediments (grey) in figure 6.3C follow the normal weathering trends in the A-NC-K diagram. Higher smectite/clay mineral contents force the palaeosol samples to the mafic/basaltic trend (Fig. 6.3C, A-NC-K plot). An observation, which can also be made in the A-NCK-FM plot. The position of the clayey palaeosols (blue) in the ternary diagrams indicates low weathering rates, which coincides with their low average CIA-value of 53.59.

6.2.3 Provenance

Provenance diagrams based on discriminant functions, (e.g. Bhatia, 1983; Roser and Korsch, 1988) involve several of the major elements and thus reduce possible errors in the concentration of single elements. Diagrams, based on the combination of single elements in ternary or XY-plots (e.g. Bhatia (1983) and Roser and Korsch (1986)), proved to be inadequate for the studied extreme quartz-rich sediments and therefore have been neglected.

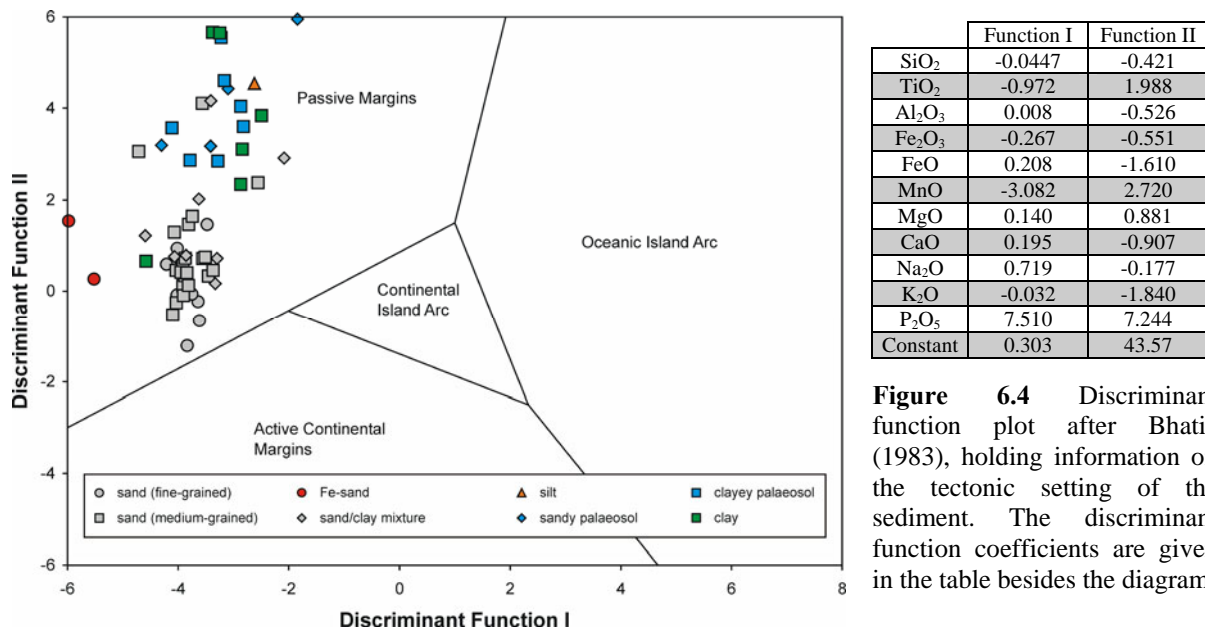
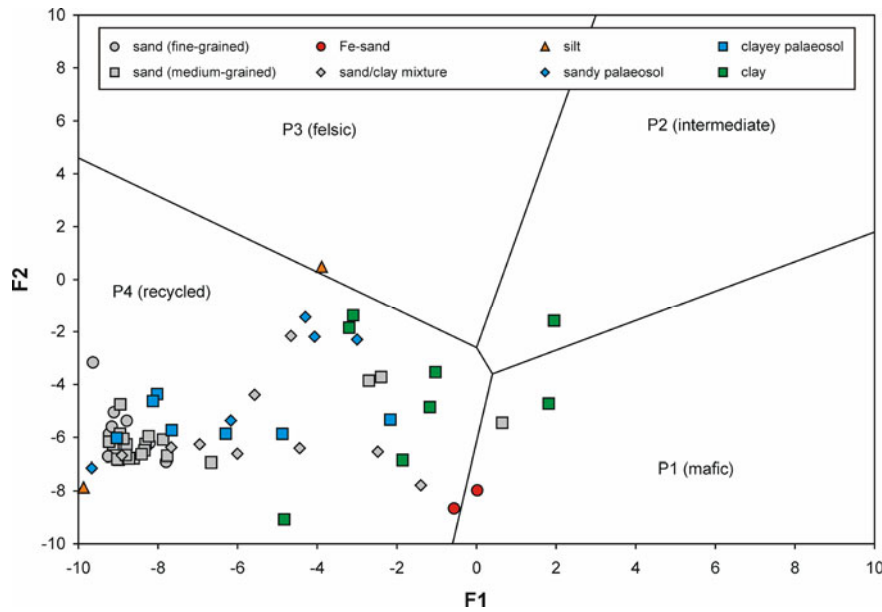


Figure 6.4 Discriminant function plot after Bhatia (1983), holding information on the tectonic setting of the sediment. The discriminant function coefficients are given in the table besides the diagram.

The discriminant function plot after Bhatia (1983) gives information on the general tectonic setting of the studied samples. The result shows that all samples gather in the passive margin field (Fig. 6.4). The plot after Roser & Korsch (1988) (Fig. 6.5) holds information on the source material. The clustering of the samples points to a recycling of older sedimentary material (field P4, Roser & Korsch, 1988) as the main source of the Cretaceous sediments. Due to higher contents of clay minerals and iron oxides, causing higher concentrations of Al_2O_3 and Fe_2O_3 , some samples plot more in the middle part of the diagram.



	F1	F2
TiO ₂	-1.773	0.445
Al ₂ O ₃	0.607	0.070
Fe ₂ O ₃ Total	0.760	-0.250
MgO	-1.500	-1.142
CaO	0.616	0.438
Na ₂ O	0.509	1.475
K ₂ O	-1.224	1.426
Constant	-9.090	-6.861

Figure 6.5
Discriminant Function plot after Roser and Korsch (1988). The function coefficients are given in the table above.

6.2.4 Hierarchical cluster analysis of the major elements

The aim of this method is to group the geochemical data so that it can be used for sediment classification (Fischer, 1989). Hierarchical cluster analysis (squared Euclidean distance, Ward method) was carried out on a data matrix consisting sample numbers and major element oxides (LOI-free, 100 wt.% normalized). The Ward-method was chosen because it produces hyperspherical clusters and well proportioned hierarchical structures (Swan and Sandilands, 1995). Prior to the cluster analysis the significance of all element oxides were tested with a factor analysis (Fig. 6.6).

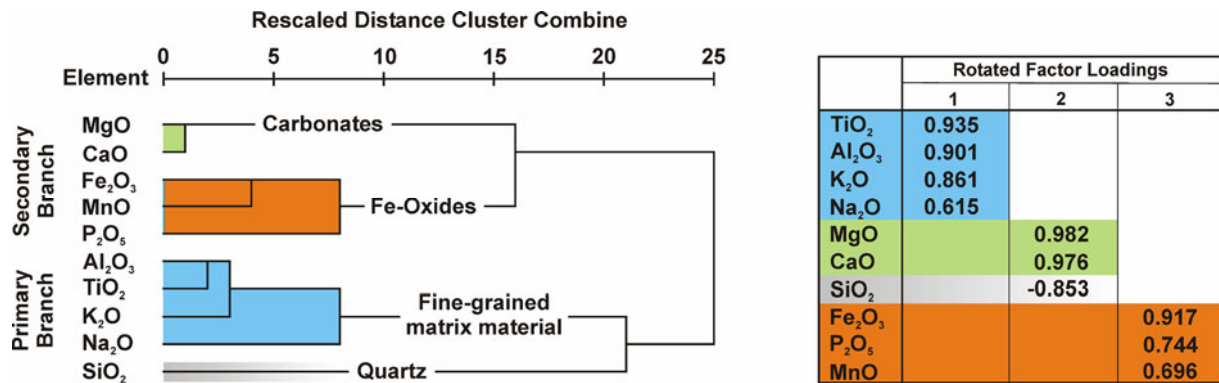


Figure 6.6 Results of the R-mode clustering (squared Euclidean distance, Ward Method, $n = 70$) and the factor analysis (right hand side). Both methods were applied to the complete data set. The colours match the colours of the resulting clusters in the dendrogram of figure 6.7. Note that both methods produce basically the same oxide-groups and the negative correlation of SiO₂ with MgO and CaO. For further explanation, see text.

Rationale

It was expected that SiO₂ represents mainly the quartz portion of the sediment. Al₂O₃, Na₂O and K₂O were assumed to mirror the clay mineral/sheet silicate and feldspar content. The iron impregnation, producing ferri-bands in the outcrops, is represented by Fe₂O₃ and MnO. However, these oxides also occur in heavy minerals and there especially in the opaque heavy mineral fraction. TiO₂ and P₂O₅ represent the heavy mineral fraction. TiO₂ stands for the rutile (TiO₂) content and P₂O₅ for apatite (Ca₅(PO₄)₃(F, OH, Cl)) in the sediment. It has to be considered that phosphorous fossil remains like fish scales, teeth, or bones are also composed of apatite and therefore might bias the P₂O₅ content. MgO and CaO represent the carbonate content (cement) of the sediment either as calcite (CaCO₃) or as dolomite (MgCa(CO₃)₂).

However, it has to be considered that CaO might be part of clays, feldspars and apatite; as well that MgO occurs in heavy minerals and iron oxides. In general this rational should allow distinguishing between the major sandstone types due to their major oxide content (Tab. 6.4). The cluster analysis provides a new tool for the geochemical classification of sediments with the advantage that all major elements are used.

Table 6.4 Summary of the expected geochemical characteristics.

Rock type	Expected geochemical characteristics
quartzarenite	dominance of SiO ₂ , possible raised TiO ₂ and P ₂ O ₅ due to enrichment of heavy minerals
arkose	medium SiO ₂ , medium to raised Al ₂ O ₃ , Na ₂ O and K ₂ O
litharenite	medium SiO ₂ , medium to high Al ₂ O ₃ , Na ₂ O and K ₂ O, possibly CaO; general geochemistry depends on the type and frequency of lithic fragments
calcareous sediments	high values of CaO and MgO, low SiO ₂
clay dominated sediments	high Al ₂ O ₃ , raised Na ₂ O and K ₂ O, general geochemistry depends on primary rock type (clayey arenite, wacke, sandy palaeosol etc.)
clay	high Al ₂ O ₃ , raised TiO ₂ , possibly raised K ₂ O and Na ₂ O
ferri-bands	high Fe ₂ O ₃ and MnO, medium SiO ₂ , possible raised P ₂ O ₅ due to phosphate scavenging

Result of the Q-mode cluster analysis

The dendrogram resulting from the hierarchical cluster analysis (Fig. 6.7) displays five key clusters: quartzarenites, clayey quartzarenites, Fe-sands, clays and palaeosols and calcareous clays. The general element distribution for each cluster is given in table 6.5. Cluster 1 (quartzarenites) represents all quartzarenites with an average SiO₂ content of 97.26 %. Cluster 2 (clayey quartzarenites) consists of quartzarenite with a higher clay mineral content (i.e. indicated by a higher Al₂O₃-value as in cluster 1). Increased values of TiO₂ and P₂O₅, point to a higher heavy mineral content. This indicates cluster 2 holds the finer grain size fractions compared to cluster 1. The examined fine sands often contain a higher amount of finer grained material like silt and clay. Generally heavy minerals will be enriched in finer grained sands.

Table 6.5 Result of the Q-mode cluster analysis of the major elements (squared Euclidean distance, Ward method, n = 70). Major element concentrations in wt.%.

Cluster No.		SiO ₂	Al ₂ O ₃	Fe ₂ O ₃	MnO	MgO	CaO	Na ₂ O	K ₂ O	TiO ₂	P ₂ O ₅
1 quartzarenites n = 28	mean	97.26	1.28	0.62	0.01	0.08	0.10	0.09	0.36	0.17	0.03
	σ	1.53	0.67	0.48	0.02	0.08	0.14	0.14	0.35	0.11	0.03
	range	94.24- 99.52	0.23- 2.27	0.13- 2.03	0- 0.06	0-0.39	0-0.69	0- 0.68	0.03- 1.29	0.04- 0.41	0- 0.10
2 clayey quartzarenites n = 22	mean	84.69	6.54	4.32	0.04	1.22	0.69	0.76	1.03	0.61	0.11
	σ	5.59	4.15	2.91	0.05	1.33	0.62	0.65	0.82	0.39	0.23
	range	74.81- 93.95	1.30- 17.97	0.68- 11.50	0- 0.19	0.06- 4.65	0.04- 1.97	0.07- 2.11	0.03- 2.72	0.15- 1.66	0.02- 1.10
3 clays and palaeosols n = 13	mean	65.99	17.80	7.56	0.03	1.87	0.66	0.84	3.49	1.51	0.24
	σ	3.34	6.06	4.00	0.04	0.73	0.91	0.54	1.14	0.50	0.32
	range	60.12- 71.25	7.55- 29.53	3.58- 17.11	0- 0.14	1.14- 3.18	0.02- 2.72	0- 1.96	1.35- 5.11	0.75- 2.52	0.05- 1.20
4 Fe-sands n = 2	mean	65.34	2.31	30.40	0.23	0.29	0.23	0.18	0.32	0.19	0.54
	σ	2.02	0.41	3.28	0.09	0.11	0.08	0.25	0.39	0.05	0.28
	range	63.91- 66.77	2.02- 2.60	28.08- 32.72	0.16- 0.29	0.21- 0.36	0.17- 0.29	0- 0.36	0.04- 0.59	0.15- 0.22	0.34- 0.73
5 calcareous clays n = 5	mean	24.33	5.82	6.95	0.13	25.13	35.69	0.09	1.47	0.30	0.09
	σ	4.28	1.22	4.11	0.07	4.43	3.31	0.19	0.69	0.05	0.06
	range	20.04- 30.51	4.33- 7.45	4.84- 14.29	0.08- 0.24	18.57- 29.53	30.73- 38.78	0- 0.43	0.62- 2.20	0.23- 0.35	0.05- 0.19

Cluster 3 (clays and palaeosols) combines Al_2O_3 -rich samples. Still a high SiO_2 content points to a certain amount of quartz grains in the sediment. Increased values of TiO_2 and Fe_2O_3 indicate the presence of heavy minerals and iron oxides in the sediments. Cluster 4 represents the iron-oxide rich sand samples, the so called Fe-sands. The high SiO_2 content marks these sediments as quartzarenites. The high Fe_2O_3 content results from intensive iron impregnation.

Cluster 5 (calcareous clays) is characterized by high MgO and high CaO , pointing to the presence of dolomite in the sediment. Relatively high amounts of Al_2O_3 indicate high clay mineral content. All samples in this cluster were taken from clayey sediments with marine influence, and contain small dolomite crystals. The expected results are met to a major extend.

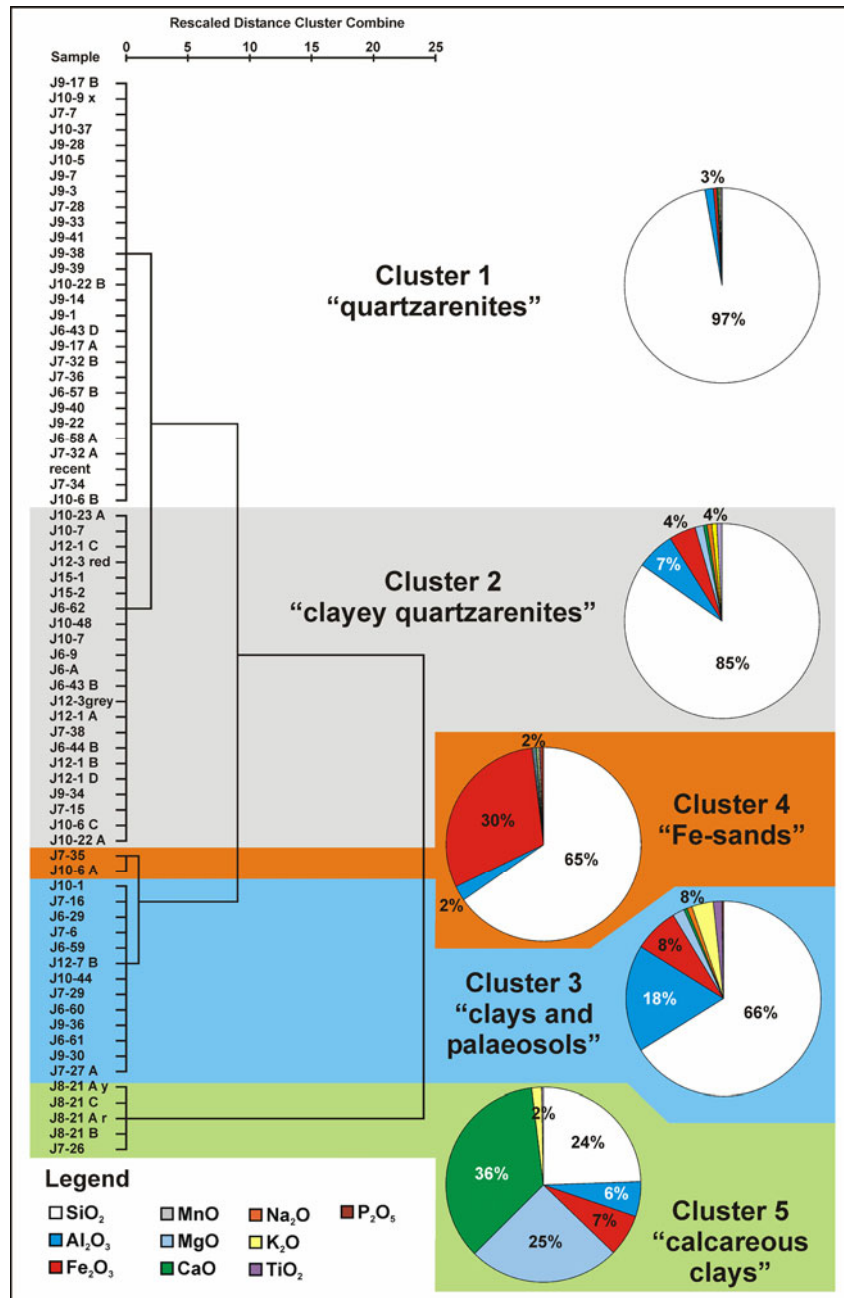


Figure 6.7

Result of the major element Q-mode cluster analysis (squared Euclidean distance, Ward Method, $n = 70$). The examined sediments are grouped in 5 clusters and classified by their dominating major elements.

Result of the R-mode cluster analysis

The R-mode cluster analysis indicates 4 assemblages divided into 2 branches (Fig. 6.6). The primary branch comprises the dominating primary mineral content, quartz respectively fine-grained matrix material, of the samples. It contains the quartz assemblage, characteristic for

the two quartzarenitic clusters, and the clay mineral assemblage, typical for the clays and palaeosol cluster. The presence of TiO_2 in the matrix material cluster displays the affinity of TiO_2 to retain in the fine-grained alteration products, together with Al_2O_3 (Garcia et al., 1994).

The secondary branch includes two assemblages whose geochemical character is determined by authigenic minerals (diagenetic calcite/dolomite and iron-oxide). Generally speaking these are the carbonate assemblage, characteristic for the calcareous clays, and the Fe-oxide assemblage, distinctive for the Fe-sands. MgO and CaO are the main elements forming the carbonate minerals calcite and dolomite. Fe_2O_3 and MnO are tied to iron-oxides. P_2O_5 is also connected to iron-oxides. Dissolved phosphate which occurs only in small quantities, can be scavenged in iron oxihydroxides (Föllmi, 1995; Gunnars et al., 2002). Solid inorganic phosphate (besides apatite) is carried with iron oxihydroxide in form of aggregated colloidal suspensions or coatings around suspended clay particles (Föllmi, 1995; Gunnars et al., 2002).

A direct comparison of the R-mode cluster analysis and the factor analysis (Fig. 6.6) shows similar results. Both methods combine the same element oxides in the same groups, pointing to the reliance of the results.

6.3 Rare earth (REE) and trace elements

Many trace elements and rare earth elements (REE) are immobile during sedimentary processes (e.g. Th, Sc, high field strength elements (HFSE) like Zr, Hf, Ta, Nb, and Y). Therefore they are transported quantitatively into sedimentary rocks during weathering (Bhatia and Crook, 1986; Roser and Nathan, 1997; Toulkerides et al., 1999). This can be used to apply trace element geochemistry to provenance aspects, since the amount of element enrichment and dilution, respectively, is generally contingent on the original source material.

6.3.1 Rare earth element geochemistry

Rare earth elements (REE) comprise the lanthanide elements, La to Lu, which are divided into light rare earth elements (LREE; La to Sm) and heavy rare earth elements (HREE; Gd to Lu). The lithophile REE are generally considered to be chemically immobile. Thus it is assumed that average REE patterns of source rocks are nearly quantitatively transferred to siliciclastic sediments during erosion and sedimentation (McLennan, 1989). Diagenesis, does not affect bulk-rock REE patterns significantly (Fleet, 1984; McLennan et al., 1993). In most rock-forming minerals, REE fill lattice sites in eight-fold coordination. Since there is no common, geochemically similar mineral-forming element, the trivalent REE cations have to replace analogues. Close analogues are Ca^{2+} and Na^+ , with existing charge and size imbalances which restrict the REE entry. For major rock-forming minerals, REE primarily substitute Ca. An excellent example for this replacement is plagioclase, where Eu^{2+} substitutes for Ca^{2+} , in place of Sr^{2+} (McLennan, 1989). This process is the reason for the positive Eu-anomaly of plagioclase (see Fig. 6.9F). Quartz contains little or no REE. Therefore quartz-rich sediments, have low REE values since the quartz dilutes the REE concentrations of the other minerals.

The REE pattern of average sediments is interpreted to reflect the average upper continental crust (McLennan, 1989). Besides the immobile character of the REEs this can be attributed to the homogenizing effects of sedimentary processes (Taylor and McLennan, 1985). The average REE pattern of the quartzarenitic Cretaceous sediments of South Jordan continues this (Fig. 6.8). The displayed pattern is similar to the upper continental crust. The lowered REE concentrations are caused by the dilution of the REE content by quartz.

For this study the chondrite normalizing scheme is used since the average chondritic REE pattern is likely parallel to bulk earth patterns (McLennan, 1989). The chondrite data was

taken from Taylor and McLennan (1985). The chondrite-normalized patterns of REEs of the studied sediments are shown in figure 6.9A-D. In addition to the patterns of the samples, which are presented stratigraphically from the footwall to the hanging wall, each plot includes the REE patterns of active and passive margins as presented by Taylor and McLennan (1985).

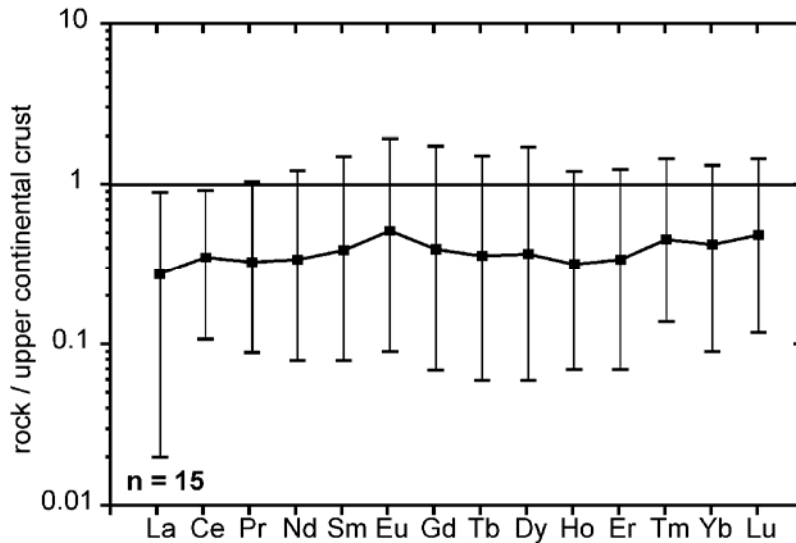


Figure 6.8
Average REE pattern of Cretaceous sands from South Jordan (with range indicated), normalized to the upper continental crust cf. Taylor and McLennan (1985).

Comparing the data set with the active and passive margin patterns shows no clear result. Enrichment in the HREE, which is typically for the passive margin pattern, is clearly present in all samples. The distinct negative Eu-anomaly of the passive margin is only present in some samples (e.g. J9-1 and J9-39). Other samples, like J9-33 and J9-38, seem to follow the active margin pattern. Therefore the chondrite normalized REE patterns of the studied samples do not allow a statement on the tectonic setting.

Comparison of the samples with the REE patterns of heavy minerals and clays (Figs. 6.9E & F) shows that the REE content of the samples is influenced by clay minerals and zircon. Especially the enrichment in HREE might be attributed to the zircon content, since all sand sized samples are enriched in zircon (see chapter 5.2). The clay mineral influence might be seen in samples J9-17 B, J9-28, J9-33 and J9-38.

The effect of heavy minerals biasing the whole rock concentration of REE is also considered by Totten and Weaver (2000). This is also reported by McLennan (1989) and Taylor and McLennan (1985), who state that the most important heavy minerals to consider include zircon, garnet and monazite, which all are notably enriched in HREE (see Figs. 6.9 E & F). Taylor and McLennan (1985) also point to the importance of the clay fraction as a REE carrier.

For provenance studies the Eu-value is of special interest. Usually Eu is enriched (positive EU-anomaly) or depleted (negative Eu-anomaly) relative to other REE on chondrite-normalized diagrams. This can be quantified by the term Eu/Eu^* , where Eu^* is the expected Eu value for a smooth chondrite-normalized REE pattern (McLennan, 1989). Eu/Eu^* can be calculated as follows:

$$Eu/Eu^* = Eu_N / (Sm_N \times Gd_N)^{0.5},$$

where 'N' denotes chondrite-normalized values (McLennan, 1989).

Certain provenance types display distinctive Eu/Eu^* values which, in combination with other ratios like Th/Sc and Th/U, can be used for discrimination means (McLennan et al., 1993). The mean Eu/Eu^* of the fifteen Cretaceous samples presented in figure 6.9 is 0.86 (range: 0.67-1.11), where finer grained sands tend to display higher Eu contents. This value reflects a slight negative Eu-anomaly for the combined samples, while a single sample (J9-33, fine to medium-grained sand) displays a slight positive anomaly.

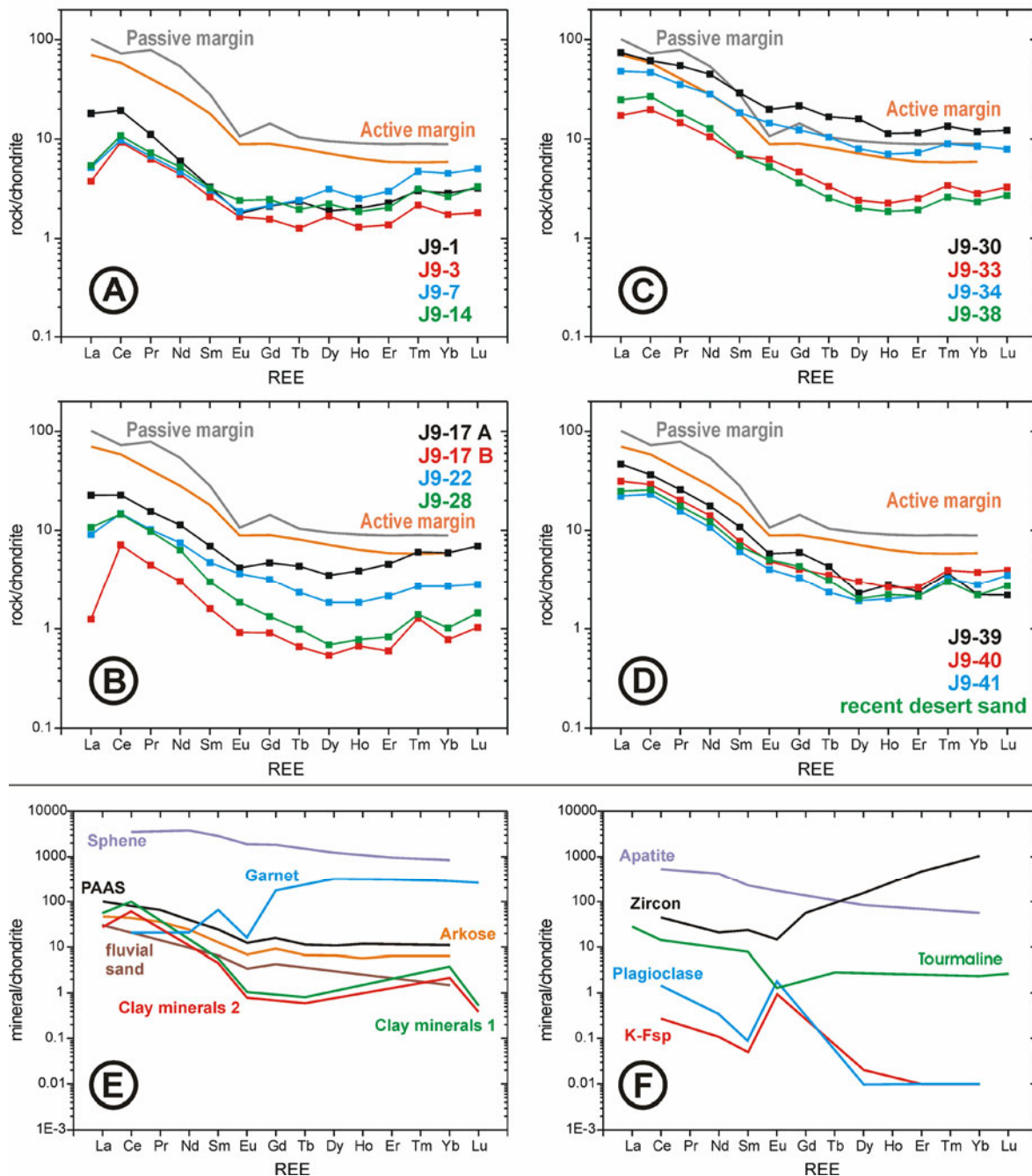


Figure 6.9 A-D: Chondrite normalized REE patterns of analysed Cretaceous sand samples from South Jordan. Passive and active margin patterns are also displayed. None of the samples fits completely with either passive or active margin. Some pattern of the Jordan samples compare partially (HREE) with the passive margin setting. **E & F:** Example REE patterns of typical rock forming minerals and three sediments (PAAS = Post-Archean average Australian shale). The enrichment of HREE in zircon and garnet should be noted. Chondrite data, active and passive margins patterns and data sets of E & F from Taylor and McLennan (1985).

6.3.2 Provenance derived from trace elements

The plot after Nagender Nath et al. (2000) and Floyd and Leveridge (1987), using La/Th and Hf, clearly shows the dominance of a sedimentary source component in the analysed samples (Fig. 6.10). The La/Th-ratio basically reflects different magmatic settings. High Hf-values are linked to higher zircon contents in the sediment and thus to upper continental crust material and recycling of a sedimentary source.

A plot using the Th/Sc- and the Zr/Sc-values, was presented by McLennan et al. (1993, Fig. 6.11). The Th/Sc-ratio is used as indicator for igneous chemical differentiation processes of the source rock: Th is typically an incompatible element, whereas Sc is compatible in igneous systems (McLennan et al., 1993) and generally preserves a signature of the provenance. Therefore the Th/Sc-values display the compositional differences of the source material. Similar to the diagram of Nagender Nath, high Zr/Sc-values point to sediment recycling (= addition of zircon). Elements like Zr and Hf are closely associated with heavy minerals (especially zircon) and their distribution is therefore controlled by heavy mineral concentrations (McLennan, 1989; McLennan et al., 1993). The grain size dependent fractionation of Zr in the sediments can be correlated to hydraulic fractionation of heavy minerals (Garcia et al., 1994; Wozazek, 2001). This causes raised Zr/Sc values for the sand sized samples in Fig. 6.11.

Fig. 6.10 and Fig. 6.11 show that the analysed samples from Jordan comprise a clear sediment recycling component. Fig. 6.10 additionally points to a felsic, upper continental crust source and a passive continental margin setting.

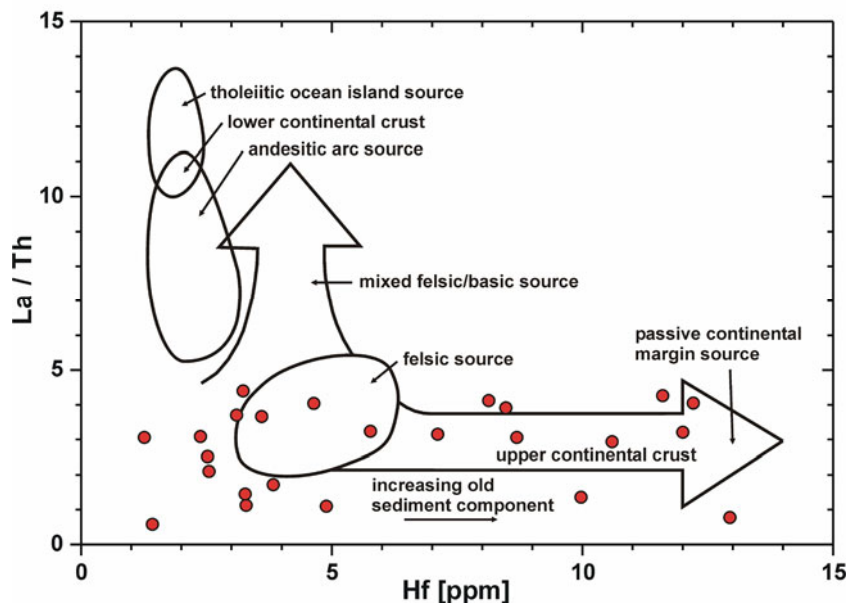


Figure 6.10

Plot after Floyd and Leveridge (1987), modified by Nagender Nath et al. (2000). Based on La/Th and Hf, it indicates possible source materials for the plotted sand sized samples. The overall source can be considered to be felsic with components of upper continental crust material. The increase in Hf is caused by an increasing component of older sediment in the samples (sediment recycling).

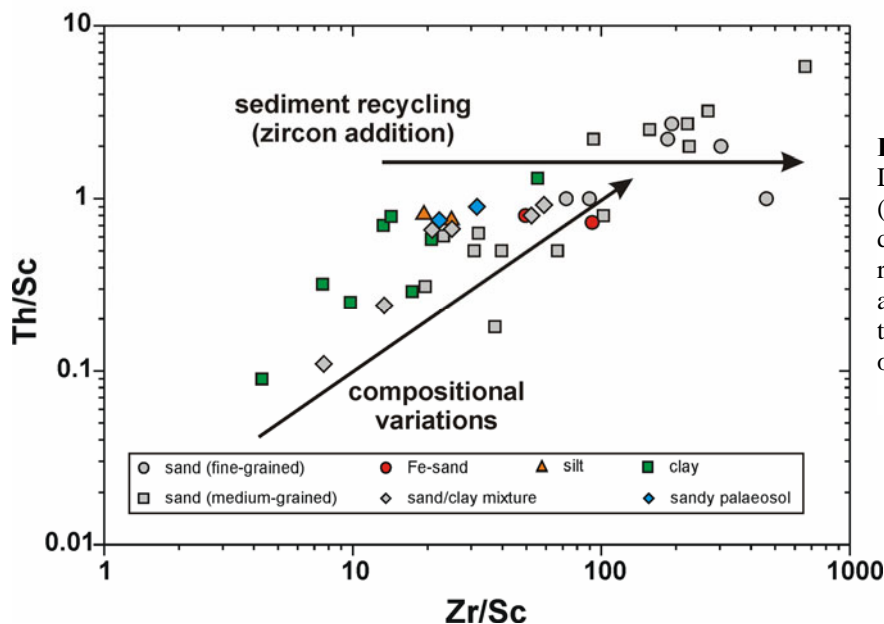


Figure 6.11

Diagram after McLennan et al. (1993). The sand samples also display a trend to high Zr/Sc-ratios, indicating zircon addition to the sediment and therefore a recycling of an older sedimentary source rock.

6.4 Multi element plots

A multi element plot, normalized to the upper continental crust, can help to identify the tectonic setting of the examined sediments (Fig. 6.12). The mean element pattern of 15 sand samples from the Cretaceous of South Jordan (see Figs. 6.9 A-D for sample identification) is plotted. In direct comparison, pattern of the Jordan samples fits no other pattern completely, but shows resemblances to the passive margin pattern in details. Especially the negative Sr peak and the enrichment in Hf and Zr are also present in the Cretaceous sediments of South Jordan. All are distinctive aspects of a passive margin setting (Floyd et al., 1991) indicating a zircon addition to the sediment by recycling of an older sedimentary source. The general low element concentrations of the Jordan sediments can be attributed to the quartzarenitic character of the samples, where the high SiO₂ concentration dilutes all other elements.

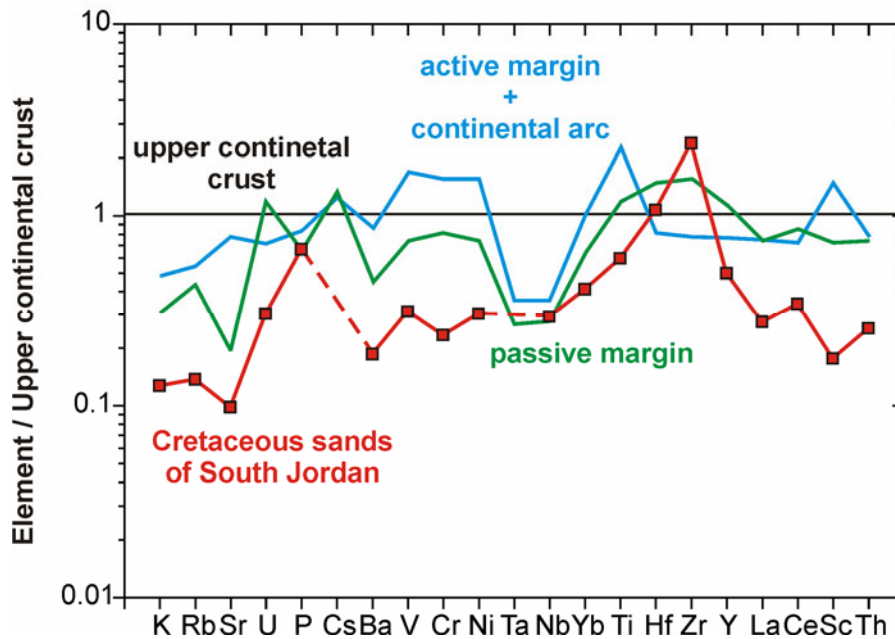


Figure 6.12 Multi-element plot comparing the mean composition of Cretaceous sands from South Jordan (red; n = 15), passive margin composition (green) and active margin/continental arc composition (blue). Continental crust data from Taylor and McLennan (1985), margin patterns from Floyd et al., (1991).

Another multi element plot after Molinaroli et al. (1991), using discriminant functions, is shown in figure 6.13. In this figure most of the samples, plot in the continental block field, which is principally comparable to a passive margin setting. Samples with a higher content of clay minerals and iron-oxides tend to plot in the magmatic arc field.

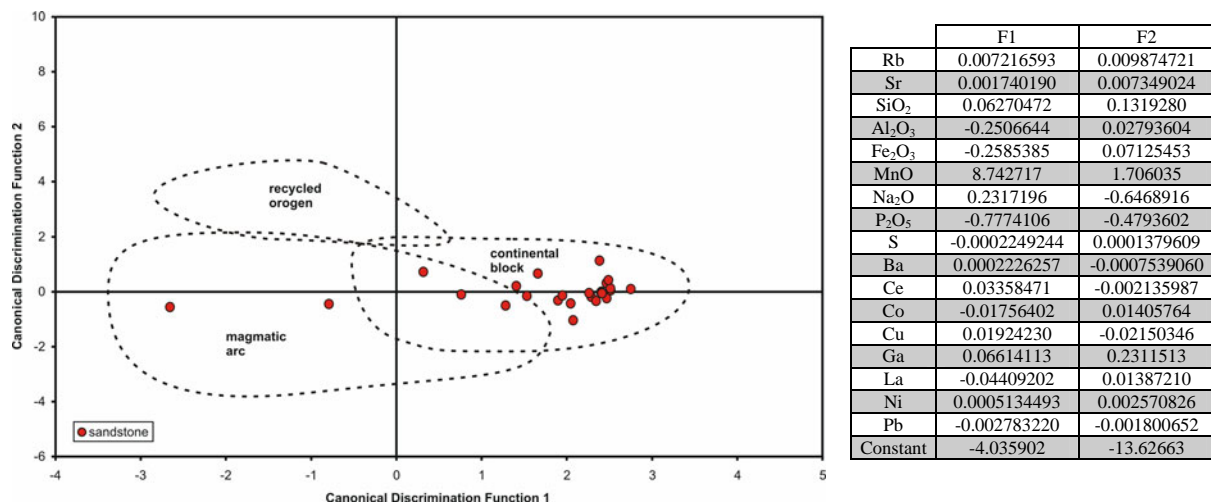


Figure 6.13 Multi element plot after Molinaroli et al. (1991) using discriminant functions. The fields correspond to typical source areas. The discriminant function coefficients are given in the table besides the diagram.

An R-mode hierarchical cluster analysis of the major and trace element analysis (major elements 100 wt.%, LOI-free) is presented in figure 6.14. The dendrogram is similar to the major element dendrogram (Fig. 6.6), though by adding the trace elements, the clusters include more detailed information and can be better interpreted.

The first two clusters mirror diagenetic features (cementation): cluster I represents the marine sandstones and cluster II the ferri-bands and Fe-sands (see 5.1.6). Cluster I holds elements which are characteristic for diagenetic carbonates (calcite and dolomite) in the sediment. Ba and Zn are elements which can be incorporated into carbonates and therefore fit well into this cluster.

The addition of U and Y to cluster II can be explained by the nature of uranium. U is carried in rivers in form of colloids together with Fe and organic carbon (Andersson et al., 2001). Brought to near shore environments, it will be sedimented with iron-oxides during the process of tidal mixing (Church et al., 1996). The element Y is generally aligned to uranium.

SiO₂, or quartz, is the sole component of cluster III, reflecting the quartz-rich character of the examined sediments. Cluster IV combines numerous elements representing the fine-grained or matrix sized fraction of the sediments (Garcia et al., 1994), including heavy minerals, feldspars, clay minerals and micas, as well as alteration products of these minerals. In general these matrix sized components are characterized by high amounts of Fe₂O₃, TiO₂ and Na₂O, which can lead to a “mafic” signal (Gu et al., 2002) in some geochemical applications, like the provenance analysis or the chemical index of weathering. K₂O and Rb are most probably aligned to potassium feldspar, where Rb can be present in small amounts (Deer et al., 1997). Na₂O and Sr are connected to plagioclase. TiO₂, Nb and Th represent Ti bearing heavy minerals like rutile and titanite, as well as their alteration products. Al₂O₃ is connected with many minerals but especially with clay minerals, micas and to feldspars. These minerals can also incorporate Na₂O and K₂O. Ga can replace alumina, while Sc can be integrated in Al₂O₃ bearing minerals. Zr is definitely linked to the heavy mineral zircon. All these elements are dominant in the fine-grained sediments like clays and palaeosols.

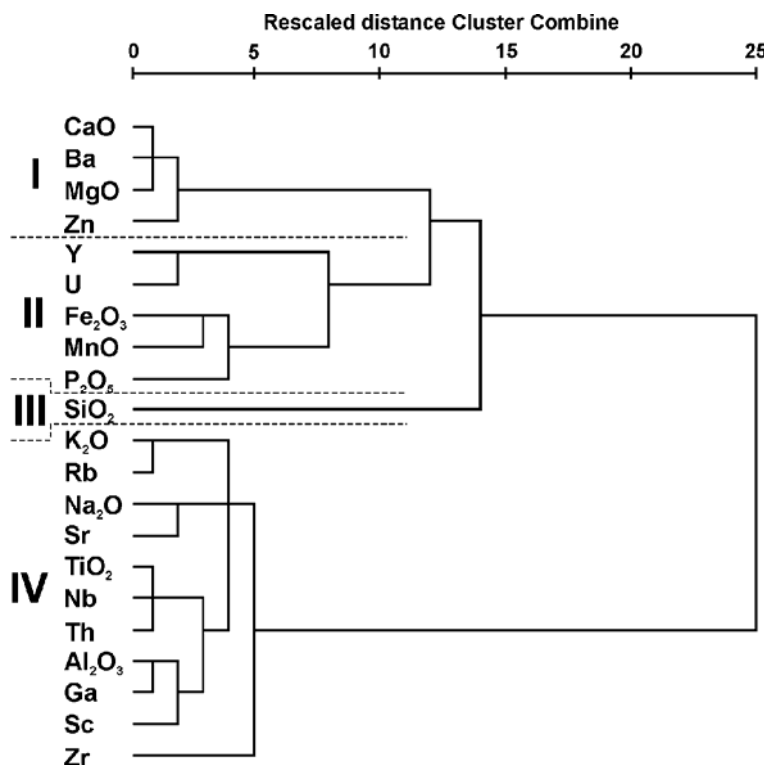


Figure 6.14

R-mode cluster analysis (squared Euclidean distance, Ward Method, $n = 70$) applied to the major and trace element data set from South Jordan. Pb, V, Cr, Ni and Cu were omitted from the analysis because they might be warped by the sample preparation (Tucker, 1996). The four groups are referred to: I = diagenetic carbonates; II = iron-oxide; III = framework quartz; IV = matrix sized materials (clay minerals, heavy minerals, feldspar, and alteration products).

6.5 Discussion and conclusion of the bulk rock geochemistry

The major element geochemistry of the sands (fine and medium-grained sand, Fe-sand and sand/clay mix) mirrors the evolved, compositional mature character of these sediments. Low $\text{Al}_2\text{O}_3/\text{SiO}_2$ values indicate a quartz-rich nature, which can also be seen in the classification plot in figure 6.2 and the cluster analysis of the major elements (Figs. 6.6 and 6.7). The distribution of the major elements depends on the grain size. The fine-grained sands contain more K_2O and Al_2O_3 than the medium-grained sand (Fig. 6.1). These two elements reflect the elevated potassium feldspar content in the fine-grained sands. This is also mirrored in the SandClass classification after Herron (1988), where the majority of fine sands plots in or close to the subarkose discrimination field (Fig. 6.2). The high $\text{K}_2\text{O}/\text{Na}_2\text{O}$ -ratio of the fine-grained sands indicates no significant plagioclase component in the sediments (Bhatia, 1983). In general low $\text{Al}_2\text{O}_3/\text{SiO}_2$, high $\text{K}_2\text{O}/\text{Na}_2\text{O}$ and decreasing $\text{Fe}_2\text{O}_{3\text{total}}+\text{MgO}$ values point to a high sedimentary maturation (Roser and Korsch, 1988).

The fine-grained sediments (silt, palaeosols and clays) hold the highest $\text{Fe}_2\text{O}_3+\text{MgO}$ values, pointing to iron oxide content in the sediments. This is also reflected in the geochemical sediment classification (Fig. 6.2). The raised value of TiO_2 in the fine-grained material is also evident (Fig. 6.1). High $\text{Al}_2\text{O}_3/\text{SiO}_2$ and $\text{K}_2\text{O}/\text{Na}_2\text{O}$ -ratios are linked to a high phyllosilicate content and remaining small (potassium-) feldspar particles in the muddy sediments. Due to the higher SiO_2 concentrations the palaeosols are classified as litharenites and wackes.

High CaO and MgO contents (Fig. 6.1 and table 6.2) in the clayey palaeosols and clays point to diagenetic formation of calcite and dolomite in the sediment. In case of the palaeosols the carbonate formation took place during the pedogenesis in form of microscopically calcrete and dolocrete veins.

Since trace elements (especially HREE and HFSE) are principally resistant to weathering effects, the weathering history is based on the major element geochemistry (Nesbitt and Young, 1982; Bhatia and Crook, 1986; McLennan et al., 1993; Roser and Nathan, 1997; Toulkerides et al., 1999). The combined use of the chemical index of alteration (CIA, table 6.3) and the A-NC-K/A-NCK-FM ternary plots (Fig. 6.3), is a helpful tool to determine weathering degrees and trends in sediments. The position of the sediments in the ternary diagrams corresponds to their CIA values. In general the mean CIA value is around 70, which is comparable to moderate weathered shale (Nesbitt and Young, 1982; McLennan et al., 1993). The weathering trends for the sediment groups follow the general weathering trends, indicated in the ternary diagrams (Fig. 6.3A-C).

Maximum CIA values of 95 for the sand-sized sediments point to a very strong weathering. The fact that the examined sands are not first cycle, but multicycle sediments, has to be considered. With each sedimentary cycle alkali and alkaline earth bearing minerals (e.g. feldspar) are removed from the sediment. Therefore a high CIA is characteristic for recycled sediments (McLennan et al., 1993). The weathering trends for the medium-grained sands follow the normal paths, while the fine-grained sands are influenced by higher (potassium-) feldspar content (Figs. 6.3A & B). Although clearly influenced by iron-oxide (see Fig. 6.3A), the CIA values for the Fe-sands are also comparable to the medium sands.

The low values for the clayey palaeosols (mean CIA: 53.59) and the extreme minimum of 30 in a sandy palaeosol point to the addition of alkali and earth alkaline elements to the palaeosols. Clay minerals, which dominate these sediments and generally raise the CIA, can not lead to such low values. The neo-formation of macroscopically invisibly calcrete/dolocrete in the palaeosols, bringing not silicate bound CaO and MgO into the sediment, has to be considered as the major disturbing influence. The addition of CaO can lower the CIA ($\text{CIA} = \text{Al}_2\text{O}_3/(\text{Al}_2\text{O}_3+\text{CaO}^*+\text{Na}_2\text{O}+\text{K}_2\text{O})\times 100$) significantly, and can explain the source rock close position of the palaeosol samples in the A-NC-K/A-NCK-FM ternary plots (Fig. 6.3), below the feldspar line. The neo-formation of carbonate in the sediment might also explain minimum values below 50 for the medium-grained sands (table 6.3).

The presence of matrix sized material with a general mafic geochemical character can also decrease the CIA of the palaeosols (Garcia et al., 1994). This material includes some heavy mineral phases, feldspar fragments, and diagenetic phases like iron-oxides and carbonates. The CIA values for the clays display the expected high values for this sediment type (Nesbitt and Young, 1982), which also accounts for the two studied silt samples. Both sediment groups show reasonable positions/weathering trends in the ternary weathering plots (Fig. 6.3).

A summary of the geochemical characteristics of the assorted sediment groups, including the CIA, is given in table 6.6.

Table 6.6 Summary of the geochemical characteristics of the sediment groups.

sediment type	geochemical characteristics
sand (fine-grained)	high SiO ₂ ; raised K ₂ O, Al ₂ O ₃ , and Zr; medium to high CIA,
sand (medium-grained)	high SiO ₂ ; raised Zr; other elements low, medium to high CIA
Fe-sand	high SiO ₂ and Fe ₂ O ₃ ; medium CIA
sand/clay mixture	raised Fe ₂ O ₃ +MgO, and Al ₂ O ₃ ; mixed CIA
silt	raised Fe ₂ O ₃ +MgO and TiO ₂ ; high Al ₂ O ₃ ; medium CIA
sandy palaeosol	raised Fe ₂ O ₃ +MgO and TiO ₂ ; high Al ₂ O ₃ ; medium CIA
clayey palaeosol	high Fe ₂ O ₃ +MgO; raised Al ₂ O ₃ and TiO ₂ ; high Ca; low CIA
clay	high Fe ₂ O ₃ +MgO and Al ₂ O ₃ ; raised Ca and TiO ₂ ; medium to high CIA

For statements on the provenance of the Cretaceous sediments of South Jordan, the combined results of major and trace element analyses worked well. The work with the dataset showed that not all geochemical provenance methods are suitable, especially when dealing with extremely quartz-rich sediments. The strong dilution of all elements by SiO₂, together with a considerable zircon enrichment due to sediment recycling renders many classic provenance diagrams (e.g. Bhatia, 1983; Bhatia and Crook, 1986; Roser and Korsch, 1986; 1988) useless.

Concerning the source rock, major elements were useful for a general overview. The trace elements and REEs proved to be a valuable and useful tool. In general the source rock of the Cretaceous siliciclastic sediments of South Jordan can be assumed to be of upper continental crust (UCC) origin (Figs. 6.8, 6.10 & 6.13), with a dominance of felsic source material. This is also evident by the element composition, e.g. low Al₂O₃/SiO₂, high K₂O/Na₂O and CIA, reflecting dominance of upper crustal granitic sources, combined with a strong weathering/recycling history (Taylor and McLennan, 1985; McLennan et al., 1993).

The mean Eu/Eu* ratio is too high for an UCC or recycled source (McLennan et al., 1993), though the corresponding Th/Sc ratios of about 1 fit well to these provenance types. In general high Eu values might be attributed to the feldspar content in sediments. Although the examined quartzarenites contain only little feldspar, their general low abundance on REE bearing minerals leads to certain Eu enrichment above usual values. Similar to the K₂O content, finer grained sands display higher Eu values, and therefore higher feldspar content.

From the results of the major (Fig. 6.5) and the trace element analyses (Figs. 6.8 & 6.10) it is quite obvious that recycling of older sediments is a dominating factor for the provenance. Especially the enrichment of the ultra stable heavy mineral zircon, clearly reflected by the enrichment of zirconium (Zr) and hafnium (Hf), points to this fact. By enrichment of Zr, Hf and HREE, the zircon enrichment in the sand sized samples is clearly visible in figures 6.10 and 6.11 and also in the REE patterns (Fig. 6.9A-D), where the HREE influence from zircon is obvious in the HREE part of the plots.

In order to get information on the tectonic setting of the source rocks, major (Fig. 6.4) and trace element methods (Figs. 6.4 & 6.10) were applied and point to a passive continental margin setting. The REE patterns however (Fig. 6.9), generally a standard tool in geochemically based provenance analysis (e.g. Taylor and McLennan, 1985; McLennan, 1989; McLennan et al., 1993; Toulkerides et al., 1999 among others), turned out to be unclear.

Only the enrichment in HREE points to a passive margin tendency. HREE enrichment in the studied samples can be attributed to zircon addition, which is caused by sediment recycling as part of the passive continental setting (McLennan et al., 1993). As “stand alone method” in this study, the REE patterns are dangerous to use.

7. Summary and conclusion

The presented study dealt with a sedimentary succession of mid to Late Cretaceous age (Albian to Santonian), which is exposed along the so called Naqb escarpment in South Jordan. Based on 15 vertical stratigraphic sections and on sediment samples from these logs, sedimentological studies were carried out. In this chapter the results of the single approaches of the thesis are summed up, discussed and compared to each other where applicable.

7.1 Part 1: Facies analysis and sequence stratigraphic results

7.1.1 Marine depositional environments and sequence stratigraphy

The examined sedimentary succession comprises ten environmental depositional facies which can be grouped into four major facies associations (Tab. 3.2). These facies associations are (i) the shelf facies association, (ii) the shoreface facies association, (iii) the marginal marine facies association and (iv) the coastal plain facies association. The recurring interfingering of these four facies associations and their lateral and vertical stacking pattern and arrangement showed that the Mid to Upper Cretaceous deposits of south Jordan can best be described as a shallow marine mixed siliciclastic-carbonate shelf to coastal system. The shelf was wave/storm dominated with minor tidal influence. Throughout transgressive relative sea-level phases the shelf system was accommodation-dominated and the coastal system was formed by estuaries and barrier/lagoon complexes. During regressive relative sea-level phases the shelf was supply-dominated and sand dominated braid deltas developed on the coast.

The vertical stacking pattern of the major facies associations displays the cyclothemic nature of the sediment succession (Fig. 3.14). An ideal shallowing upward cyclothem starts with a first siliciclastic ramp system, which is then followed by a mixed carbonate-siliciclastic ramp system. A second siliciclastic ramp system overlies the mixed carbonate-siliciclastic ramp. The last element of the cyclothem is formed by an alluvial system. This vertical stacking pattern is repeated several times along the Naqb escarpment. The repetition of the cyclothem makes the Naqb escarpment a perfect study area for shallow marine sequence stratigraphy.

The shallow, ramp like palaeogeographic setting of the study area, where relative sea-level changes are well recorded, allowed the use of a ‘new’ sequence stratigraphic model introduced by Plint and Nummedal (2000). This sequence stratigraphic model uses four systems tracts instead of the usual three of the established Exxon model. Plint and Nummedal combined the complete relative sea-level fall of the late HST and early LST to form the new falling stage systems tract (FSST). At its base the FSST is bounded by the “basal surface of forced regression”, at the top by a sequence boundary or its equivalent surfaces. The relative position of the other systems tracts and their bounding surfaces stays as it was in the Exxon model.

The sequence stratigraphic analysis resulted in eight third-order sequences (1 to 8), within the studied sections. The first four sequences are situated within the Cenomanian to Coniacian Ajlun Group (Fig. 7.1), the following four sequences are part of the Coniacian to Santonian Belqa Group. Three of the sequences, sequences number 1, 2 and 4, can be further divided into sequences of higher order (1.1, 1.2, 2.1, 2.2, 4.1 and 4.2).

An interesting feature in the study area is the repeated appearance of forced regressions. Forced regressions, that is the seaward migration of the shoreline in direct response to relative sea-level fall (Posamentier and Morris, 2000), are part of the FSST. All sequences within the Ajlun Group, including the sub-sequences, show distinguished characteristics of forced regressions in their FSSTs. Typical features of forced regressions like foreshortened stratigraphy, sharp based shoreface deposits and long distance regressions can be found. Using the classification scheme presented by Posamentier and Allen (1999) and Posamentier

and Morris (2000), the forced regressive deposits in sequences 1.1, 1.2, 3, 4.1 and 4.2 are smooth-topped attached forced regressive deposits, whereas in sequences 2.1 and 2.2 the deposits are smooth-topped and detached.

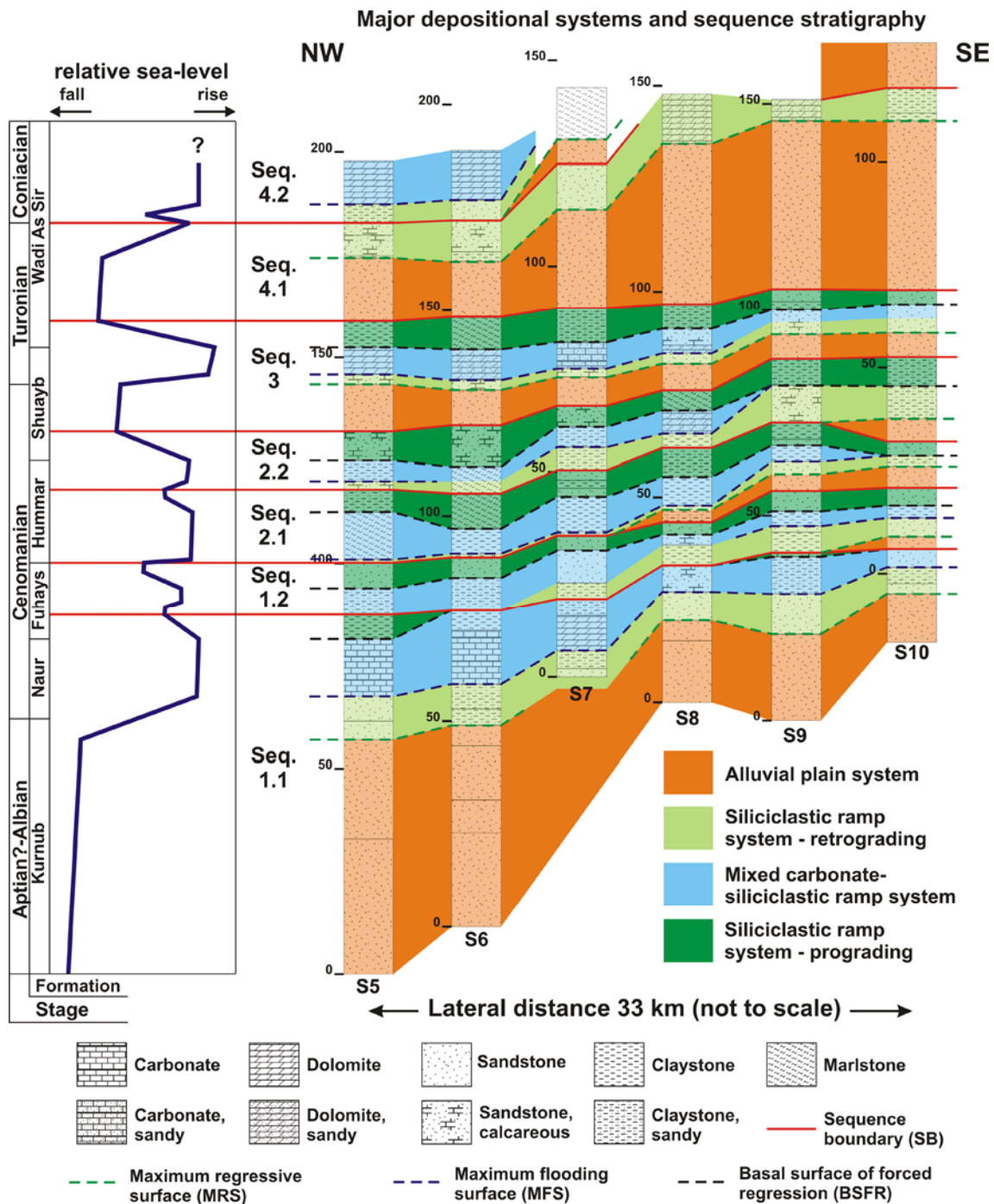


Figure 7.1 Relative sea-level, major depositional systems and sequence stratigraphy of the mid to Late Cretaceous Ajlun Group of South Jordan. The stratigraphic column is based on section 5 (S5).

Combining the results of the facies analysis with that of the sequence stratigraphy shows that the four major depositional systems, which form an ideal cyclothem, can be perfectly linked to the four systems tracts of the sequence model (Fig. 7.1). The first siliciclastic ramp system forms during the TST. The mixed carbonate-siliciclastic ramp system matches the HST. The second siliciclastic ramp develops during the FSST. During the LST the alluvial plain system forms.

Furthermore, the development of the carbonate depositional system on the shelf is linked to the systems tracts. During the LST high siliciclastic sediment input reached far into the basin and disturbed the carbonate production in the study area. During the TST the low siliciclastic input allowed the formation of a tripartite shelf system, with a calcareous to sandy outer shelf, a muddy to sandy transition zone and a sandy shoreface. During the HST the tripartite shelf was well developed. The outer shelf was carbonate dominated, sometimes marly. The transition zone included a higher portion of calcareous material. The shoreface system was still siliciclastic dominated. During the FSST the tripartite shelf system got disturbed by high siliciclastic sediment input and the influence of forced regressions, leading to an inhibited carbonate production.

7.1.2 Terrestrial deposits

Many terrestrial deposits in the study area, especially the palaeosols of the interfluves, have reddish colours. The red sediment colour and the occurrence of ferribands (“ironcrusts”) within the sediments are linked to diagenetic and soil forming processes. Especially in the muddy palaeosols both features might be connected to lateritic weathering.

The terrestrial deposits in the eastern part of the study area (east of section 10), consist of fluvial sediments of anastomosing to meandering river systems with vast interfluve areas. The interfluves were vegetated and experienced extended soil formation. The comparison of the different forms of palaeosols found along the Naqb escarpment showed that they developed under different drainage conditions. The encountered palaeosols can be classified as oxisols, vertisols, calcisols and argillisols (Mack et al., 1993), soil forms that normally develop under wet equatorial to dry subtropical palaeoclimatic conditions (Mack and James, 1994).

In the western part of the study area, west of section 11, the terrestrial deposits are made up of fluvial sediments that are best characterized as sandy braided river deposits which were part of braid delta complexes. These braid deltas formed during the LSTs at the head of incised valleys in response to high sediment supply from the hinterland (Fig. 4.9). The increased siliciclastic sediment supply was caused, in response to the rising base-level, by the upstream moving knickpoint of the river system, which triggered valley incision in the upper parts of the fluvial system.

Braid delta systems, channel stacking and aggradational conditions, filling the incised valleys mark the terrestrial depositional system of the LST. During the TSTs the rising relative sea-level/base-level strongly influenced the river system. The fluvial equilibrium profiles changed, forming accommodation space on the coastal plain and in the incised valleys. Transported sediment from the hinterland was now deposited there, filling the incised valleys and reducing the siliciclastic sediment supply to the basin to a minimum. Exposed to marine wave energy with only minimal terrestrial sediment supply, the river mouths at the front of the incised valleys were transformed to estuaries and the coastal system changed to a barrier/lagoonal one. With low rates of relative sea-level/base-level rise during the HSTs the coastal system began to prograde. The river mouths switched back to delta complexes and meandering rivers with wide interfluves developed on the coastal plain. The regressive sea-level conditions during the FSST again changed the fluvial equilibrium profile dramatically. Close to the shoreline the fluvial systems began to incise, resulting in rising sediment input into the basin. Due to the low gradient of the shelf slope and the coastal plain, the valley incision was only shallow, but relatively wide. “Forced regressive” conditions with long distance regressions, caused by the low shelf gradient and the strong eustasy, also affected the river system. The valley incision repeatedly shifted towards the shoreline bypassing wide areas of the exposed shelf. Only at the end of the FSST the incision started to move up the fluvial equilibrium profile. During the complete FSST sediment transported by the river systems was bypassed from the coastal plain onto the shoreface/basin. There the sediment was distributed by wave action and currents. Summing up it can be stated that the development of

the river systems in the study area was directly linked to relative sea-level changes and thus to sequence stratigraphy.

7.1.3 Controlling parameters of the stratigraphic/sequence architecture

An aim of this study was also to define the parameters controlling the stratigraphic and sequence architecture of the examined deposits. The sequence stratigraphic interpretation of the logged sections showed that the relative sea-level changes played an important role for the stratigraphic architecture. Evidence for the influence of synsedimentary tectonics was not found in the studied outcrops. Petrographic analysis of the sampled sandstones showed that compaction, overburden and therefore subsidence were rather low. The absence of tectonic influence and the low subsidence reveal that the relative sea-level was basically controlled by eustasy. The reconstructed relative sea-level curve (Fig. 4.10) for the Ajlun Group time interval (Cenomanian to Upper Coniacian) is relatively similar to global eustacy curves for this time period. This underlines the importance of eustasy for the examined sequence architecture.

Siliciclastic sediment supply is the second important controlling parameter for the stratigraphic/sequence architecture. By means of incised valley formation the siliciclastic sediment supply is also linked to the relative sea-level changes. During FSSTs and LSTs the siliciclastic sediment supply was relatively high. Throughout these times incised valley formation on the shelf or on the coastal plain took place. Cannibalization of older terrestrial deposits was therefore the main source for the sediment load transported to the shoreline at those times. During the FSSTs this sediment was directly bypassed to the basin (forced regression) while during the LSTs it led to the progradation of the shoreline (normal regression) and filled the incised valleys. Evidence for the high siliciclastic sediment supply during the LSTs is the repeated occurrence of thick sandstone units within the study area, e.g. within the Mid Wadi As Sir Formation.

The physiography of the shelf, that is the low gradient of the shelf slope, was a third important controlling factor for the sequence architecture of the study area. In combination with the relative sea-level changes, the low shelf gradient is the main parameter that leads to the formation and preservation of the forced regressive deposits. The occurrence of forced regressions in virtually each sequence gives rise to the assumption that even slight changes in the relative sea-level resulted in long distance regressions. This effect is strongly enhanced by a low shelf gradient. Besides that, it can be concluded that the storm/wave dominated shelf system is also mainly caused by the low shelf slope which produces wide areas with relatively shallow water conditions.

The importance of eustasy, systems tract linked sediment supply and physiography for the stratigraphic architecture of the studied succession was proved by forward stratigraphic computer modelling (Wöhrle, 2001). The outcrop based computer simulation also concludes that these three parameters were the controlling factors for the sequence architecture and for the formation of repeated forced regressions within the succession.

7.2 Part 2: Petrographic and geochemical results

7.2.1 Sandstone petrography

Light mineral studies of sampled medium- to coarse-grained sandstones showed that they are mineralogically mature and can be classified as quartz arenites (Fig. 5.3). A slightly higher content of feldspar in finer-grained sandstones often classifies them as subarkoses. The petrographic results are also reflected in the geochemical composition (Tab. 6.2 and Fig. 6.1) and the geochemical classification after Herron (1988) (Fig. 6.2).

Independent of grain-size all studied sandstone samples show very similar heavy mineral spectra. Zircon, tourmaline and rutile form the absolute majority of heavy minerals, resulting

in an average ZTR-index of about 98. Such a high ZTR-index corresponds very well with the high mineralogical maturity of the sandstones (cf. Hubert, 1962). The high zircon content is geochemically mirrored by high zirconium (Zr) and hafnium (Hf) content in the sand-sized sediments (tables 6 and 7 in Appendix II).

This study is the first that petrographically dealt with the Ajlun Group of south Jordan. Until now only the Kurnub Group of entire Jordan was covered in petrographic works for example by Amireh (1987; 1991; 1992) and Nasir and Sadeddin (1989). The results of the light and heavy mineral analysis match well the observations of the previous workers for the Kurnub Group. Therefore it can be stated that the Kurnub and the Ajlun groups of south Jordan form a petrographical continuous unit.

7.2.2 Provenance

Geochemical analysis pointed to a passive continental margin setting for the source rocks of the mid to Late Cretaceous sediments of south Jordan (Figs. 6.4, 6.9, 6.10 and 6.12). This setting was constant during the complete studied time interval, from the Kurnub Group to the Lower Belqa Group. As source rock both, petrographic and geochemical approaches point to felsic upper continental crust material of a continental block and/or craton interior (granites/granitoids and medium to high grade metamorphic rocks) (Figs. 5.8, 5.9, 5.10, 6.8 and 6.13). Furthermore a content of obviously recycled sedimentary material is indicated by both methodical approaches (Figs. 5.8, 5.9, 6.5, 6.10 and 6.11).

From the petrographic point of view the recycling is visible in form of quartz grains with rounded syntaxial quartz cement overgrowths in the light mineral fraction. In the heavy mineral fraction the dominance of zircon, tourmaline and rutile points to the recycling component (Fig. 5.12). Geochemically the recycling is noticeable in the high zirconium (Zr) and hafnium (Hf) content (Figs. 6.10 and 6.11). Both trace elements are abundant in the ultrastable heavy mineral zircon, which gets enriched in the sediment by recycling processes.

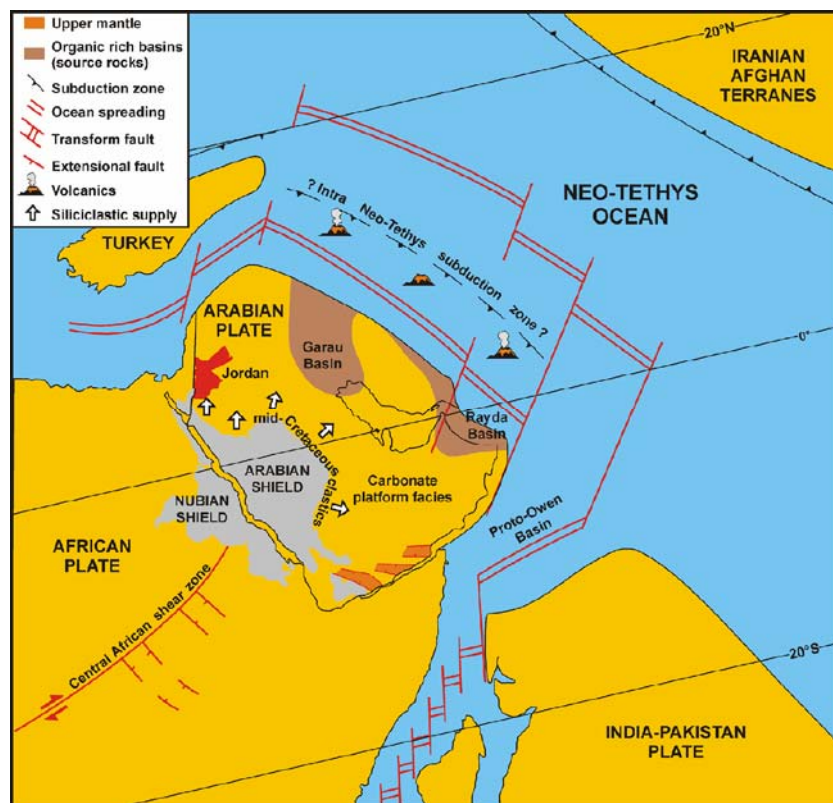


Figure 7.2

Plate tectonic reconstruction of the mid Cretaceous Arabian Plate region (modified after Sharland et al., 2001). The figure shows that during that time the Arabian-Nubian shield provided the siliciclastic sediment source for South Jordan and the surrounding region.

As source area for the mid to Late Cretaceous sediments of south Jordan the Arabian-Nubian shield is the most likely solution (Fig. 7.2). As a stable craton it matches the passive continental margin and craton interior settings, required by the provenance analysis, perfectly. The plutonic and metamorphic rocks of the shield, typical upper continental crust rocks, provided a sediment source since the Cambrian period. The Palaeozoic sediments, covering the flanks of the shield, were the source of the recycled sedimentary material found in the Cretaceous sandstones.

Discussion of the applied methods of provenance study

Concerning the provenance study of quartz-rich sediments and quartz arenites the applied petrographic and geochemical methods proved to be of different value. Especially some geochemical methods, though all well established in provenance study, proved to be less useful for quartz rich sediments as expected.

Light mineral analysis was a very useful tool. The multicycle nature of the quartz arenites and their origin from a craton source was clearly revealed by this method. Heavy mineral analysis underlined the light mineral results and demonstrated the dominance of the heavy minerals zircon, tourmaline and rutile in the sediments.

The results of the three applied bulk rock geochemical methods, major element analysis, trace element analysis and rare earth element analysis, were not necessarily useful. So was the major element analysis only of limited use for the provenance study. The SiO₂-rich nature of the sediments diluted the major element concentration in the sandstones to an extent that many established provenance diagrams were useless. Only the determination of the tectonic setting and the recycled nature of the analyzed sediments worked well, but the results were already known from the light mineral studies. Trace element analysis also offered results on the tectonic setting and the recycled nature of the studied sediments. These results were comparable to the results of the heavy mineral analysis. Analysing the REE content of the sediments was only of limited use. This was especially true for the comparison of the REE patterns with typical patterns of different tectonic settings, meanwhile a standard tool in provenance study (e.g. McLennan et al., 1993; Toulkerides et al., 1999). This comparison did not work well on the examined material due to the diluting effect of the high quartz content.

Summing up it can be concluded that a combination of light mineral study and bulk rock trace element analysis might prove to be the best approach for provenance studies of quartz rich sediments. Heavy mineral analysis helps to link the trace element geochemistry to the sediment but takes up a great deal of time. Due to the diluting dominance of SiO₂ in quartz-rich sediments and the low content of REE, bulk rock major element and REE analysis are only of limited use for provenance studies of these sediments.

7.2.3 Diagenesis

High intergranular volumes (IGV) and lacking destructive grain contacts in all samples, point to low to moderate compaction rates (Fig. 5.2). Therefore it can be assumed that the post Cretaceous overburden of the sediments was minimal and that they did not experience deep burial.

Considering the main cementing minerals, the often friable sandstones can be classified into three groups: clay mineral-, iron-oxide- and carbonate mineral-cemented sandstones. Sandstones cemented by clay minerals are all friable and have the highest intergranular porosities of all examined samples. The clay minerals, sometimes accompanied by iron-oxide, occur as rims and coatings around framework grains. This and the lack of pore filling clay mineral phases point to an infiltrated nature of the clay minerals (Gaupp et al., 1993).

Sandstones cemented by iron-oxides are well lithified and display low intergranular porosities. In marine environments the iron-oxide cementation is most probably an early diagenetic feature linked to high continental runoff. In terrestrial environments this

cementation can be attributed to ground water influence and soil forming processes. Lateritic weathering in a warm humid climate was in both cases the source of the iron-oxide.

The sandstones cemented by carbonate minerals (calcite, dolomite) have a low intergranular porosity and are well lithified. Due to the low sediment compaction observed in the samples, the carbonate cementation can be said to be of early diagenetic origin. A precipitation from marine or marine derived waters at the sediment-water interface or the solution and re-precipitation of biogenic carbonate material are possible mechanism for this kind of cementation. Due to the low burial depth of the sediments, the dolomite cementation must also have taken place during the early diagenesis. Its origin is most probably linked to the sulphate reduction zone or to a mixed-water aquifer. Occurring de-dolomitization in the samples points to a post dolomite formation meteoric influence within the south Jordan clastic sediments. Facies analysis showed that all samples of this cementation group were of marine origin. Terrestrial samples did not contain carbonate minerals as cement. For that reason it can be stated that the carbonate cementation in the study area is facies dependant.

Summing up it can be concluded that minor compaction and facies dependant cementation are the only diagenetic features of the studied samples. Consequently the mid to Late Cretaceous sediments of south Jordan experienced only minor diagenesis.

7.3 Stratigraphic correlation of North/Central Jordan and South Jordan

Besides the establishment of a sequence stratigraphic framework for the mid to Late Cretaceous sediments of South Jordan, the improvement of the correlation of these deposits with North/Central Jordan was a major aim of the study. The logged sections in Appendix I show that, by combining lithostratigraphic with sequence stratigraphic criteria, a correlation was achieved up to section 10, west of Batn El Ghul. East of section 10, which is similar to the type section for the Batn El Ghul Formation (Teimeh et al., 1990), the terrestrial dominated succession can only be described by using the undifferentiated Batn El Ghul Formation.

By applying these criteria (Tab. 7.1) it is possible to use the Cretaceous stratigraphy of North and Central Jordan in South Jordan, too. As a result the change from a carbonate platform in North and Central Jordan to a clastic dominated, terrestrial influenced shallow shelf in South Jordan is no longer a hindrance. Only east of Batn El Ghul, where the terrestrial deposits dominate, this correlation is not accomplished yet and the use of the term 'Batn El Ghul Formation' is still necessary.

Table 7.1 Summary of features used to determine the top of the Formations in the study area

Stratigraphic Formation	Criteria defining the top of the formation
Amman Formation	-
Wadi Umm Ghudran Formation	The base of the first marine bed within the thick terrestrial deposits of the Wadi Umm Ghudran Formation or the maximum regressive surface (MRS) of sequence 6
Wadi As Sir Formation	The lithologic change from limestones/dolomites to sandstone and/or the base of the first glaucony bearing sandstone bed above limestones/dolomites
Shuayb Formation	The maximum regressive surface (MRS) of sequence 3
Hummar Formation	The basal surface of forced regression (BSFR) of sequence 2.2
Fuhays Formation	The sequence boundary of sequences 1.2/2.1
Naur Formation	Lithologic change from limestone to claystone or the basal surface of forced regression (BSFR) of sequence 1.1
Kurnub Group	The base of the bed with the first marine body or trace fossils between the sandstones of the Kurnub Formation and the limestones/dolomites of the Naur Formation

It has to be kept in mind that by using sequence stratigraphic criteria/boundaries, the single formation boundaries get a diachronous character. Since this is also often the case with

established lithologic criteria, for example the change from the Kurnub Group sandstones to the carbonates of the Naur Formation along the Naqb escarpment, this should hold no difficulty.

7.4 Discussion of the mid to Late Cretaceous climatic conditions of the study area

Information on the climatic conditions during the mid to Late Cretaceous in the study area can be found in outcrops, petrographical and geochemical studies. Though isolated the single datasets are sometimes difficult to use, their combination is usually helpful.

In the outcrops the palaeosols were used for climatic interpretations (Chapter 3.6.3). Applying the classification after Mack and James (1994), the encountered palaeosols (oxisols, vertisols, calcisols and argillisols after Mack et al., 1993) formed most probably under wet equatorial to dry subtropical palaeoclimatic conditions. The frequent occurrence of plant material in form of wood and plant fragments and roots within terrestrial deposits of the study area, point to climatic conditions that allowed at least seasonal growing vegetation. Such vegetation can cope without problem with the above mentioned climatic conditions.

From a petrographic point of view, the dominance of quartz arenites in the study area can also be interpreted with regard to palaeoclimate. First-cycle quartz-arenites form in warm humid climates under slow sedimentation rates and within a low relief (Pettijohn et al., 1987). Such conditions are indicated for the studied samples in figure 5.12, the log-ratio plot after Weltje (1994). Considering the fact that all samples contain recycled material and therefore are multicycle quartz arenites, this evidence can not be used. The quartz rich character of the sandstones is basically inherited from the underlying Palaeozoic sediments. It might be possible though, that a warm humid Cretaceous climate furthered the quartz arenitic character of the sandstones.

Geochemically the use of the chemical index of alteration (CIA, Tab. 6.3) and the A-NC-K/A-NCK-FM plots (Fig. 6.3) are useful for palaeoclimatic interpretations. Unfortunately to conclude on the Cretaceous palaeoclimate of the studied region by means of CIA values and weathering trends is difficult. An average CIA value of about 70 for all studied sediments (Chapter 5) implies a low to moderate weathering rate (Nesbitt and Young, 1982), which would fit temperate humid climatic conditions. Since this mean CIA is influenced by factors like sediment recycling and neo-formation of carbonates in the sediment, it is critical to use. Maximum CIAs of 90 and above in single claystone samples, which are NOT recycled and uninfluenced by authigenic minerals, point to a very high weathering, expected under humid tropical conditions.

Linked to the principles of the CIA, the weathering trends in the A-NC-K/A-NCK-FM plots (Fig. 6.3) are similarly difficult to use for clear statements on the Cretaceous climate of the study area. On the whole most of the samples follow normal weathering trends, but only the clay-rich sediments can be used for a climatic interpretation. The trend of the claystones to the Al_2O_3 /kaolinite corner of the diagrams can be interpreted as an indicator for weathering under warm humid climate, since kaolinite forms under these conditions (Velde, 1995).

Based on the data presented in this study, an exact statement on the climatic conditions in south Jordan during the studied time interval (Cenomanian to Coniacian) can not be made. The field observations allow the statement that during the studied time period climatic conditions were warm and most probably humid. To a certain extend this is supported by the CIA results of the claystones. So the observed results fit the general statement of a warm and humid Cretaceous climate (Frakes et al., 1992).

Discussion of the influence of the Cretaceous climatic conditions on the depositional architecture of the study area

It can be assumed, that the changes in the Cretaceous climate also affected the study area. As shown above, it is difficult to find direct climatic indicators, especially in an overall warm period. Therefore the concept of 'warm' and 'cold' phases in Cretaceous climate (Chapter 2.6) was used, in the hope that the change in sediment composition within the Cretaceous formations of Jordan might offer a hint for the climatic development during the mid to Late Cretaceous. Applying this concept means that 'warm' phases are linked to times with raised precipitation and thus high continental runoff. 'Cold' phases are times with lower precipitation rates, but overall still warm temperatures. Applying this concept to the studied sedimentary succession results in the following model:

The clastic dominated Kurnub Group, comprising the complete Lower Cretaceous succession, was deposited in a 'warm' period with high continental runoff/sediment supply rates. The overlying carbonate dominated Naur Formation was sedimented under 'cold' conditions during the Cenomanian. The carbonate predominance of this formation is connected to lowered siliciclastic supply and therefore most probably to low precipitation rates. During the deposition of the F/H/S formations in the still 'cold' Late Cenomanian to mid-Turonian (Frakes and Francis, 1990), a raised precipitation lead to a higher clastic input, causing the predominance of clays with only few carbonate intercalations in these formations. The sedimentation of the Wadi As Sir Formation during the Late Turonian and Coniacian, carbonate dominated in North/Central Jordan and of mixed carbonate-siliciclastic character in the study area, occurred again under 'cold', arid conditions. The overlying Santonian Wadi Umm Ghudran Formation with its siliciclastics was sedimented in a 'warm' climate with raised precipitation and therefore raised continental runoff.

Though this model might seem reasonable on the first look, it is based on 'modelled' global climatic conditions alone and does not consider other important factors like plate tectonics, possibly local tectonics and sea-level changes.

During the Cretaceous period the Arabian Craton drifted northward from an equatorial position (Early Cretaceous) up to about 20 degrees N by Maastrichtian time (Powell et al., 1996). This latitudinal change rises the question of a 'forced' climate change, since the equatorial position was left, bringing the Cretaceous Jordan in changing climatic regions. Local tectonic effects, like the uplift of a hinterland region, might lead to increased siliciclastic sediment supply, consequently disturbing the sedimentation scheme produced by continental runoff alone. Though the study area revealed no direct evidence for such effects, the mechanism has to be kept in mind.

Even more important, the Cretaceous sea-level changes also have to be considered. A change in sea-level/base-level influences the erosional power of river systems dramatically (e.g. Miall, 1996). A low sea-level/base-level raises the erosion potential in an otherwise stable hinterland. A raised erosion potential leads to a higher sediment supply to the basin which disturbs the runoff-linked sedimentation pattern completely.

As the sequence stratigraphic results of the presented study show, the sedimentation pattern/stratigraphic architecture of the Cretaceous sediments of south Jordan is mainly controlled by eustasy and sediment supply. Therefore a direct connection of climate changes and sedimentation patterns, as discussed in the model above, is very unlikely. Nevertheless there is an indirect influence since climate changes affect the eustatic sea-level.

8. References

- Abd Elwahab, A.** 1999. Petrography, Fabric Analysis and Diagenetic History of Upper Cretaceous Sandstone, Kharga Oasis, Western Desert, Egypt. *Sedimentology of Egypt*, **7**: 99-117.
- Abed, A.M.** 1978. Depositional Environments of the Kurnub (Lower Cretaceous) Sandstones: I. A Coal Horizon at the Lowermost Kurnub, Northern Jordan. *Dirasat*, **5**: 31-44.
- Abed, A.M.** 1982a. Depositional environments of the Early Cretaceous Kurnub (Hathira) sandstones, north Jordan. *Sedimentary Geology*, **31**: 267-279.
- Abed, A.M.** 1982b. Microfacies and Paleoenvironment of the Wadi Sir Formation (Upper Cretaceous), North Jordan. *Facies*, **7**: 229-236.
- Abed, A.M.** 1984. Emergence of Wadi Mujib (Central Jordan) during Lower Cenomanian time and its regional tectonic implications. In: *The Geological Evolution of the Eastern Mediterranean* (Eds J.E. Dixon and A.H.F. Robertson), pp. 824. Blackwell Scientific Publications, Oxford.
- Abed, A.M. and Amireh, B.S.** 1999. Sedimentology, geochemistry, economic potential and palaeogeography of an Upper Cretaceous phosphorite belt in the southeastern desert of Jordan. *Cretaceous Research*, **20**: 119-133.
- Abed, A.M. and El-Hiyari, M.** 1986. Depositional environments and paleogeography of the Cretaceous gypsum horizon in west-central Jordan. *Sedimentary Geology*, **47**: 109-123.
- Abed, A.M. and Kraishan, G.M.** 1991. Evidence for Shallow-Marine Origin of a 'Monterey-Formation Type' Chert-Phosphorite-Dolomite Sequence: Amman Formation (Late Cretaceous), Central Jordan. *Facies*, **24**: 25-38.
- Abed, A.M. and Mansour, H.** 1982. Petrography and Chemistry of Some Lower Cretaceous Glauconites from Jordan. *Dirasat*, **9**: 67-80.
- Abed, A.M. and Sadaqah, R.** 1998. Role of Upper Cretaceous Oyster Bioherms in the Deposition and Accumulation of High-Grade Phosphorites in Central Jordan. *Journal of Sedimentary Research*, **68**: 1009-1020.
- Abed, A.M. and Schneider, W.** 1980. A General Aspect in the Genesis of Nodular Limestones Documented by the Upper Cretaceous Limestones of Jordan. *Sedimentary Geology*, **26**: 329-335.
- Abed, A.M. and Schneider, W.** 1982. The Cenomanian Nodular limestone Member of Jordan - from subtidal to supratidal environments. *N. Jb. Geol. Paläont. Mh.*, **1982**: 513-522.
- Abu Saad, L. and Al Bashish, M.** 1996. *Surface and Subsurface Lithostratigraphic Relationships of the Kurnub Sandstone Group in Jordan*. Subsurface Geology Bulletin, **No. 9**. The Hashemite Kingdom of Jordan, Ministry of Energy and Mineral Resources, Natural Resources Authority, Amman, 74 pp.
- Abu Saad, L. and Al Bashish, M.** 1999. *Surface and Subsurface Lithostratigraphic Relationships of the Cretaceous Amman Silicified Limestone Formation (Belqa Group) in Jordan*. Subsurface Geology Bulletin, **No. 10**. The Hashemite Kingdom of Jordan, Ministry of Energy and Mineral Resources, Natural Resources Authority, Amman, 58 pp.
- Adams, A.E., McKenzie, W.S. and Guilford, C.** 1986. *Atlas der Sedimentgesteine in Dünnschliffen*. Enke Verlag, Stuttgart, 103 pp.
- Aigner, T.** 1985. *Storm Depositional Systems: Dynamic Stratigraphy in Modern and Ancient Shallow-Marine Sequences*. Lecture Notes in Earth Sciences, **3**. Springer-Verlag, Berlin, 174 pp.
- Ainsworth, R.B., Bosscher, H. and Newall, M.J.** 2000. Forward stratigraphic modelling of forced regressions: evidence for the genesis of attached and detached lowstand

- systems. In: *Sedimentary Responses to Forced Regression* (Eds D. Hunt and R.L. Gawthorpe), *Geological Society Special Publication*, **172**, pp. 163-176. The Geological Society, London.
- Alsharhan, A.S. and Nairn, A.E.M.** 1997. *Sedimentary Basins and Petroleum Geology of the Middle East*. Elsevier, Amsterdam, 843+99 pp.
- Amireh, B.S.** 1987. *Sedimentological and Petrological Interplays of the Nubian Series in Jordan with Regard to Paleogeography and Diagenesis*. Dissertation, Universität Braunschweig, Braunschweig, 232 pp.
- Amireh, B.S.** 1991. Mineral composition of the Cambrian-Cretaceous Nubian Series of Jordan: provenance, tectonic setting and climatological implications. *Sedimentary Geology*, **71**: 99-119.
- Amireh, B.S.** 1992. Sedimentology and mineral composition of the Kurnub Sandstone in Wadi Qsieb, SW Jordan. *Sedimentary Geology*, **78**: 267-283.
- Amireh, B.S.** 1993a. New Occurrences of the Disi Sandstone Formation (Early Ordovician) in Central Jordan. *Dirasat*, **20 B**: 21-44.
- Amireh, B.S.** 1993b. Three Paleosols of the Nubian Series of Jordan: Climatologic, Tectonic and Paleogeographic Implications. *Dirasat*, **20 B**: 33-62.
- Amireh, B.S.** 1997. Sedimentology and palaeogeography of the regressive-transgressive Kurnub Group (Early Cretaceous) of Jordan. *Sedimentary Geology*, **112**: 69-88.
- Amireh, B.S.** 2000. The Early Cretaceous Kurnub Group of Jordan: Subdivision, characterization and depositional environment development. *Neues Jahrbuch für Geologie und Paläontologie, Monatshefte* 29-57.
- Amireh, B.S. and Abed, A.M.** 1999. Depositional environments of the Kurnub Group (Early Cretaceous) in northern Jordan. *Journal of African Earth Sciences*, **29**: 449-468.
- Amireh, B.S., Jarrar, G., Henjes-Kunst, F. and Schneider, W.** 1998. K-Ar dating, X-Ray diffractometry, optical and scanning electron microscopy of glauconies from the early Cretaceous Kurnub Group of Jordan. *Geological Journal*, **33**: 49-65.
- Andersson, P.S., Porcelli, D., Gustafsson, Ö., Ingri, J. and Wasserburg, G.J.** 2001. The importance of colloids for the behavior of uranium isotopes in the low-salinity zone of a stable estuary. *Geochimica et Cosmochimica Acta*, **65**: 13-25.
- Andrews, I.J.** 1992. *Cretaceous and Paleogene Lithostratigraphy in the Subsurface of Jordan*. Subsurface Geology Bulletin, **5**. The Hashemite Kingdom of Jordan, Ministry of Energy and Mineral Resources, Natural Resources Authority, Amman, 60 pp.
- Aqrabawi, M.** 1993. Oysters (Bivalvia-Pteriomorpha) of the Upper Cretaceous rocks of Jordan; Palaeontology, Stratigraphy and Comparison with the Upper Cretaceous oysters of Northwest Europe. *Mitteilungen aus dem Geologisch-Palaeontologischen Institut der Universität Hamburg*, **75**: 1-135.
- Baaske, U.P.** 1999. *Untersuchungen zur Diagenese des Buntsandsteins am Westrand des Rheingrabens (Region Bad Dürkheim / Neustadt a. d. Weinstraße)*. Diplomarbeit, Johannes Gutenberg Universität Mainz, Mainz, 90 pp.
- Baaske, U.P. and Krawinkel, H.E.** 2001a. Controls on Depositional Facies and Sequence Architecture of Cretaceous Sediments of Southern Jordan. In: *J. Conf. Abs.*, **6**, pp. 745. European Union of Geosciences, Strasbourg.
- Baaske, U.P. and Krawinkel, H.E.** 2001b. Provenance and Geochemistry of Upper Cretaceous Sediments from Southern Jordan. In: *IAS 2001, 21st Meeting, International Association of Sedimentologists: Abstracts & Programme* (Eds U. Wortmann and H. Funk), pp. 120-121. International Association of Sedimentologists, Davos, Switzerland.
- Baaske, U.P., Krawinkel, H.E., Fürsich, F.T., Berndt, R., Schmidt-Kittler, N. and Moumani, K.** 2001a. Depositional sequences of Upper Cretaceous sediments

- (Cenomanian to Santonian, southern Jordan). In: *7th Jordanian Geological Conference: Book of Abstracts*, pp. 89, Amman.
- Baaske, U.P., Wöhrle, A., Krawinkel, H.E., Al-Bashish, M. and Moumani, K.** 2001b. Sequence Stratigraphy and Outcrop Based Stratigraphic Modelling of Mid-Cretaceous Deposits of Southern Jordan. In: *2001 Margins Meeting: Program and Abstracts* (Eds S. Roth and A. Rüggeberg), *Schriftenreihe der Deutschen Geologischen Gesellschaft*, **14**, pp. 15-16. Deutsche Geologische Gesellschaft, Hannover.
- Bandel, K. and Geys, J.** 1984. Regular echinoids in the Upper Cretaceous of the Hashemite Kingdom of Jordan. *Ann. Soc. Geol. Nord*, **104**: 97-115.
- Bandel, K. and Vávra, N.** 1981. Ein fossiles Harz aus der Unterkreide Jordaniens. *N. Jb. Geol. Paläont. Mh.*, **1981**: 19-33.
- Basu, A.** 1985a. Influence of Climate and Relief on Compositions of Sands at Source Areas. In: *Provenance of Arenites* (Ed G.G. Zuffa), *NATO ASI Series C*, **148**, pp. 1-18. D. Reidel Publishing Company, Dordrecht.
- Basu, A.** 1985b. Reading Provenance From Detrital Quartz. In: *Provenance of Arenites* (Ed G.G. Zuffa), *NATO ASI Series, C* **148**, pp. 231-247. D. Reidel Publishing Company, Dordrecht.
- Bender, F.** 1963. Stratigraphie der "Nubischen Sandsteine" in Süd-Jordanien. *Geol. Jb.*, **81**: 237-276.
- Bender, F.** 1968. *Geologie von Jordanien*. Beiträge zur Regionalen Geologie der Erde, **7**. Borntraeger, Berlin, 230 pp.
- Bender, F.** 1974. *Geology of Jordan*. Beiträge zur Regionalen Geologie der Erde, **7**. Gebrüder Bornträger, Berlin, 196 pp.
- Bender, F. and Mädler, K.** 1969. Die sandige Schichtenfolge der Kreide mit einer Angiospermen-Flora in Süd-jordanien. *Beih. geol. Jb.*, **81**: 35-92.
- Bender, F., van den Boom, G., Busse, R., Heimbach, W., Khdeir, K., Lahloub, M., Lillich, W. and Wiesemann, G.** 1968. Geologische Karte von Jordanien: Blatt Aqaba - Ma'an 1:250000. Bundesanstalt für Bodenforschung, Hannover.
- Berndt, R.** 2002. *Palaeoecology and taxonomy of the macrobenthic fauna from the Upper Cretaceous Ajlun Group, southern Jordan*. Dissertation, Würzburg.
- Beydoun, Z.R.** 1988. *The Middle East: Regional geology and petroleum resources*. Scientific Press Ltd., Beaconsfield, 292 pp.
- Beydoun, Z.R.** 1995. Productive Middle East clastic oil and gas reservoirs: their depositional settings and origins of their hydrocarbons. In: *Sedimentary Facies Analysis* (Ed A.G. Plint), *Spec. Publs int. Ass. Sediment.*, **22**, pp. 331-354. Blackwell Science, Oxford.
- Bhatia, M.R.** 1983. Plate tectonics and geochemical composition of Sandstones. *Journal of Geology*, **91**: 611-627.
- Bhatia, M.R. and Crook, A.W.** 1986. Trace element characteristics of graywackes and tectonic setting discrimination of sedimentary basins. *Contrib. Mineral. Petrol.*, **92**: 181-193.
- Bhattacharya, J.P. and Walker, R.G.** 1992. Deltas. In: *Facies Models: response to Sea Level Change* (Eds R.G. Walker and N.P. James), pp. 157-177. Geological Association of Canada, St. John's.
- Bjørlykke, K.** 1989. *Sedimentology and Petroleum Geology*. Springer-Verlag, Berlin, 363 pp.
- Boenigk, W.** 1983. *Schwermineralanalyse*. Ferdinand Enke Publishers, Stuttgart, 158 pp.
- Boggs, S.** 1995. *Principles of Sedimentology and Stratigraphy*. Prentice Hall, Upper Saddle River, 774 pp.
- Bouma, A.H., Berryhill, H.L., Brenner, R.L. and Knebel, H.J.** 1982. Continental Shelf and Epicontinental Seaways. In: *Sandstone Depositional Environments* (Eds P.A. Scholle and D. Spearing), *AAPG Memoir*, **31**, pp. 281-327. The American Association of Petroleum Geologists, Tulsa/Oklahoma.

- Bowen, R. and Jux, U.** 1987. *Afro-Arabian geology - A kinematic view*. Chapman and Hall Ltd, London, 295 pp.
- Bown, T.M. and Kraus, M.J.** 1981. Lower Eocene Alluvial Paleosols (Willwood Formation, Northwest Wyoming, U.S.A.) and Their Significance for Paleocology, Paleoclimatology, and Basin Analysis. *Palaeogeography, Palaeoclimatology, Palaeoecology*, **34**: 1-30.
- Bromley, R.G.** 1996. *Trace Fossils: Biology, taphonomy and applications*. Chapman & Hall, London, 361 pp.
- Bromley, R.G. and Ekdale, A.A.** 1984. Trace fossil preservation in flint in the European chalk. *J. Paleont.*, **58**: 298-311.
- Buchbinder, B., Benjamini, C. and Lipson-Benitah, S.** 2000a. Sequence development of Late Cenomanian-Turonian carbonate ramps, platforms and basins in Israel. *Cretaceous Research*, **21**: 813-843.
- Buchbinder, B., Benjamini, C. and Lipson-Benitah, S.** 2000b. Sequence expression in the Late Cenomanian-Turonian differs in northern, central and southern Israel. In: *Israel Geological Society Annual Meeting 2000* (Eds G. Baer and Y. Avni), pp. 24. Israel Geological Society, Ma'alot.
- Bussert, R.** 1998. *Die Entwicklung interkratonaler Becken im Nordsudan*. Berliner geowiss. Abh., (A) **196**. Selbstverlag Fachbereich Geowissenschaften, FU Berlin, Berlin, 329 pp.
- Buurman, P.** 1980. Palaeosols in the Reading Beds (Paleocene) of Alun Bay, Isle of Wight, U.K. *Sedimentology*, **27**: 593-606.
- Castelltort, S. and Van Den Driessche, J.** 2003. How plausible are high-frequency sediment supply-driven cycles in the stratigraphic record? *Sedimentary Geology*, **157**: 3-13.
- Catuneanu, O.** 2002. Sequence stratigraphy of clastic systems: concepts, merits, and pitfalls. *Journal of African Earth Sciences*, **35**: 1-43.
- Chaimov, T.A., Barazangi, M., Al-Saad, D., Sawaf, T. and Gebran, A.** 1992. Mesozoic and Cenozoic deformation inferred from seismic stratigraphy in the southwestern intracontinental Palmyride fold-thrust belt, Syria. *Geological Society of America Bulletin*, **104**: 704-715.
- Church, T.M., Sarin, M.M., Fleischer, M.Q. and Ferdelman, T.G.** 1996. Salt marshes: An important coastal sink for dissolved uranium. *Geochimica et Cosmochimica Acta*, **60**: 3879-3887.
- Clifton, H.E.** 1981. Progradational sequences in miocene shoreline deposits, southeastern Caliente Ridge, California. *Journal of Sedimentary Petrology*, **51**: 165-184.
- Collinson, J.D.** 1996. Alluvial sediments. In: *Sedimentary Environments: Processes, Facies and Stratigraphy* (Ed H.G. Reading) 3rd edn, pp. 37-82. Blackwell Science, Oxford.
- Collinson, J.D. and Thompson, D.B.** 1989. *Sedimentary Structures*. Chapman & Hall, London, 207 pp.
- Crowley, T.J. and North, G.R.** 1991. *Paleoclimatology*. Oxford Monographs on Geology and Geophysics, **18**. Oxford University Press, New York, 339 pp.
- Dalrymple, R.W.** 1992. Tidal Depositional Systems. In: *Facies Models: Response to Sea Level Change* (Eds R.G. Walker and N.P. James), pp. 195-218. Geological Association of Canada, St. John's.
- Dalrymple, R.W., Zaitlin, B.A. and Boyd, R.** 1992. Estuarine Facies Models: Conceptual Basis and Stratigraphic Implications. *Journal of Sedimentary Petrology*, **62**: 1130-1146.
- Davis, R.A., Jr.** (Ed), 1985a. *Coastal Sedimentary Environments*, Second edn. Springer-Verlag, New York, 716 pp.
- Davis, R.A., Jr.** 1985b. Beach and Nearshore Zone. In: *Coastal Sedimentary Environments* (Ed R.A. Davis, Jr.) Second edn, pp. 379-444. Springer-Verlag, New York.

- de Graciansky, P.-C., Hardenbol, J., Jacquin, T. and Vail, P.R.** (Eds) 1998. *Mesozoic and Cenozoic Sequence Stratigraphy of European Basins*, *SEPM Spec. Pub.*, **60**. SEPM, Tulsa/Oklahoma, 786 pp.
- Deer, W.A., Howie, R.A. and Zussman, J.** 1997. *An Introduction to the Rock-Forming Minerals*. Longman, Harlow, 696 pp.
- Dercourt, J., Gaetani, M., Vrielynck, B., Barrier, E., Biju-Duval, B., Brunet, M.F., Cadet, J.P., Crasquin, S. and Sandulescu, M.** (Eds) 2000. *Atlas Peri-Tethys, Palaeogeographical Maps*. CCGM/CGMW, Paris, 24 maps and explanatory notes: 1-XX; 1-269 pp.
- Dickinson, W.R.** 1985. Interpreting Provenance Relations From Detrital Modes Of Sandstones. In: *Provenance of Arenites* (Ed G.G. Zuffa), *NATO ASI Series*, **C 148**, pp. 333-361. D. Reidel Publishing Company, Dordrecht.
- Dickinson, W.R., Beard, L.S., Brakenridge, G.R., Erjavec, J.L., Ferguson, R.C., Inman, K.F., Knepp, R.A., Lindberg, F.A. and Ryberg, P.T.** 1983. Provenance of North American Phanerozoic sandstones in relation to tectonic setting. *Geological Society of America Bulletin*, **94**: 222-235.
- Diener, R.** 2002. *Die siliziklastischen Sedimente der synorogenen Hochwipfel-Formation im Karbon der Westkarawanken (Österreich/Slowenien/Italien) - Sedimentologie, Geochemie und Provenienz*. Dissertation, Universität Stuttgart, Stuttgart, 366 pp.
- Dinelli, E., Lucchini, F., Mordenti, A. and Paganelli, L.** 1999. Geochemistry of Oligocene-Miocene sandstones of the northern Apennines (Italy) and evolution of chemical features in relation to provenance changes. *Sedimentary Geology*, **127**: 193-207.
- Dunham, R.J.** 1962. Classification of carbonate rocks according to depositional texture. In: *Classification of carbonate rocks* (Ed W.E. Ham), *AAPG Memoir*, **1**, pp. 108-121. The American Association of Petroleum Geologists, Tulsa/Oklahoma.
- Einsele, G.** 2000. *Sedimentary Basins: Evolution, Facies, and Sediment Budget*. Springer, Berlin, 792 pp.
- Emery, D. and Myers, K.** (Eds) 1996. *Sequence Stratigraphy*. Blackwell Science, Oxford, 297 pp.
- Faure, G.** 1986. *Principles of Isotope Geology*. John Wiley & Sons, New York, 590 pp.
- Fischer, K.** 1989. *Prozesse und Produkte lateritischer Verwitterung in oberkretazischen Sedimenten Oberägyptens und des Sudan*. Berliner geowiss. Abh., (A) **115**. Selbstverlag Fachbereich Geowissenschaften, FU Berlin, Berlin, 123 pp.
- Fleet, A.J.** 1984. Aqueous and Sedimentary Geochemistry of the Rare Earth Elements. In: *Rare Earth Element Geochemistry* (Ed P. Henderson), *Developments in Geochemistry*, **2**, pp. 343-373. Elsevier, Amsterdam.
- Flexer, A. and Reymont, R.** 1989. The Cretaceous transgressive peaks and their relation to geodynamic events. The Arabo-Nubian and the Northern African shields. *Journal of African Earth Sciences*, **8**: 172-192.
- Floyd, P.A. and Leveridge, B.E.** 1987. Tectonic environment of the Devonian Gramscatho basin, south Cornwall: framework mode and geochemical evidence from turbiditic sandstones. *J. Geol. Soc. London*, **144**: 531-542.
- Floyd, P.A., Shail, R., Leveridge, B.E. and Franke, W.** 1991. Geochemistry and provenance of Rhenohercynian synorogenic sandstones: implications for tectonic environment discrimination. In: *Developments in Sedimentary Provenance Studies* (Eds A.C. Morton, S.P. Todd and P.D.W. Haughton), *Geological Society Special Publication*, **57**, pp. 173-188. The Geological Society, London.
- Folk, R.L.** 1959. Practical petrographic classification of limestones. *American Association of Petroleum Geologists Bulletin*, **43**: 1-38.

- Folk, R.L.** 1962. Spectral subdivision of limestone types. In: *Classification of carbonate rocks* (Ed W.E. Ham), *AAPG Memoir*, **1**, pp. 62-84. The American Association of Petroleum Geologists, Tulsa/Oklahoma.
- Föllmi, K.B.** 1996. The phosphorus cycle, phosphogenesis and marine phosphate-rich deposits. *Earth-Science Reviews*, **40**: 55-124.
- Frakes, L.A. and Francis, J.E.** 1990. Cretaceous Palaeoclimates. In: *Cretaceous Resources, Events and Rhythms - Background and Plans for Research* (Eds R.N. Ginsburg and B. Beaudoin), *NATO ASI Series C: Mathematical and Physical Sciences*, **304**, pp. 273-287. Kluwer Academic Publishers, Dordrecht.
- Frakes, L.A., Francis, J.E. and Syktus, J.I.** 1992. *Climate Modes of the Phanerozoic*. Cambridge University Press, Cambridge, 274 pp.
- Fralick, P.W. and Kronberg, B.I.** 1997. Geochemical discrimination of clastic sedimentary rock sources. *Sedimentary Geology*, **113**: 111-124.
- Francis, J.E. and Frakes, L.A.** 1993. Cretaceous climates. In: *Sedimentology Review* (Ed P. Wright), **1**, pp. 17-30. Blackwell Scientific Publications, London.
- Frey, R.W. and Basan, P.B.** 1985. Coastal Salt Marshes. In: *Coastal Sedimentary Environments* (Ed R.A. Davis, Jr.) Second edn, pp. 225-301. Springer-Verlag, New York.
- Füchtbauer, H.** 1967. Der Einfluss des Ablagerungsmilieus auf die Sandsteindiagenese im Mittleren Buntsandstein. *Sedimentary Geology*, **1**: 159-179.
- Füchtbauer, H.** 1988. Sandsteine. In: *Sediment-Petrologie Teil II: Sedimente und Sedimentgesteine* (Ed H. Füchtbauer) 4th edn, pp. 97-184. E. Schweizerbart'sche Verlagsbuchhandlung, Stuttgart.
- Füchtbauer, H. and Valetton, I.** 1988. Kieselgesteine. In: *Sediment-Petrologie Teil II: Sedimente und Sedimentgesteine* (Ed H. Füchtbauer) 4th edn, pp. 501-542. E. Schweizerbart'sche Verlagsbuchhandlung, Stuttgart.
- Gale, A.S.** 2000. The Cretaceous World. In: *Biotic Response to Global Change - The Last 145 Million Years* (Eds S.J. Culver and P.F. Rawson), pp. 4-19. Cambridge University Press, Cambridge.
- Galloway, W.E. and Hobday, D.K.** 1996. *Terrigenous Clastic Depositional Systems: Applications to Fossil Fuel and Groundwater Resources*. Springer, Berlin, 489 pp.
- Garcia, D., Fonteilles, M. and Moutte, J.** 1994. Sedimentary Fractionations between Al, Ti, and Zr and the Genesis of Strongly Peraluminous Granites. *Journal of Geology*, **102**: 411-422.
- Gaupp, R., Matter, A., Platt, J., Ramseyer, K. and Walzebeck, J.** 1993. Diagenesis and Fluid Evolution of Deeply Buried Permian (Rotliegendes) Gas Reservoirs, Northwest Germany. *Amer. Assoc. Pet. Geol. Bull.*, **77**: 1111-1128.
- Germann, K., Fischer, K. and Schwarz, T.** 1990. Accumulation of lateritic weathering products (kaolins, bauxitic laterites, ironstones) in sedimentary basins of northern Sudan. *Berliner geowiss. Abh. (A)*, **120.1**: 109-148.
- Gradstein, F.M., Agterberg, F.P., Ogg, J.G., Hardenbol, J., van Veen, P., Thierry, J. and Zehui, Z.** 1995. A Triassic, Jurassic and Cretaceous time scale. In: *Geochronology, Time Scales and Global Stratigraphic Correlation* (Eds W.A. Berggren, D.V. Kent, M.-P. Aubry and J. Hardenbol), **54**, pp. 95-126. SEPM Special Publication, Tulsa/Oklahoma.
- Grumbt, E.** 1969. Beziehungen zwischen Korngröße, Schichtung, Materialbestand und anderen sedimentologischen Merkmalen in feinklastischen Sedimenten. *Geologie*, **18**: 151-167.
- Gruszczynski, M. and Rudorobek, J.** 1993. Rip currents as a geological tool. *Sedimentology*, **40**: 217-236.

- Gu, X.X., Liu, J.M., Zheng, M.H., Tang, J.X. and Qi, L.** 2002. Provenance and Tectonic Setting of the Proterozoic Turbidites in Hunan, South China: Geochemical Evidence. *Journal of Sedimentary Research*, **72**: 393-407.
- Gunnars, A., Blomqvist, S., Johansson, P. and Andersson, C.** 2002. Formation of Fe(III) oxyhydroxide colloids in freshwater and brackish seawater, with incorporation of phosphate and calcium. *Geochimica et Cosmochimica Acta*, **66**: 745-758.
- Haq, B.U., Hardenbol, J. and Vail, P.R.** 1987. Chronology of Fluctuating Sea Levels Since the Triassic. *Science*, **235**: 1156-1167.
- Haq, B.U., Hardenbol, J. and Vail, P.R.** 1988. Mesozoic and Cenozoic Chronostratigraphy and Cycles of Sea-Level Change. In: *Sea-Level Changes - An Integrated Approach* (Eds C.K. Wilgus et al.), *SEPM Special Publication*, **42**, pp. 71-108. Society of Economic Paleontologists and Mineralogists (SEPM), Tulsa/Oklahoma.
- Hardenbol, J., Thierry, J., Farley, M.B., Jacquin, T., de Graciansky, P.-C. and Vail, P.R.** 1998. Mesozoic and Cenozoic sequence chronostratigraphic framework of European basins. In: *Mesozoic and Cenozoic Sequence Stratigraphy of European basins* (Eds P.-C. de Graciansky, J. Hardenbol, T. Jacquin and P.R. Vail), *SEPM Spec. Pub.*, **60**, pp. 3-13. SEPM, Tulsa/Oklahoma.
- Harris, P.M., Frost, S.H., Seiglie, G.A. and Schneidermann, N.** 1984. Regional Unconformities and Depositional Cycles, Cretaceous of the Arabian Peninsula. In: *Interregional unconformities and hydrocarbon accumulation* (Ed J.S. Schlee), *AAPG Mem.*, **36**, pp. 67-80. AAPG, Tulsa/Oklahoma.
- Haughton, P.D.W., Todd, S.P. and Morton, A.C.** 1991. Sedimentary provenance studies. In: *Developments in Sedimentary Provenance Studies* (Eds A.C. Morton, S.P. Todd and P.D.W. Haughton), *Geological Society Special Publications*, **57**, pp. 1-12. Geological Society, Bath.
- Herron, M.M.** 1988. Geochemical Classification of Terrigenous Sands and Shales from Core or Log Data. *Journal of Sedimentary Petrology*, **58**: 820-829.
- Holail, H., Lohman, K.C. and Sanderson, I.** 1988. Dolomitization and Dedolomitization of Upper Cretaceous Carbonates Bahariya Oasis, Egypt. In: *Sedimentology and Geochemistry of Dolostones* (Eds V. Shukla and P.A. Baker), *SEPM Special Publication*, **43**, pp. 191-207. The Society of Economic Paleontologists and Mineralogists, Tulsa, Oklahoma.
- Holmes, A.** 1965. *Principles of Physical Geology*. Thomas Nelson, London, 1288 pp.
- Houseknecht, D.W.** 1987. Assessing the Relative Importance of Compaction Processes and Cementation to Reduction of Porosity in Sandstones. *Amer. Assoc. Pet. Geol. Bull.*, **71**: 633-642.
- Hubert, J.F.** 1962. A Zircon-Tourmaline-Rutile Maturity Index and the Interdependence of the Composition of Heavy Mineral Assemblages with the Gross Composition and Textures of Sandstones. *Journal of Sedimentary Petrology*, **32**: 440-450.
- Hunt, D. and Gawthorpe, R.L.** (Eds) 2000. *Sedimentary Responses to Forced Regressions*. (Eds A.J. Hartley, R.E. Holdsworth, A.C. Morton and M.S. Stoker), *Geological Society Special Publication*, **172**. The Geological Society, London, 383 pp.
- Hunt, D. and Tucker, M.E.** 1992. Stranded parasequences and the forced regressive wedge systems tract: deposition during base-level fall. *Sedimentary Geology*, **81**: 1-9.
- Ibrahim, A.M.** 2000. Elgunna Cambrian - Lower Cretaceous Sandstones, Southern Sinai, Egypt: Composition and Paleoclimatic Inferences. *Sedimentology of Egypt*, **8**: 119-132.
- Ibrahim, K.M.** 1987. Wadi Rahma 3049 IV. The Hashemite Kingdom of Jordan, Natural Resources Authority, Geology Directorate, Amman.

- Johnson, H.D. and Baldwin, C.T.** 1996. Shallow clastic seas. In: *Sedimentary Environments: Processes, facies and Stratigraphy* (Ed H.G. Reading) 3rd edn, pp. 232-280. Blackwell Science, Oxford.
- Johnsson, M.J.** 1993. The system controlling the composition of clastic sediments. In: *Processes Controlling the Composition of Clastic Sediments* (Eds M.J. Johnsson and A. Basu), *Special Paper*, **284**, pp. 1-19. Geological Society of America, Boulder, Colorado.
- Kendall, A.C.** 1992. Evaporites. In: *Facies Models: Response to Sea Level Change* (Eds R.G. Walker and N.P. James), pp. 375-409. Geological Association of Canada, St. John's.
- Kendall, A.C. and Harwood, G.M.** 1996. Marine evaporites: arid shorelines and basins. In: *Sedimentary Environments: Processes, Facies and Stratigraphy* (Ed H.G. Reading) 3rd edn, pp. 281-324. Blackwell Science, Oxford.
- Houry, H.N.** 1986. Depositional environment and diagenesis of the lower part of the Kurnub Sandstone Formation (Lower Cretaceous), Mahis area, Jordan. *Sedimentary Geology*, **49**: 129-141.
- Kohler, E.E. and Köster, H.M.** 1982. Remarks on the Influence of Depositional Environment on Radiometric Age Measurements. *Geol. Jb.*, **D 52**: 101-111.
- Kraus, M.J.** 1999. Paleosols in clastic sedimentary rocks: their geologic applications. *Earth-Science Reviews*, **47**: 41-70.
- Kraus, M.J. and Gwinn, B.** 1997. Facies and facies architecture of Paleogene floodplain deposits, Willwood Formation, Bighorn Basin, Wyoming, USA. *Sedimentary Geology*, **114**: 33-54.
- Kreuzer, H., Kuster, H., Daniels, C.H.v., Hinsch, W., Spiegler, D. and Harre, W.** 1980. K-Ar Dates for Late Oligocene Glauconites from NE Lower Saxony (NW Germany). *Geol. Jb.*, **A 54**: 61-74.
- Kuss, J.** 1992. The Aptian-Paleocene Shelf Carbonates of Northeast Egypt and Southern Jordan: Establishment and Break-up of Carbonate Platforms along the Southern Tethyan Shores. *Z. dt. geol. Ges.*, **143**: 107-132.
- Kuss, J. and Conrad, M.A.** 1991. Calcareous algae from Cretaceous carbonates of Egypt, Sinai and Jordan. *Journal of Paleontology*, **65**: 869-882.
- Kuss, J., Scheibner, C. and Gietl, R.** 2000. Carbonate Platform to Basin Transition along an Upper Cretaceous to Lower Tertiary Syrian Arc Uplift, Galala Plateaus, Eastern Desert of Egypt. *GeoArabia*, **5**: 405-424.
- Kutterolf, S.** 2001. *Die klastischen Sedimente der karbonen Hochwipfel- und Auernig-Formation der Ostkarawanken (Österreich/Slowenien):. Sedimentologie, Geochemie und Provenanz.* Dissertation, Universität Stuttgart, Stuttgart, 182 pp.
- Le Nindre, Y.-M., Vaslet, D., Le Métour, J., Bertrand, J. and Halawani, M.** 2003. Subsidence modelling of the Arabian Platform from Permian to Paleogene outcrops. *Sedimentary Geology*, **156**: 263-285.
- Lewy, Z.** 1990. Transgressions, Regressions and Relative Sea Level Changes on the Cretaceous Shelf of Israel and Adjacent Countries. A Critical Evaluation of Cretaceous Global Sea Level Correlations. *Paleoceanography*, **5**: 619-637.
- Lewy, Z., Kuss, J., Schulze, F. and Gharaibeh, A.** 2000. Cretaceous palaeogeography, palaeoecology and sedimentary settings of the southeastern margins of the Tethys, Western Jordan (Central Jordan working group: Initial report), pp. 10.
- Lihou, J.C. and Mange-Rajetzky, M.A.** 1996. Provenance of the Sardona Flysch, eastern Swiss Alps: example of high-resolution heavy mineral analysis applied to an ultrastable assemblage. *Sedimentary Geology*, **105**: 141-157.
- Lovelock, P.E.R.** 1984. A review of the tectonics of the northern Middle East region. *Geol. Mag.*, **121**: 577-587.

- Lüning, S., Kuss, J., Bachmann, M., Marzouk, A.M. and Morsi, A.M.** 1998a. Sedimentary Response to Basin Inversion: Mid Cretaceous - Early Tertiary Pre- to Syndeformational Deposition at the Areif El Naqa Anticline (Sinai, Egypt). *Facies*, **38**: 103-136.
- Lüning, S., Marzouk, A.M., Morsi, A.M. and Kuss, J.** 1998b. Sequence stratigraphy of the Upper Cretaceous of central-east Sinai, Egypt. *Cretaceous Research*, **19**: 153-196.
- Mack, G.H. and James, W.C.** 1994. Paleoclimate and the Global Distribution of Paleosols. *Journal of Geology*, **102**: 360-366.
- Mack, G.H., James, W.C. and Monger, H.C.** 1993. Classification of paleosols. *Geol. Soc. Am. Bull.*, **105**: 129-136.
- MacKenzie, F.T.** 1990. Sea Level Change, Sediment Mass and Flux and Chemostratigraphy. In: *Cretaceous Resources, Events and Rhythms - Background and Plans for Research* (Eds R.N. Ginsburg and B. Beaudoin), *NATO ASI Series C: Mathematical and Physical Sciences*, **304**, pp. 197-202. Kluwer Academic Publishers, Dordrecht.
- Makhlouf, I., Abu-Azzam, H. and Al-Hiayri, A.** 1996. *Surface and Subsurface Lithostratigraphic Relationships of the Cretaceous Ajlun Group in Jordan*. Subsurface Geology Bulletin, **No. 8**. The Hashemite Kingdom of Jordan, Ministry of Energy and Mineral Resources, Natural Resources Authority, Amman, 95 pp.
- Makhlouf, I.M.** 1998. Storm-Generated Channels in the Middle Dubaydib Sandstone Formation, South Jordan. *Journal of King Saud University*, **10**: 61-77.
- Mange, M.A. and Maurer, H.F.W.** 1991. *Schwerminerale in Farbe*. Ferdinand Enke Verlag, Stuttgart, 148 pp.
- Masri, A.** 1991. Ath Thulaythuwat 3249 II. The Hashemite Kingdom of Jordan, Natural Resources Authority, Geology Directorate, Amman.
- Masri, A.** 1992. *The Geology of the Ath-Thulaythuwat Area - Map Sheet No. 3249 III*. Bulletin, **No. 23**. The Hashemite Kingdom of Jordan, Ministry of Energy and Mineral Resources, Natural Resources Authority, Amman, 31 pp.
- Masri, A.** 1998. Geological Map of Batn Al Ghul (Jabal Al Harad) 3149 II. The Hashemite Kingdom of Jordan, Natural Resources Authority, Geology Directorate, Amman.
- Masri, M.** 1963. *Geological report Amman-Zerqa area*. Report of the Central Water Authority. Unpublished, Amman, Jordan, 74 pp.
- Matthes, S.** 1990. *Mineralogie*. Springer-Verlag, Berlin, 448 pp.
- McBride, E.F.** 1963. A Classification of Common Sandstones. *Journal of Sedimentary Petrology*, **33**: 664-669.
- McCann, T.** 1991. Petrological and geochemical determination of provenance in the southern Welsh Basin. In: *Developments in Sedimentary Provenance Studies* (Eds A.C. Morton, S.P. Todd and P.D.W. Haughton), *Geological Society Special Publication*, **57**, pp. 215-230. Geological Society, London.
- McCubbin, D.G.** 1982. Barrier-Island and Strand-Plain Facies. In: *Sandstone Depositional Environments* (Eds P.A. Scholle and D. Spearing), *AAPG Memoir*, **31**, pp. 247-279. The American Association of Petroleum Geologists, Tulsa/Oklahoma.
- McLennan, S.M.** 1989. Rare Earth Elements in Sedimentary Rocks: Influence of Provenance and Sedimentary Processes. In: *Geochemistry and Mineralogy of Rare Earth Elements* (Eds B.R. Lipin and G.A. McKay), *Reviews in Mineralogy*, **21**, pp. 169-200. Mineralogical Society of America, Chelsea.
- McLennan, S.M., Hemming, S., McDaniel, D.K. and Hanson, G.N.** 1993. Geochemical approaches to sedimentation, provenance and tectonics. In: *Processes Controlling the Composition of Clastic Sediments* (Eds M.J. Johnsson and A. Basu), *Special Paper*, **284**, pp. 21-40. Geological Society of America, Boulder/ Colorado.

- McPherson, J.G., Shanmugam, G. and Moiola, R.J.** 1988. Fan deltas and braid plains: conceptual problems. In: *Fan Deltas: Sedimentology and Tectonic Settings* (Eds W. Nemeo and R.J. Steel), pp. 14-22. Blackie, Glasgow.
- Miall, A.D.** 1977. A review of the braided river depositional environment. *Earth-Science Reviews*, **13**: 1-62.
- Miall, A.D.** 1985. Architectural-Element Analysis: A New Method of Facies Analysis Applied to Fluvial Deposits. *Earth-Science Reviews*, **22**: 261-308.
- Miall, A.D.** 1996. *The Geology of Fluvial Deposits: Sedimentary Facies, Basin Analysis, and Petroleum Geology*. Springer-Verlag, Berlin, 582 pp.
- Miall, A.D.** 1997. *The Geology of Stratigraphic Sequences*. Springer-Verlag, Berlin, 433 pp.
- Miall, A.D.** 1999. *Principles of Sedimentary Basin Analysis*. Springer, Berlin, 616 pp.
- Miall, A.D.** 2000. Suggestions for researching and publishing regional stratigraphic research. *Sedimentary Geology*, **132**: 1-3.
- Miall, A.D. and Miall, C.E.** 2001. Sequence stratigraphy as a scientific enterprise: the evolution and persistence of conflicting paradigms. *Earth-Science Reviews*, **54**: 321-348.
- Mohs, M.A.** 2001. *The Upper Cretaceous Wadi Umm Ghudran Formation of Southern Jordan: Sedimentology and Clay Mineralogy*. Diplomarbeit, Universität Stuttgart, Stuttgart, 50 pp.
- Molinaroli, E., Blom, M. and Basu, A.** 1991. Methods of Provenance Determination Tested with Discriminant Function Analysis. *Journal of Sedimentary Petrology*, **61**: 900-908.
- Moore, E.M., Robinson, P.T., Malpas, J. and Xenophonotos, C.** 1984. Model for the origin of the Troodos massif, Cyprus, and other mid-east ophiolites. *Geology*, **12**: 500-503.
- Morad, S.** 1998. Carbonate cementation in sandstones: distribution patterns and geochemical evolution. In: *Carbonate Cementation in Sandstones* (Ed S. Morad), *IAS Special Publication*, No. **26**, pp. 1-26. Blackwell Science, Oxford.
- Moraes, M.A.S. and De Ros, L.F.** 1992. Depositional, infiltrated and authigenic clays in fluvial sandstones of the Jurassic Sergi Formation, Recôncavo Basin, Northeastern Brazil. In: *Origin, Diagenesis, and Petrophysics of Clay Minerals in Sandstones* (Eds D.W. Houseknecht and E.D. Pittman), *SEPM Spec. Publ.*, **47**, pp. 197-208, Tulsa /Oklahoma.
- Morrow, D.W.** 1990. Dolomite Part 2: Dolomitization Models and Ancient Dolostones. In: *Diagenesis* (Eds I.A. McIlreath and D.W. Morrow), *Geoscience Canada reprint series*, **4**, pp. 125-139. Geological Association of Canada, Ottawa, Ontario.
- Morton, A.C.** 1985. Heavy Minerals in Provenance Studies. In: *Provenance of Arenites* (Ed G.G. Zuffa), pp. 249-277. D. Reidel Publishing Company, Dordrecht.
- Morton, A.C. and Hallsworth, C.R.** 1999. Processes controlling the composition of heavy mineral assemblages in sandstones. *Sedimentary Geology*, **124**: 3-30.
- Moumani, K., Masri, A. and Tarawneh, K.** 2001. First Record Of An Enormous Drifted Fossil Tree Trunk From The Upper Cretaceous Of Batn Al Ghul Area, SE/Jordan. In: *Geology of Jordan and Adjacent Areas - Proceedings of the Sixth Jordanian Geological Conference 5-8 October, 1998, Amman* (Eds K. Moumani, M. Al-Saiden and M. Abu Qudaira), *Special Publication*, **6**, pp. 41-46. The Jordanian Geologists Association, Amman.
- Mücke, A.** 2000. Environmental conditions in the Late Cretaceous African Tethys: conclusions from a microscopic-microchemical study of ooidal ironstones from Egypt, Sudan and Nigeria. *Journal of African Earth Sciences*, **30**: 25-46.
- Mustafa, H.** 2000. Fish teeth from the Upper Umm Ghudram Formation (Late Santonian) of NW-Jordan. *N. Jb. Geol. Paläont. Mh.*, **10**: 595-612.

- Nagender Nath, B., Kunzendorf, H. and Plüger, W.L.** 2000. Influence of Provenance, Weathering, and Sedimentary Processes on the Elemental Ratios of the Fine-Grained Fraction of the Bedload Sediments from the Vembanad Lake and the Adjoining Continental Shelf, Southwest Coast of India. *Journal of Sedimentary Research*, **70**: 1081-1094.
- Nasir, S. and Sadeddin, W.** 1989. The heavy minerals of the Kurnub Sandstone (Early Cretaceous) of Jordan. *Sedimentary Geology*, **62**: 101-107.
- Nasir, S. and Safarjalani, A.** 2000. Lithosperic petrology beneath the northern part of the Arabian Plate in Syria: evidence from xenoliths in alkali basalts. *Journal of African Earth Sciences*, **30**: 149-168.
- Nemec, W.** 1990. Deltas - remarks on terminology and classification. In: *Coarse-Grained Deltas* (Eds A. Colella and D.B. Prior), *Spec. Publs int. Ass. Sediment.*, **10**, pp. 3-12. Blackwell Scientific Publications, Oxford.
- Nemec, W. and Steel, R.J.** 1988. What is a fan delta and how do we recognize it? In: *Fan Deltas: Sedimentology and Tectonic Settings* (Eds W. Nemec and R.J. Steel), pp. 3-13. Blackie, Glasgow.
- Nesbitt, H.W. and Young, G.M.** 1982. Early Proterozoic climates and plate motions inferred from major element chemistry of lutites. *Nature*, **299**: 715-717.
- Niedoroda, A.W., Swift, D.J.P. and Hopkins, T.S.** 1985. The Shoreface. In: *Coastal Sedimentary Environments* (Ed R.A. Davis, Jr.) Second edn, pp. 533-624. Springer-Verlag, New York.
- Odin, G.S.** 1994. Geological time scale. *Courier de l'academie des Sciences de Paris*, **t318, Serie II**: 59-71.
- Odin, G.S. and Dodson, M.H.** 1982. Zero isotopic age of glauconites. In: *Numerical Dating in Stratigraphy* (Ed G.S. Odin), pp. 277-305. John Wiley & Sons, Ltd., Chichester.
- Odin, G.S. and Matter, A.** 1981. De glauconiarum origine. *Sedimentology*, **28**: 611-641.
- Odin, G.S. and Rex, D.C.** 1982. Potassium-argon dating of washed, leached, weathered and reworked glauconies. In: *Numerical Dating in Stratigraphy* (Ed G.S. Odin), pp. 363-385. John Wiley & Sons, Ltd., Chichester.
- Orton, G.J.** 1988. A spectrum of Middle Ordovician fan deltas and braidplain deltas, North Wales: a consequence of varying fluvial clastic input. In: *Fan Deltas: Sedimentology and Tectonic Settings* (Eds W. Nemec and R.J. Steel), pp. 23-49. Blackie, Glasgow.
- Osborn, G.** 1985. Evolution of the Late Cenozoic Inselberg Landscape of Southwestern Jordan. *Palaeogeography, Palaeoclimatology, Palaeoecology*, **49**: 1-23.
- Paola, C.** 2000. Quantitative models of sedimentary basin filling. *Sedimentology*, **47**: 121-178.
- Parker, D.H.** (Ed), 1970. *The hydrogeology of the Mesozoic-Cainozoic aquifers of the western highlands and plateau of East Jordan. Investigation of the aquifers of east Jordan, Report of United Nations Development Project/Food and Agriculture Organization Project 212, Technical Report No. 2.* Unpublished, Rome, 424 pp.
- Pemberton, S.G., MacEachern, J.A. and Frey, R.W.** 1992. Trace Fossil Facies Models: Environmental and Allostratigraphic Significance. In: *Facies Models: Response to Sea Level Change* (Eds R.G. Walker and N.P. James), pp. 47-72. Geological Association of Canada, Stittsville, Ontario.
- Petters, S.W.** 1991. *Regional Geology of Africa.* Lecture Notes in Earth Sciences, **40**. Springer-Verlag, Berlin, 722 pp.
- Pettijohn, F.J., Potter, P.E. and Siever, R.** 1987. *Sand and Sandstone.* Springer, Berlin, 553 pp.
- Plint, A.G. and Nummedal, D.** 2000. The falling stage systems tract: recognition and importance in sequence stratigraphic analysis. In: *Sedimentary Responses to Forced*

- Regressions* (Eds D. Hunt and R.L. Gawthorpe), *Geological Society Special Publications*, **172**, pp. 1-17. The Geological Society, London.
- Posamentier, H.W. and Allen, G.P.** 1999. *Siliciclastic Sequence Stratigraphy - Concepts and Applications*. Concepts in Sedimentology and Paleontology, **7**. SEPM, Tulsa/Oklahoma, 210 pp.
- Posamentier, H.W., Jervey, M.T. and Vail, P.R.** 1988. Eustatic Controls on Clastic Deposition I - Conceptual Framework. In: *Sea-Level Changes: An Integrated Approach* (Eds C.K. Wilgus et al.), **No. 42**, pp. 109-124. Society of Economic Paleontologists and Mineralogists (SEPM), Tulsa/Oklahoma.
- Posamentier, H.W. and Morris, W.R.** 2000. Aspects of the stratal architecture of forced regressive deposits. In: *Sedimentary Responses to Forced Regressions* (Eds D. Hunt and R.L. Gawthorpe), *Geological Society Special Publication*, **172**, pp. 19-46. The Geological Society, London.
- Posamentier, H.W. and Vail, P.R.** 1988. Eustatic Controls on Clastic Deposition II - Sequence and Systems Tract Models. In: *Sea-Level Changes: An Integrated Approach* (Eds C.K. Wilgus et al.), **No. 42**, pp. 125-154. Society of Economic Paleontologists and Mineralogists (SEPM), Tulsa/Oklahoma.
- Postma, G.** 1990. Depositional architecture and facies of river and fan deltas: a synthesis. In: *Coarse-Grained Deltas* (Eds A. Colella and D.B. Prior), *Spec. Publs int. Ass. Sediment.*, **10**, pp. 13-27. Blackwell Scientific Publications, Oxford.
- Powell, J.H.** 1989. *Stratigraphy and Sedimentation of the Phanerozoic Rocks in Central and South Jordan - Part B: Kurnub, Ajlun and Belqa Groups*. Geological Bulletin, **No. 11**. The Hashemite Kingdom of Jordan, Ministry of Energy and Mineral Resources, Natural Resources Authority, Amman, 130 pp.
- Powell, J.H., El-Hiyari, M. and Khalil, B.M.** 1996. *Evolution of Cretaceous to Eocene alluvial and carbonate platform sequences in central and south Jordan*. Internal Report, Amman, 57 pp.
- Pye, K.** 1983. Red Beds. In: *Chemical sediments and geomorphology: precipitates and residua in the near-surface environment* (Eds A.S. Goudie and K. Pye), pp. 227-263. Academic Press, London.
- Quenell, A.M.** 1951. The geology and mineral resources of (former) Transjordan. *Colon. Geol. Min. Resource*, **2**: 85-115.
- Rashdan, M.** 1987. Wadi 'Araba 2949 II / Al 'Aqaba 3049 III. The Hashemite Kingdom of Jordan, Natural Resources Authority, Geology Directorate, Amman.
- Reading, H.G.** (Ed), 1996. *Sedimentary Environments: Processes, Facies and Stratigraphy*, 3rd edn. Blackwell Science, Oxford, 688 pp.
- Reading, H.G. and Collinson, J.D.** 1996. Clastic coasts. In: *Sedimentary Environments: Processes, Facies and Stratigraphy* (Ed H.G. Reading) 3rd edn, pp. 154-231. Blackwell Science, Oxford.
- Reineck, H.-E. and Singh, I.B.** 1980. *Depositional Sedimentary Environments*. Springer-Verlag, Berlin, 549 pp.
- Reinson, G.E.** 1992. Transgressive barrier island and estuarine systems. In: *Facies Models: response to Sea Level Change* (Eds R.G. Walker and N.P. James), pp. 179-218. Geological Association of Canada, St. John's.
- Remane, J., Faure-Muret, A., Odin, G.S., Cita, M.B., Dercourt, J., Bouysse, P., Repetto, F., Roche, G. and Dumas, L.** 2002. International Stratigraphic Chart. International Union of Geological Sciences, International Commission on Stratigraphy, Commission on the Geological Map of the World, UNESCO.
- Richards, M.T.** 1996. Fluvial Systems. In: *Sequence Stratigraphy* (Eds D. Emery and K. Myers), pp. 111-133. Blackwell Science, Oxford.

- Rigo De Righi, M. and Cortesini, A.** 1964. Gravity Tectonics in Foothills Structure Belt of Southeast Turkey. *American Association of Petroleum Geologists Bulletin*, **48**: 1911-1937.
- Rock-Color Committee, T.** 1963. *The Rock-Color Chart*. The Geological Society of America, New York.
- Roser, B.P. and Korsch, R.J.** 1986. Determination of tectonic setting of sandstone-mudstone suites using SiO₂ content and K₂O/Na₂O Ratio. *Journal of Geology*, **94**: 635-650.
- Roser, B.P. and Korsch, R.J.** 1988. Provenance signatures of sandstone-mudstone suites determined using discriminant function analysis of major-element data. *Chem. Geol.*, **67**: 119-139.
- Roser, B.P. and Nathan, S.** 1997. An evaluation of element mobility during metamorphism of a turbidite sequence (Greenland Group, New Zealand). *Geological Magazine*, **134**: 219-234.
- Salem, A.M., Abd Elhameed, A.T., Hassanein, I. and Fouda, A.M.** 2001. Diagenetic Implications and Provenance of Pre-Cenomanian Sandstones, Sheikh Attia Area, East-Central Sinai, Egypt. *Sedimentology of Egypt*, **9**: 57-72.
- Salvador, A.** (Ed), 1994. *International Stratigraphic Guide: A Guide to Stratigraphic Classification, Terminology, and Procedure*, 2nd edn. The International Union of Geological Sciences and The Geological Society of America, Boulder/Colorado, 214 pp.
- Sandler, A.** 1996. A Turonian Subaerial Event in Israel: Karst, Sandstone and Pedogenesis. *Geol. Surv. Isr. Bull.*, **85**: 1-52.
- Scheffer, F. and Schachtschabel, P.** 1992. *Lehrbuch der Bodenkunde*. Enke, Stuttgart, 491 pp.
- Scholle, P.A.** 1979. *A Color Illustrated Guide To Constituents, Textures, Cements, and Porosities of Sandstones and Associated Rocks*. AAPG Memoir, **28**. The American Association of Petroleum Geologists, Tulsa/Oklahoma, 201 pp.
- Scholle, P.A. and Spearing, D.** (Eds) 1982. *Sandstone Depositional Environments*. (Ed M.K. Horn), *AAPG Memoir*, **31**. The American Association of Petroleum Geologists, Tulsa/Oklahoma, 410 pp.
- Scotese, C.R.** 2000. Late Cretaceous Climate. PALEOMAP Project, <http://www.scotese.com/lcretcli.htm>; F080_zonef.jpg.
- Sharland, P.R., Archer, R., Casey, D.M., Davies, R.B., Hall, S.H., Heward, A.P., Horbury, A.D. and Simmons, M.D.** 2001. *Arabian Plate Sequence Stratigraphy*. GeoArabia Special Publication, **2**. Gulf PetroLink, Manama, Bahrain, 371 pp.
- Shinn, E.A.** 1983. Tidal Flat Environment. In: *Carbonate Depositional Environments* (Eds P.A. Scholle, D.G. Bebout and C.H. Moore), *AAPG Memoir*, **33**, pp. 171-210. The American Association of Petroleum Geologists, Tulsa/Oklahoma.
- Singer, A.** 1975. A Cretaceous laterite in the Negev Desert, southern Israel. *Geol. Mag.*, **112**: 151-162.
- Steinitz, G.** 1981. Enigmatic Chert Structures in the Senonian Cherts of Israel. *Geol. Surv. Isr. Bull.*, **75**: 1-46.
- Swan, A.R.H. and Sandilands, M.** 1995. *Introduction to Geological Data Analysis*. Blackwell Science Ltd., Oxford, 446 pp.
- Taylor, S.R. and McLennan, S.M.** 1985. *The Continental Crust: its Composition and Evolution*. Geoscience Texts. Blackwell Scientific Publications, Oxford, 312 pp.
- Teimeh, M., Abu Lihie, O., Taani, Y. and Abu Saad, L.** 1990. *A Study of the Palaeozoic Formations of Jordan at Outcrop and in the Subsurface - Including Measured Sections and Regional Isopach Maps*. Subsurface Geology Bulletin, **No. 1**. The Hashemite Kingdom of Jordan, Ministry of Energy and Mineral Resources, Natural Resources Authority, Amman, 72 pp.

- Télez Duarte, M.A. and López Martínez, M.** 2002. K-Ar dating and geological significance of clastic sediments of the Paleocene Sepultura Formation, Baja California, México. *Journal of South American Earth Sciences*, **15**: 725-730.
- Terwindt, J.H.J.** 1988. Palaeo-tidal reconstructions of inshore tidal depositional environments. In: *Tide-Influenced Sedimentary Environments and Facies* (Eds P.L. de Boer, A. van Gelder and S.D. Nio), *Sedimentology and Petroleum Geology*, pp. 233-263. D. Reidel Publishing Company, Dordrecht.
- Tibert, N.E. and Gibling, M.R.** 1999. Peat accumulation on a drowned coastal braidplain: the Mullins Coal (Upper Carboniferous), Sydney Basin, Nova Scotia. *Sedimentary Geology*, **128**: 23-28.
- Tortosa, A., Palomares, M. and Arribas, J.** 1991. Quartz grain types in Holocene deposits from the Spanish Central System: some problems in provenance analysis. In: *Developments in Sedimentary Provenance Studies* (Eds A.C. Morton, S.P. Todd and P.D.W. Haughton), *Geological Society Special Publication*, **57**, pp. 47-54.
- Totten, M.W. and Weaver, B.L.** 2000. Beyond whole-rock geochemistry of shales: The importance of assessing mineralogic controls for revealing tectonic discrimination of multiple sediment sources for the Ouachita Mountain flysch deposits. *GSA Bulletin*, **112**: 1012-1022.
- Toulkerides, T., Clauer, N., Kröner, A., Reimer, T. and Todt, W.** 1999. Characterization, provenance, and tectonic setting of Fig Tree greywackes from the Archaean Barberton Greenstone Belt, South Africa. *Sedimentary Geology*, **124**: 113-129.
- Tucker, M.** 1996a. *Methoden der Sedimentologie*. Enke, Stuttgart, 366 pp.
- Tucker, M.E.** 1996b. *Sedimentary Rocks In The Field*. The Geological Field Guide Series. John Wiley & Sons, Chichester, 153 pp.
- Tucker, M.E. and Wright, V.P.** 1990a. Carbonate depositional systems I: marine shallow-water and lacustrine carbonates. In: *Carbonate Sedimentology* (Eds M. Tucker and P. Wright), pp. 101-227. Blackwell Science, Oxford.
- Tucker, M.E. and Wright, V.P.** 1990b. *Carbonate Sedimentology*. Blackwell Science, Oxford, 482 pp.
- Valeton, I.** 1988. Verwitterung und Verwitterungslagerstätten. In: *Sediment-Petrologie Teil II: Sedimente und Sedimentgesteine* (Ed H. Füchtbauer) 4th edn, pp. 11-68. E. Schweizerbart'sche Verlagsbuchhandlung, Stuttgart.
- Van Wagoner, J.C., Mitchum, R.M., Campion, K.M. and Rahmanian, V.D.** 1990. *Siliciclastic Sequence Stratigraphy in Well Logs, Cores, and Outcrops: Concepts for High-Resolution Correlation of Time and Facies*. AAPG Methods in Exploration Series, **7**, Tulsa/Oklahoma, 55 pp.
- Van Wagoner, J.C., Posamentier, H.W., Mitchum, R.M., Vail, P.R., Sarg, J.F., Loutit, T.S. and Hardenbol, J.** 1988. An Overview of the Fundamentals of Sequence Stratigraphy and Key Definitions. In: *Sea-Level Changes: An Integrated Approach* (Eds C.K. Wilgus et al.), *SEPM Special Publication*, **No. 42**, pp. 39-45. Society of Economic Paleontologists and Mineralogists (SEPM), Tulsa/Oklahoma.
- Velde, B.** (Ed), 1995. *Origin and Mineralogy of Clays - Clays and the Environment*. Springer, Berlin, 334 pp.
- Walker, R.G. and James, N.P.** (Eds) 1992. *Facies Models: Response to Sea Level Change*. Geological Association of Canada, St. John's, 454 pp.
- Walker, R.G. and Plint, A.G.** 1992. Wave- and Storm-Dominated Shallow Marine Systems. In: *Facies Models: Response to Sea Level Change* (Eds R.G. Walker and N.P. James), pp. 219-238. Geological Association of Canada, St. John's.
- Walker, T.R.** 1974. Formation of Red Beds in Most Tropical Climates: A Hypothesis. *Geological Society of America Bulletin*, **85**: 633-638.

- Walker, T.R.** 1976. Diagenetic Origin of Continental Red Beds. In: *The Continental Permian in Central, West, and South Europe* (Ed H. Falke), pp. 240-282. D. Reidel Publishing Company, Dordrecht.
- Weissbrod, T. and Nachmias, J.** 1986. Stratigraphic significance of heavy minerals in the Late Precambrian-Mesozoic clastic sequence ("Nubian Sandstone") in the Near East. *Sedimentary Geology*, **47**: 263-291.
- Weltje, G.J.** 1994. *Provenance and Dispersal of Sand-sized Sediments: Reconstruction of dispersal patterns and sources of sand-sized sediments by means of inverse modelling techniques*. Geologica Ultraiectina: Mededelingen van de Faculteit Aardwetenschappen, **121**. Faculteit Aardwetenschappen, Universiteit Utrecht, Utrecht, 208 pp.
- Weltje, G.J.** 2002. Quantitative analysis of detrital modes: statistically rigorous confidence regions in ternary diagrams and their use in sedimentary petrology. *Earth-Science Reviews*, **57**: 211-253.
- West, I., Ali, Y.A. and Hilmy, M.E.** 1979. Primary gypsum nodules in a modern sabkha on the Mediterranean coast of Egypt. *Geology*, **7**: 354-358.
- Wilgus, C.K., Hastings, B.S., Kendall, C.G.S.C., Posamentier, H.W., Ross, C.A. and Van Wagoner, J.C.** (Eds) 1988. *Sea-Level Change: An Integrated Approach*. (Ed B.H. Lidz), *Special Publication*, **42**. Society of Economic Paleontologists and Mineralogists (SEPM), Tulsa/Oklahoma, 407 pp.
- Wöhrle, A.** 2001. *Das Oberkreide-Becken Südjordaniens - Beckenanalyse und stratigraphische Modellierung mit SEDPAK und STRATA*. Diplomarbeit, Universität Stuttgart, Stuttgart, 155 pp.
- Wozazek, S.** 2001. *Die klastischen Sedimente von Süd-Elfenbeinküste: Provenanz, Umlagerungsprozesse und Entwicklung des Goldvorkommens "Belle Ville"*. Dissertation, Universität Stuttgart, Stuttgart, 184 pp.
- Wright, V.P. and Burchette, T.P.** 1996. Shallow-water carbonate environments. In: *Sedimentary Environments: Processes, Facies and Stratigraphy* (Ed H.G. Reading) Third edn, pp. 325-394. Blackwell Science, Oxford.
- Zaitlin, B.A., Dalrymple, R.W. and Boyd, R.** 1994. The Stratigraphic Organization of Incised-Valley Systems Associated with Relative Sea-Level Change. In: *Incised-valley Systems: Origin and Sedimentary Sequences* (Eds R.W. Dalrymple, R. Boyd and B.A. Zaitlin), *SEPM Special Publication*, **51**, pp. 45-60. SEPM, Tulsa, Oklahoma.
- Zimmerle, W.** 1972. Sind detritische Zirkone rötlicher Farbe auch in Mitteleuropa Indikatoren für präkambrische Liefergebiete? *Geologische Rundschau*, **61**: 116-139.

Appendix I

Graphic logs and sample overview

Legend to graphic logs

Lithologies

	Sand/sandstone
	Calcareous sand
	Dolomitic sand
	Silt/siltstone
	Calcareous silt
	Dolomitic silt
	Clay/claystone
	Marl
	Limestone
	Limestone, sandy
	Dolomitic limestone
	Nodular limestone
	Dolomite
	Dolomite, sandy

Sedimentary structures

	Massive bedding
	Trough cross-bedding
	Planar cross-bedding
	Horizontal lamination
	Wavy lamination
	Ripple lamination
	Faint cross-bedding
	Hummocky cross strat.
	Convolute lamination
	Flaser bedding
	Graded bedding
	Load casts

Bed boundaries

	Sharp
	Gradational
	Erosional
	Irregular

Abbreviations:

LST= lowstand systems tract, TST= transgressive systems tract, HST= highstand systems tract, FSST= falling stage systems tract, SB= sequence boundary, BSFR= basal surface of forced regression, MFS= maximum flooding surface, MRS= maximum regressive surface

B.= Beach, C. P./Coastal PI = Coastal Plain, Est.= Estuarine, Fluvial= Fluvial Channels and Floodplain, M.= Marsh, Lag.= Lagoon, O. S.= Open Shelf, S. F.= Shoreface, T. F.= Tidal Flat, T. Z./Transition Z.= Transition Zone, W. U. G. F.= Wadi Umm Ghudran Formation

Sedimentary features

	Colour mottling
	Slickensides
	Clay chips
	Gravel
	Shell bed

Diagenetic minerals

	Glauconite
	Baryte
	Calcite
	Dolomite
	Gypsum
	Pyrite

Nodules/ concretions

	Concretions (undif.)
	Baryte concretions
	Caliche
	Iron oxide concretions
	Chert nodules

Bioturbation

	Rare
	Common
	Abundant

Trace fossils

	<i>Bergaueria isp.</i>
	<i>Chondrites isp.</i>
	<i>Diplocraterion isp.</i>
	<i>Rhizocorallium irregulare</i>
	<i>Rhizocorallium jenense</i>
	<i>Thalassinoides isp.</i>
	<i>Zoophycos isp.</i>

Body fossils

	Ammonites
	Bivalves
	Brachiopods
	Bryozoas
	Coralls
	Crustaceans
	Foraminiferans
	Gastropods
	Oysters
	Rudists
	Sea urchins
	Serpulids
	Bone fragments
	Fish scales
	Shark teeth
	Roots
	Wood
	Plant material

1 = Ferri-band

2 = Red colours

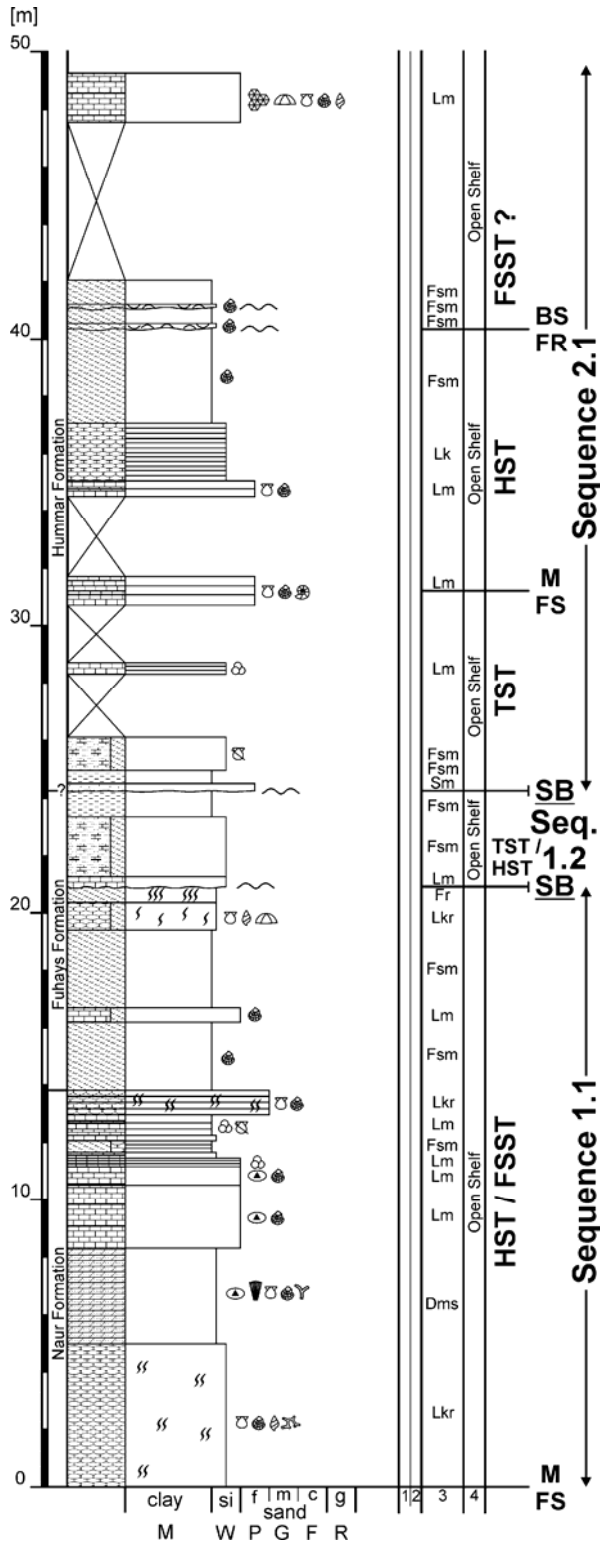
3 = Lithofacies

4 = Depositional environment

Section 1

GPS-Coordinates: N30° 14' 21.6"; E35° 27' 17.1"

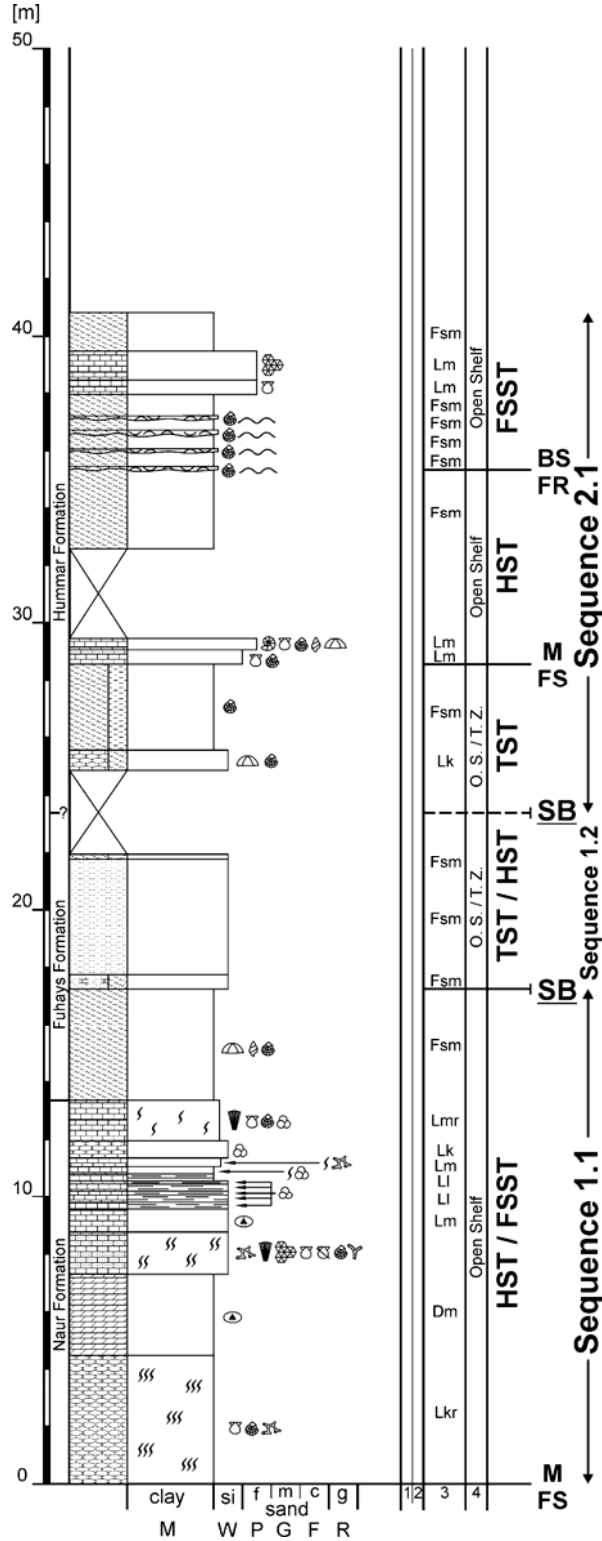
Distance from S1 to S2: 13.12 km; Bearing: 202° (true)



Section 2

GPS-Coordinates: N30° 07' 45.6"; E35° 24' 11.0"

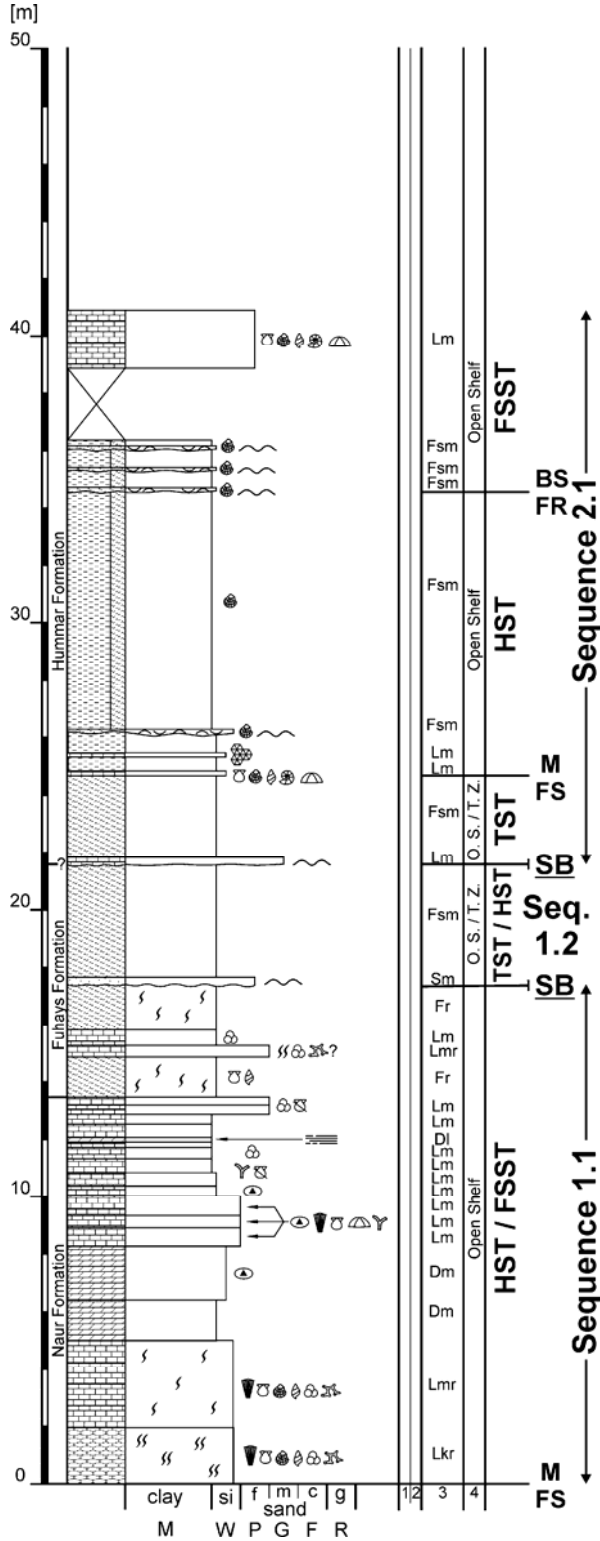
Distance from S2 to S3: 6.80 km; Bearing: 166° (true)



Section 3

GPS-Coordinates: N30° 04' 14.6"; E35° 25' 13.1"

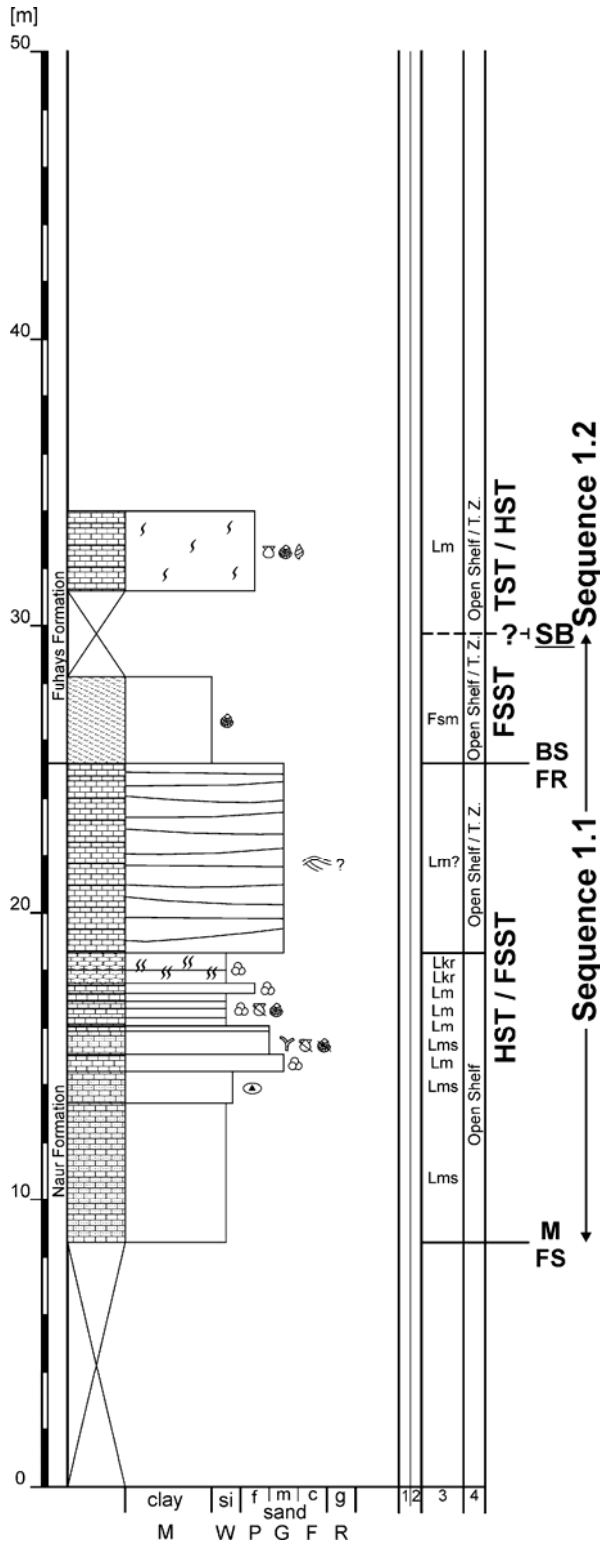
Distance from S3 to S4: 13.83 km; Bearing: 139° (true)



Section 4

GPS-Coordinates: N29° 58' 32.9"; E35° 30' 50.5"

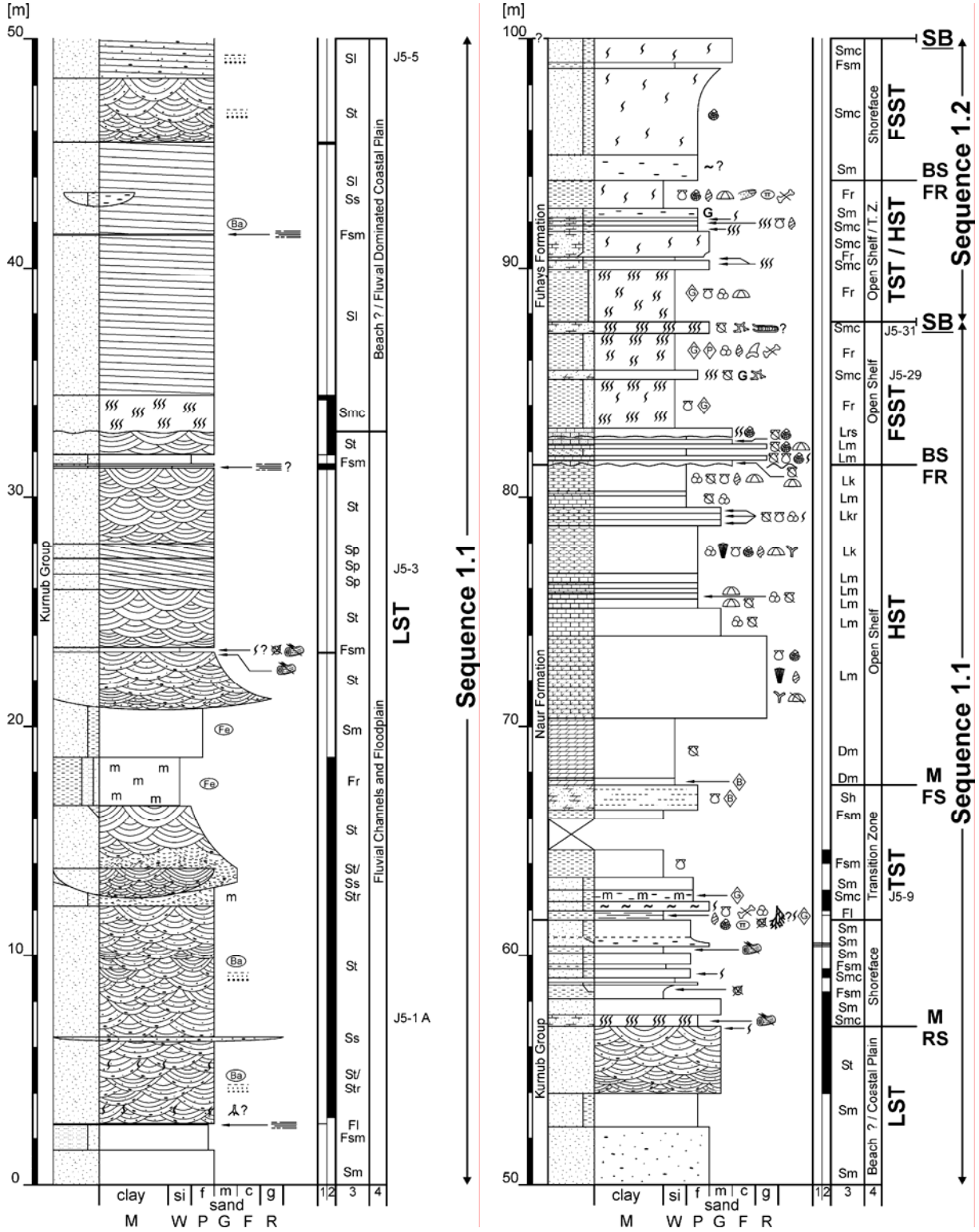
Distance from S4 to S5: 7.54 km; Bearing: 136° (true)



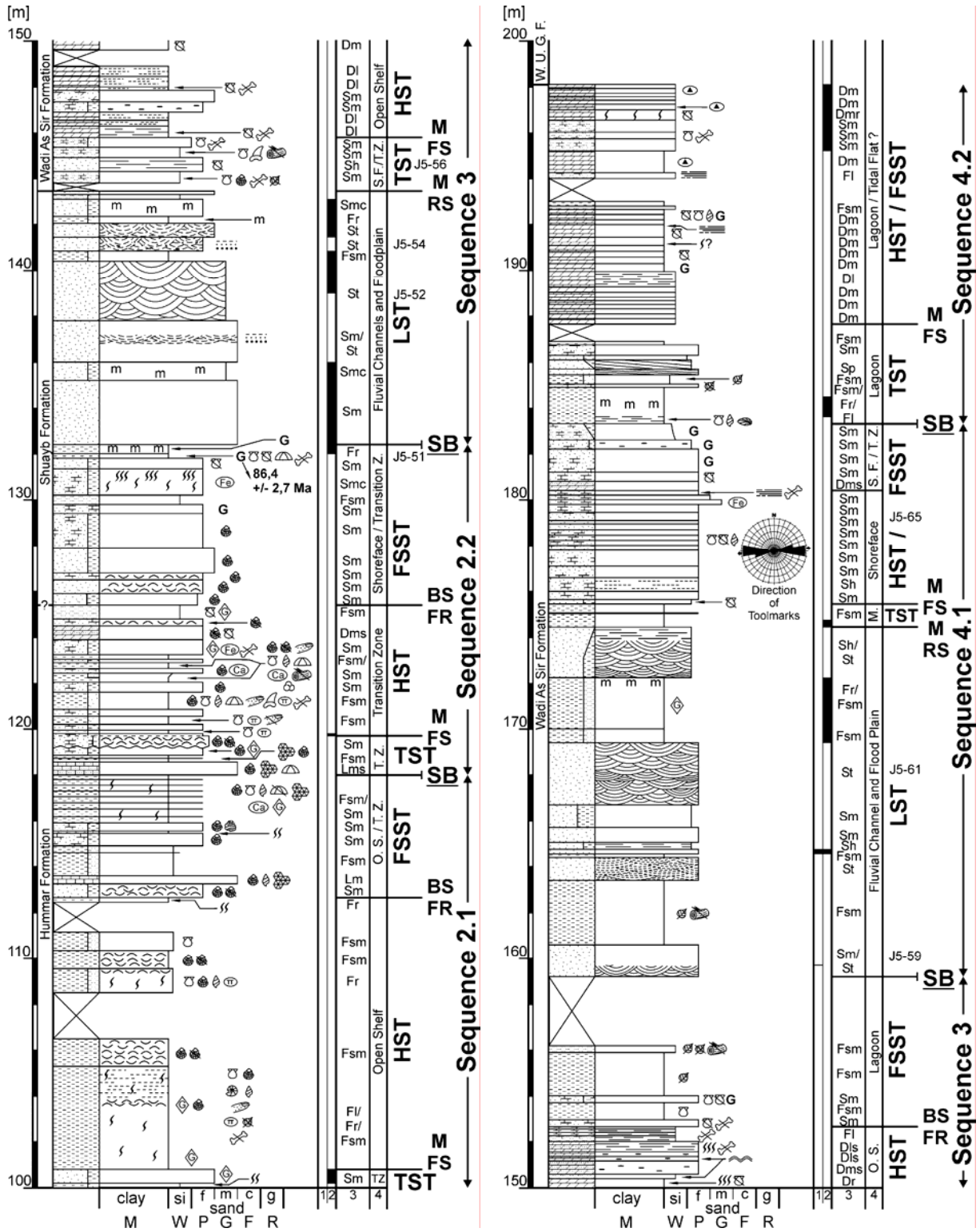
Section 5

GPS-Coordinates: N29° 55' 37.4"; E35° 34' 04.4"

Distance from S5 to S6: 4.33 km; Bearing: 166° (true)



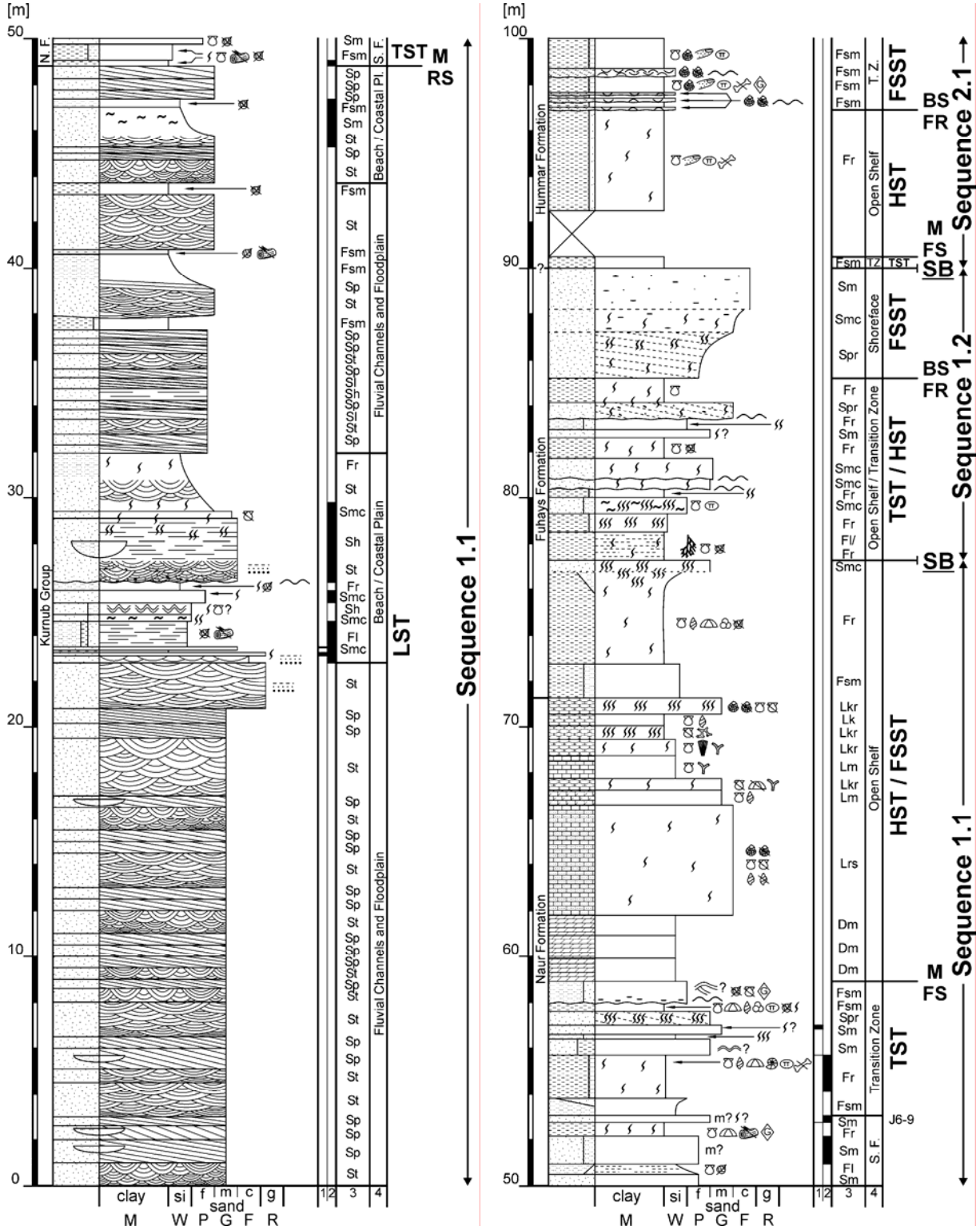
Section 5 continued



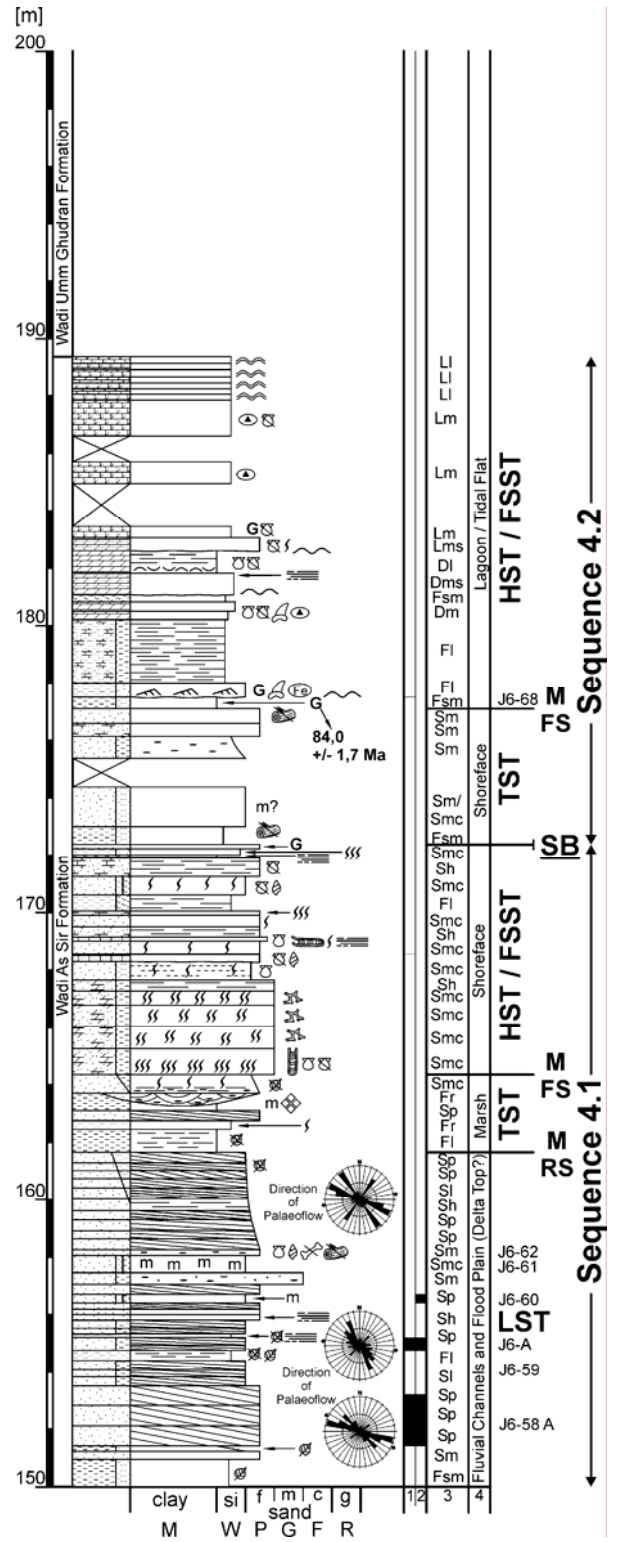
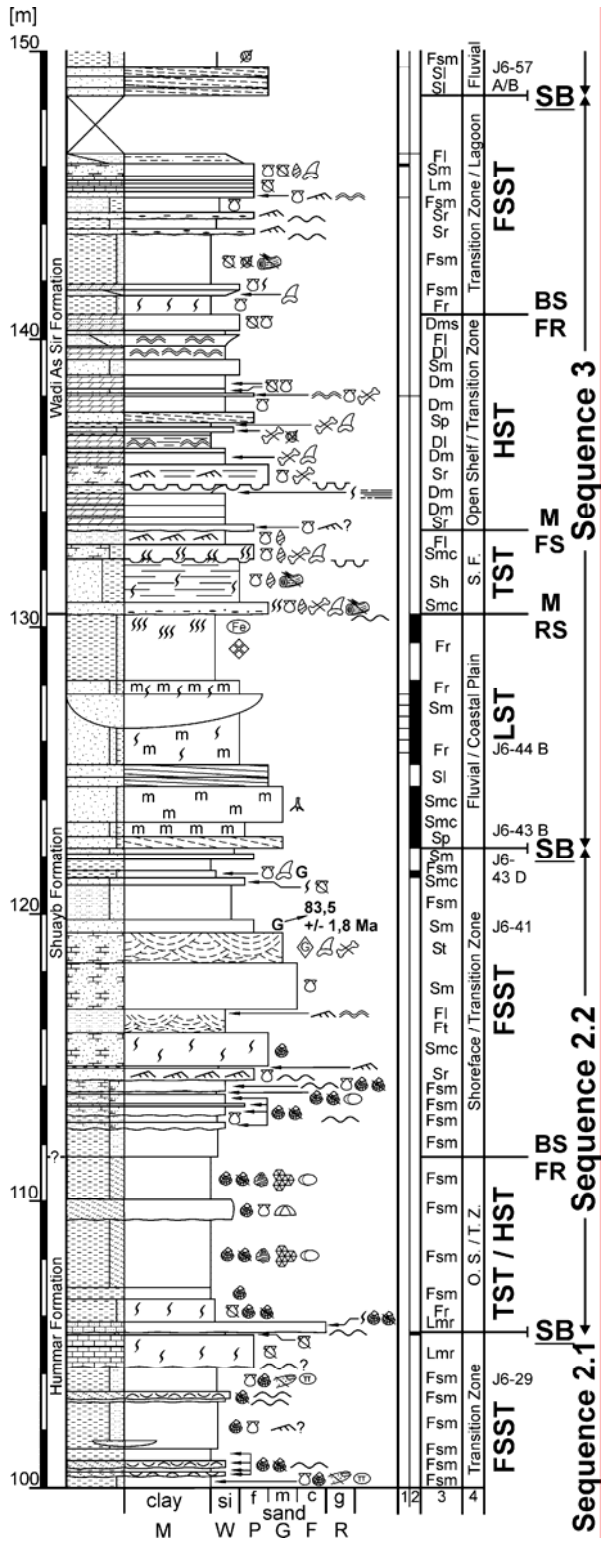
Section 6

GPS-Coordinates: N29° 53' 21.6"; E35° 34' 43.2"

Distance from S6 to S7: 5.35 km; Bearing: 128° (true)



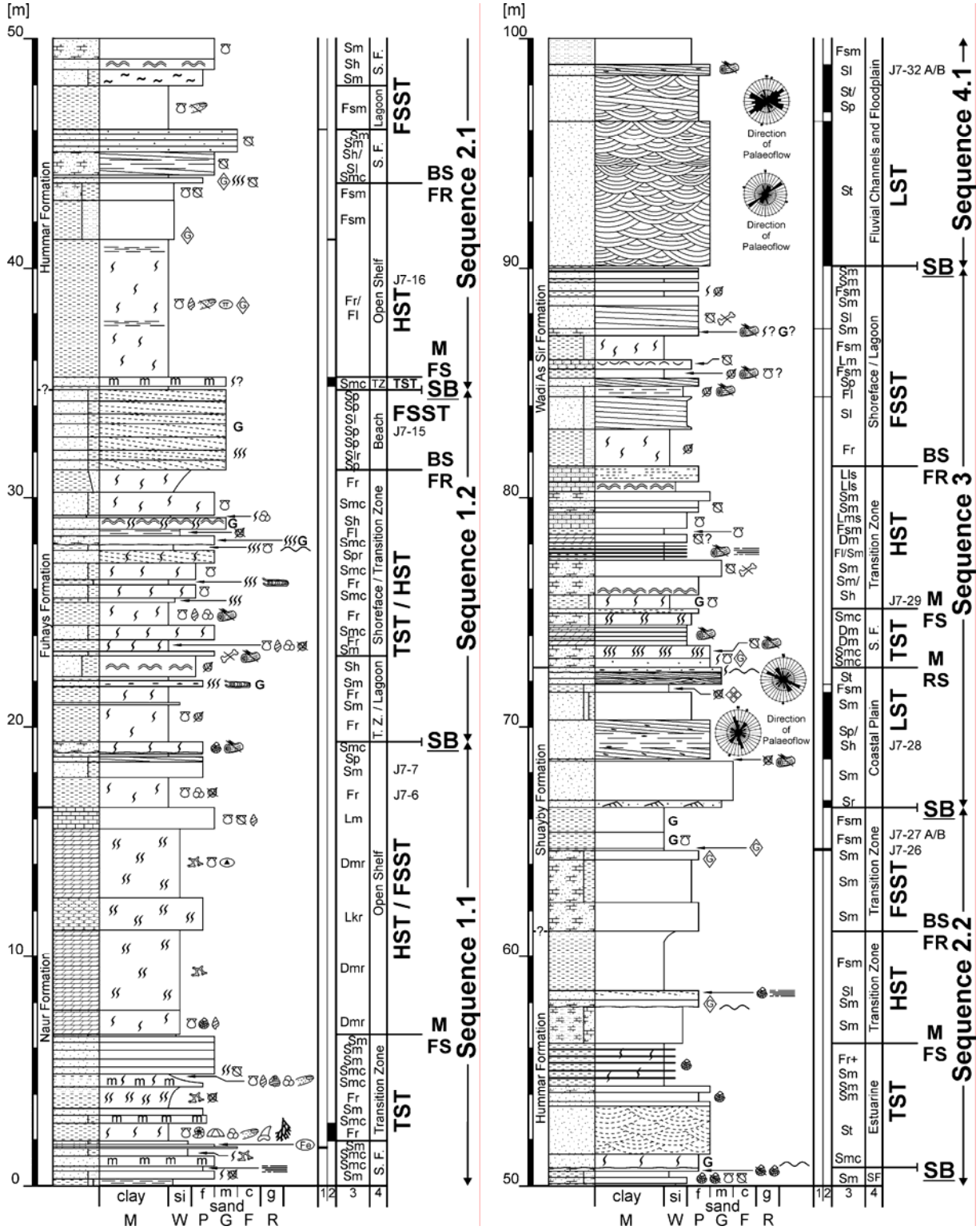
Section 6 continued



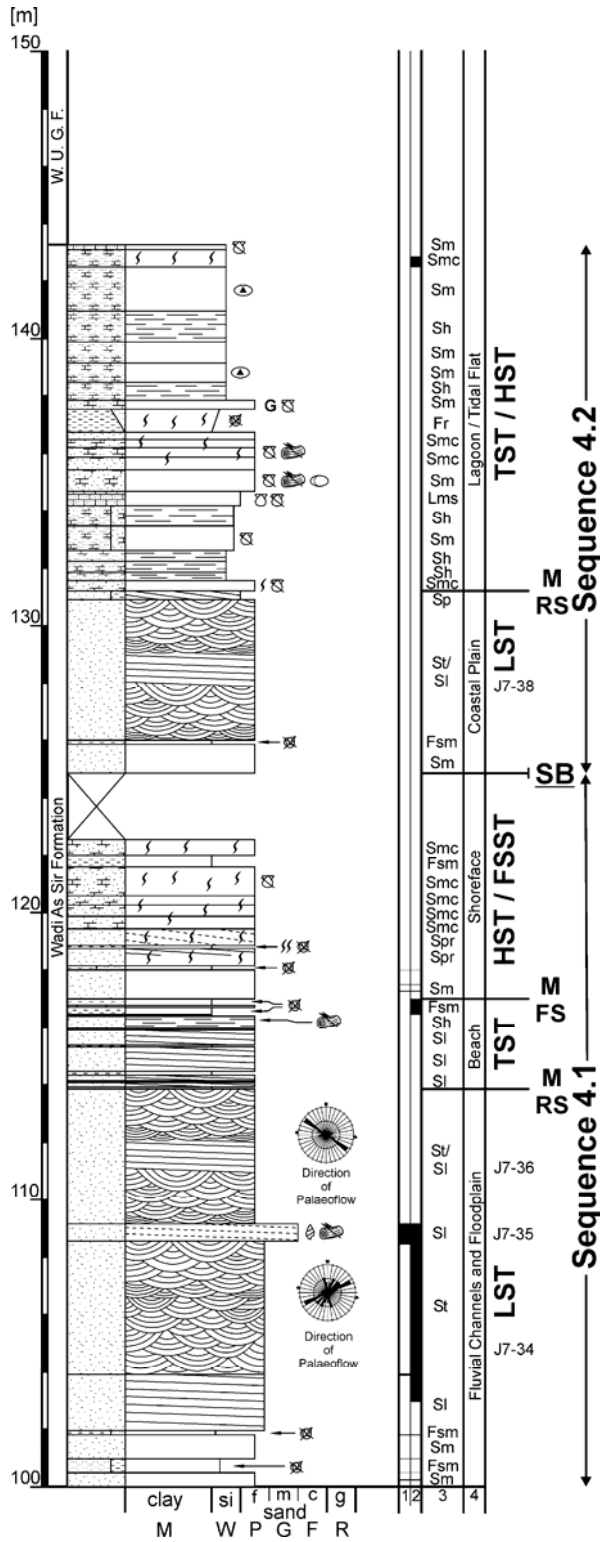
Section 7

GPS-Coordinates: N29° 51' 38.7"; E35° 37' 20.9"

Distance from S7 to S8: 7.90 km; Bearing: 129° (true)



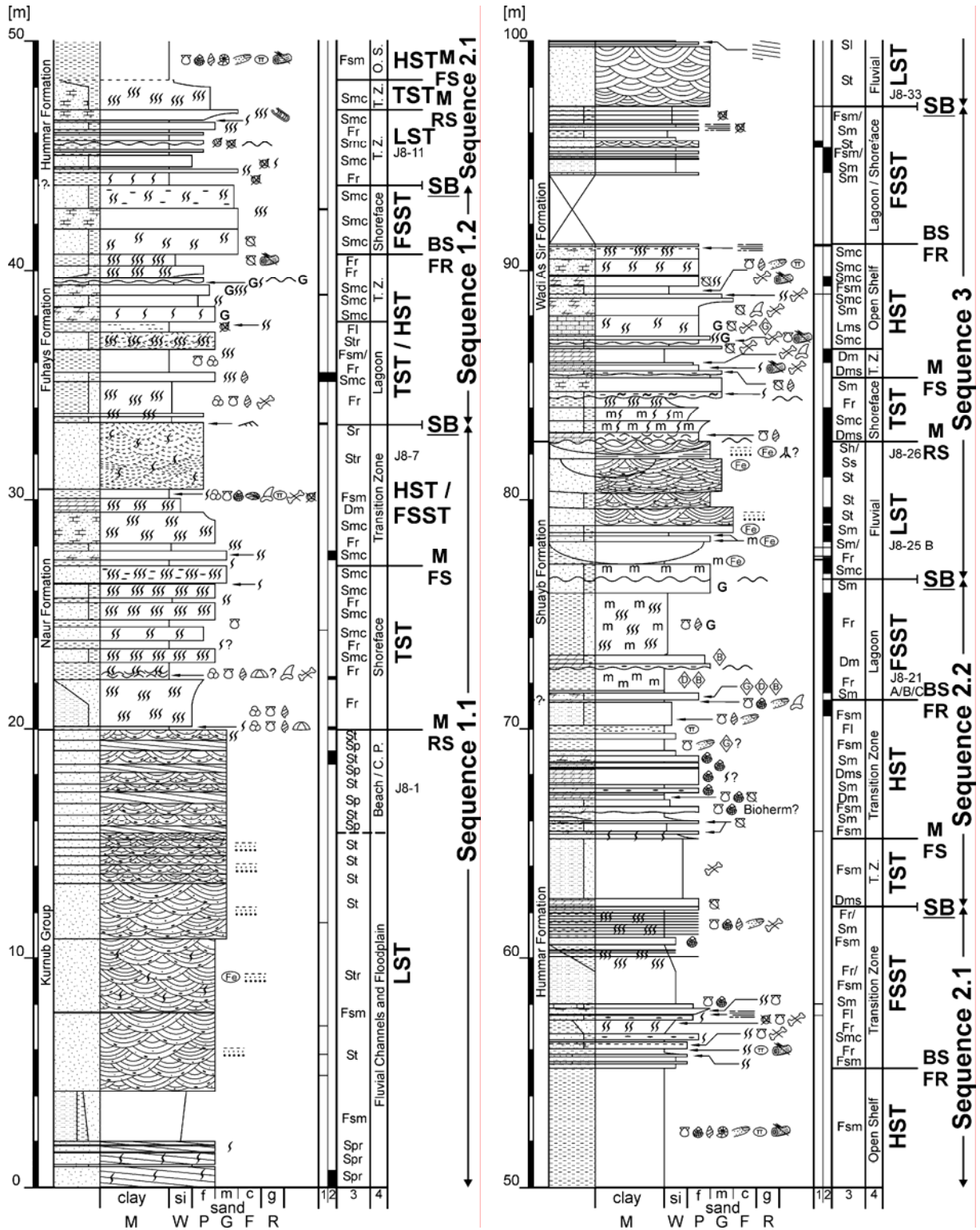
Section 7 continued



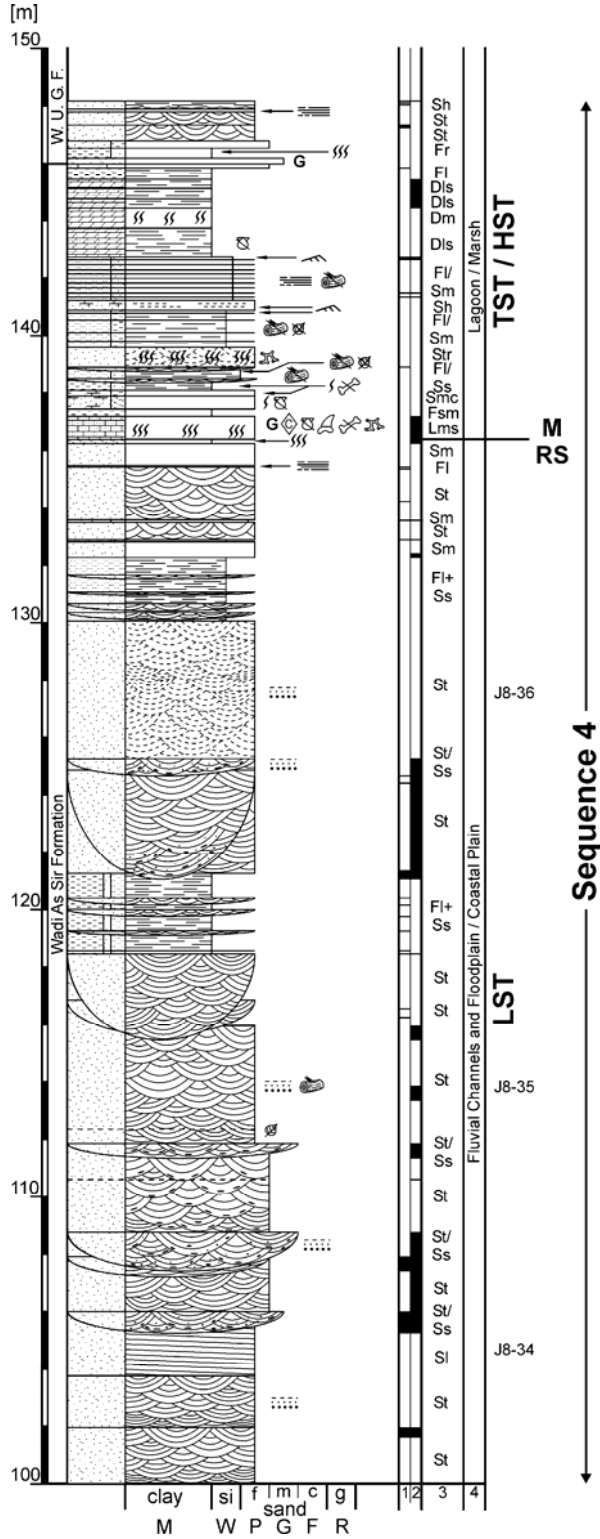
Section 8

GPS-Coordinates: N29° 48' 55.1"; E35° 41' 13.2"

Distance from S8 to S9: 3.31 km; Bearing: 093° (true)



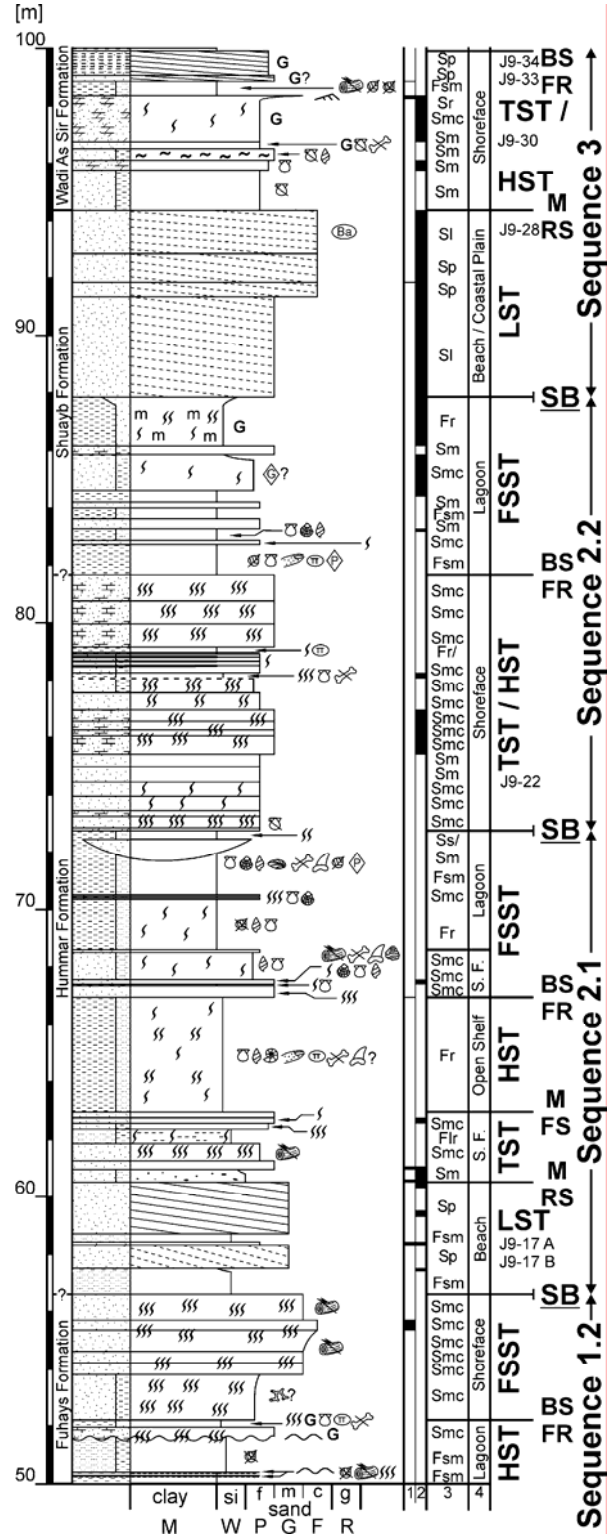
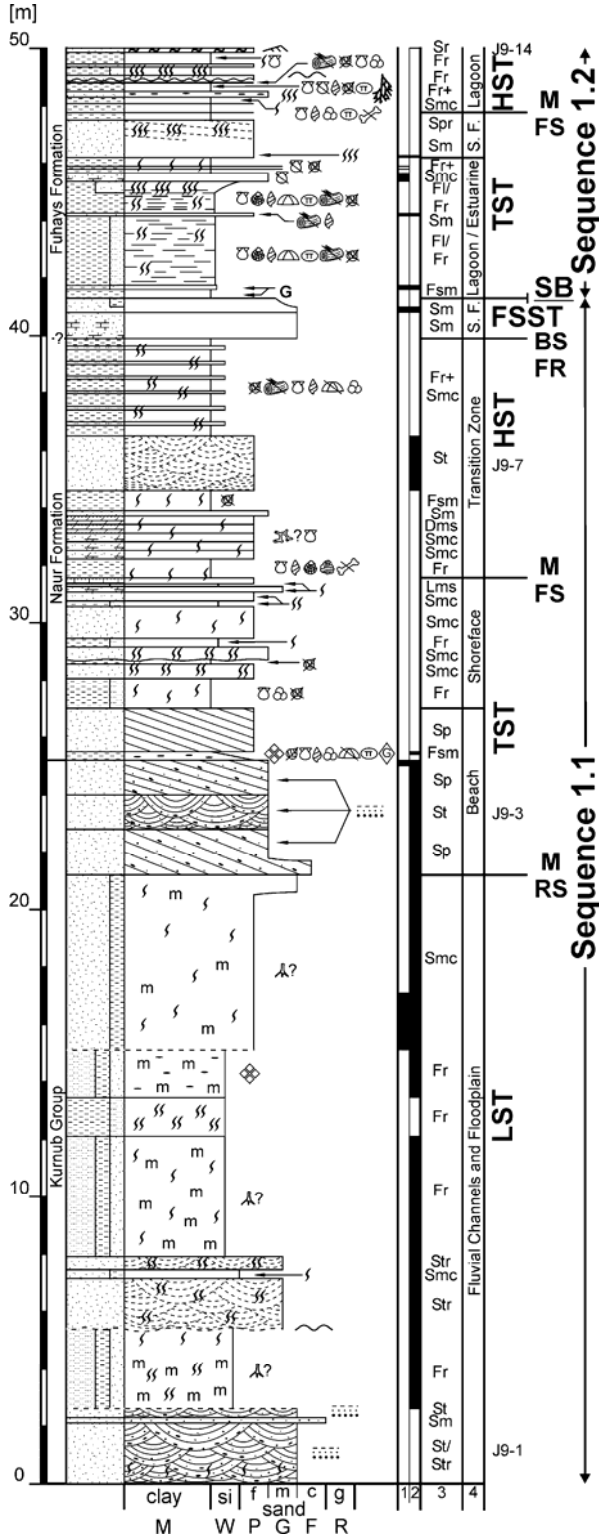
Section 8 continued



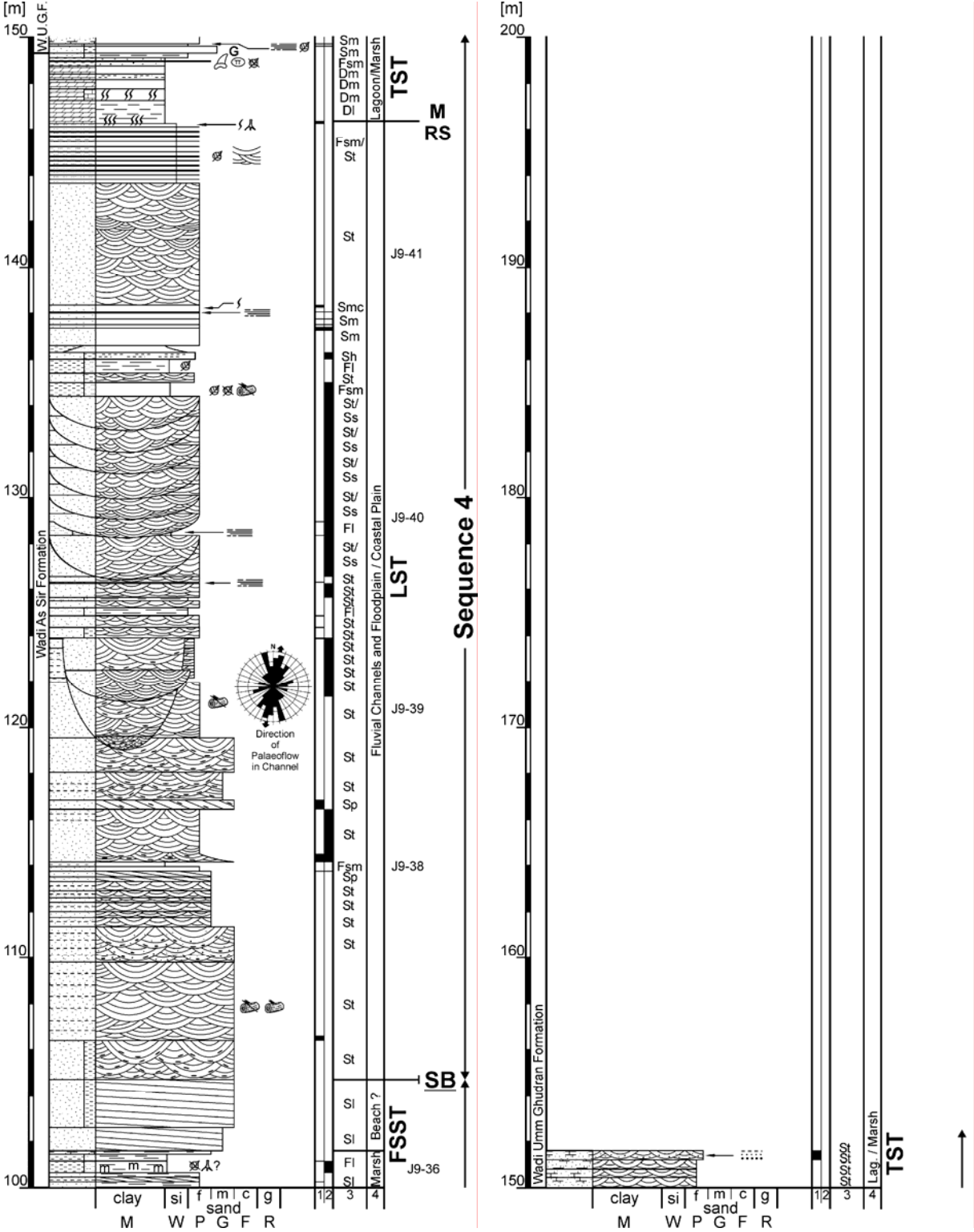
Section 9

GPS-Coordinates: N29° 48' 52.0"; E35° 43' 15.0"

Distance from S9 to S10: 13.28 km; Bearing: 135° (true)



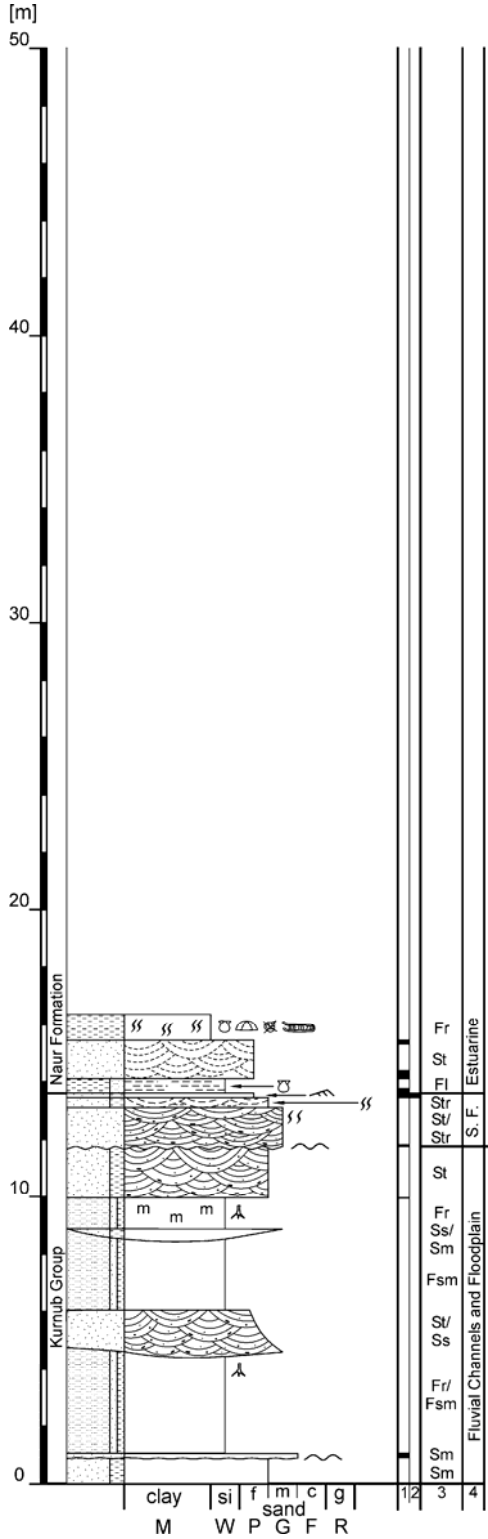
Section 9 continued



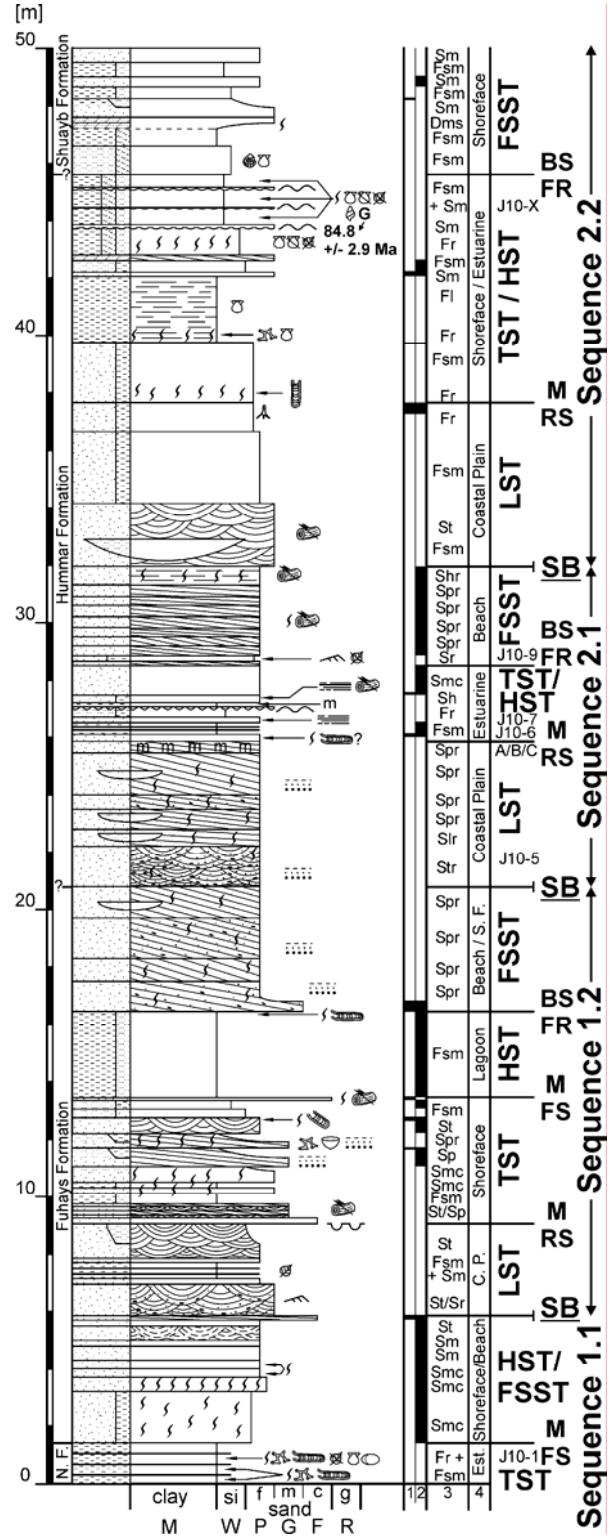
Section 10

GPS-Coordinates: N29° 43' 46.5"; E35° 49' 05.5"

Distance from S10 to S11: 19.31 km; Bearing: 134° (true)

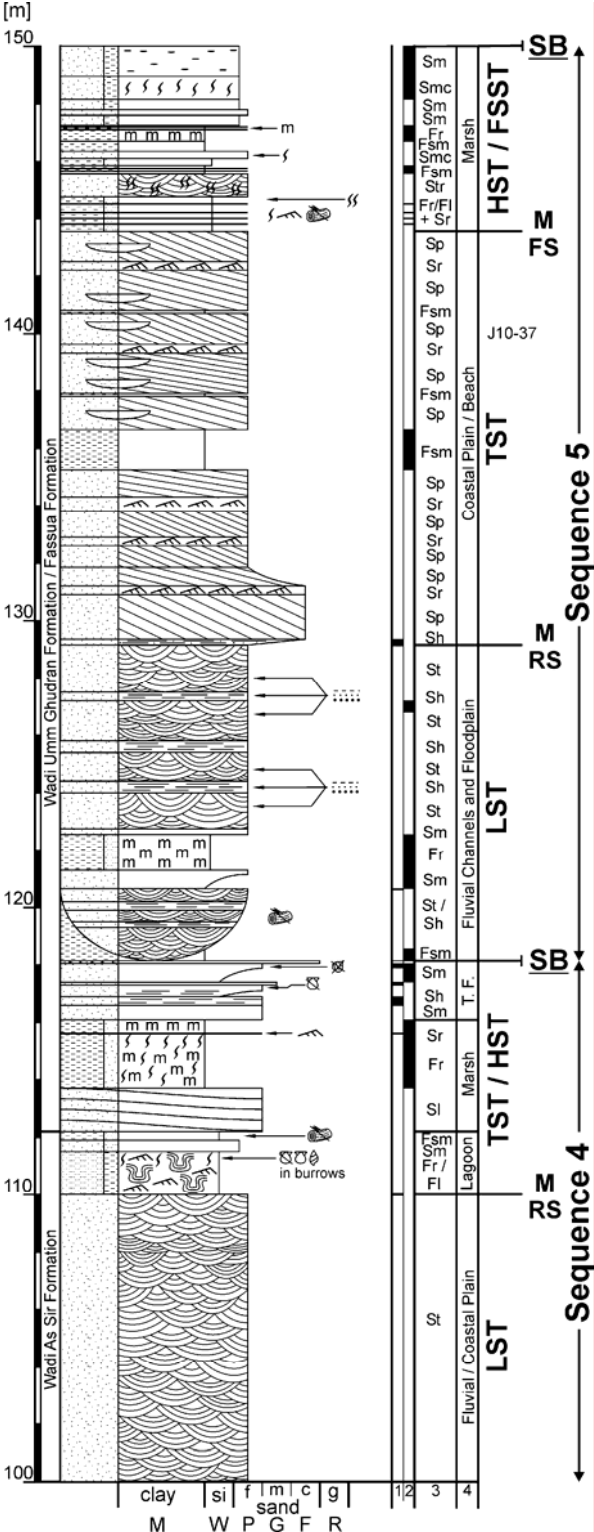
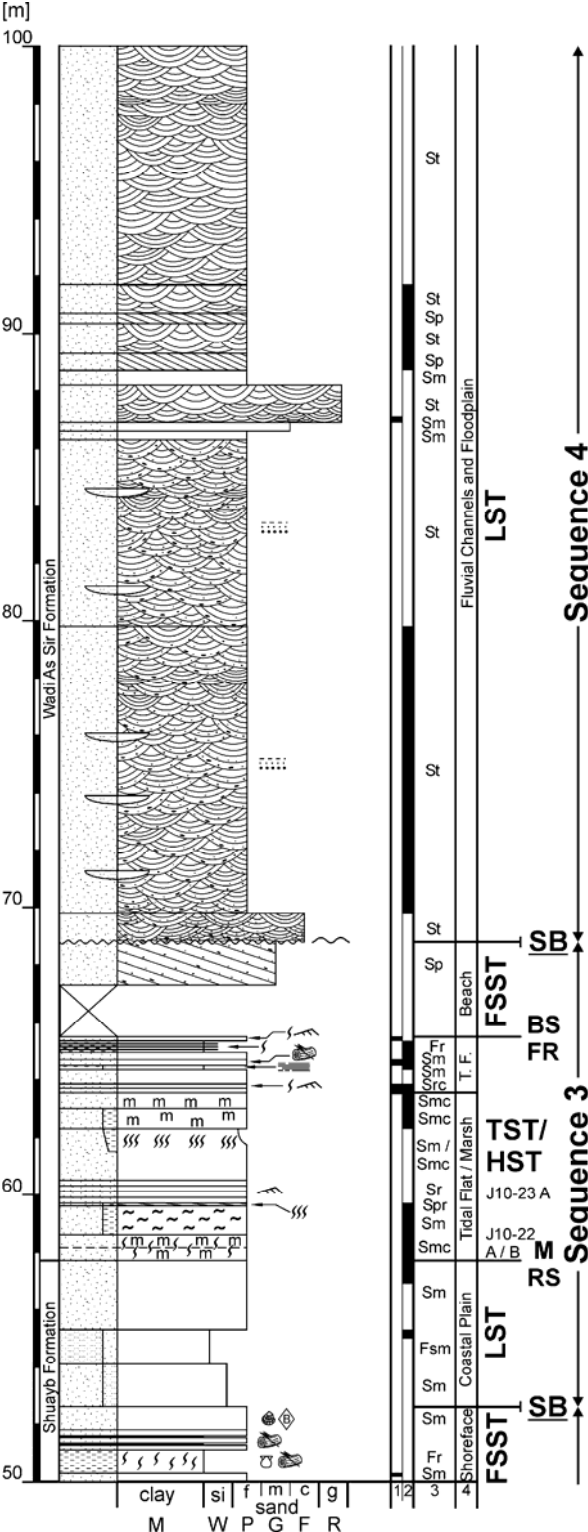


Sequence 1.1

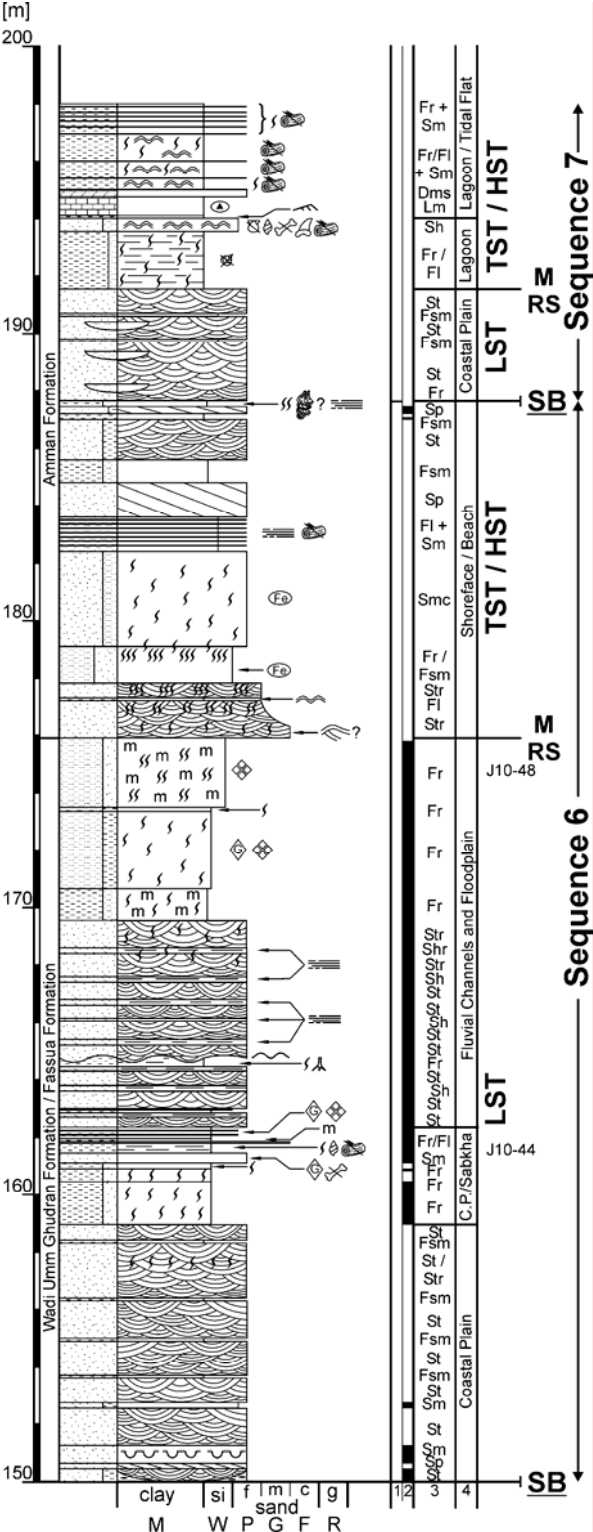


Sequence 1.1

Section 10 continued



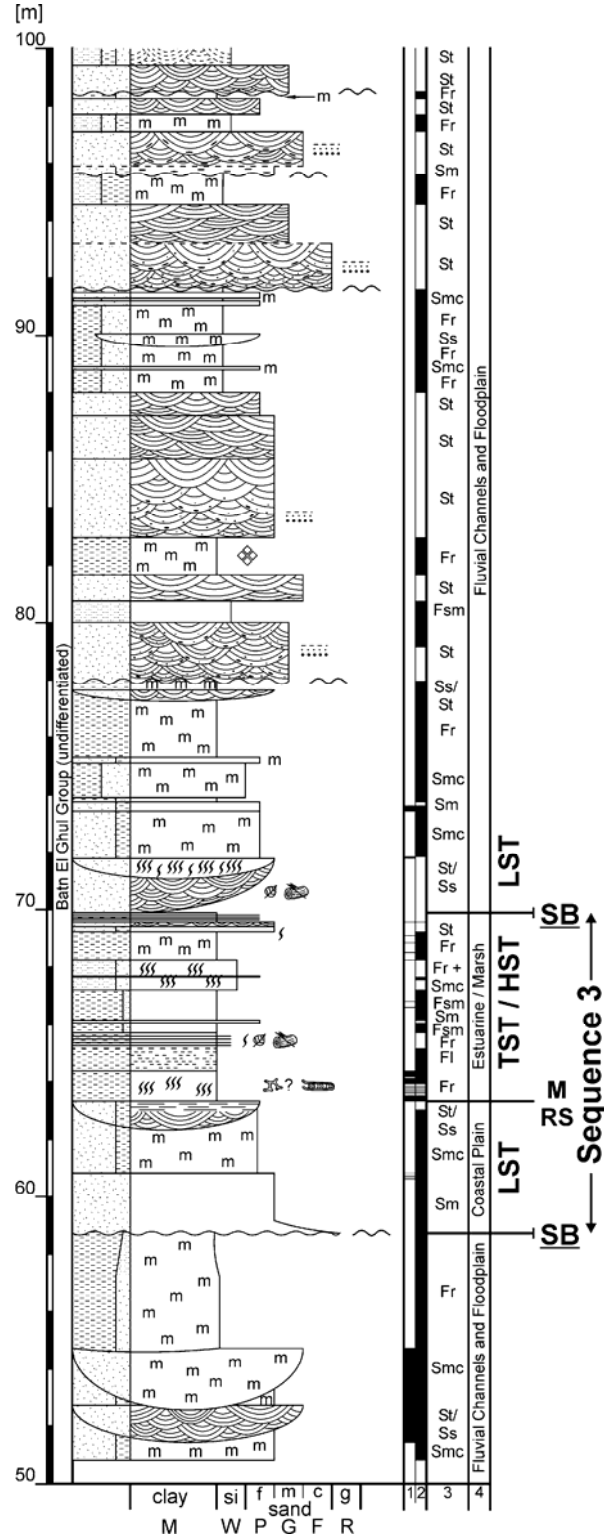
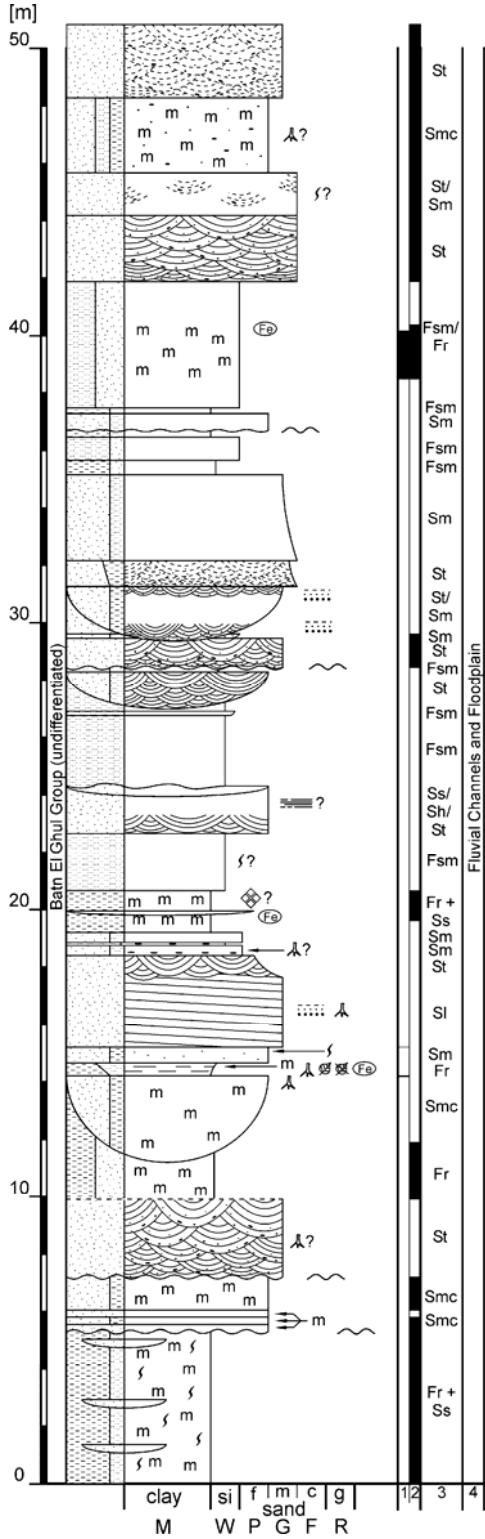
Section 10 continued



Section 11

GPS-Coordinates: N29° 36' 32.0"; E35° 57' 39.6"

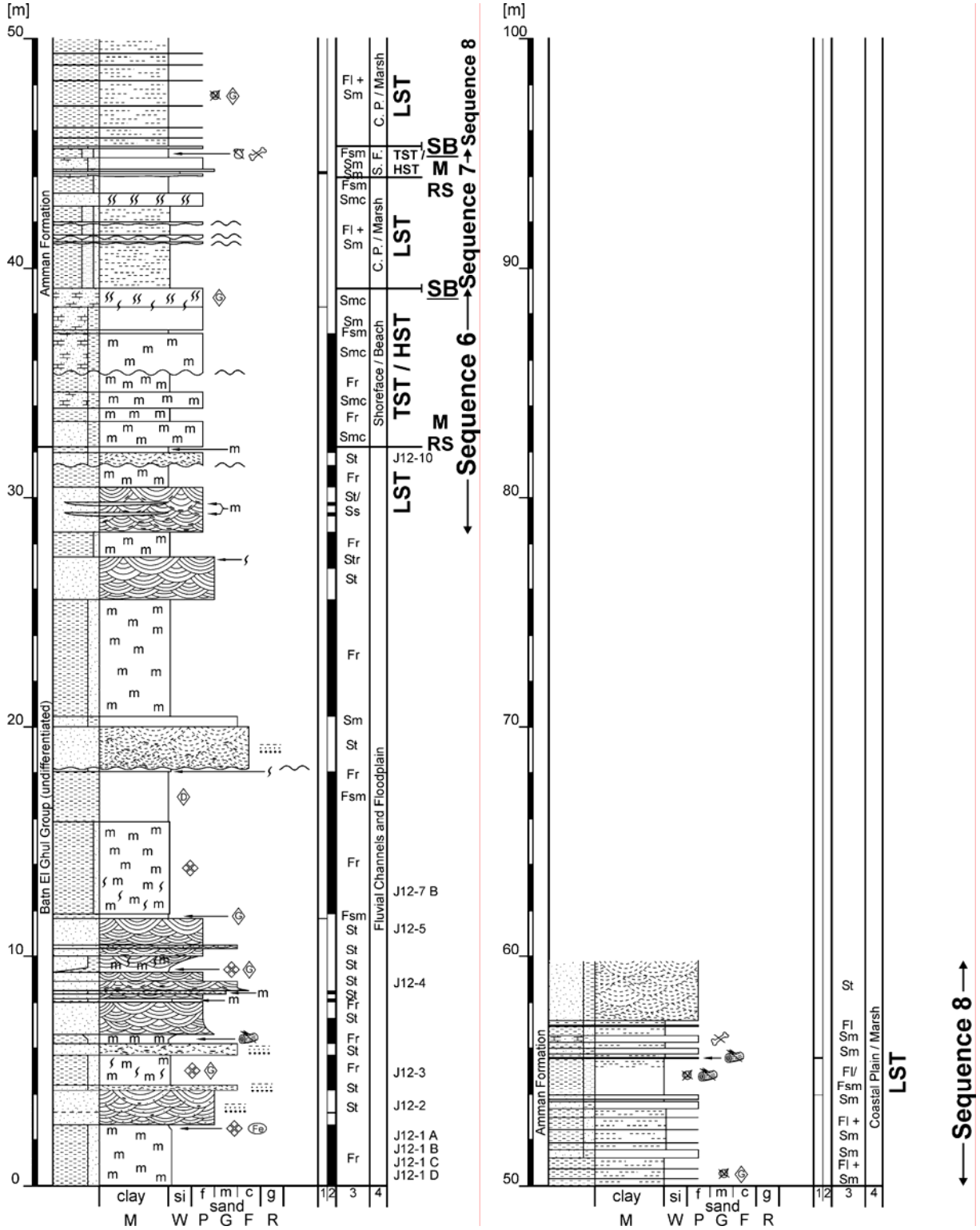
Distance from S11 to S12: 9.95 km; Bearing: 023° (true)



Section 12

GPS-Coordinates: N29° 41' 24.5"; E36° 00' 01.2"

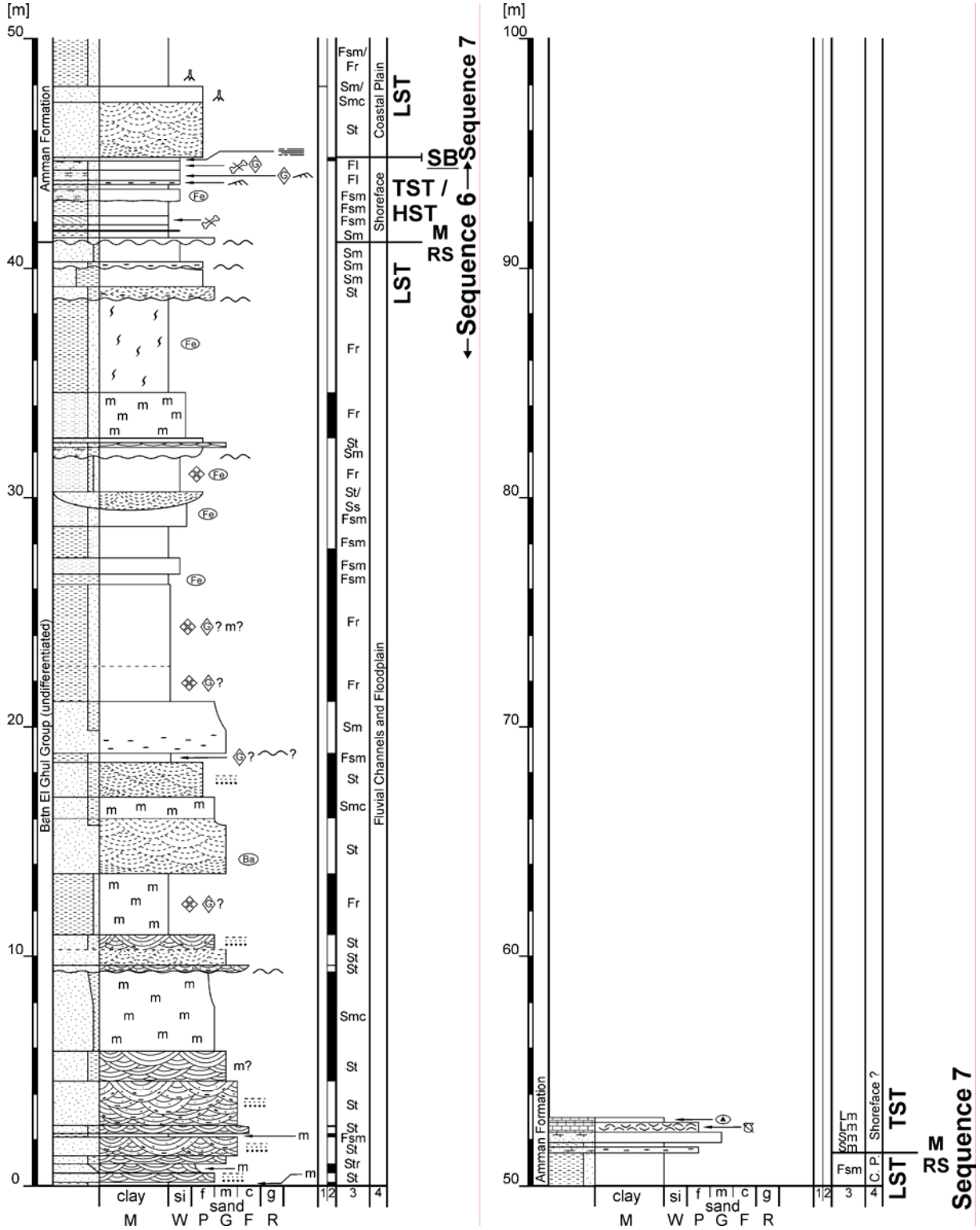
Distance from S12 to S13: 12.05 km; Bearing: 081° (true)



Section 13

GPS-Coordinates: N29° 36' 32.0"; E35° 57' 39.6"

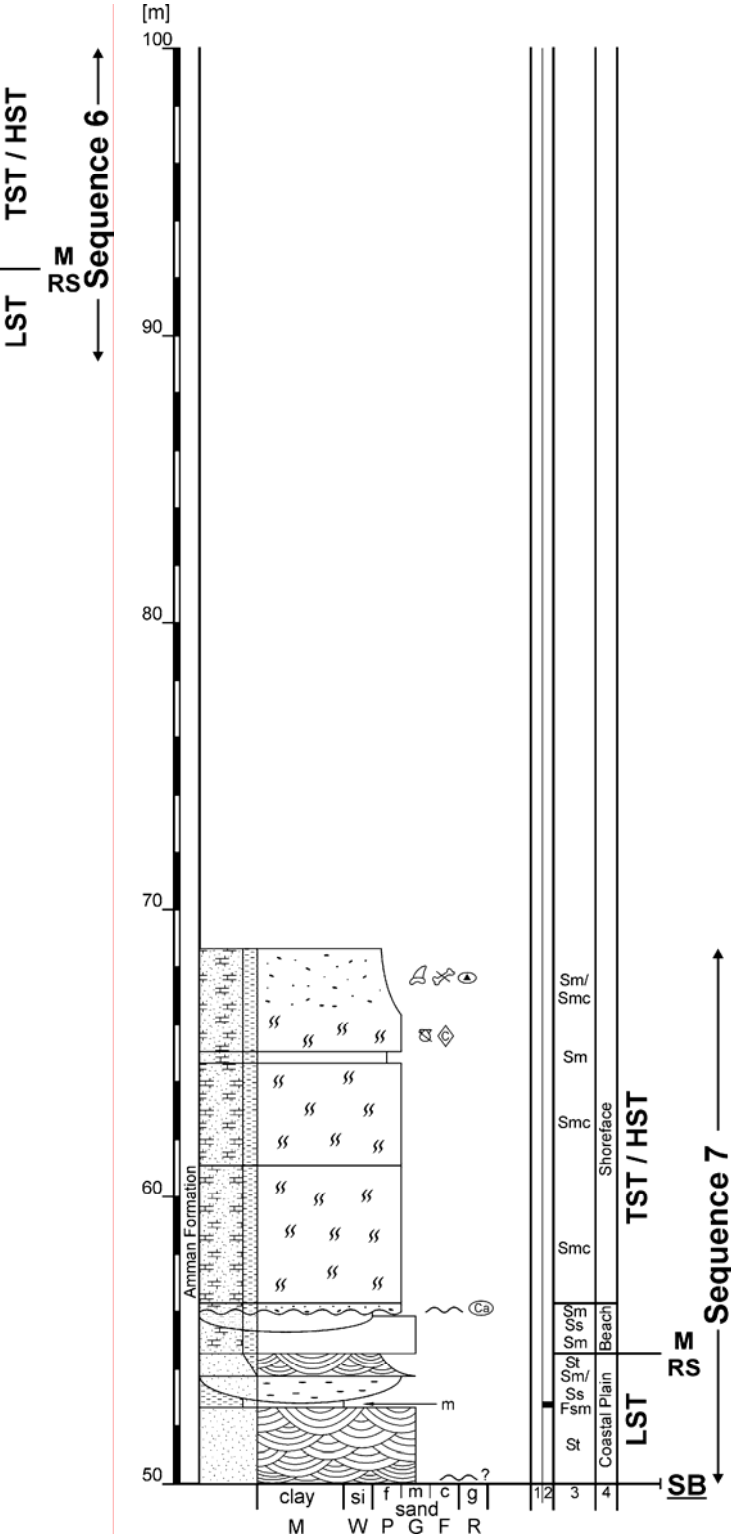
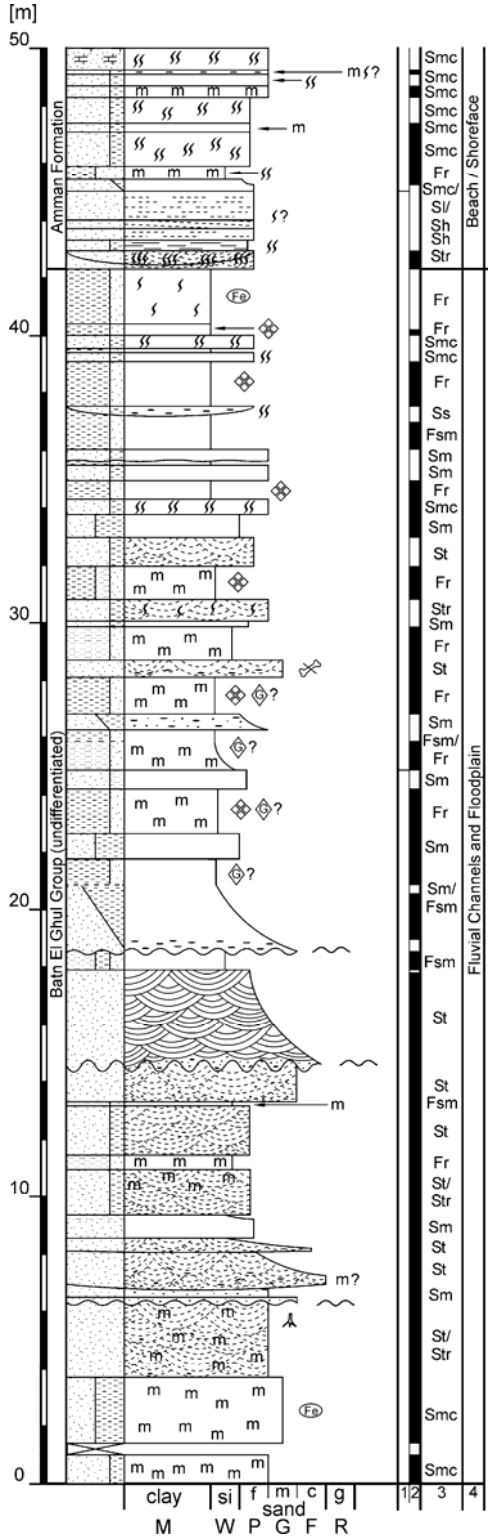
Distance from S13 to S14: 14.19 km; Bearing: 064° (true)



Section 14

GPS-Coordinates: N29° 45' 45.8"; E36° 15' 25.7"

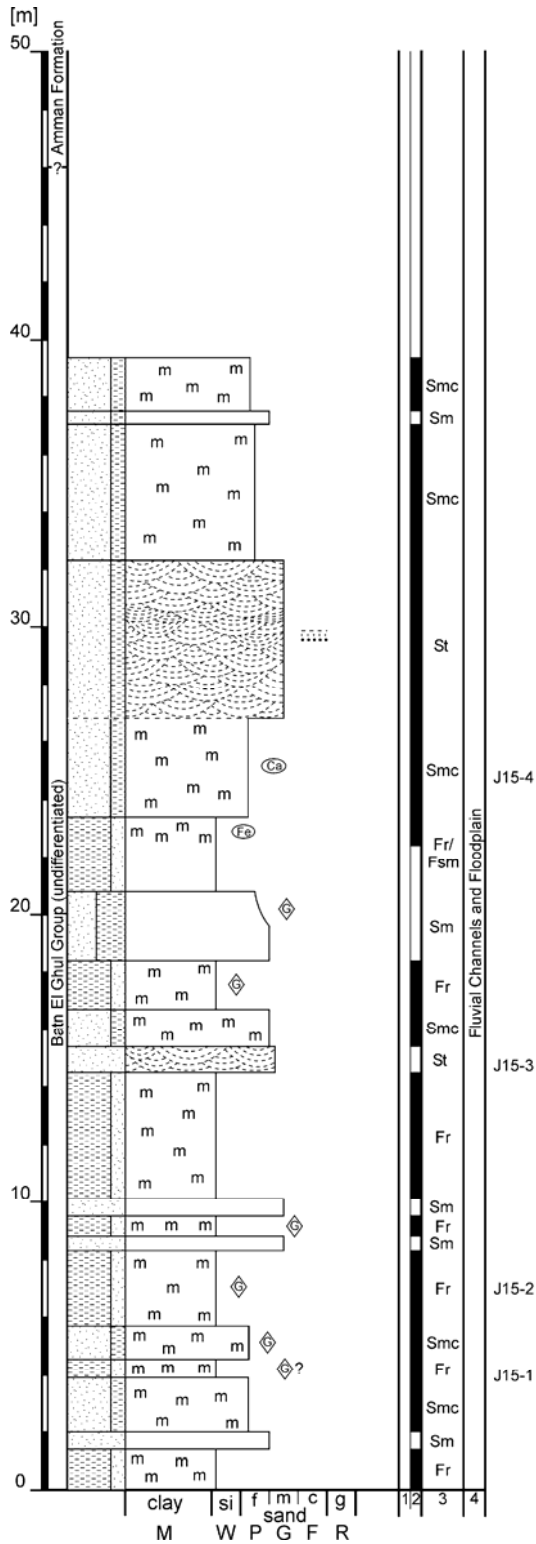
Distance from S14 to S15: 13.08 km; Bearing: 071° (true)



Section 15

GPS-Coordinates: N29° 48' 09.8"; E36° 23' 03.9"

Distance from S1 to S15: 102 km; Bearing: 118° (true)



Overview of samples and applied examination methods

Sample ID	Sediment	Stratigraphy	Light min.	Heavy min.	XRF	REE	K-Ar date
J5-1 A	f/m-sand	Kurnub Gr	X	X			
J5-3	f/m-sand	Kurnub Gr		X			
J5-5	f/m-sand	Kurnub Gr	X	X			
J5-9	f-sand	Naur Fm		X			
J5-29	f-sand	Fuhays Fm	X				
J5-31	f/m-sand	Fuhays Fm	X				
J5-51	glaucony	Shuayb Fm					X
J5-52	m-sand	Shuayb Fm	X	X			
J5-54	f-sand	Shuayb Fm		X			
J5-56	f-sand	WAS Fm		X			
J5-59	f-sand	WAS Fm	X	X			
J5-61	f-sand	WAS Fm		X			
J5-65	f-sand	WAS Fm	X				
J6-9	f/m-sand	Naur Fm	X	X	X	X	
J6-29	claystone	Hummar Fm			X		
J6-41	glaucony	Shuayb Fm					X
J6-43 B	palaeosol	Shuayb Fm			X	X	
J6-43 D	f-sand	Shuayb Fm	X	X	X		
J6-44 B	palaeosol	Shuayb Fm			X	X	
J6-57 A	Ferry band	WAS Fm	X				
J6-57 B	f/m-sand	WAS Fm	X	X	X		
J6-58 A	f-sand	WAS Fm	X	X	X		
J6-59	f-sand	WAS Fm			X		
J6-A	Fe-sand	WAS Fm			X		
J6-60	palaeosol	WAS Fm			X		
J6-61	palaeosol	WAS Fm			X		
J6-62	f-sand	WAS Fm			X		
J6-68	glaucony	WAS Fm					X
J7-6	clay	Fuhays Fm			X		
J7-7	f-sand	Fuhays Fm	X	X	X		
J7-15	m-sand	Fuhays Fm			X	X	
J7-16	clay	Hummar Fm			X		
J7-26	clay	Shuayb Fm			X		
J7-27 A	clay/glaucony	Shuayb Fm			X		X
J7-27 B	glaucony	Shuayb Fm					X
J7-28	f/m-sand	Shuayb Fm	X	X	X		
J7-29	clay	WAS Fm			X		
J7-32 A	f/m-sand	WAS Fm	X	X	X		
J7-32 B	f/m-sand	WAS Fm	X	X	X		
J7-34	f-sand	WAS Fm			X		
J7-35	m/c-sand	WAS Fm			X	X	
J7-36	f-sand	WAS Fm	X	X	X		
J7-38	f-sand	WAS Fm	X	X	X		
J8-1	m-sand	Kurnub Gr		X			
J8-7	f-sand	Fuhays Fm	X	X			
J8-11	f-sand	Hummar Fm		X			
J8-21 A-y.	palaeosol	Shuayb Fm			X		
J8-21 A-r.	palaeosol	Shuayb Fm			X		
J8-21 B	palaeosol	Shuayb Fm			X		
J8-21 C	palaeosol	Shuayb Fm			X		
J8-25 B	f-sand	Shuayb Fm		X			
J8-26	f/m-sand	Shuayb Fm	X	X			
J8-33	f/m-sand	WAS Fm	X	X			
J8-34	f-sand	WAS Fm	X	X			
J8-35	f-sand	WAS Fm	X	X			
J8-36	f-sand	WAS Fm		X			

Sample ID	Sediment	Stratigraphy	Light min.	Heavy min.	XRF	REE	K-Ar date
J9-1	m/c-sand	Kurnub Gr	X	X	X	X	
J9-3	f/m-sand	Kurnub Gr	X	X	X	X	
J9-7	f-sand	Naur Fm	X	X	X	X	
J9-14	f-sand	Fuhays Fm	X		X	X	
J9-17 A	f-sand	Hummar Fm.	X	X	X	X	
J9-17 B	m-sand	Hummar Fm.	X	X	X	X	
J9-22	f-sand	Hummar Fm.	X	X	X	X	
J9-28	c-sand	Shuayb Fm	X	X	X	X	
J9-30	f-sand	WAS Fm			X	X	
J9-33	f/m-sand	WAS Fm	X	X	X	X	
J9-34	f-sand	WAS Fm	X	X	X	X	
J9-36	palaeosol	WAS Fm			X		
J9-38	f-sand	WAS Fm	X	X	X	X	
J9-39	f-sand	WAS Fm	X	X	X	X	
J9-40	f-sand	WAS Fm	X	X	X	X	
J9-41	f-sand	WAS Fm	X	X	X	X	
J10-1	clay	Naur Fm			X		
J10-5	f-sand	Hummar Fm	X	X	X	X	
J10-6 A	clay	Hummar Fm			X		
J10-6 B	clay	Hummar Fm			X		
J10-6 C	clay	Hummar Fm			X		
J10-7	clay	Hummar Fm			X	X	
J10-7 x	Fe-sand	Hummar Fm			X		
J10-9	f-sand	Hummar Fm	X	X	X		
J10-X	glaucony	Hummar Fm					X
J10-22 A	f-sand/palaeosol	WAS Fm	X	X	X	X	
J10-22 B	f-sand/palaeosol	WAS Fm	X	X	X	X	
J10-23 A	f-sand	WAS Fm			X		
J10-37	f-sand	WUG Fm	X		X	X	
J10-44	clay	WUG Fm			X		
J10-48	silt/palaeosol	WUG Fm			X		
J12-1 A	palaeosol	BEG Gr			X		
J12-1 B	palaeosol	BEG Gr			X		
J12-1 C	palaeosol	BEG Gr			X		
J12-1 D	palaeosol	BEG Gr			X		
J12-2	f/m-sand	BEG Gr	X	X			
J12-3 g.	palaeosol	BEG Gr			X		
J12-3 r.	palaeosol	BEG Gr			X		
J12-4	m/c-sand	BEG Gr	X	X			
J12-5	f-sand	BEG Gr	X	X			
J12-7 B	palaeosol	BEG Gr			X		
J12-10	f-sand	BEG Gr	X	X			
J15-1	palaeosol	BEG Gr			X		
J15-2	palaeosol	BEG Gr			X		
J15-3	f/m-sand	BEG Gr	X	X			
J15-4	f-sand	BEG Gr	X	X			
Desert sand	f/m-sand	recent	X	X	X	X	

- f-sand = fine-grained sand/sandstone
 m-sand = medium-grained sand/sandstone
 c-sand = coarse-grained sand/sandstone
 Fe-sand = iron-oxide bearing sand/sandstone
 Fm = Formation
 Gr = Group
 BEG Gr = Batn El Ghul Group
 WUG Fm = Wadi Umm Ghudran Formation
 WAS Fm = Wadi As Sir Formation

Appendix II

Tables

Table 1: Light minerals

Table 2: Rock fragments

Table 3: Cement types

Table 4: Heavy minerals

**Table 5: Main elements normalised
to 100% LOI-free**

Table 6: Trace elements in ppm

Table 7: REE and Hf in ppm

Table 1: Light minerals

Sample ID	Kind	Qm	Qu <5°	Qu >5°	Qp 2-3	Qp >3	Chert	Plag	K-Fsp	Rock Frag.	Hvy.-Min.	Opak	Cement	Pore-space
J5-1 A	Sandst.	51.40	4.00	6.00	1.40	0.40	0	0	1.40	0	0	0	4.80	30.60
J5-5	Sandst.	47.80	2.80	8.40	2.60	0.80	0.40	0	1.40	1.00	0	0	8.80	26.00
J5-29	Sandst.	39.80	2.00	8.00	0.40	0.40	0	0	1.80	0.20	1.20	0	38.20	8.00
J5-31	Sandst.	51.40	2.80	9.20	0.60	0	0	0	1.60	0.40	0	0.20	22.40	11.60
J5-52	Sand	57.00	5.67	24.67	0.67	0.33	0	0	1.33	0	0	0	10.33	0
J5-59	Sand	57.67	5.33	12.00	3.33	1.00	0	1.33	6.67	1.00	0	0	11.67	0
J5-65	Sandst.	30.60	1.80	4.20	0.60	0.20	0	1.20	2.00	0	0.60	0.60	45.40	12.80
J6-9	Sandst.	45.80	2.40	8.00	0	1.00	0.20	0	1.00	4.00	0	1.20	23.20	17.20
J6-43 D	Sandst.	47.00	2.80	9.00	1.00	0.20	0	0	1.80	3.20	0	0	8.80	28.40
J6-57 A	Sandst.	44.60	4.40	12.60	1.00	0.40	0	0.60	1.40	0	1.00	0.20	28.00	5.80
J6-57 B	Sand	61.33	3.67	15.67	1.33	0.67	0	0.33	4.00	1.67	0	0.33	11.00	0
J6-58 A	Sand	60	5.00	14.33	2.33	1.00	0	0.33	4.67	3.33	0.33	0.33	8.33	0
J7-7 (2)	Sand	55.00	8.00	19.33	1.67	0.33	0	0.33	2.33	1.33	0	0	11.67	0
J7-7 (3)	Sand	55.00	9.00	18.00	2.00	0.67	0	0	3.67	0.33	0	0	11.33	0
J7-7	Sand x2	53.33	4.33	25.67	2.33	0.33	0	0	5.67	1.33	0	0	7.00	0
J7-28	Sandst.	42.20	1.80	13.40	1.20	0.40	0	0	1.40	1.00	0	0	22.40	16.20
J7-28	Sand	67.00	2.33	24.33	0.67	0.33	0	0	1.33	0.67	0.33	0	3.00	0
J7-32 A	Sand	57.67	2.33	26.00	1.00	1.00	0	0.33	2.00	1.67	0	0.67	7.33	0
J7-32 B	Sand	62.00	3.67	21.33	2.00	1.00	0	0	2.33	2.67	0.33	0	4.67	0
J7-36	Sand	64.67	2.00	14.33	2.00	2.00	0	0.33	4.33	3.00	0	0	7.33	0
J7-38	Sand	51.33	1.33	16.00	3.00	1.33	0	1.67	8.67	2.00	0.33	0.33	14.00	0
J8-7	Sand	73.00	5.67	12.00	2.00	0	0	0	3.33	0.33	0	0	3.67	0
J8-26	Sandst.	51.60	3.40	15.60	1.20	0.40	0	0	1.00	0.20	0.20	0	10.20	16.40
J8-33	Sand	63.00	4.33	23.00	1.67	1.33	0	0	1.00	0.33	0.67	0	4.67	0
J8-34	Sandst. x3	41.80	5.00	12.60	1.00	0.20	0	0.60	3.60	1.20	0.60	0.40	10.20	22.80
J8-35	Sand	61.00	6.33	17.00	1.33	0.67	0.33	0	6.67	0.67	0.33	0	5.67	0
J9-1	Sandst. x2	39.20	3.60	10	2.20	2.40	0.20	0.20	6.20	2.20	0	0	17.20	16.60
J9-3	Sandst. x2	48.40	3.00	6.40	1.00	0.40	0	0	4.80	0	0.20	0	7.00	28.80
J9-7	Sand	68.67	5.00	16.00	2.00	0.33	0	0	2.00	0.67	0	0	5.33	0
J9-14	Sand	68.33	4.67	12.67	1.33	1.33	0	0	2.33	1.67	0	0.33	7.33	0
J9-17 A	Sand	61.00	1.33	13.00	3.67	1.67	0	0.67	3.33	3.33	0.67	0.33	11.00	0
J9-17 A	Sandst.	46.40	2.40	8.00	0.80	0.60	0	0.20	0.60	0.40	0	0	6.40	34.20
J9-17 B	Sand	63.00	4.00	24.33	1.33	2.67	0	0	1.67	0.67	0	0	2.33	0
J9-17 B	Sandst.	42.71	3.59	6.99	1.00	1.20	0	0.20	3.59	0.20	0.40	0	8.78	31.34
J9-17 B (2)	Sandst.	42.89	3.21	15.83	1.80	0.40	0	0	0.80	0	0	0	7.62	27.45
J9-17 B (3)	Sandst.	38.60	3.40	9.80	2.60	0.80	0	0	2.00	0	0	0	8.80	34.00
J9-22	Sand	59.00	1.67	18.00	3.00	2.00	0	2.33	7.33	0.67	0	0	6.00	0
J9-28	Sand	67.00	3.33	21.67	1.33	0.67	0	0.33	1.00	0.67	0.33	0	3.67	0
J9-33	Sand	67.00	4.67	17.67	1.00	1.67	0	0	1.00	1.67	0.33	0.33	4.67	0
J9-34	Sandst. x2	36.80	1.80	6.80	1.20	0	0	0.80	5.40	5.60	0.40	0.60	15.60	25.80
J9-38	Sand	65.00	2.00	16.33	2.00	1.33	0	0.33	2.67	2.67	0	0	7.67	0
J9-39	Sand	56.33	5.00	24.67	1.00	0.67	0	0.33	2.67	2.33	0.33	0.33	6.33	0
J9-40	Sand	62.00	3.33	16.67	2.33	1.33	0	1.67	6.00	1.67	0.33	0	4.67	0
J9-41	Sand	62.67	3.33	19.33	3.67	1.33	0	0.33	3.00	1.67	0.33	0	4.33	0
J10-5	Sand	64.33	3.00	23.67	1.67	1.33	0	0	4.00	0.33	0	0	1.67	0
J10-9	Sandst.	57.20	1.40	12.00	0.80	0.60	0.20	0	2.60	0	0.20	0	5.00	20
J10-22 A	Sand	53.33	1.67	8.00	0.33	0	0.33	0	2.67	6.00	0	0	28.33	0
J10-22 B	Sand	62.00	4.00	18.00	2.00	0.67	0	0	2.00	2.67	0	0	8.67	0
J10-37	Sand	63.00	6.33	23.00	0.33	0.67	0	0	3.00	0.33	0	0	3.33	0
J12-2	Sand	62.33	11.67	19.00	0.33	0.67	0	0.33	1.67	0.33	0	0	3.67	0
J12-4	Sand	60.33	8.33	20	0.33	1.00	0	0.33	1.67	0.67	0.33	0	7.00	0
J12-5	Sand	57.00	10	22.00	0.33	0.33	0	0	3.33	0	0	0	7.00	0
J12-10	Sandst.	50.60	5.00	8.40	0.60	0	0	0	2.00	1.00	0	0.40	11.60	20.80
J15-3	Sand	57.33	6.33	17.33	1.67	1.00	0	0	1.67	0	0.33	0	14.33	0
J15-4	Sandst. x2	42.20	3.60	8.40	1.00	0	0	0	0.60	0.80	0	0.80	32.40	10.20
Desert sand	Sand	56.67	3.00	16.67	1.67	3.00	0	1.00	1.67	10.33	0.33	0	5.67	0

Table 2: Rock fragments

Sample ID	Kind	FSP-Mica	Hematite	Sediment	Clay	Silt	Carbonate	Phosphate	Volcanic	Metamorph
J5-1 A	Sandst.	0	0	0	0	0	0	0	0	0
J5-5	Sandst.	0	0.20	0	0	0	0	0	0.40	0.40
J5-29	Sandst.	0	0	0	0	0	0	0	0.20	0
J5-31	Sandst.	0	0	0	0	0	0	0.20	0	0.20
J5-52	Sand	0	0	0	0	0	0	0	0	0
J5-59	Sand	0	0.33	0	0.67	0	0	0	0	0
J5-65	Sandst.	0	0	0	0	0	0	0	0	0
J6-9	Sandst.	0	0	0	0	0	0	4.00	0	0
J6-43 D	Sandst.	0	0.20	0	0.80	0	0	2.20	0	0
J6-57 A	Sandst.	0	0	0	0	0	0	0	0	0
J6-57 B	Sand	0	1.00	0	0.33	0.33	0	0	0	0
J6-58 A	Sand	0	1.33	0	1.67	0.33	0	0	0	0
J7-7 (2)	Sand x0	0	0.67	0	0	0.33	0	0	0	0.33
J7-7 (3)	Sand x1	0	0	0	0	0	0	0	0	0.33
J7-7	Sand x2	0	0.33	0	0.67	0	0.33	0	0	0
J7-28	Sandst.	0	1.00	0	0	0	0	0	0	0
J7-28	Sand	0	0	0	0.67	0	0	0	0	0
J7-32 A	Sand	0	1.00	0	0.33	0	0	0	0	0.33
J7-32 B	Sand	0	0.33	0	1.00	1.33	0	0	0	0
J7-36	Sand	0	1.33	0	0.33	1.00	0	0	0	0.33
J7-38	Sand	0	1.67	0.33	0	0	0	0	0	0
J8-7	Sand	0	0.33	0	0	0	0	0	0	0
J8-26	Sandst.	0	0	0	0	0	0	0.20	0	0
J8-33	Sand	0	0.33	0	0	0	0	0	0	0
J8-34	Sandst. x3	0	0.80	0	0	0.20	0	0	0	0.20
J8-35	Sand	0	0.33	0	0.33	0	0	0	0	0
J9-1	Sandst. x2	0	0.20	0	1.00	0.20	0	0	0.60	0.20
J9-3	Sandst. x2	0	0	0	0	0	0	0	0	0
J9-7	Sand	0.33	0	0	0	0	0	0	0	0.33
J9-14	Sand	0	0.67	0	0	0.33	0	0	0	0.67
J9-17 A	Sand	0	1.33	0	0.33	1.00	0	0	0.33	0.33
J9-17 A	Sandst.	0	0.20	0	0	0	0	0	0.20	0
J9-17 B	Sand	0	0.67	0	0	0	0	0	0	0
J9-17 B	Sandst.	0	0	0	0.20	0	0	0	0	0
J9-17 B (2)	Sandst.	0	0	0	0	0	0	0	0	0
J9-17 B (3)	Sandst.	0	0	0	0	0	0	0	0	0
J9-22	Sand	0	0.67	0	0	0	0	0	0	0
J9-28	Sand	0	0.33	0	0	0.33	0	0	0	0
J9-33	Sand	0	1.00	0	0	0	0	0	0	0.67
J9-34	Sandst. x2	0.40	1.80	0	2.40	0.20	0	0.80	0	0
J9-38	Sand	0	1.67	0	1.00	0	0	0	0	0
J9-39	Sand	0	1.33	0	0	0	0	0	0.67	0.33
J9-40	Sand	0	1.00	0	0.33	0	0	0	0	0.33
J9-41	Sand	0	0	0	0.33	0.33	0	0	0.67	0.33
J10-5	Sand	0	0	0	0	0	0	0	0	0.33
J10-9	Sandst.	0	0	0	0	0	0	0	0	0
J10-22 A	Sand	0	1.33	0.33	1.33	0.33	2.00	0.67	0	0
J10-22 B	Sand	0	1.67	0	0.67	0	0	0	0	0.33
J10-37	Sand	0	0	0	0.33	0	0	0	0	0
J12-2	Sand	0	0	0	0	0	0	0	0	0.33
J12-4	Sand	0	0	0.33	0.33	0	0	0	0	0
J12-5	Sand	0	0	0	0	0	0	0	0	0
J12-10	Sandst.	0	0	0	0.40	0	0	0.40	0	0.20
J15-3	Sand	0	0	0	0	0	0	0	0	0
J15-4	Sandst. x2	0	0	0	0.80	0	0	0	0	0
Desert sand	Sand	0	4.00	0	0.67	2.33	2.67	0	0	0.67

Qm = Monocrystalline quartz

Qu = Undulose monoquartz

Qp = Polycrystalline quartz

Plag = Plagioclase

K-Fsp = K-Feldspar

Rock Frag. = Rock fragments (undif.)

Hvy.-Min. = Heavy minerals

Table 3: Cement types

Sample ID	Kind	Qz	K-Fsp	Plag	Cc	Dol	Gy	Bar	Phos	Clay	Illte	Smec	Glau	FeOx (Hem)	FeOx (undif)
J5-1 A	Sandst.	0.20	0	0	0	0	0	0	0	2.40	0	0	0	0	2.20
J5-5	Sandst.	0.40	0	0	0	0	0	0.20	0	3.60	0	0.40	0	0	4.20
J5-29	Sandst.	0.80	0	0	28.00	0.20	1.60	0	0	1.20	0	0	0	0	6.40
J5-31	Sandst.	1.00	0	0	15.20	0	0	0	0.20	0.60	0	0	0	0	5.40
J5-52	Sand	2.00	0	0	0	0	0	0	0	2.33	0	0.33	0	0	5.67
J5-59	Sand	4.67	1.00	0	0	0	0	0	0	1.33	0	0	0	0	4.67
J5-65	Sandst.	0.40	0	0	26.80	0.20	1.80	0.20	0	0.40	0	0	0	0	15.60
J6-9	Sandst.	0.80	0	0	0	0	0	0	4.00	0.80	0	0	0	0	17.60
J6-43D	Sandst.	2.80	0	0	0	0	0	0	2.20	2.60	0	0	0.40	0	0.80
J6-57A	Sandst.	0.40	0	0	0	0	0	0	0	0	0	0	0	2.00	25.60
J6-57B	Sand	2.67	0	0	0	0	0	0	0	1.00	0	0	0	7.33	0
J6-58A	Sand	2.67	0.33	0	0.33	0	0	0.33	0	0.33	0	0	0	0	4.33
J7-7(2)	Sand	3.67	0.33	0	0	0	0	0	0	4.00	0	0	0	3.67	0
J7-7(3)	Sand	2.00	0	0	0	0	0	0	0	4.67	0	0	0	4.67	0
J7-7	Sand x2	2.67	0	0	0	0	0	0	0	1.00	0	0	0	3.33	0
J7-28	Sandst.	0.20	0	0	0	0	0	0	0	1.20	0	0	0	0	21.00
J7-28	Sand	1.67	0	0	0	0	0	0	0	0.33	0	0	0	1.00	0
J7-32A	Sand	1.33	0	0	0	0	0	0	0	0	0	0	0	6.00	0
J7-32B	Sand	2.67	0	0	0	0	0	0	0	1.00	0	0	0	1.00	0
J7-36	Sand	3.33	0	0	0	0	0	0	0	0.67	0	0	0	3.33	0
J7-38	Sand	4.00	1.00	0	1.67	0	0	0	0	2.00	0	0	0	5.33	0
J8-7	Sand	1.67	0	0	0	0	0	0	0	1.00	0	0	0	0	1.00
J8-26	Sandst.	0.40	0	0	0	0	0	0	0.20	4.60	0	0	0	0	5.00
J8-33	Sand	2.33	0	0	0	0	0	0	0	1.00	0	0	0	0	1.33
J8-34	Sandst. x3	2.00	0.40	0	0	0	0	0	0	4.00	0	0.20	0	0	3.60
J8-35	Sand	1.33	0.33	0	0	0	0	0	0	1.33	0	0	0	0	2.67
J9-1	Sandst. x2	2.40	0	0	0	0	0	0.40	0	1.80	0	0	0	12.60	0
J9-3	Sandst. x2	2.40	0	0	0	0	0	0	0	3.60	0	0	0	1.00	0
J9-7	Sand	3.67	0	0	0.33	0	0	0	0	0.33	0	0	0	1.00	0
J9-14	Sand	2.33	0	0	0	0	0	0	0	0	0	0	0	5.00	0
J9-17A	Sand	2.67	0	0	0	0	0	0	0	0	0	0	0	8.33	0
J9-17A	Sandst.	0.80	0	0	0	0	0	0	0	4.80	0	0	0	0	0.80
J9-17B	Sand	1.67	0	0	0	0	0	0	0	0.33	0	0	0	0.33	0
J9-17B	Sandst.	3.19	0	0	0	0	0	0	0	2.79	0	0	0	0	2.79
J9-17B (2)	Sandst.	1.20	0	0	0	0	0	0	0	4.21	0	0	0	0	2.20
J9-17B (3)	Sandst.	2.20	0	0	0	0	0	0	0	4.40	0	0	0	0	2.20
J9-22	Sand	3.00	0.67	0	0	0	0	0	0	0.67	0	0	0	1.67	0
J9-28	Sand	2.00	0	0	0	0	0	0	0	0.67	0	0	0	1.00	0
J9-33	Sand	3.00	0	0	0	0	0	0	0	1.00	0	0	0	0.67	0
J9-34	Sandst. x2	3.60	0.60	0.20	0.20	0	0	1.20	0.80	3.00	0	0	0	6.00	0
J9-38	Sand	1.67	0	0	0	0	0	0	0	0.33	0	0	0	5.67	0
J9-39	Sand	4.33	0	0	0	0	0	0	0	0	0	0	0	2.00	0
J9-40	Sand	3.00	0.33	0	0	0	0	0	0	0.33	0	0	0	1.00	0
J9-41	Sand	3.00	0	0	0	0	0	0	0	1.00	0	0	0	0.33	0
J10-5	Sand	1.67	0	0	0	0	0	0	0	0	0	0	0	0	0
J10-9	Sandst.	4.40	0	0	0	0	0	0.20	0	0.40	0	0	0	0	0
J10-22 A	Sand	0	0	0	0	0	0	0	0.67	1.33	0	0	0	26.33	0
J10-22 B	Sand	2.33	0	0	0	0	0	0	0	1.00	0	0	0	0	5.33
J10-37	Sand	2.00	0	0	0.33	0	0	0	0	0.33	0	0	0	0	0.67
J12-2	Sand	1.00	0	0	0	0	0	0	0	1.33	0	0	0	0	1.33
J12-4	Sand	2.67	0	0	0	0	0	0	0	3.00	0	0	0	0	1.33
J12-5	Sand	2.67	0	0	0	0	0	0	0	2.67	0	0.33	0	0	1.33
J12-10	Sandst.	2.40	0	0	0.20	0	0	0.60	0.40	2.00	0.60	3.20	0	0	2.20
J15-3	Sand	2.00	0	0	0	0	0	0	0	6.33	0	0.33	0	0	5.67
J15-4	Sandst. x2	2.20	0	0	0.20	0	0	0	0	6.60	0	0.20	0	12.00	11.20
Desert sand	Sand	1.33	0	0	0	0	0	0	0	1.67	0	0	0	2.67	0

Qz = Quartz
K-Fsp = K-Feldspar
Plag = Plagioclase

Cc = Calcite
Dol = Dolomite
Gy = Gypsum

Bar = Baryte
Phos = Phosphate
Smec = Smectite

Glau = Glaucony
FeOx = Iron-oxide
Hem = Hematite

Table 4: Heavy minerals

Sample ID	Zircon					Tourmaline						Rut	Mon	Stau	Ky	Ti	Gar
	round	anhedral	euhedral	zone.	pink	round blue	ang. blue	round brown	ang. brown	round green	ang. green						
J5-1 A	41.0	14.5	14.0	7.0	4.5	0	0.5	0.5	2.0	0.5	1.0	13.5	0	1.0	0	0	0
J5-3	29.0	18.5	12.5	5.0	4.0	0.5	1.0	3.5	3.0	1.0	0.5	19.0	0	1.0	1.5	0	0
J5-5	16.0	15.5	9.0	4.5	0.5	1.5	1.0	11.0	1.5	11.5	3.0	23.0	0	0.5	1.0	0.5	0
J5-9	6.0	9.0	2.0	1.0	2.0	1.0	4.5	11.5	15.0	12.5	12.5	21.0	1.0	1.0	0	0	0
J5-52	49.0	12.0	10	4.5	6.0	0.5	0	2.0	0.5	1.0	1.0	13.5	0	0	0	0	0
J5-54	19.0	15.5	10	3.5	5.0	3.0	1.0	6.0	5.5	4.0	3.5	22.5	0	1.0	0.5	0	0
J5-56	1.5	11.5	3.0	0	1.5	3.0	6.0	19.5	21.0	14.0	6.0	12.0	0	1.0	0	0	0
J5-59	27.5	10	5.0	3.0	5.5	1.5	1.5	6.5	1.5	7.0	3.5	21.5	0.5	2.0	1.0	0	2.5
J5-61	26.5	11.5	8.5	3.0	4.0	3.0	0.5	10	3.5	9.0	1.0	18.5	0	0.5	0.5	0	0
J6-9	7.0	11.0	6.5	0.5	2.0	3.5	5.0	20	10	10	8.5	14.5	0.5	0.5	0	0	0.5
J6-43 D	27.5	7.0	7.5	0.5	3.5	1.0	1.5	7.5	3.5	6.5	3.0	30.5	0	0	0.5	0	0
J6-57 B	33.0	13.5	6.0	2.5	4.0	1.0	2.5	8.0	3.0	7.5	4.0	14.0	0	0.5	0.5	0	0
J6-58 A	29.5	11.5	10.5	3.5	3.5	2.0	0	9.0	3.0	9.5	1.5	16.5	0	0	0	0	0
J7-7	36.5	8.0	3.5	3.5	6.5	0.5	2.5	4.5	3.0	3.5	3.0	24.0	0.5	0.5	0	0	0
J7-28	30.5	8.5	6.5	3.0	4.0	0.5	1.0	10	4.0	5.0	5.0	20	0.5	0.5	1.0	0	0
J7-32 A	36.0	8.5	13.0	5.0	4.0	2.5	0.5	5.0	1.0	4.5	1.5	16.5	0.5	1.0	0.5	0	0
J7-32 B	33.0	12.5	10.5	5.5	4.0	1.0	0	6.5	2.5	5.5	3.0	15.5	0	0	0.5	0	0
J7-36	32.5	13.0	8.0	4.0	3.5	3.0	1.0	8.0	1.5	7.0	1.0	16.0	0.5	0	0.5	0.5	0
J7-38	17.5	19.0	5.0	4.0	3.5	1.5	2.5	8.0	3.0	6.5	4.5	16.0	2.5	1.5	3.5	0.5	1.0
J8-1	30	17.0	15.5	5.5	5.5	0	0	1.0	0.5	0	0.5	21.5	0	2.0	1.0	0	0
J8-7	7.0	9.5	5.0	1.0	1.5	6.5	3.0	18.5	7.0	15.0	7.5	16.5	1.0	0.5	0.5	0	0
J8-11	7.5	25.5	4.5	1.5	1.0	1.5	3.0	6.0	6.5	7.0	8.5	25.0	0.5	1.0	1.0	0	0
J8-25 B	22.5	12.5	6.0	2.0	3.0	1.5	1.5	12.5	5.5	9.0	2.5	20.5	1.0	0	0	0	0
J8-26	24.0	16.0	12.0	2.5	4.0	0.5	1.0	2.5	4.5	3.0	6.5	23.0	0	0	0	0.5	0
J8-33	37.5	15.5	16.0	2.0	4.0	0.5	0	6.0	1.0	3.0	4.5	9.0	0.5	0.5	0	0	0
J8-34	25.5	13.5	8.5	0.5	6.0	2.5	1.0	10	5.5	7.5	2.5	16.5	0	0.5	0	0	0
J8-35	20	20	9.5	2.0	3.0	2.0	1.0	6.5	3.0	8.0	2.5	21.5	0	0	1.0	0	0
J8-36	12.0	19.0	6.5	2.0	4.0	1.5	5.0	9.0	10	9.5	5.5	14.0	1.0	0.5	0.5	0	0
J9-1	38.5	18.0	12.5	4.0	6.5	0	0	1.5	1.0	1.0	0.5	16.0	0	0	0.5	0	0
J9-3	36.5	10	9.0	4.5	7.0	2.5	0.5	5.0	1.5	4.5	2.0	16.5	0	0	0.5	0	0
J9-7	25.0	12.0	5.0	2.0	1.0	1.5	2.5	11.5	6.0	8.0	3.5	19.5	0	1.0	1.0	0.5	0
J9-17 A	17.5	10	3.0	1.0	4.0	8.0	3.5	7.0	4.5	10	5.0	23.0	0	2.5	1.0	0	0
J9-17 B	35.0	15.0	5.0	5.0	2.5	1.5	0	9.5	3.5	1.0	0	20	0.5	0.5	1.0	0	0
J9-22	24.0	12.0	4.0	1.5	2.5	2.5	2.5	9.0	9.5	5.0	2.0	23.0	0	1.0	1.5	0	0
J9-28	45.5	7.0	5.0	1.0	5.5	1.5	0.5	5.0	0.5	2.5	0	25.0	0	1.0	0	0	0
J9-33	38.0	7.5	5.5	5.0	1.5	0.5	0.5	11.5	1.0	5.5	1.0	19.5	0	1.5	0.5	1.0	0
J9-34	12.5	19.0	4.0	1.5	7.5	3.5	2.0	9.0	6.0	8.5	4.0	16.5	1.0	1.5	3.0	0.5	0
J9-38	34.0	8.5	4.0	3.5	2.5	2.5	0.5	11.5	2.5	4.0	1.0	22.0	0	1.0	2.0	0.5	0
J9-39	25.5	15.5	9.5	2.5	6.0	2.0	1.0	6.5	2.5	7.0	1.5	20.5	0	0	0	0	0
J9-40	17.0	9.5	3.0	5.5	1.5	4.0	2.0	9.5	4.0	4.5	3.5	28.0	0.5	2.5	4.0	1.0	0
J9-41	35.0	5.0	5.0	2.5	4.0	4.0	0.5	10	4.5	7.5	2.0	16.0	0	1.5	1.5	1.0	0
J10-5	41.5	10	12.0	3.0	5.0	1.0	1.0	4.0	0	3.0	1.0	17.5	0	1.0	0	0	0
J10-9	14.0	19.5	10	3.0	1.5	2.0	1.5	8.5	8.0	7.0	2.5	20	1.0	1.0	0.5	0	0
J10-22 A	14.0	10.5	8.5	3.0	4.0	5.0	5.0	3.5	6.0	10	5.5	22.5	1.5	0	0	0.5	0
J10-22 B	11.0	13.5	7.5	1.5	3.0	1.5	4.0	12.0	8.0	13.0	5.5	17.5	0.5	0	1.0	0	0.5
J12-2	39.5	9.5	6.0	1.5	4.0	1.0	0.5	4.0	1.5	7.0	1.5	22.5	0	0.5	0.5	0.5	0
J12-4	35.5	10	10	3.0	5.5	1.5	0.5	3.5	0	3.5	1.5	24.5	0	1.0	0	0	0
J12-5	31.0	11.5	8.5	0.5	2.5	1.5	0	8.5	3.0	7.5	4.5	19.0	0	1.0	0	1.0	0
J12-10	32.5	12.0	4.0	2.5	3.0	4.0	2.0	5.5	2.5	7.0	3.5	19.0	0	1.0	1.0	0.5	0
J15-3	40	12.0	7.0	3.5	6.0	1.5	1.0	2.0	1.0	3.5	0.5	20	0	2.0	0	0	0
J15-4	29.5	19.0	5.5	2.5	6.5	1.5	3.0	5.5	1.0	5.5	3.0	17.0	0	0.5	0	0	0
Desert sand	13.0	10.5	10	1.0	2.5	4.0	1.5	13.0	10.5	7.5	4.0	17.5	1.0	1.0	1.0	0	2.0

zone. = zoned
round = rounded
ang. = angular

Rut = Rutile
Mon = Monazite
Stau = Staurolite

Ky = Kyanite
Ti = Titanite
Gar = Garnet

Table 5: Main elements normalised to 100% LOI-free

Sample ID	SiO ₂ [%]	Al ₂ O ₃ [%]	Fe ₂ O ₃ [%]	MnO [%]	MgO [%]	CaO [%]	Na ₂ O [%]	K ₂ O [%]	TiO ₂ [%]	P ₂ O ₅ [%]	LOI	CO ₂	H ₂ O
J6-9	86.06	3.76	8.47	0.03	0.22	0.57	0.21	0.33	0.23	0.10	5.04	0.11	2.43
J6-29	65.46	22.03	4.42	0.01	1.90	0.06	0.43	4.32	1.25	0.12	12.06	1.17	6.62
J6-43B	86.66	7.07	4.45	0	0.41	0.28	0.68	0.12	0.27	0.04	5.10	0.11	2.72
J6-43D	97.27	1.61	0.41	0	0.17	0.06	0.16	0.18	0.09	0.04	1.41	0.15	0.54
J6-44B	93.95	4.29	1.26	0	0.06	0.04	0.12	0.03	0.21	0.02	2.08	0.07	1.44
J6-57B	96.65	1.60	0.63	0	0.09	0.02	0.08	0.64	0.25	0.03	0.69	0.15	0.38
J6-58A	95.51	2.27	0.67	0	0.11	0.11	0.13	0.90	0.25	0.05	0.91	0.11	0.51
J6-59	61.33	21.83	6.05	0.02	1.52	0.44	1.03	5.06	2.42	0.29	12.18	0.37	7.01
J6-A	86.07	1.30	11.50	0.02	0.12	0.05	0.30	0.38	0.16	0.09	2.06	0.11	0.85
J6-60	68.02	13.68	10.01	0.07	1.19	0.09	1.01	3.89	1.85	0.21	9.38	0.26	4.91
J6-61	71.25	14.47	6.48	0.01	1.40	0.19	1.18	3.41	1.48	0.13	9.92	0.18	5.40
J6-62	74.81	8.57	8.98	0.04	0.65	1.63	0.46	2.72	1.04	1.10	5.77	0.26	3.24
J7-6	68.66	19.89	3.61	0	1.61	0.03	1.51	3.39	1.24	0.06	12.94	0.59	5.75
J7-7	98.95	0.34	0.31	0	0.04	0.15	0.04	0.10	0.05	0.01	0.70	0.15	0.18
J7-15	90.05	2.87	2.87	0.03	1.24	1.97	0.19	0.46	0.17	0.16	4.30	2.27	1.33
J7-16	60.12	29.53	3.59	0.01	1.29	0.02	0.76	3.23	1.41	0.05	14.04	1.32	9.59
J7-26	20.04	4.92	14.29	0.24	18.57	38.78	0.43	2.20	0.35	0.19	31.41	19.82	4.21
J7-27A	61.37	11.51	17.11	0.01	2.82	0.33	0.77	5.11	0.75	0.20	10.32	0.18	7.39
J7-28	98.45	0.76	0.40	0	0.05	0.08	0.15	0.04	0.05	0.01	0.82	0.07	0.33
J7-29	65.46	17.75	6.41	0.01	2.80	0.10	1.96	3.70	1.64	0.17	13.39	0.26	7.09
J7-32A	95.73	1.72	1.25	0.01	0.09	0.15	0.12	0.60	0.23	0.10	0.79	0.11	0.47
J7-32B	96.82	1.82	0.38	0	0.10	0.04	0.06	0.50	0.25	0.02	0.79	0.07	0.37
J7-34	94.24	2.13	1.44	0.06	0.07	0.08	0.24	1.29	0.41	0.05	0.65	0.15	0.39
J7-35	66.77	2.60	28.08	0.16	0.21	0.29	0.36	0.59	0.22	0.73	3.82	0.18	2.82
J7-36	96.72	1.60	0.43	0	0.08	0.06	0.08	0.80	0.19	0.03	0.57	0.11	0.29
J7-38	91.92	4.02	0.68	0	0.14	0.17	0.07	2.33	0.60	0.05	0.95	0.18	0.78
J8-21A-y	21.59	4.33	4.84	0.15	29.53	38.34	0	0.92	0.23	0.07	38.52	26.71	2.12
J8-21A-r	26.87	6.30	5.25	0.09	25.37	34.22	0	1.51	0.31	0.08	36.11	30.26	2.08
J8-21B	30.51	7.45	5.27	0.08	23.45	30.73	0	2.08	0.34	0.08	34.03	28.58	2.29
J8-21C	22.64	6.08	5.11	0.10	28.75	36.39	0	0.62	0.25	0.05	38.24	32.79	1.52
J9-1	97.23	1.86	0.60	0.04	0.02	0.02	0.06	0.05	0.11	0.01	1.40	0.07	0.80
J9-3	98.68	0.81	0.29	0	0.02	0.04	0	0.05	0.09	0.01	0.45	0.11	0.34
J9-7	99.17	0.26	0.21	0	0.03	0.03	0	0.08	0.20	0.01	0.17	0.07	0.06
J9-14	96.87	1.38	1.35	0.01	0.06	0.01	0	0.13	0.17	0.01	0.89	0.07	0.72
J9-17A	97.02	1.96	0.28	0	0.04	0.02	0	0.29	0.39	0.01	0.84	0.07	0.70
J9-17B	99.50	0.24	0.14	0	0.02	0.01	0	0.04	0.04	0.01	0.17	0.15	0.04
J9-22	95.96	2.13	0.30	0	0.05	0.22	0.04	1.13	0.13	0.03	0.87	0.04	0.49
J9-28	99.21	0.36	0.21	0	0.02	0.06	0.02	0.05	0.05	0.01	0.34	0.07	0.16
J9-30	68.91	7.55	13.21	0.02	1.56	1.95	0.51	4.01	1.08	1.20	6.18	0.15	4.31
J9-33	97.66	0.92	0.48	0.01	0.06	0.12	0	0.38	0.27	0.09	0.38	0.07	0.23
J9-34	89.41	4.95	1.45	0.02	0.23	0.19	0.35	2.06	1.17	0.16	1.90	0.07	1.10
J9-36	68.61	13.52	8.30	0.04	1.14	0.68	1.11	3.53	2.52	0.57	5.42	0.22	4.61
J9-38	96.56	1.67	0.87	0.02	0.07	0.08	0.14	0.36	0.20	0.02	1.11	0.07	0.67
J9-39	96.22	1.83	1.02	0.01	0.06	0.07	0.01	0.46	0.27	0.05	0.79	0.04	0.44
J9-40	97.09	1.48	0.40	0	0.05	0.03	0	0.64	0.28	0.02	0.41	0.07	0.33
J9-41	98.07	0.91	0.22	0	0.04	0.13	0	0.41	0.21	0.01	0.33	0.11	0.19
J10-1	65.61	26.24	3.58	0.01	1.28	0.15	0.15	1.42	1.49	0.06	12.67	0.59	10.80
J10-5	99.17	0.41	0.26	0	0	0.06	0.02	0.03	0.05	0	0.46	0.11	0.20
J10-6A	63.91	2.02	32.72	0.29	0.36	0.17	0	0.04	0.15	0.34	4.94	0.18	3.62
J10-6B	94.43	1.70	2.03	0.04	0.39	0.35	0.68	0.14	0.15	0.08	2.68	0.07	1.29
J10-6C	91.20	1.84	3.49	0.06	0.41	0.25	2.11	0.35	0.15	0.13	5.06	0.15	1.51
J10-7	77.05	16.33	2.21	0	0.35	0.72	1.33	0.32	1.66	0.03	9.27	0.18	5.22
J10-7x	82.96	5.21	9.89	0.19	0.21	0.32	0.30	0.25	0.61	0.07	3.56	0.18	1.94
J10-9	99.52	0.23	0.13	0	0	0	0	0.03	0.07	0.01	0.25	0.07	0.01
J10-22A	89.13	4.12	4.73	0.01	0.44	0.12	0.65	0.52	0.24	0.03	3.52	0.07	1.70
J10-22B	96.31	1.65	1.13	0	0.16	0.08	0.31	0.22	0.06	0.07	1.54	0.11	0.57
J10-23A	77.32	17.97	2.71	0.01	0.21	0.19	0.19	0.25	1.09	0.07	7.22	0.11	5.45
J10-37	99.02	0.42	0.22	0	0.07	0.02	0.10	0.09	0.04	0.01	0.35	0.07	0.07
J10-44	66.97	16.25	7.58	0.14	3.18	2.72	0.49	1.35	1.26	0.06	17.83	0.22	15.50
J10-48	75.18	10.81	4.98	0.01	4.65	0.47	0.41	2.40	1.01	0.09	10.35	0.18	5.79
J12-1A	86.02	4.71	3.16	0.03	1.68	0.71	1.60	1.51	0.55	0.03	5.78	0.07	2.89
J12-1B	88.25	4.40	2.26	0.07	1.44	0.38	1.58	1.12	0.49	0.03	6.20	0.11	2.78
J12-1C	80.51	7.34	4.52	0.04	2.64	1.38	0.91	1.82	0.80	0.03	9.69	0.04	4.97
J12-1D	88.59	4.45	2.06	0.15	1.75	0.70	0.62	1.13	0.53	0.03	5.47	0.07	3.86
J12-3-g	85.51	7.20	2.50	0.01	1.45	1.34	0.42	0.98	0.55	0.03	6.40	0.07	3.84
J12-3-r	80.71	9.03	4.12	0.01	1.79	1.95	0.48	1.19	0.68	0.04	8.89	0.11	5.77

Sample ID	SiO ₂ [%]	Al ₂ O ₃ [%]	Fe ₂ O ₃ [%]	MnO [%]	MgO [%]	CaO [%]	Na ₂ O [%]	K ₂ O [%]	TiO ₂ [%]	P ₂ O ₅ [%]	LOI	CO ₂	H ₂ O
J12-7B	66.13	17.16	7.89	0.03	2.68	1.88	0	2.93	1.24	0.05	8.74	0.11	7.55
J15-1	79.93	7.26	3.48	0.01	4.46	1.25	1.71	1.26	0.62	0.02	10.18	0.11	7.01
J15-2	81.96	6.30	5.21	0.09	2.27	0.40	1.96	1.21	0.59	0.03	6.98	0.11	4.93
Desert sand	95.34	1.70	1.18	0.03	0.23	0.69	0.12	0.49	0.13	0.08	1.42	0.59	0.60

Table 6: Trace elements in ppm

Sample ID	Pb	Th	U	Sc	V	Cr	Co	Ni	Cu	Zn	Ga	Rb	Sr	Y	Zr	Nb	Ba
J6-9	30	2	1	2	39	24	48	20	2	51	6	13	2	7	78	4	96
J6-29	10	5	1	22	134	133	34	27	11	37	22	69	27	16	215	15	130
J6-43B	18	8	2	9	69	27	74	12	7	9	8	3	108	40	370	6	98
J6-43D	6	1	3	4	8	5	383	6	8	5	5	5	87	48	149	3	33
J6-44B	16	5	1	4	20	16	50	4	4	5	6	0	92	6	333	5	99
J6-57B	8	3	1	1	14	11	310	6	6	6	5	12	37	8	269	7	119
J6-58A	7	2	1	1	20	10	213	9	7	19	5	18	44	7	185	7	210
J6-59	17	15	3	19	140	113	49	62	19	80	26	127	123	36	367	48	338
J6-60	16	12	3	13	142	82	31	56	0	68	19	97	115	34	411	35	427
J6-61	17	12	1	16	122	79	25	43	7	43	20	93	130	48	357	29	334
J6-62	38	10	4	17	173	55	169	141	74	23	12	60	99	74	393	20	335
J6-A	30	2	0	2	53	11	182	27	3	586	6	7	45	10	99	5	86
J7-6	14	10	4	17	94	104	27	22	12	31	21	73	132	21	353	19	148
J7-7	5	0	0	0	5	1	338	2	6	7	4	1	11	3	63	3	25
J7-15	5	2	1	2	24	16	123	13	5	9	5	11	55	13	100	3	107
J7-16	10	7	2	22	167	160	21	50	16	72	29	50	23	17	166	14	83
J7-26	2	2	3	16	34	20	84	71	0	1044	0	22	84	40	69	4	161
J7-27A	6	5	4	16	58	82	46	68	1	155	15	121	123	47	277	10	87
J7-28	10	1	1	0	11	3	257	3	8	3	4	0	20	3	42	3	25
J7-29	22	11	3	17	107	86	11	25	12	26	24	103	124	17	353	32	86
J7-32A	7	3	1	1	19	9	311	6	6	7	6	11	36	11	222	6	105
J7-32B	19	2	0	0	11	8	93	4	6	7	5	10	36	6	172	6	74
J7-34	8	6	2	1	20	13	253	6	6	9	5	24	54	13	661	9	261
J7-35	20	4	3	3	43	16	74	35	0	35	5	14	111	34	247	5	58
J7-36	8	3	1	0	14	8	205	6	7	5	4	15	42	7	187	5	170
J7-38	10	5	2	2	38	26	133	7	7	10	7	41	65	15	384	11	420
J8-21A-y	1	n.a.	n.a.	n.a.	9	n.a.	n.a.	19	n.a.	20	n.a.	32	60	n.a.	100	n.a.	55
J8-21A-r	4	n.a.	n.a.	n.a.	15	5	n.a.	19	n.a.	23	n.a.	40	60	n.a.	100	n.a.	20
J8-21B	2	n.a.	n.a.	n.a.	20	10	n.a.	23	n.a.	28	n.a.	42	59	n.a.	100	n.a.	27
J8-21C	1	n.a.	n.a.	n.a.	12	2	n.a.	18	n.a.	20	n.a.	34	60	n.a.	100	n.a.	17
J9-1	4	2	1	2	15	8	154	3	11	6	4	3	19	4	130	4	114
J9-3	3	1	1	1	9	3	265	2	9	5	3	3	11	3	140	3	27
J9-7	6	2	1	1	5	1	152	3	6	5	2	3	10	8	877	7	57
J9-14	15	2	1	0	12	6	132	7	10	76	3	5	11	5	251	5	76
J9-17A	7	6	1	2	12	8	45	4	9	5	3	7	16	9	455	7	98
J9-17B	4	1	0	0	4	1	226	3	9	2	2	2	7	1	20	2	20
J9-22	4	2	1	2	9	4	106	4	6	6	3	20	42	5	157	3	190
J9-28	8	1	0	0	4	0	217	3	7	5	3	3	25	2	64	2	35
J9-30	7	7	2	12	106	38	28	24	7	36	14	99	50	32	700	17	113
J9-33	7	2	1	0	12	6	159	7	8	7	3	7	23	6	254	5	90
J9-34	8	6	2	5	44	30	96	10	9	23	7	29	36	16	541	21	200
J9-36	12	12	3	n.a.	182	87	13	51	n.a.	58	n.a.	81	94	n.a.	600	n.a.	269
J9-38	5	2	1	2	16	7	140	6	5	11	4	12	45	5	248	5	118
J9-39	6	1	0	1	19	8	103	10	6	15	3	15	175	61	226	23	169
J9-40	6	4	1	1	12	3	183	5	9	7	4	15	45	7	465	6	177
J9-41	4	3	1	0	9	2	91	1	6	6	2	8	32	5	384	4	107
J10-1	16	15	3	22	113	130	14	29	17	62	28	64	44	43	292	25	120
J10-5	7	1	1	1	6	6	336	4	8	10	3	0	50	4	91	3	102
J10-6A	8	3	7	n.a.	148	72	25	94	n.a.	184	n.a.	7	33	n.a.	200	n.a.	246
J10-6B	6	4	4	n.a.	62	5	8	21	n.a.	28	n.a.	9	55	n.a.	300	n.a.	67
J10-6C	8	5	6	n.a.	78	12	10	30	n.a.	61	n.a.	9	47	n.a.	200	n.a.	78
J10-7x	11	6	3	4	53	44	57	21	2	68	8	10	110	23	839	10	54
J10-7	25	19	4	14	86	103	40	21	11	53	19	11	120	40	776	27	97
J10-9	11	1	1	1	3	3	198	3	5	4	4	0	50	3	94	3	105
J10-22A	6	4	2	12	27	29	84	12	5	30	8	14	67	9	220	4	101
J10-22B	3	1	8	5	8	8	224	8	6	12	4	6	61	322	35	2	106

Sample ID	Pb	Th	U	Sc	V	Cr	Co	Ni	Cu	Zn	Ga	Rb	Sr	Y	Zr	Nb	Ba
J10-23A	12	8	3	27	67	69	45	15	9	25	17	6	95	19	528	14	98
J10-37	6	1	0	1	7	1	132	2	5	4	3	2	49	3	39	2	110
J10-44	9	13	2	16	102	99	36	51	15	42	18	35	163	23	228	21	196
J10-48	7	10	1	13	74	94	17	33	3	24	14	72	47	20	325	18	159
J12-1A	4	6	3	n.a.	52	24	6	25	n.a.	20	n.a.	55	78	n.a.	400	n.a.	50
J12-1B	5	6	3	n.a.	58	16	7	27	n.a.	24	n.a.	48	49	n.a.	400	n.a.	180
J12-1C	2	7	3	n.a.	83	55	7	40	n.a.	34	n.a.	66	112	n.a.	500	n.a.	94
J12-1D	4	5	3	n.a.	59	19	15	54	n.a.	39	n.a.	49	65	n.a.	600	n.a.	337
J12-3-g	4	8	3	n.a.	82	29	12	23	n.a.	20	n.a.	46	119	n.a.	400	n.a.	71
J12-3-r	4	10	2	n.a.	74	45	10	27	n.a.	20	n.a.	51	149	n.a.	400	n.a.	69
J12-7B	2	19	2	n.a.	113	91	29	43	n.a.	37	n.a.	106	156	n.a.	400	n.a.	130
J15-1	3	8	2	n.a.	44	31	8	31	n.a.	30	n.a.	70	159	n.a.	400	n.a.	55
J15-2	8	7	3	n.a.	61	45	8	33	n.a.	30	n.a.	55	72	n.a.	400	n.a.	162
Desert sand	20	4	1	31	17	8	129	5	8	18	6	12	50	5	62	4	171

Table 7: REE and Hf in ppm

Sample ID	La	Co	Pr	Nd	Sm	Eu	Gd	Tb	Dy	Ho	Er	Tm	Yb	Lu	Hf
J6-9	13.34	15.89	10.78	n.a.	n.a.	n.a.	4.81	4.69	4.29	3.10	n.a.	n.a.	n.a.	3.55	2.55
J6-43 B	74.11	82.48	74.03	n.a.	n.a.	n.a.	30.89	31.12	19.01	n.a.	n.a.	n.a.	n.a.	n.a.	12.00
J6-44 B	53.67	48.15	33.52	n.a.	4.05	n.a.	2.74	2.67	3.34	n.a.	n.a.	n.a.	n.a.	4.58	11.60
J7-15	21.96	26.13	21.25	n.a.	10.29	12.16	9.38	7.72	5.99	5.46	n.a.	n.a.	n.a.	5.09	3.10
J7-35	44.28	40.05	34.38	n.a.	25.90	n.a.	34.11	27.96	19.66	17.86	n.a.	n.a.	n.a.	12.15	8.47
J9-1	18.09	19.36	11.13	6.01	3.28	1.78	2.12	2.36	1.89	2.01	2.27	3.03	2.86	3.20	3.60
J9-3	3.77	9.33	6.29	4.43	2.61	1.65	1.56	1.27	1.68	1.30	1.37	2.17	1.74	1.81	3.29
J9-7	5.16	9.76	6.74	4.71	3.07	1.86	2.15	2.42	3.13	2.53	2.99	4.73	4.52	5.02	12.94
J9-14	5.43	10.78	7.27	5.25	3.20	2.41	2.47	1.96	2.22	1.86	2.04	3.15	2.62	3.32	4.89
J9-17 A	22.61	22.80	15.55	11.36	6.93	4.20	4.71	4.34	3.50	3.89	4.57	6.05	5.94	6.93	9.97
J9-17 B	1.25	7.13	4.47	3.03	1.60	0.92	0.91	0.66	0.54	0.67	0.60	1.28	0.78	1.03	1.42
J9-22	9.06	14.84	10.20	7.48	4.73	3.64	3.19	2.34	1.84	1.84	2.15	2.69	2.70	2.82	3.83
J9-28	10.74	14.58	9.78	6.33	2.99	1.85	1.33	0.99	0.69	0.78	0.83	1.40	1.02	1.44	2.38
J9-30	73.92	61.27	54.60	44.90	29.04	19.77	21.58	16.69	15.93	11.35	11.57	13.46	11.78	12.23	12.21
J9-33	17.25	19.74	14.56	10.52	6.79	6.25	4.64	3.34	2.41	2.25	2.52	3.40	2.82	3.27	5.77
J9-34	48.07	46.91	35.37	28.27	18.40	14.45	12.33	10.44	7.98	7.03	7.30	8.91	8.45	7.89	10.59
J9-38	24.81	26.78	18.11	12.76	7.05	5.23	3.62	2.54	2.01	1.86	1.93	2.59	2.33	2.70	4.64
J9-39	46.64	36.47	25.81	17.61	10.83	5.81	5.99	4.31	2.29	2.79	2.39	3.66	2.21	2.19	3.44
J9-40	31.36	29.08	20.24	14.13	7.76	4.87	4.04	3.52	3.01	2.63	2.61	3.93	3.76	3.96	8.69
J9-41	22.24	23.13	15.63	10.71	6.09	4.03	3.29	2.35	1.92	2.02	2.13	3.26	2.81	3.50	7.11
J10-5	14.96	19.45	15.26	n.a.	4.63	n.a.	4.34	3.33	3.34	n.a.	n.a.	n.a.	n.a.	1.94	3.23
J10-7	31.08	33.12	29.57	n.a.	19.50	n.a.	16.13	14.81	11.48	13.15	n.a.	n.a.	n.a.	14.40	28.48
J10-22 A	40.80	56.28	55.57	n.a.	n.a.	n.a.	20.09	13.41	8.74	5.93	n.a.	n.a.	n.a.	5.74	8.13
J10-22 B	127.48	213.10	226.16	n.a.	n.a.	n.a.	n.a.	n.a.	n.a.	n.a.	n.a.	n.a.	n.a.	n.a.	1.16
J10-37	11.08	13.74	10.51	n.a.	n.a.	n.a.	2.07	1.82	2.30	n.a.	n.a.	n.a.	n.a.	0.98	1.26
Desert sand	24.84	25.68	17.59	12.24	6.93	5.05	4.32	3.09	2.02	2.21	2.15	3.00	2.19	2.73	2.52

LEBENSLAUF / CURRICULUM VITAE

Persönliche Daten

Vor- und Familienname: Uwe Peter Baaske
Geburtsdatum: 13.05.1971
Geburtsort: Kaiserslautern
Staatsangehörigkeit: deutsch
Familienstand: verheiratet

Schulischer Werdegang

1977-1981 Gemeinsame Grundschule Selberg, Rothselberg
1981-1987 Staatliche Realschule, Kusel
1987-1990 Technisches Gymnasium, Kaiserslautern
Mai 1990 Allgemeine Hochschulreife

Studium

WS 1991-SS 1994 Grundstudium der Geologie und Paläontologie an der Julius-Maximilians-Universität, Würzburg
Juli 1994 Vordiplom
WS 1994-WS 1998/99 Hauptstudium der Geologie und Paläontologie an der Johannes-Gutenberg-Universität, Mainz
März 1999 Diplom
Thema der Diplomarbeit: *Untersuchungen zur Diagenese des Buntsandsteins am Westrand des Rheingrabens (Region Bad Dürkheim / Neustadt a. d. Weinstraße)*“, Betreuer: Prof. Dr. R. Gaupp
Seit April 1999 Promotionsstudium am Institut für Geologie und Paläontologie der Technischen Universität Stuttgart

Stipendien

Juli-Dezember 1997 Förderstipendium der Johannes-Gutenberg-Universität Mainz

Praktika/Berufspraxis

Dezember 1990 und April-Juli 1991 Produktionsarbeiter in der Adam Opel AG, Kaiserslautern
August-September 1996 Praktikum am Alfred-Wegener-Institut für Polar- und Meeresforschung (AWI), Bremerhaven
1996-1999 Verschiedene Tätigkeiten als wissenschaftliche Hilfskraft am Institut für Geowissenschaften der Johannes-Gutenberg-Universität, Mainz
Oktober 1997 Praktikum am Institut für Allgemeine und Angewandte Geophysik der Ludwig-Maximilians-Universität, München
August-Oktober 1998 Mitarbeit an einem Drittmittelprojekt der Preussag-Energie; Projektleitung: Prof. Dr. R. Gaupp, Institut für Geowissenschaften der Friedrich-Schiller-Universität, Jena
April 1999-Oktober 2001 Wissenschaftlicher Mitarbeiter am Institut für Geologie und Paläontologie der Technischen Universität Stuttgart; Verwaltung des DFG-Projektes KR 1333/1 & 3; Verschiedene Lehrtätigkeiten
Mai 2002-September 2002 Wissenschaftlicher Mitarbeiter am Institut für Geologie und Paläontologie der Technischen Universität Stuttgart für ein Drittmittelprojekt der Firma Edison Gas; Projektleitung: Prof. Dr. M. Mutti